The Dendritic NMDA Spike as a Fundamental Mechanism Initiating Associative Plasticity in the CA3 Region of the Hippocampus

Dissertation

zur

Erlangung der naturwissenschaftlichen Doktorwürde (Dr. sc. nat.)

vorgelegt der

Mathematisch-naturwissenschaftlichen Fakultät

der

Universität Zürich

von

FEDERICO BRANDALISE

aus

Italien

Promotionskomitee

Prof. Dr. Urs Gerber

Prof. Dr. Fritjof Helmchen (Vorsitz)

Prof. Dr. Kevan Martin

Zürich, 2016

"*One cell to rule them all,*

and in the dendrites bind them"

Rui P. Costa and P. Jesper Sjöström

TABLE OF CONTENT

ABSTRACT

A major goal in neuroscience is to understand how changes in synaptic strength allow neurons to store information. A related question concerns the mechanisms through which neurons distinguish between relevant and non-relevant input. It is in fact a general assumption that a neuronal stimulus would have a significant impact on the surrounding network only in the case in which it will provide a depolarization, on a postsynaptic neuron, sufficient to exceed the action potential threshold. This concept is hardly applicable in brain regions such as the dentate gyrus of the hippocampus, which exhibits exceptionally sparse activity that rarely elicits action potentials in targeted CA3 pyramidal cells. It is thus unclear how weak input from the dentate granule cells, which represents a major conduit of information to the hippocampus, sustains adequate levels of synaptic plasticity for memory storage in the CA3 network. For my doctoral project, I have assessed the functional consequences of mossy fiber input to the hippocampal CA3 network, a matrix-like structure implicated in pattern completion and navigational learning.

Repetitive pairing of a synaptic response mediated by the recurrent fibers that interconnect CA3 pyramidal cells and of a subsequent subthreshold mossy fiber response induced long-term potentiation (LTP) at the CA3 recurrent synapses in rat hippocampus *in vitro*. Reversing the timing of the inputs induced long-term depression (LTD). Investigation of the mechanism underlying this form of input-timing-dependent synaptic plasticity (ITDP) revealed that the giant excitatory postsynaptic potential evoked by mossy fiber stimulation enhanced glutamatergic current at activated CA3 recurrent synapses by relieving magnesium block from NMDA receptor channels. Furthermore, the repetitive pairing protocol frequently led to the generation of localized supralinear dendritic responses, whose probability of induction correlated with the magnitude of LTP. Candidate mechanisms for active dendritic responses are sodium spikes, calcium spikes, and NMDA spikes. Experiments with pharmacological blockers allowed us to rule out a role for sodium

or calcium spikes and identified NMDA spikes as the source of the supralinear dendritic signals associated with LTP. We then designed experiments to provide evidence for a causal relationship between the generation of NMDA spikes and associative LTP. Using a combination of dendritic recording and calcium imaging we were able to show that NMDA spikes evoke regenerative branch-specific calcium transients that are critical for LTP induction. Moreover, we examined the role of back-propagating spikes and found that a burst of back-propagating action potentials, but not a single back-propagating action potential, can lead to the generation of an NMDA spike. In conclusion, our data indicate that the current textbook paradigm positing the back-propagating action potential as the ultimate effector for LTP induction is incorrect. Instead, our experiments show that NMDA spikes are necessary and sufficient to produce the critical postsynaptic depolarization required for associative LTP between hippocampal pyramidal cells and this event can be triggere both under subthreshold input (ITDP) and suprathreshold responses (STDP).

ZUSAMMENFASSUNG

Eines der Hauptziele der Neurowissenschaft ist zu verstehen, wie Unterschiede in der Synapsenstärke neuronaler Schaltkreise es erlauben Information zu speichern. In diesem Zusammenhang ist es wichtig die Mechanismen zu verstehen, durch welche Neuronen in der Lage sind zwischen wichtigen und unwichtigen synaptischen Eingängen zu unterscheiden. Es wird weitgehend angenommen, dass ein exzitatorischer synaptischer Eingang nur dann einen signifikanten Einfluss hat, wenn er zu einer Depolarisierung führt, welche ein Aktionspotential induziert. Diese Annahme trifft jedoch wahrscheinlich nicht für die Körnerzellen des Gyrus dentatus zu, deren ausserordentlich spärliche Aktivität nur selten ein Aktionspotential in den CA3 Pyramidenzellen auslöst. Daher ist es ungewiss, wie die schwachen Signale der Körnerzellen, welche den Hauptsignalweg von Informationen zum Hippocampus bilden, genügend synaptische Plastizität für die Speicherung von Gedächtnisinhalten im CA3-Netzwerk entfalten können. Für mein Dissertations-Projekt habe ich die funktionellen Auswirkungen der Aktivierung von Moosfasern, den Axonen der Körnerzellen, auf das hippocampale CA3-Netzwerk im Detail erforscht. Die Struktur des CA3-Netzwerkes ähnelt einer Matrix und dient vor allem der Komplettierung von Mustern sowie der Navigation.

Wiederholtes Paaren von synaptischen Antworten, ausgelöst durch die Stimulation von rekurrenten CA3 Fasern, gefolgt von unterschwelligen Moosfaserantworten, induzierten im Hippocampus *in vitro* eine Langzeitpotenzierung (LTP) an den rekurrenten CA3-Synapsen. Die Umkehr der Stimulationssequenz führte, hingegen, zu einer Langzeitdepression (LTD). Genauere Nachforschungen über den Mechanismus dieser zeit- und sequenzabhängigen synaptischen Plastizität (ITDP) zeigten, dass die starken exzitatorischen postsynaptischen Potentiale, welche durch die Stimulation von Moosfasern ausgelöst wurden, die Antworten an rekurrenten CA3-Synapsen durch die Aufhebung der Magnesiumblockade von NMDA-Rezeptorkanälen verstärken. Darüber hinaus hat dieses wiederholte

Paarungsprotokoll vermehrt zu der Entstehung von lokalen, supralinearen dendritischen Antworten geführt. Deren Wahrscheinlichkeit einer Entstehung korrelierte mit der Stärke der LTP. Mögliche Auslöser von aktiven, dendritischen Antworten sind Natrium-, Kalzium- oder NMDA-Spikes. Unsere Experimente mit pharmakologischen Inhibitoren ermöglichten uns Natrium- und Kalzium-Spikes auszuschliessen und NMDA-Spikes als Ursache für die supralinearen, dendritischen Signale zu identifizieren, welche mit der LTP assoziiert sind. Wir haben daher Experimente entworfen, um den Beweis für einen kausalen Zusammenhang zwischen der Entstehung von NMDA-Spikes und der assoziierten LTP zu erbringen. Durch die Kombination von dendritischen Ableitungen mit bildgebenden Verfahren zur Messung von Kalziumsignalen konnten wir zeigen, dass die NMDA-Spikes in den Dendritenästen regenerierende, Ast-spezifische Kalziumströme auslösen, welche für die Induktion von LTP essenziell sind. Zusätzlich haben wir die Rolle der Backpropagation von Aktionspotentialen untersucht. Dabei stellte sich heraus, dass kurze Salven, jedoch nicht einzelne, backpropagating Aktionspotentiale einen NMDA-Spike auslösen können.

Zusammenfassend lässt sich sagen, dass unsere Daten den aktuellen Wissensstand über Backpropagation von Aktionspotentialen als Auslöser einer LTP mindestens für das CA3 Gebiet des Hippocampus widerlegen. Mit unseren Versuchen konnten wir zeigen, dass NMDA-Spikes sowohl notwendig wie auch ausreichend sind, um die entscheidende, postsynaptische Depolarisierung auszulösen, welche für die assoziative LTP zwischen den CA3 Pyramidenzellen des Hippocampus erforderlich ist.

INTRODUCTION

INDUCTION OF SYNAPTIC PLASTICITY

Long term potentiation (LTP) of synaptic transmission is considered to represent the cellular substrate for learning and memory (Tonegawa et al., 2015). Experiments utilizing recent technical innovations such as optogenetic stimulation in conjunction with mouse lines expressing calcium indicators in specific neuronal types are providing evidence that extends beyond a simple correlation between the induction of synaptic potentiation (or depression) and the learning capability of an animal. Thus, a number of recent studies have presented data supporting a causal relationship between synaptic plasticity and memory. For example, using a pharmacosynthetic approach it was possible to express a modified neurotransmitter receptor (DREADD) only in neurons in which c-fos was upregulated in association with the encoding of a neutral contextual memory (context A). Next, the mice were subjected to fear conditioning in a different context (context B). Subsequently, the mice only exhibited freezing behavior in context B. However, if the neurons activated in context A were chemically stimulated during fear conditioning in context B, a hybrid memory was created (Garner et al. 2012). In other publications, the optogenetic approach was used to selectively stimulate a specific neuronal connection and to alter artificially the synaptic strength of that input. With this approach Nabavi et al. 2014 used a classical fear conditioning paradigm in which inputs converging in the amygdala were then optogenetically stimulated to induce LTD that inactivated or LTP that reactivated the previously induced conditioning fear.

If synaptic plasticity is the substrate of memory then an artificial alteration of certain synapses might create a false memory *de novo*. This was the question addressed in study by Ramirez et al. 2013, where optogenetic activation of a population of granule cells in the dentate gyrus of the hippocampus (known to be active during fear conditioning) was sufficient to cause the animal to freeze in a context that should not have induced such behavior.

In their original publication describing synaptic plasticity, Bliss and Lømo (1973) noted that brief tetanic stimulation (60 action potentials at 100 Hz repeated three times) at perforant path-granule cell synapses in the hippocampus was particularly effective at inducing LTP that could last for hours. This protocol to strengthen synaptic transmission was widely adopted for its ease and reproducibility and has led to numerous breakthroughs elucidating the cellular and molecular

foundations of LTP (for achievements in this field, G. Collingridge, R. Morris and T. Bliss received the Brain Prize in 2016). Major efforts during the last decades have revealed a variety of processes involved in synaptic plasticity, including transduction mechanisms initiated by activation of metabotropic receptors and endocannabinoid receptors (Blitzer, 2005). However, the most thorough characterization has been performed at the glutamatergic synapses onto pyramidal cells in hippocampus and cortex, where it is well established that LTP is triggered by the activation of NMDA receptors. The NMDA receptor is a heteromeric nonspecific cation channel comprising two NR1 subunits combined with two subunits generated by the NR2 gene family (see Fig. 1; Aizenman et al. 1989; Bloodgood and Sabatini, 2007). The main NR2 subunits are NR2A, NR2B, NR2C and NR2D and they confer different physiological and pharmacological properties to the channel. Interestingly, NR2 subunits are known to change during development. During early stages the NMDA receptors are composed mainly of NR1/NR2B subunits, whereas NR2A is mainly expressed at mature synapses (Shi et al. 1997; Sans et al. 2000; Yoshii et al. 2003).

A unique biophysical feature of this receptor is that two requirements must be met for the channel to open: first the receptor must bind glutamate (EC_{50} in the 1 μM range) to open the pore; second, strong depolarization of the postsynaptic membrane is necessary to expel magnesium ions that are blocking conduction through the channel (Mayer et al. 1984; Nowak et al. 1984). The channel is permeable to Na^+, K^+ and Ca^{2+} ions, but only 6% to 12% of the total cationic fraction is carried by Ca^{2+} (Burnashevet al., 1995; Garaschuk et al., 1996; Rogers and Dani, 1995; Schneggenburger et al., 1993).

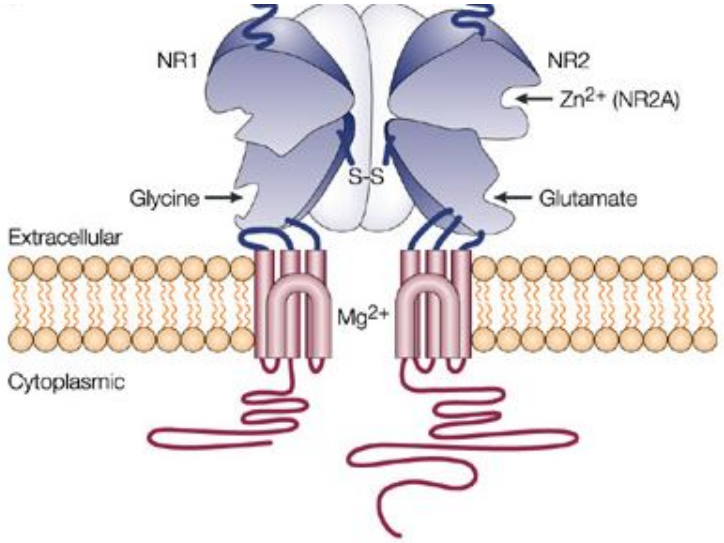

Fig.1. Scheme of the molecular structure of the NMDA channel: model of the NMDA receptor showing the binding site for the glutamate and glycine. Note also the presence of the Mg^{2+} that is blocking the pore of the channel (Witt et al. 2004).

The resulting influx of calcium into the dendritic spine initiates well-described signaling cascades that culminate with the enhanced expression of synaptic AMPA receptors in the synaptic density (Huganir & Nicoll, 2013). Calcium influx through NMDA receptors activates calmodulin which in turn activates calcium/calmodulin-dependent protein kinase II (CaMKII) that then associated with the postsynaptic density (PSD). Consequently AMPA receptor-mediated responses are enhanced as a result of phoshorylation of the GluR1 subunit at S831 that augments conductance of the channel. Furthermore, CaMKII phosphorylates the AMPAR-binding protein stargazin, which then binds to PSD95 leading to an increase in the number of AMPARs at the synapse (Lisman et al. 2012).

Although high frequency stimulation has proven to be an excellent method for investigating the basic properties of LTP, experiments with *in vivo* recordings demonstrate that such sustained high frequency neuronal discharge does not conform to the subtle and dynamic patterns of activity characteristic for hippocampal pyramidal neurons (Henze et al. 2002) or cortical pyramidal cells (Gambino et al. 2014). In an attempt to mimic more faithfully physiological conditions and to take into account the temporal parameters necessary for associative learning, novel protocols were developed in which the order and precise timing between repetitive presynaptic input and postsynaptic action potentials can either potentiate or depress synapses (Debanne et al., 1994, 1998; Markram et al., 1997; Bi & Poo, 1998). This temporally sensitive form of plasticity is referred to as spike-timing-dependent plasticity (STDP). In its simplest form, a STDP protocol consists of the pairing of a weak input, (normally an excitatory post synaptic potential (EPSP)), with a strong input, which elicits an action potential (AP). The pairing of the weak and the strong input is normally repeated 50 to 60 times at a frequency between 10 and 50 Hz. In general, if the EPSP precedes the AP, the synapse is strengthened, whereas if the AP occurs before the EPSP, the synapse becomes weaker (see Fig.2). However another form of spike timing dependent plasticity called anti-STDP with the opposite temporal dependence has been described in the electrosensory lobe of electric fish (Bell et al. 1997; Han et al. 2000), the dorsal cochlear nucleus (Tzounopoulos et al. 2004) and the cerebellum (Wang et al. 2000).

According to Hebb's cell assembly theory of neuronal learning, a synapse is potentiated when activity in the presynaptic neuron is associated in time with AP discharge in the postsynaptic neuron (Hebb, 1949). This postulate was summarized

by Shatz (1992) as: “Cells that fire together, wire together”. Experimental evidence for this statement is provided by the demonstration that synapses undergo LTP in response to STDP protocols in many different brain areas. A further major advance came with the observation that LTP is an NMDA-dependent mechanism (Collingridge et al., 1983). In the case of STDP, the fact that conduction of current by the channel requires both glutamate binding to the receptor and postsynaptic depolarization to alleviate Mg^{2+} block makes the NMDA receptor the perfect substrate for coincidence detection (Magee & Johnston, 1997).

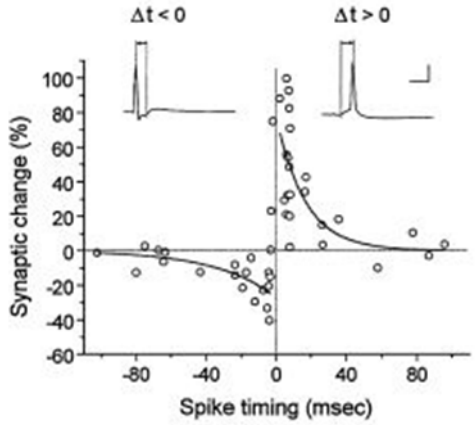

Fig.2. Spike timing dependent plasticity time windows: Percentage of variation of the EPSP amplitudes as a function of the time difference Δt = tpost – tpre between the post- and pre-synaptic spike. Induction protocol: 60 spike pairs at 1 Hz. Inset: postsynaptic action potential, relative to the time of the EPSP occurrence (vertical line). Scale bars: 10 ms, 50 mV. (Bi & Poo, 2001).

According to Hebb’s postulate, for a synapse to undergo potentiation it must obtain a feedback message relaying whether the EPSP that it generated was successful in contributing to evoking an action potential. The discovery of active dendritic back-propagation of the AP in which the action potential generated at the axon hillock is conducted not only down the axon but also retrogradely into the dendritic tree (Stuart & Sakmann, 1994), provided an ideal candidate for the synaptic feedback signal. Thus, the back-propagating AP is thought to relieve Mg^{2+} block from NMDA receptors thereby allowing calcium influx, but only if the receptor is concurrently activated by glutamate released from a presynaptic neuron.

Even though the bAP is considered an “all or none” event (digital signal), numerous processes have been demonstrated to modulate the spatial “backward” propagation of the dendritic AP into the dendritic arbor. These factors can augment or reduce the depolarization induced by the bAP in response to a specific input depending on its location. A well-described example occurs in the CA1 pyramidal cell where, under physiological conditions, the bAP normally fails to invade the distal dendritic tree so that only proximal synapses are depolarized and potentiated

(Spruston et al. 1995; Stuart et al. 1997). The spatial extent of the bAP is extremely variable among different neuronal types: in Purkinje cells for example, due to the fact that Na^+ channel density decreases rapidly with increasing distance from the soma (Lev-Ram et al. 1992; Stuart and Hausser 1994; Callaway and Ross 1997), Na^+-dependent action potentials do not actively propagate back to dendrites. In contrast, mitral cells express predominantly slow activating K^+ channels on their apical dendrites such that the amplitude of the bAP is not significantly reduced. Consequently, bAPs can invade even very distal dendrites in these cells.

At the branch-point level, local up-down regulation of Na^+ and K^+ channels can actively regulate the spatial propagation of the bAP. Additional factors affecting backpropagation include branch point failures related to structural biophysical constraints (Jaffe et al. 1992; Magee and Johnston 1997), inhibitory synaptic inputs (Tsubokawa and Ross 1996), and neuromodulatory transmitters (Hoffman and Johnston 1999; Sandler and Ross 1999).

In addition to providing a biological basis for Hebb's learning theory, STDP also conforms to the theoretically derived Bienenstock-Cooper-Munro (BCN) plasticity function (Bienenstock et al., 1982), which predicted the existence of a critical threshold of postsynaptic activity determining whether LTP or LTD is induced. CaMKII has been proposed as a molecular candidate for this threshold detection (Lisman et al., 2012), as the state of phosphorylation at its subunits depends on the calcium concentration within the synapse: high and fast transients of calcium lead to LTP, whereas prolonged low levels of calcium favor LTD (Coultrap et al., 2014).

On the basis of these findings, STDP has become a *leitmotif* for most experimentalists and modelers working in the field of synaptic plasticity (Caporale & Dan, 2008; Feldman, 2012). However, even though STDP is attractive in its elegance and simplicity as a synaptic learning rule, a number of criticisms have arisen over the past ten years (reviewed in Lisman & Spruston, 2005, 2010). The main issue lies in establishing the functional role of the back-propagating action potentials. Indeed, several observations have called into question the importance of this phenomenon in inducing synaptic plasticity. First and foremost, in experiments where a synaptically triggered back-propagating spike is pharmacologically blocked, LTP is not prevented, nor is its magnitude diminished (Gustafsson et al., 1987; Golding et al., 2002; Remy & Spruston, 2007; Hardie & Spruston, 2009). Why was this problem not noted, earlier? In the first investigations to characterize STDP, the back-propagating AP was

induced artificially by brief current injection into the postsynaptic cell, which simplified the precise timing of EPSPs and APs. However, in more recent studies where the AP was evoked by an EPSP, thus mimicking physiological conditions, LTP was not affected by blocking the back-propagating action potential, pointing to the presence of a different mechanism mediating the dendritic depolarization required to unblock NMDA receptors (Kampa et al. 2004; Kampa et al. 2007; Sjöström et al. 2008). Second, it is possible that the back-propagating action potential is a causal factor in synaptic plasticity, even if it acts indirectly by activating some other processes that initiate LTP. However, pairing an EPSP with a single back-propagating action potential has been found to be insufficient to generate LTP. The duration of a single back-propagating action potential (1–2 ms) is too short to counter the slow kinetics of Mg^{2+} unblock from NMDA channels (Spruston et al., 1995; Kampa et al., 2004), for which a high frequency burst of two to three APs is necessary to allow the integration of a signal sufficient to open NMDA channels (Sjöström et al., 2001). However, the probability that three action potentials will occur with the appropriate frequency and the precise timing relative to a preceding EPSP to induce LTP is low. In addition, the amplitude of a back-propagating AP is reduced with increasing distance from the soma because of cable filtering and can therefore fail in distal dendritic segments (Stuart & Häusser, 2001).

Taken together these findings demonstrate that in cases where LTP is induced with an STDP protocol, the back-propagating action potential alone is unlikely to generate sufficient depolarization of dendritic spines to trigger LTP. The validity of STDP as a general model of synaptic plasticity induced by back-propagating AP also becomes questionable when taking into account synapses characterized by strong input but sparse spiking activity, as is the case for hippocampal mossy fibers. If the back-propagating AP is not essential, what other events might be implicated in LTP induction? Recent work has indicated several candidates (London & Häusser, 2005; Major et al., 2013):

1) dendritic NMDA spikes
2) dendritic calcium spikes
3) AMPA receptor-mediated EPSPs

My work in the Gerber laboratory as a PhD student has demonstrated the crucial role played by dendritic NMDA spikes in LTP induction at recurrent synapses of hippocampal CA3 pyramidal cells (rCA3), which will be presented below (Brandalise & Gerber, 2014, Brandalise et al., 2016 *in revision*).

ACTIVE DENDRITIC SIGNALING

When an action potential is generated in the axon hillock of a neuron, a bAP is conducted to the dendrite tree, which under certain conditions is able to trigger a supralinear response known as a dendritic spike (dSpike). dSpikes exhibit a number of features that delineate them from bAPs. First, a dSpike is a localized regenerative event whereas a bAP can propagate throughout the dendritic tree as long as dendritic filtering does not impede regenerative depolarization. Second, dSpikes exhibit a lower activation threshold than bAPs (Grunditz et al., 2008; Harnett et al., 2012). Substantial dendritic depolarization is required to generate a signal sufficient to induce a suprathreshold response at the axon hillock. Under physiological conditions, dSpikes and bAPs often occur together; for example, summation of multiple dSpikes can generate a response sufficient to attain the threshold for triggering an action potential. With *in vitro* experiments it is, however, straightforward to investigate each event individually by selectively silencing one or the other component.

There are three main types of dSpikes and these have distinct properties (Antic et al. 2010):

1) dendritic NMDA spikes
2) dendritic calcium spikes
3) dendritic sodium spikes

The dendritic NMDA spike was described for the first time by Schiller et al. (1997; 2000). This response requires the clustered activation on a dendritic branch of at least 10 synapses (Makara &Magee 2013). Furthermore, NMDA spikes cannot be triggered by dendritic depolarization alone, as NMDA channels require both glutamate as well as depolarization to allow current flow. An NMDA spike amplifies synaptic input through ion influx conducted exclusively through NMDA channels. The

amplitude of NMDA spikes is not reduced by voltage dependent sodium channels blockers. In fact, an increased response is observed after sodium channel blockade (Brandalise & Gerber 2014; Palmer et al. 2014), which is probably due to increased membrane input resistance and improved space clamp.

The dendritic calcium spike is generated by calcium influx through both voltage-gated calcium channels as well as NMDA receptor channels as it was confermed in CA1 pyramidal cells (Golding et al. 2002) and in layer 5 pyramidal neurons (Kampa et al. 2006). Similar to NMDA spikes they have a duration of 20 to100 ms. The induction of calcium spikes is facilitated by theta burst stimulation of inputs (Stuart & Spruston 2015).

Dendritic sodium spikes are sensitive to voltage-dependent sodium channel antagonist and manifest as a fast events referred to as a spikelets with a duration of 2-5 ms (Golding and Spruston, 1998) The generation of a dendritic sodium spike greatly increases the probability of triggering an AP (Muller et al. 2012).

The type of dSpike that is evoked depends on the cell type, the dendritic compartment, the constellation and density of dendritic ion channels (Antic et al. 2010), and additionally, in the case of NMDA spikes, the appropriate activation of synaptic and extrasynaptic NMDA receptors (Chalifoux & Carter 2011). Furthermore, dSpikes often consist of multiple components (complex spikes) in which the individual dSpikes exhibit synergistic behavior (Major et al., 2013). At the time of their discovery, dSpikes were thought to occur only in the very thin dendrites of cortical neurons. Subsequent studies have, however, shown that they can be evoked throughout the dendritic tree in many different neuronal types and are likely to be present in the majority of the spiny neurons (Oikonomou et al. 2014).

Even though dSpikes were discovered more than a decade ago, their roles and physiological relevance remain poorly understood. Only recently has a series of studies begun to elucidate the fundamental roles of dSpikes in dendritic computation and induction of plasticity (see Table 1).

A comprehensive characterization of dSpike function will be essential for clarifying the integrative capabilities of neurons and for the development of more realistic computational models. Recent investigations in vivo have demonstrated that dSpikes compute a threshold for local integration of inputs within individual dendritic segments, which is important for processing sensory input in cortical pyramidal cells (Smith et al., 2013; Gambino et al., 2014; Palmer et al., 2014), for triggering burst

discharge in CA1 pyramidal cells when multiple NMDA spikes occur (Grienberger et al., 2014), and for the representation of space by place cells in the CA1 area (Sheffield & Dombeck, 2015).

Table 1

Role of NMDA spike in the brain	**Brain location**	**References**
LTP induction	Layer 5 pyramidal neurons in motor cortex	Chicon & Gan, 2015
	CA3 pyramidal cells	Brandalise & Gerber, 2014
	CA1 pyramidal cells	Sheffield & Dombek, 2015
		Kim et al., 2015; Basu et al., 2016
	Layer 2/3 pyramidal neurons in somatosensory cortex	Gambino et al., 2014
UP/DOWN state regulation	Thalamocortical neurons	Augustinaite et al., 2014
	Spiny striatal neurons	Oikonomou et al., 2014
Input/output bistability	Layer 2/3 pyramidal neurons in somatosensory cortex	Palmer et al., 2014
	CA3 pyramidal cells	Makara & Magee, 2013
	Layer 2/3 pyramidal neurons in primary visual cortex	Smith et al., 2013

The impact of dSpikes is strongly modulated by the activity of inhibitory interneurons. Interneurons preferentially targeting the soma regulate action potential output, whereas dendritic inhibition can both shunt the passive summation of excitatory inputs as well as modulate dSpike threshold and duration (Tsubokawa & Ross 1996; Larkum et al. 1999; Lovett-Barron et al. 2012), thereby controlling the communication between the dendritic and the somatic compartment (Markram et al.

2004; Muller et al. 2012; Muller et al. 2014: Basu et al. 2016; Dombeck et al. personal comm.).

As then induction of dSpikes requires clustered input onto a dendritic segment, their observation in diverse cortical neurons challenges the assumption that these neurons receive sparse distributed inputs (Jia et al. 2010; Varga et al. 2011). However, recent work has provided evidence for clustered input in the visual system (Bollmann & Engert, 2009 in the fish larvae; Wilson et al. 2016 in ferrets) and in cortical and hippocampal pyramidal cells, where synaptic plasticity during development results in compartmentalization of correlated inputs onto single dendritic segments with preferential targeting of neighboring spines (Kleindienst et al., 2011; Makino & Malinow, 2011; Takahashi et al., 2012).

DENDRITIC SPIKES IN CA3 PYRAMIDAL CELLS

In our laboratory we are investigating synaptic signaling in CA3 pyramidal cells (Fig.3) in which dSpikes have only recently been shown to contribute to dendritic processing.

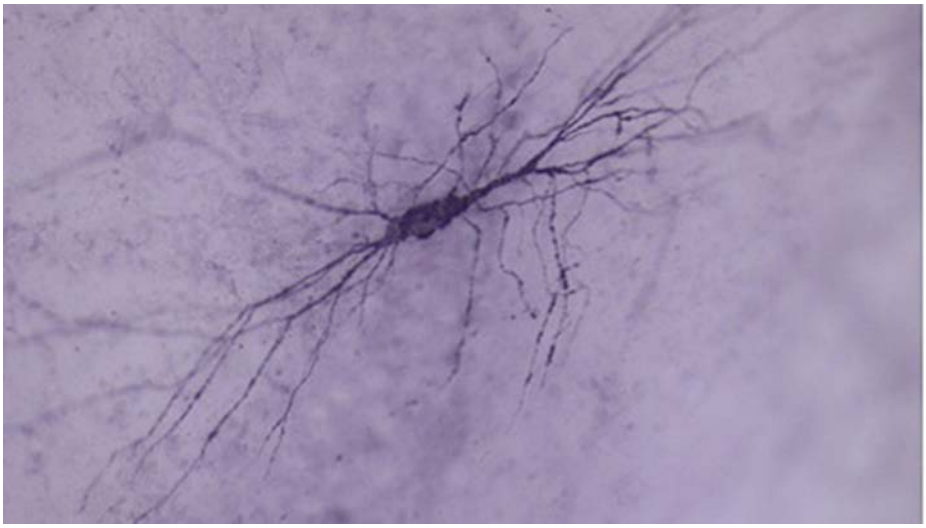

Fig.3. A biocytin labelled CA3 pyramidal cell from organotypic slice cultures.

CA3 pyramidal cells are unique with respect to their connectivity and synaptic features (Fig.4). They receive three different types of excitatory inputs that are segregated within distinct portions of the dendritic tree.

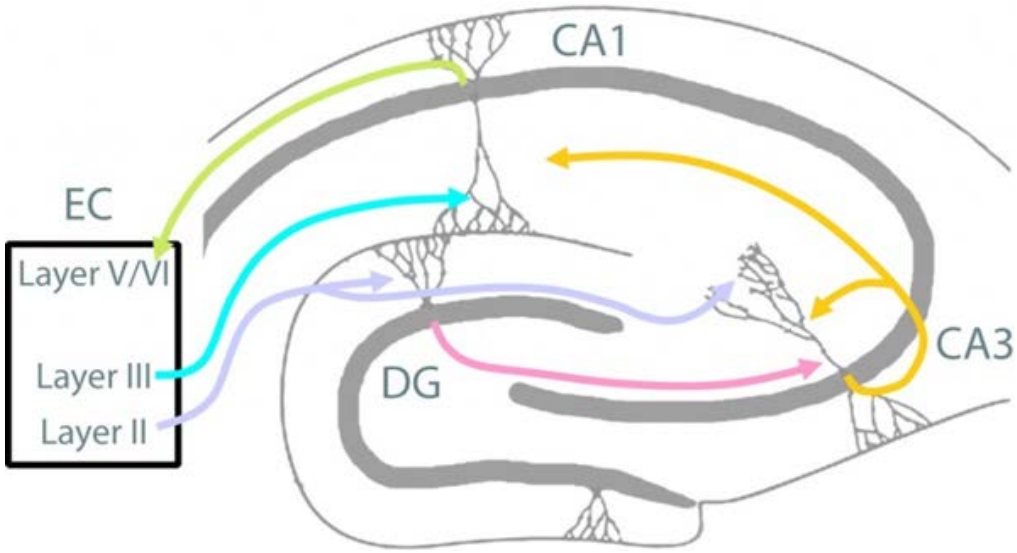

Fig.4. An illustration of the hippocampal circuitry. Diagram of the hippocampal neural network. Excitatory connections are labelled in different colours. EC: enthorinal cortex; DG: dentate gyrus. The axons of layer II neurons in the entorhinal cortex send afferents to the dentate gyrus through the perforant pathway (PP). The dentate gyrus contacts the pyramidal cells in CA3 through mossy fibres. CA3 pyramidal neurons axons excite other CA3 pyramidal cells (recurrent syanpses) and the CA1 pyramidal neurons through Schaffer collaterals. CA1 pyramidal neurons send back-projections into deep-layer neurons of the EC. CA3 is also excited by projections from EC layer II neurons through the PP. CA1 receives on the distal part of its dendrites direct inputs from EC layer III neurons through the temporoammonic pathway (Layer III EC).

The proximal region of both the apical and basal dendrites receives input from about 50 mossy fibers, whose giant terminals can contain upto 40 active zones for a total of ~2000 release sites (Urban et al., 2001). These inputs have been referred to as detonators as a single mossy fiber input can depolarize a CA3 pyramidal cell by over 10 mV. Despite this huge effect on the post-synaptic neuron, experiments in vivo have shown that even bursts of activity in granule cells have a relatively low probability (~30%) of evoking action potentials in a targeted CA3 (Henze et al., 2002). Because of extremely sparse activity levels in the dentate gyrus, the probability that a given CA3 pyramidal cell will receive concurrent input from more than one mossy fiber is close to zero (Lisman 1997; de Almeida et al. 2009). Furthermore, mossy fiber activation induces strong feedforward inhibition (Mori et al. 2007) that curtails temporal summation of repetitively activated inputs. It is thus unlikely that the action potential is the preferred instructional signal at the mossy fiber synapse onto a CA3 pyramidal cell. Can the giant EPSPs generated by mossy fibers

compensate for the low incidence of action potentials evoked in the postsynaptic CA3 pyramidal neuron? This is one of the hypotheses that I have tested during my PhD project.

The intermediate domain of the apical and distal dendritic arbor of a CA3 pyramidal cell receives excitatory input through the recurrent collaterals from neighboring CA3 pyramidal cells (Fig. 5). Compared to mossy fiber inputs, recurrent synapses evoke relatively weak responses of 0.5-1.5 mV (Henze et al. 2000) but with a much higher frequency and higher NMDA/AMPA receptor ratio (Debanne et al. 1998; Min et al. 1998; Takumi et al. 1999). Each CA3 pyramidal cell is targeted by approximately 12,000 recurrent synapses, which results in a matrix-like neuronal network making this hippocampal subfield ideal for memory formation (Marr, 1991; McNaughton & Morris, 1987; Lisman, 1999) and pattern completion (Nakazawa et al., 2002).

The distal apical dendrites receive excitatory input from the grid cells in the entorhinal cortex via the perforant path (Nakazawa et al. 2002; Witter et al. 2006).

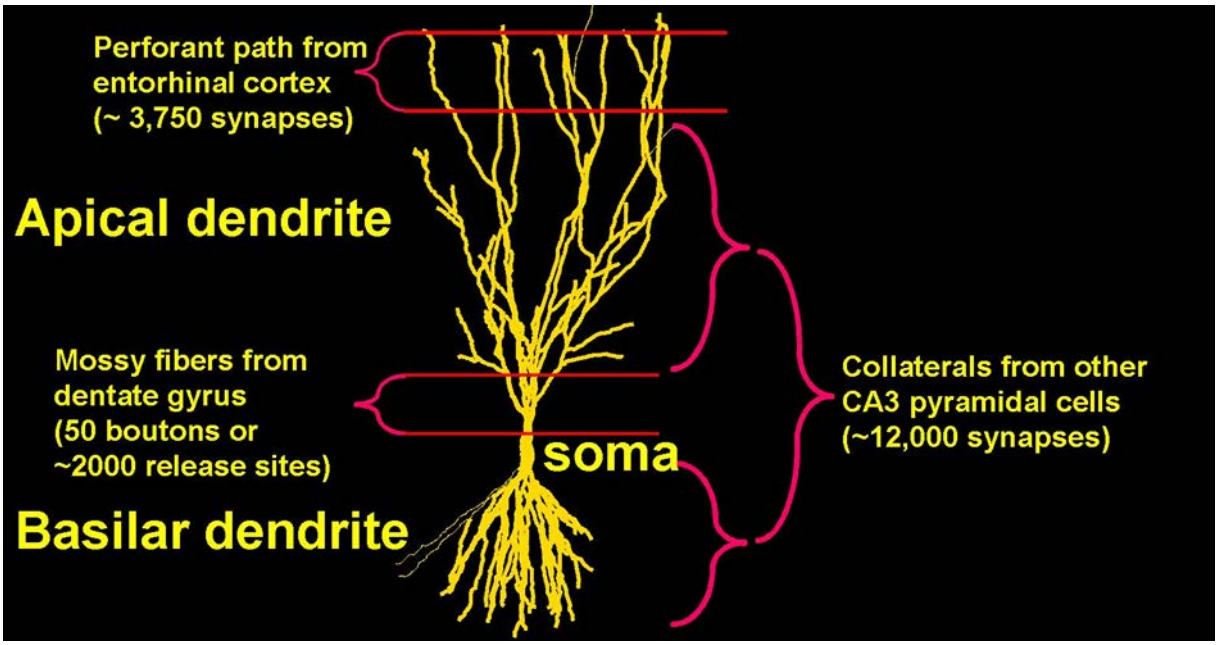

Fig.5. Input organization on CA3 pyramidal cell dendritic tree (Ishizuka et al. 1995)

The principles of dendritic integration in CA3 pyramidal cells is based solely on in vitro evidence because these neurons are too deep in the brain for conventional in vivo imaging and are difficult to maintain in acute slices because of the almost unavoidable damage caused by lesioning of dendrites during slice preparation (Gibb & Edwards, 1994), a problem that is avoided with slice cultures. The first study to

examine how dendritic inputs are integrated in CA3 pyramidal cells focused on the effects mediated by perforant path synapses on the very distal dendrites (~400 µm from the soma; Kim et al., 2012). These experiments show that bAPs cause negligible depolarization of distal dendrites, whereas dendritic sodium spikes are elicited with a low threshold in this compartment reflecting a high ratio of sodium to potassium channels. As the dendritic responses were evoked by current injection into the dendrite, glutamate was not released, and it was thus not possible to test for the presence of NMDA spikes. A more recent investigation has addressed mechanisms of dendritic integration in the intermediate portion of the dendritic tree expressing CA3 recurrent synapses (Makara & Magee, 2013). In this domain the synchronous activation of 15 synapses in a dendritic branch by two-photon glutamate uncaging resulted in pronounced supralinear integration of responses mediated by NMDA spikes. Interestingly, two types of NMDA spikes were observed with either fast or slow decay kinetics. Further analysis revealed that the fast decay kinetics resulted from the activation of voltage-gated potassium channels, $GABA_B$ receptor-gated channels, and HCN1 (hyperpolarization-activated cyclic nucleotide-gated) channels. By controlling decay time, these channels regulate the duration of the depolarizing window mediated by dSpikes, which may be critical in determining the UP state of the neuron. It remains to be investigated whether such modulation of dSpike decay also affects the induction of NMDA spike-mediated LTP.

NMDA spikes can also be evoked when glutamate uncaging is dispersed over long dendritic segments (50-80 µm), which is not consistent with the clustered synaptic input described for the dendrites of CA3 pyramidal cells (Kleindienst et al. 2011; Takahashi et al. 2012). It must be pointed out, however, that this finding may be due to the fact that glutamate uncaging preferentially stimulates extrasynaptic NMDA receptors, which are known to facilitate the induction of NMDA spikes (Chalifoux & Carter, 2011), whereas synaptic activation generally leads to limited spillover of glutamate and hence minor recruitment of extrasynaptic NMDA receptors. In previous studies in the CA3 area (Kim et al. 2012 and Makara & Magee, 2013), no evidence for a contribution of calcium spikes to the investigated responses was observed. In our experiments, however, calcium spikes in CA3 pyramidal cells could be readily evoked by increasing the intensity of the extracellular stimulation of synaptic afferents by 30% above that required to induce NMDA spikes (Brandalise & Gerber, 2014).

NMDA SPIKES AND LTP

Dendritic sodium spikes, calcium spikes and NMDA spikes have all been implicated in the induction of LTP (Kim et al. 2015, Golding et al. 2002; Brandalise & Gerber 2014). Among these, the NMDA spike is an especially attractive candidate for synaptic plasticity because it is the only spike that requires both glutamate binding to the NMDA receptors and sufficient depolarization to remove magnesium that blocks channel conduction at resting potential. Why does glutamate binding and magnesium unblock make it an attractive candidate? As the NMDA receptor channel is permeable to calcium, in addition to sodium and potassium, it is particularly effective at activating Ca^{2+}/calmodulin-dependent protein kinase II (CaMKII), which is highly concentrated in the synaptic density and whose activation is a key step in initiating LTP (Lisman et al., 2012). Furthermore, the duration of membrane depolarization is the critical parameter for removal of magnesium from NMDA receptors (Kampa et al., 2004), making the NMDA spike, which lasts 20 to 100 ms, a more reliable trigger of plasticity than the shorter-duration bAP. The NMDA spike is also the only dSpike that requires the activation of clustered inputs to be evoked. This requirement may act as a filter to impede input patterns that do not possess a specific spatial structure representing meaningful content, thereby minimizing indiscriminate synaptic plasticity. Thus, the NMDA spike appears to be an ideal candidate to initiate LTP. Nevertheless, there is currently little direct evidence for its role in synaptic plasticity.

dSpikes sufficient to induce LTP were first described in CA pyramidal cells where they were identified as calcium spikes (Golding et al., 2002). The authors concluded that NMDA receptor activation also contributed to this phenomenon as LTP was reduced when these receptors were blocked. The first demonstration that NMDA spikes can trigger LTP came from an investigation in pyramidal cells of the somatosensory cortex, but this effect was only observed with concomitant application of BDNF (Gordon et al., 2006). Only recently have studies from our laboratory (Brandalise & Gerber, 2014) and from the Holtmaat group (Gambino et al., 2014) shown that NMDA spikes alone, under conditions where back-propagating APs were prevented, could induce LTP. In both of these studies, however, the evidence is correlative and a causal link between NMDA spikes and LTP remains to be provided.

In our first study we found that a subthreshold signal evoked in a CA3 pyramidal cell by mossy fiber stimulation can act as a cooperative excitatory input to

generate an NMDA spike that initiates the induction of synaptic plasticity at recurrent CA3 synapses (Brandalise & Gerber, 2014) [paper #1]. However, it is unclear whether the NMDA spike is the ultimate effector in timing-dependent plasticity, as previously suggested (Lisman & Spruston, 2005) or whether it represents a mechanism distinct from other forms of associative plasticity as, for example, spike timing dependent plasticity (STDP). Therefore, in a second investigation (Brandalise et al., 2016, *under revision*) [paper #2], we performed a series of experiments where we used several approaches to modulate the probability of inducing NMDA spikes so as to establish a *causal relationship* between the occurrence of NMDA spikes and the induction of plasticity at recurrent CA3 synapses. With these experiments we show for the first time that dendritic NMDA spikes are necessary and sufficient for the initiation of LTP in CA3 pyramidal cells. This mechanism may prove to be of importance at a diversity of synapses, considering that NMDA spikes have now been described in several other brain areas.

BRANCH-SPECIFIC LTP AND HOMEOSTATIC PLASTICITY

As discussed above, dendrites can generate branch-restricted spikes that initiate local induction of LTP at stimulated synapses confined to a single dendritic segment. However, dendrites also participate in more global and, widely-distributed adaptations to activity. A prominent example of such a role is in homeostatic plasticity (HP) where a neuron's output can be equilibrated by altering synaptic gain control (Murthy et al. 2001; Burrone et al. 2002; Thiagarajan et al. 2005), synaptic release probability (Turrigiano et al. 1999; Wierenga et al. 2005) and ion channel conductance (Franklin et al. 1992; Turrigiano et al. 1994; Desai et al. 1999). During my PhD, in collaboration with Prof Rodney Douglas (Soldado-Magraner, Brandalise et al. 2016, *in preparation*), we have addressed this question by characterizing a novel form of HP in CA3 neurons. We investigated the discharge patterns of neurons in response to constant current injection before and after a conditioning phase of prolonged paired-pulse stimulation at low frequency (1 Hz) of mossy fibers. Briefly, we demonstrated that this conditioning protocol changes the firing pattern of the recorded neuron from tonic discharge to a burst spiking form of activity [paper #3]. We found that this result can be explained by input-dependent recruitment of D-type and M-type potassium ion channels. Interestingly this effect was observed even

though the selected stimulation protocol induced only subthreshold depolarizing responses in the postsynaptic neuron. This finding thus provides a further example of a process in which subthreshold EPSPs can compensate for the extreme sparseness of suprathreshold signals resulting from mossy fiber input.

How would this novel form of HP affect the induction of NMDA spikes in the CA3 pyramidal cell? We predict that the transition to a more robust firing pattern occurring during bursting would favor the generation of NMDA spikes in the intermediate part of the CA3 pyramidal cell arbor by prolonging the time window of NMDA channel activation at stimulated synapses. Moreover, the increased release of neurotransmitter evoked by a burst of APs favors the activation of extrasynaptic NMDA receptors thereby promoting the induction of NMDA spikes (see Brandalise et al. 2016). HP may also modulate the induction of branch-specific NMDA spikes through locally delimited mechanisms that can compensate for regional variations in synaptic activity and in dendritic calcium concentration. Detailed studies in CA1 pyramidal cells have revealed restricted up/down regulation of I_h channels in the vicinity of stimulated synapses that counterbalance previously induced plasticity triggered either by theta burst stimulation (for LTP) or spike timing dependent depression (for LTD) (Fan et al. 2005; Brager & Johnston, 2007).

In a preliminary set of experiments, we observed that prolonged generation of NMDA spikes induced by doubling the duration of our ITP protocol led to an upregulation of calcium-dependent potassium current (mediated by putative SK channels) that reduced the spatial extent of dendritic calcium transients (see Fig.2 in the GENERAL DISCUSSION section).

Taken together, these findings reveal the complexity of dendritic properties, which provide the functional substrate for their operations as nonlinear input-output devices. The next challenge will be to quantify the contribution of individual dendritic nonlinearities to the functional capability of entire neuronal networks. Further insights into the mechanisms underlying these interactions can be guided by a framework based on modeling. I hope that the results obtained during my thesis project will provide a basis for further progress in this field.

RESULTS

MOSSY FIBER-EVOKED SUBTHRESHOLD RESPONSES INDUCE TIMING-DEPENDENT PLASTICITY AT HIPPOCAMPAL CA3 RECURRENT SYNAPSES

Federico Brandalise and Urs Gerber

PNAS; March 18, 2014
vol. 111, no. 11, 4303–4308

Contribution to this study: F. Brandalise designed the study together with U.G., performed the experiments, analyzed the data, wrote the paper with U.G.

SUMMARY

Dentate granule cells exhibit exceptionally low levels of activity and rarely elicit action potentials in targeted CA3 pyramidal cells. It is thus unclear how such weak input from the granule cells sustains adequate levels of synaptic plasticity in the targeted CA3 network. We report that subthreshold potentials evoked by mossy fibers are sufficient to induce synaptic plasticity between CA3 pyramidal cells, thereby complementing the sparse action potential discharge. Repetitive pairing of a CA3-CA3 recurrent synaptic response with a subsequent subthreshold mossy fiber response induced long-term potentiation at CA3 recurrent synapses in rat hippocampus in vitro. Reversing the timing of the inputs induced long-term depression. The underlying mechanism depends on a passively conducted giant excitatory postsynaptic potential evoked by a mossy fiber that enhances NMDA receptor-mediated current at active CA3 recurrent synapses by relieving magnesium block. The resulting NMDA spike generates a supralinear depolarization that contributes to synaptic plasticity in hippocampal neuronal ensembles implicated in memory.

INTRODUCTION

The CA3 area of the hippocampus exhibits a distinctive, highly recurrent circuitry proposed to support auto-associative memory representation (1, 2). This prediction has been confirmed by experimental work demonstrating the pattern completion capabilities of CA3 networks (3), as well as their roles in the spatial tuning of CA1 pyramidal cells, in one trial contextual learning (4) and in certain forms of memory consolidation (5). CA3 pyramidal cells receive, via the mossy fibers, information processed by granule cells important for both pattern separation (6, 7) and pattern completion functions (7). The faithful transmission of mossy fiber input appears to be ensured by giant synapses composed of presynaptic boutons with up to 45 release sites (8) that target massive spines, the thorny excrescences, on the apical dendrite of CA3 pyramidal cells. Thus, the mossy fiber synapse is often referred to as a detonator synapse (9). In fact, mossy fiber signaling is more compatible with a gatekeeper function than a high-throughput data relay. Although high-frequency

bursts of action potentials in a hippocampal granule cell can discharge a targeted CA3 pyramidal cell, the majority of responses evoked by granule cells in CA3 pyramidal cells do not attain the firing threshold (10). Nevertheless, mossy fibers generate powerful signals evoking subthreshold responses that are much larger than typical synaptic events in the brain, with excitatory postsynaptic potentials (EPSPs) and excitatory postsynaptic currents (EPSCs) reaching amplitudes of 10 mV and 1 nA, respectively (11). Here we examined in rat slice cultures how EPSPs generated at mossy fiber synapses are processed in CA3 pyramidal cell dendrites, and evaluated whether subthreshold synaptic responses evoked by mossy fiber stimulation can act as instructive signals to induce plasticity at the pyramidal cell synapses forming the CA3 recurrent network.

RESULTS

We recorded evoked synaptic responses in single CA3 pyramidal cells voltage-clamped at −70 mV in which $GABA_A$ receptor-mediated responses were reduced with intracellular picrotoxin (1 mM). During pairing protocols, to induce synaptic plasticity, recordings were performed in current-clamp mode at resting potential (−64.4 ± 3.8 mV; n = 18). One stimulating electrode was positioned in the CA3 stratum radiatum to stimulate recurrent afferents, and the other was placed in the dentate gyrus to activate mossy fibers (Fig. S1 A), which form synapses on the trunk of the apical dendrite of CA3 pyramidal cells (12). The identity of the stimulated fiber tracts was ascertained using standard criteria (Fig. S1).

We studied synaptic plasticity at CA3 recurrent inputs. Plasticity was induced by pairing an evoked CA3 recurrent EPSP with a mossy fiber EPSP that followed with a delay of 10 ms, repeated 60 times at 0.1 Hz (Fig. 1A), comparable to standard spike timing-dependent plasticity (STDP) protocols (13). We chose this low frequency of stimulation because we were interested in studying plasticity solely at CA3 recurrent synapses, and thus avoided frequency facilitation and long-term potentiation (LTP) of mossy fiber-evoked responses (−6.9 ± 5.4%; n = 18; P = 0.32) (14). Furthermore, high-frequency mossy fiber stimulation evokes synaptic release of zinc (15), which can depress heterosynaptic potentiation at CA3 recurrent inputs (16).

CA3 recurrent synaptic EPSPs were enhanced during the pairing protocol (by 179 ± 93%; n = 18; P < 0.001) (Fig. 1B and Fig. S2 A and B), whereas mossy fiber-evoked EPSPs remained unchanged.

Action potentials were never observed at the stimulation intensities used (Figs. S2–S4). The potentiation of EPSCs at CA3 recurrent synapses persisted for more than 1 h, corresponding to LTP (54.4 ± 4.8%; n = 18 of 21; P < 0.001; 3 of 21 cells did not exhibit plasticity) (Fig. 1C). A subsequent STDP protocol did not lead to any further significant enhancement of LTP (65.9 ± 8.7%; n = 3; P = 0.14).

If the timing of the inputs was reversed such that the delay between the evoked CA3 recurrent EPSP and the subthreshold mossy fiber EPSP was −35 ms, then long-term depression (LTD) was induced (reduction of 42.9 ± 8.5%; n = 5; P < 0.001) (Fig. 1D). When the pairing latency was zero or increased to +40 ms, no significant plasticity at the CA3–CA3 recurrent synapse was obtained (0 ms: 1.9 ± 9.4%; n = 4; P = 0.12; +40 ms: −5.5 ± 8.8%; n = 3; P = 0.18) (Fig. 1E). Blocking sodium channels with intracellularly applied QX-314 (17) did not significantly change the magnitude of LTP (65.7 ± 10.4%; n = 3; P = 0.18), confirming that action potentials are not required for this form of plasticity (Fig. 1F). Significant LTP was induced even when $GABA_A$ receptors were not blocked (Fig. S2 E and F). Furthermore, EPSP-dependent LTP exhibited input specificity (Fig. S3).

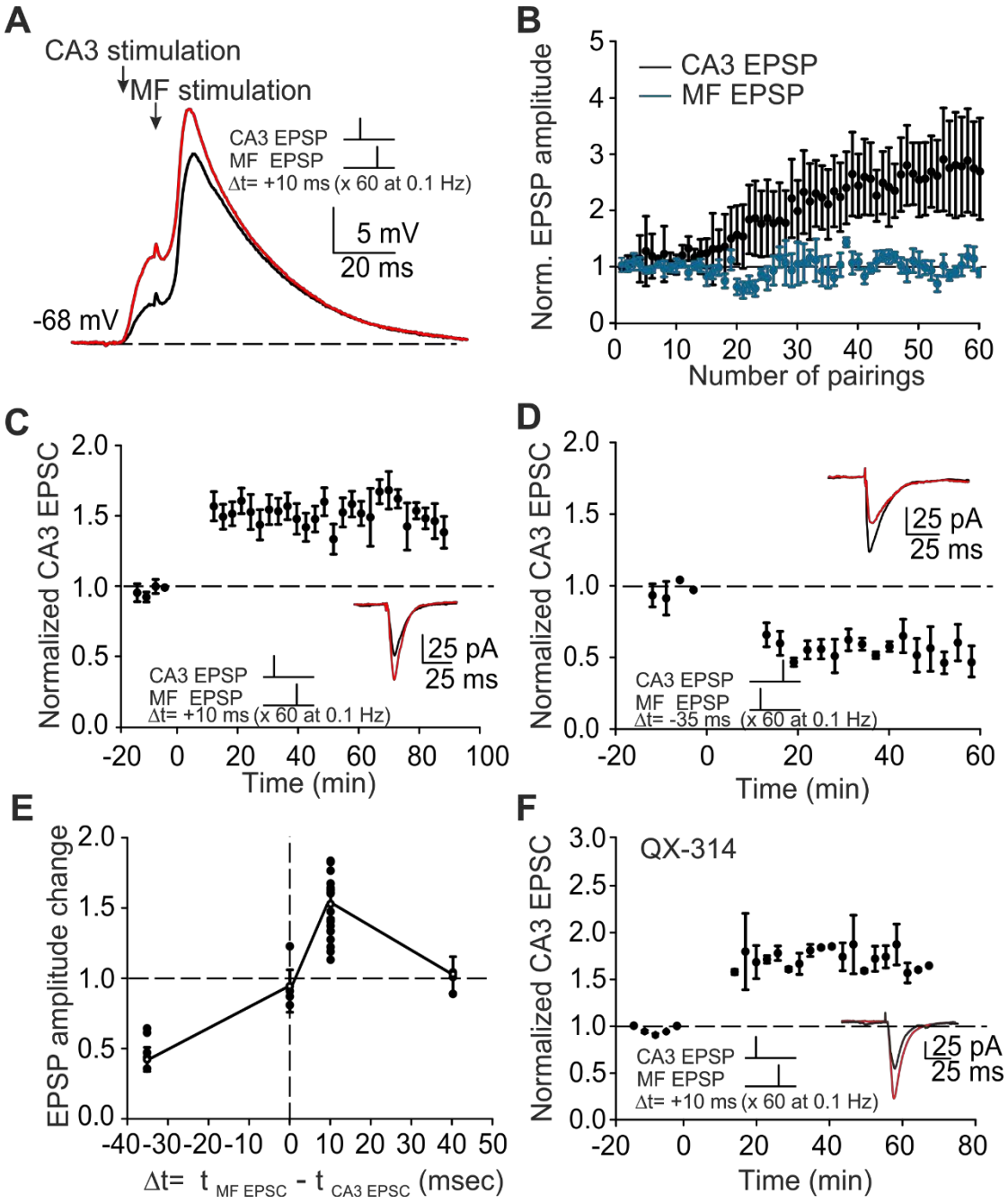

Fig. 1. Pairing of subthreshold CA3 and mossy fiber responses induces plasticity at CA3 recurrent synapses. (A) Subthreshold pairing protocol for LTP induction in a CA3 pyramidal cell at resting potential, in which activation of a CA3 recurrent input is followed after 10 ms by activation of a mossy fiber input. Shown are the first (black) and last 10 averaged traces (red) of the 60 pairings. (B) Time course of responses during the pairing protocol in current-clamp mode. Mossy fiber-evoked EPSPs did not exhibit facilitation at the stimulation frequency of 0.1 Hz, whereas CA3 recurrent-evoked EPSPs were potentiated. (C) LTP induced at CA3 recurrent synapses in cells voltage-clamped at −70 mV, before and after the 10-min pairing protocol in current-clamp mode applied at time 0. Data points are values averaged over 3 min. Example traces show averaged EPSCs before (black) and after (red) repetitive pairing. (D) LTD was induced when the timing of the pairingwas reversed such that the stimulation of the mossy fiber input preceded stimulation of the CA3 recurrent input by 35 ms. (E) Summary data for timing intervals of −35, 0, +10, and +40 ms. (F) Blocking sodium channels with QX- 314 (500 μM) did not reduce heterosynaptic LTP.

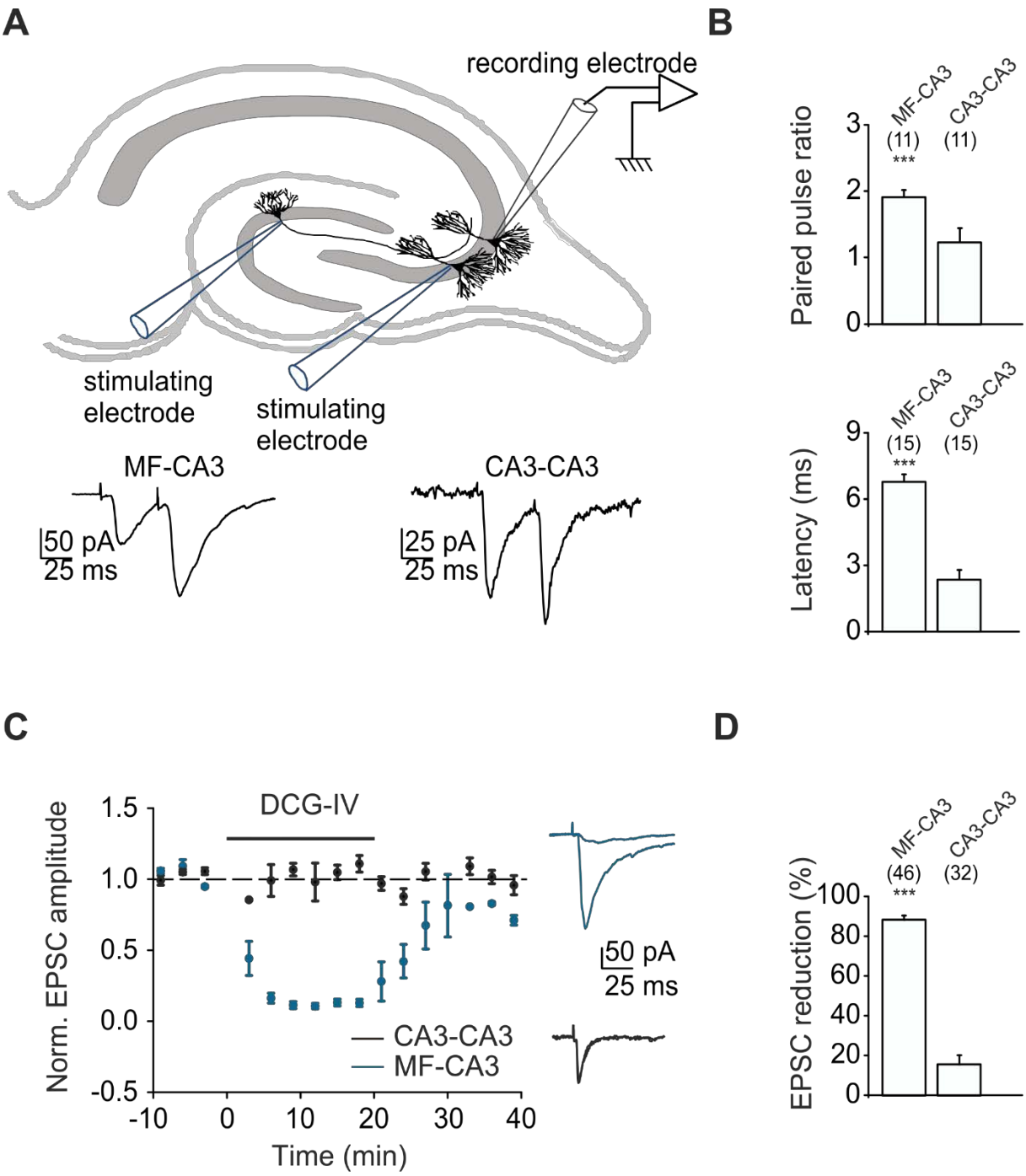

Fig. S1. Criteria for differentiating between synaptic responses evoked by mossy fibers and CA3 recurrent fibers. (A) Schematic of recording configuration. (Insets) Representative current traces evoked by paired-pulse stimulation with a 50-ms interval. (B) Pooled data. Mossy fiber stimulation always resulted in paired-pulse facilitation (1.96 ± 0.3; $P < 0.001$), whereas CA3 recurrent fiber stimulation induced either paired-pulse facilitation or depression (1.2 ± 0.2; $P = 0.15$) (64). In addition, the latency of evoked responses is longer when stimulating mossy fibers (6.8 ± 0.3 ms; $P < 0.001$) (65) versus CA3 recurrent fibers (2.3 ± 0.4 ms; $P < 0.001$) (66). (C) DCG-IV (2 μM), an mGlu2 agonist that blocks glutamate release from mossy fiber but not CA3 pyramidal cell terminals (67), reduced mossy fiber responses by 88.2 ± 2.1% ($P < 0.001$) and CA3 responses by 14.6 ± 5% ($P > 0.74$). (D) Pooled data for DCG-IV experiments.

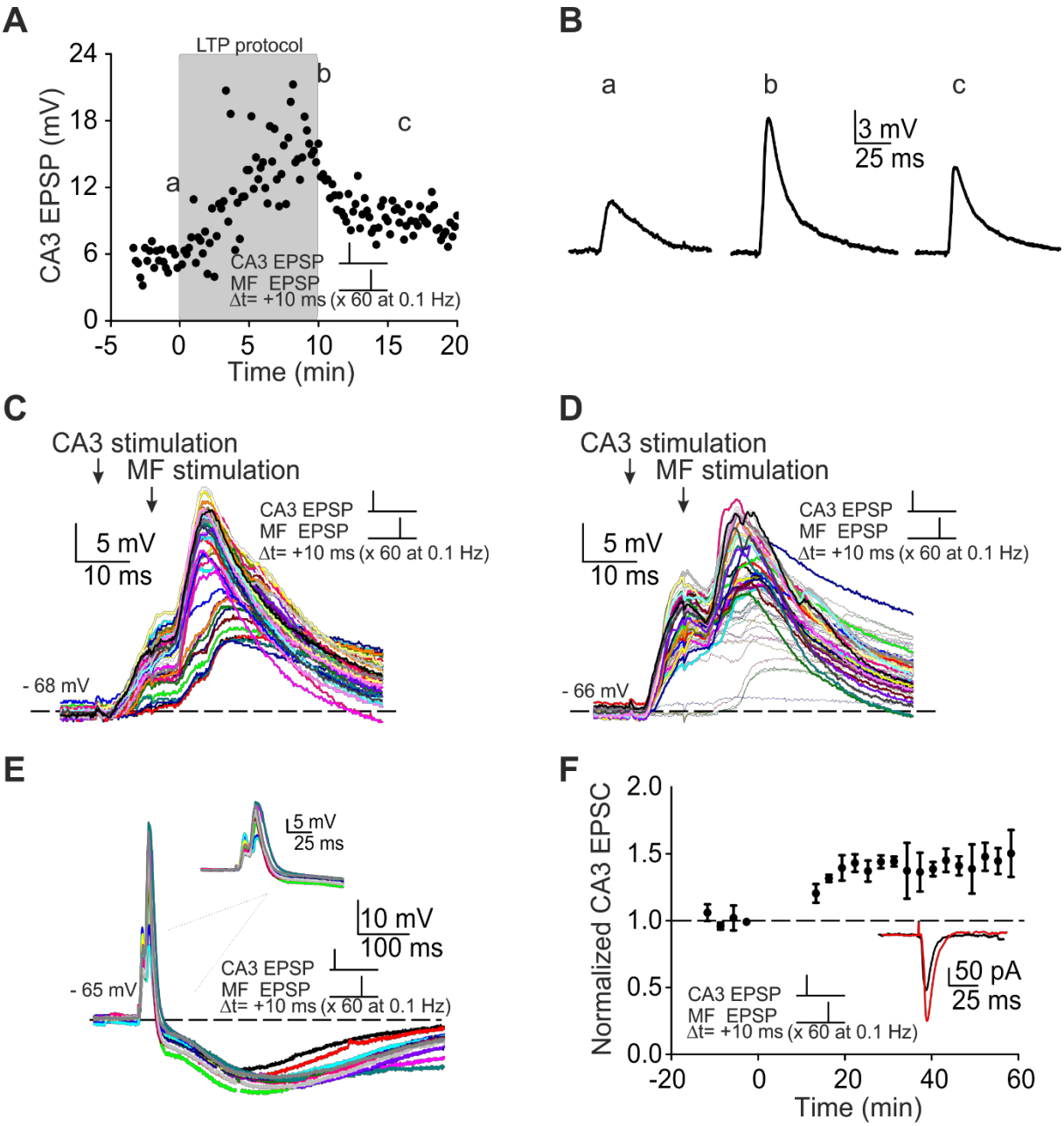

Fig. S2. Characterization of excitatory postsynaptic potential (EPSP)-dependent long-term potentiation (LTP). (A) Data from a representative cell with a resting potential of −65 mV showing the time course of potentiation both during and after the pairing protocol in an experiment in which the entire

recording was performed in current-clamp mode. (B) Traces from time points indicated in A. (C and D) Action potentials were never observed during the pairing protocol. (E) Mossy fiber EPSP-dependent LTP is maintained with intact $GABA_A$ receptor-mediated inhibition. In the absence of $GABA_A$-receptor antagonists, EPSPs recorded during the pairing protocol are followed by IPSPs. (F) Pooled data for LTP with $GABA_A$ receptor-mediated inhibition intact (35.8 ± 9.8%; n = 6; P < 0.001).

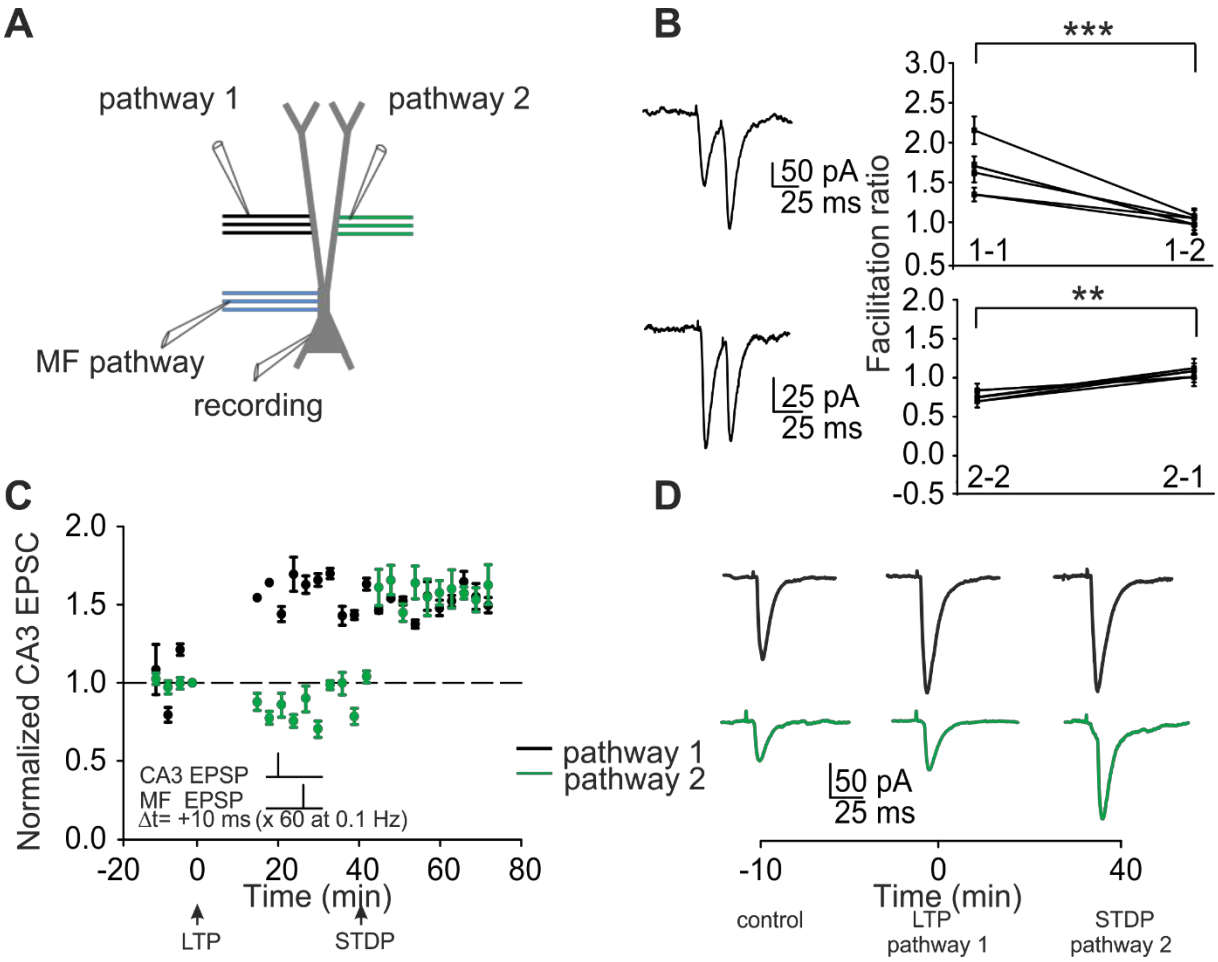

Fig. S3. (A) Experimental configuration to examine whether LTP is input-specific. (B) Pathway independence was determined for two extracellularly stimulated CA3 inputs by selecting one pathway that was facilitating (1.9 ± 0.4; n = 4; P < 0.001) and one pathway that was depressing (0.8 ± 0.03; n = 4; P < 0.01). After determining the paired-pulse ratio for pathways 1 and 2, the absence of paired-pulse modulation in the cross-pathway configuration establishes independence of the two pathways (1.1 ± 0.09; n = 4) (68). (C) The subthreshold pairing protocol applied at time 0 induced LTP in the paired (black) pathway (54.2 ± 9.8%; n = 4; P < 0.001), but not in the unpaired (green) pathway (−14.7% ± 8.5%; n = 4; P < 0.03). To rule out dysfunction in the unpotentiated pathway, a standard spike-timing-dependent plasticity protocol applied at time 40 min showed that the unpotentiated input underwent LTP (58 ± 6.2%; n = 4; P < 0.001), whereas the previously potentiated pathway was not further potentiated (−3.6 ± 7.7%; n = 4; P = 0.5). (D) Representative traces from the experiment shown in C.

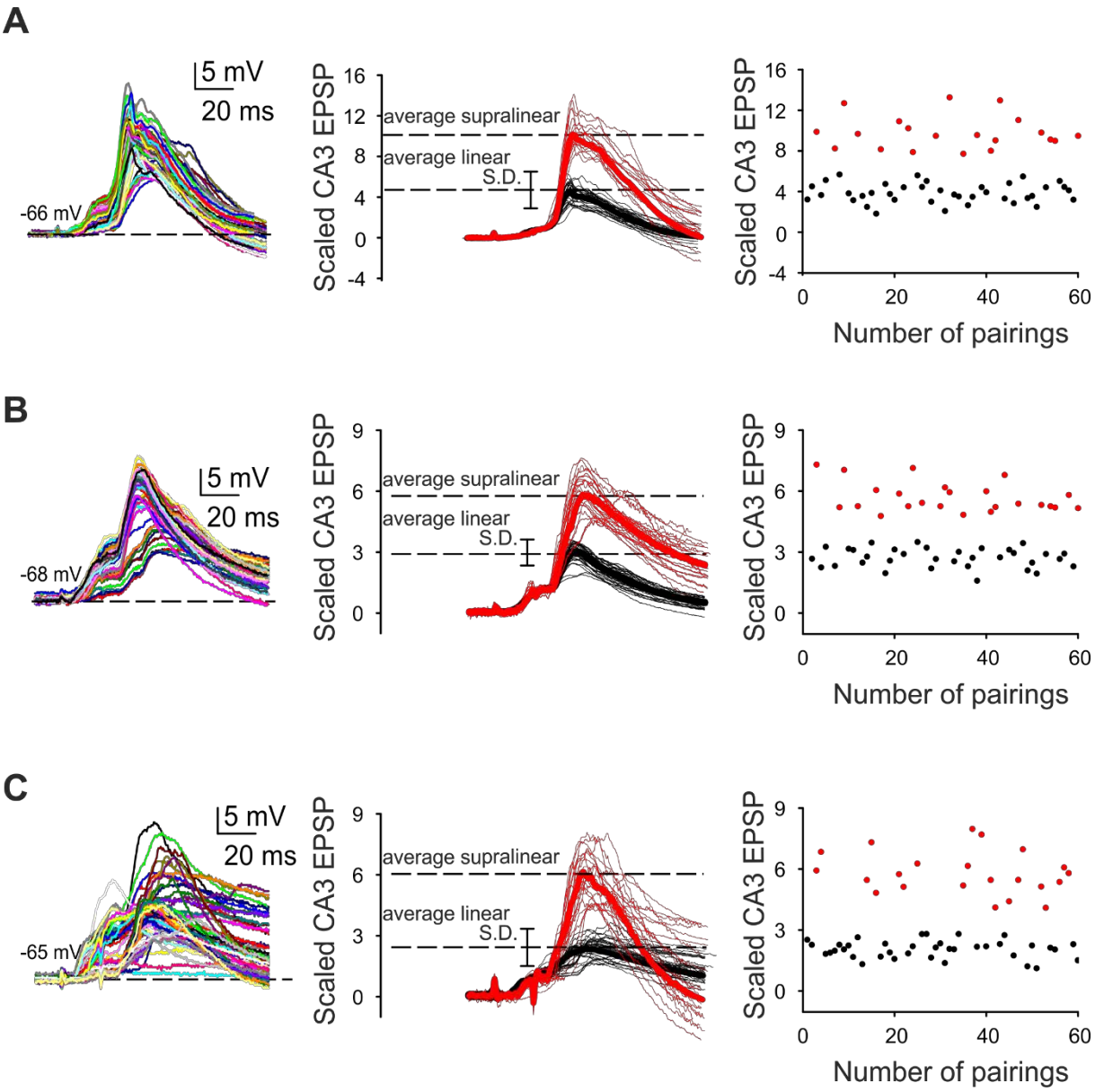

Fig. S4. (A–C) Examples of data from three cells. The left column depicts all 60 traces during pairing, demonstrating that action potentials are not elicited during the LTP protocol. The middle and right columns show that scaling responses to the amplitude of the evoked CA3 recurrent EPSP segregates the summed events into linear and supralinear responses.

Synaptic plasticity at CA3 recurrent synapses is NMDA receptor dependent (18–20), as is associative plasticity at CA3 recurrent synapses induced by mossy fiber-evoked spiking (21, 22). Thus, we tested whether EPSP-dependent LTP is also NMDA receptor dependent.

To evaluate the potential roles of NMDA receptors at CA3 recurrent synapses and mossy fiber synapses separately, we used MK801 (40 μM), an irreversible use-dependent NMDA receptor antagonist. Our results indicate that activation of NMDA receptors at CA3 recurrent synapses, but not at mossy fiber synapses, is necessary for mossy fiber EPSP-dependent LTP (Fig. 2 A–D).

Previous investigations of heterosynaptic plasticity at CA3 recurrent synapses by mossy fiber stimulation used suprathreshold signals in the form of trains of action potentials (21, 22). In those studies, activation of extrasynaptic group I metabotropic glutamate (mGlu) receptors was involved in plasticity. In our experiments, heterosynaptic potentiation of CA3 recurrent synapses was achieved without mGlu receptor activation, because plasticity was not modified in the presence of a specific antagonist (MCPG 500 μM; 58.3 ± 13.6%; $n = 3$; $P < 0.001$), and the low-frequency, single-pulse pairing that we used resulted in negligible glutamate spillover to extrasynaptic receptors. Taken together with our observation that mossy fiber stimulation can be mimicked by a subthreshold voltage step applied to the CA3 pyramidal cell to induce LTP of comparable magnitude (Fig. 2 E and F), these findings are consistent with a passive electrical signal rather than a biochemical mechanism as the process underlying EPSP-dependent plasticity.

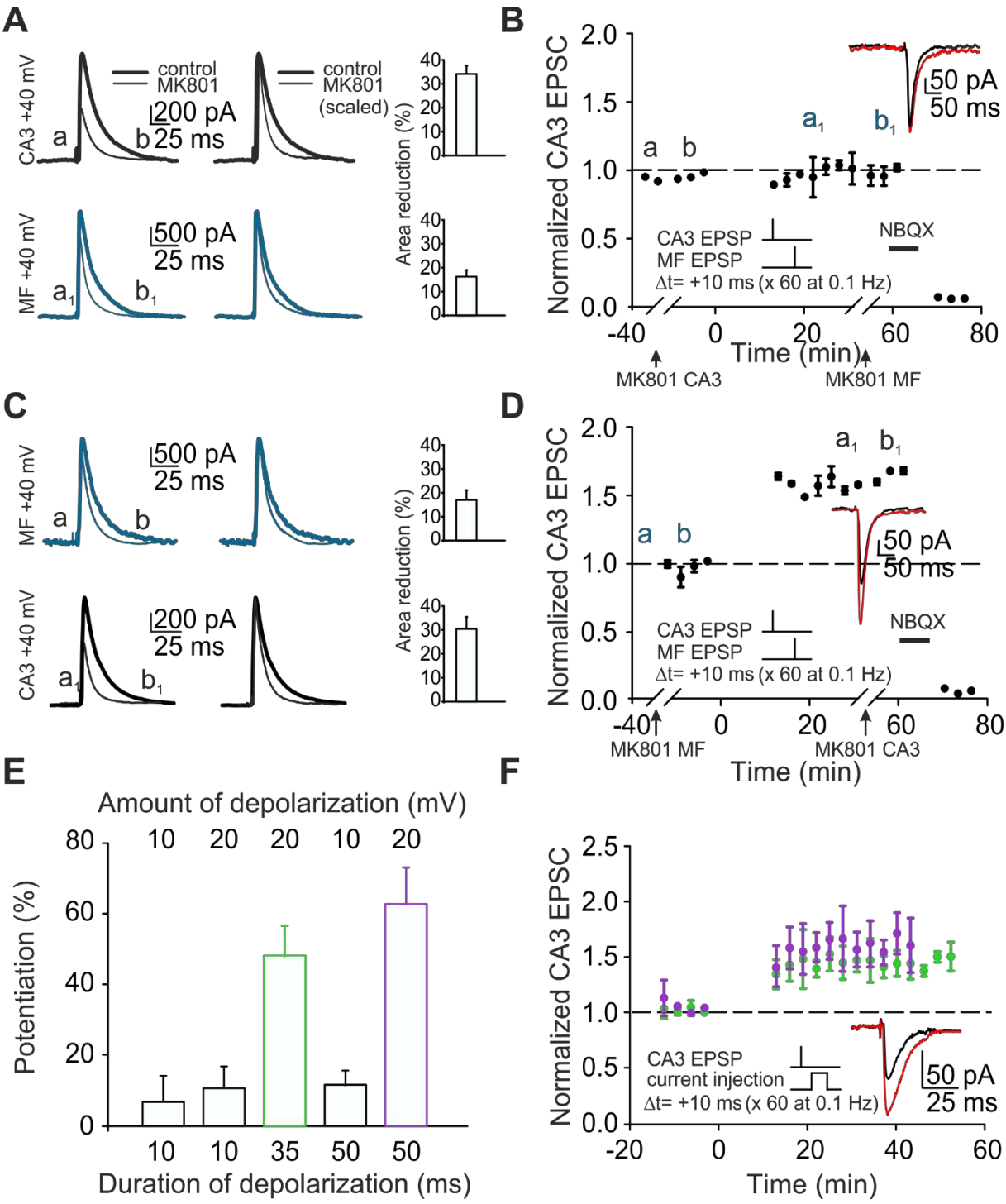

Fig. 2. The mossy fiber signal that induces EPSP-dependent LTP does not require activation of postsynaptic NMDA receptors and can be mimicked by passive current injection. (A and B) NMDA receptors were blocked selectively at the CA3 recurrent input (black traces, a, b) by application of the use-dependent antagonist MK801 in a CA3 pyramidal cell voltage-clamped at +40 mV (charge transfer reduced by 30.9 ± 4.5%; n = 3). This prevented subsequent induction of LTP in current clamp mode (0.5 ± 3.6%; n = 3; P = 0.42). A second application of MK801 at +40 mV reduced mossy fiber responses (blue traces, a1, b1) by 16 ± 2.6% (n = 3), similar to that seen in a previously unexposed cell (17.9 ± 4.1%; n = 3) (blue traces in C), demonstrating that the initial application of MK801 did not block mossy fiber NMDA receptors. (C and D) Use-dependent block of NMDA receptors only at mossy fibers (blue traces, a, b) had no significant effect on LTP (50.4 ± 3.6%; n = 3; P < 0.001) compared

with control (54.4 ± 4.8%; n = 11; P < 0.001). Subsequent application of MK801 reduced the CA3 recurrent-evoked response by 29.1 ± 3.6% (n = 3), comparable to the reduction observed for an initial application (P = 0.27) (black traces in A). (B and D) NBQX (10 μM) blocked residual currents. (E and F) A subthreshold depolarization induced by current injection can substitute for mossy fiber stimulation, consistent with a mechanism involving electrotonic dendritic signaling. The magnitude of LTP is a function of the amplitude and duration of the stimulus.

During the pairing protocol (i.e., before the development of LTP), arithmetic summation of the EPSPs was evoked by the CA3 recurrent input and the mossy fiber input in some trials, whereas in others, the summation was supralinear (34.3 ± 5.1%; n = 18) (Fig. 3A). These two distinct populations of response became readily apparent when traces were scaled to the amplitude of the evoked CA3 EPSP (Fig. 3B and Fig. S4), with supralinear response amplitude exceeding linear response amplitude by 96.9 ± 10.3% (n = 18; P < 0.001). Supralinear responses were almost completely blocked when NMDA receptors were antagonized pharmacologically (Fig. S5), suggesting that these events could be dendritic NMDA spikes, as originally described in cortical pyramidal cells (23–25). NMDA spikes were subsequently observed in hippocampal pyramidal cells as well (26, 27).

We then asked whether the mossy fiber EPSP is passively conducted distally along the dendrite to CA3 recurrent synapses to alleviate the magnesium block from NMDA receptors. If this were the case, then the likelihood of evoking an NMDA spike at a CA3 recurrent synapse should diminish as a function of the distance between the mossy fiber synapse and the CA3 recurrent synapse. As an indicator of the distance between the juxtasomatic mossy fiber input and the more distal CA3 recurrent input, we measured the rise time, under control conditions, of the somatically recorded CA3 EPSC (Fig. 3C, inset), which because of dendritic filtering declines with increasing distance from the site of the somatic recording electrode (28, 29). Plotting EPSC rise time against the magnitude of LTP induced at the CA3 recurrent synapse revealed a correlation (r = 0.66; P < 0.001) (Fig. 3C), suggesting that proximity of the CA3 input to the mossy fiber input is a critical factor for inducing EPSP-dependent LTP. A plot of EPSC rise time against the number (expressed in percent) of supralinear events evoked during the 60 pairings also revealed a positive correlation (r = 0.68; P < 0.001) (Fig. 3D). Furthermore, the number of supralinear events observed during the 60 pairings was correlated with the magnitude of LTP (r = 0.74; P < 0.001) (Fig. 3E).

It is of particular interest that in the absence of supralinear events (<10% of 60 pairings; n = 4), LTP was never induced (Fig. 3E and Fig. S6).

We also observed a correlation between the EPSC rise time and the mean amplitude of supralinear events, calculated in relation to linear event amplitude, suggesting more effective activation of NMDA receptors at more proximal recurrent synapses compared with those at distal synapses ($r = 0.69$; $P < 0.001$) (Fig. 3F). Finally, after the induction of LTP with the pairing protocol, the probability of evoking a supralinear response was significantly increased (control: 38.7 ± 7.6%; after pairing: 67.3 ± 8.8%; $n = 3$; $P < 0.05$).

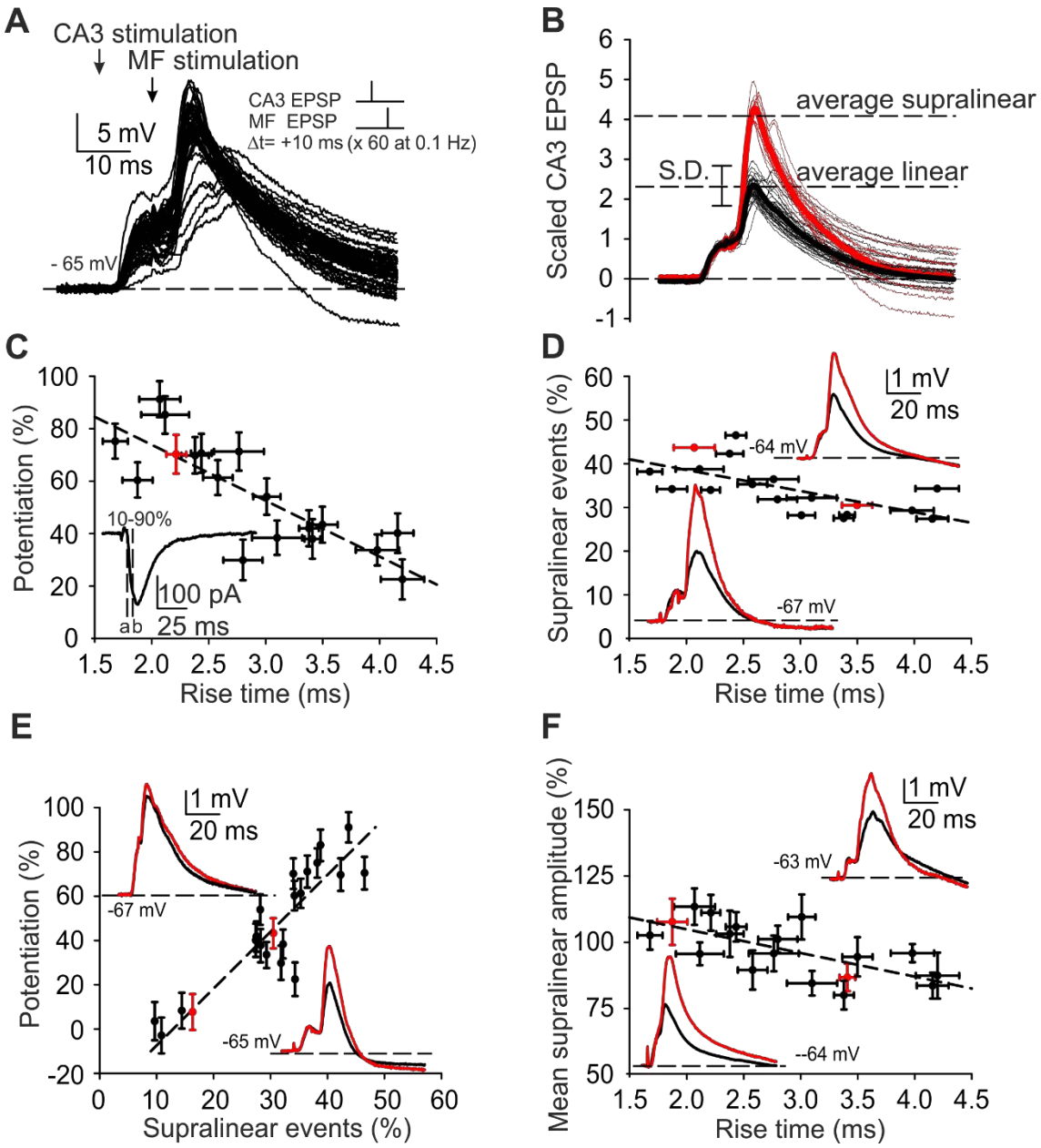

Fig. 3. Supralinear responses induced by pairing subthreshold CA3 recurrent and mossy fiber EPSPs. (A) Both linear and supralinear responses were induced during pairing of evoked EPSPs. (B) Illustration of the criterion used to distinguish between linear and supralinear summation of CA3 recurrent and mossy fiber evoked responses. Traces are scaled to the amplitude of the evoked CA3 recurrent EPSP, thereby revealing two discrete populations of responses. (C) A correlation is revealed when plotting the EPSC rise time, as a reflection of the distance between juxtasomatic mossy fiber input and more distal CA3 synaptic input, and the magnitude of LTP, suggesting that the proximity of CA3 input to mossy fiber input is critical for LTP induction. (Inset) Rise time measured from 10% of minimum (a) to 90% of maximum (b) of the EPSC evoked at −70 mV by stimulation of the CA3 recurrent input. The red data point corresponds to traces in the Inset. (D) EPSC rise time correlates with the probability of generating a supralinear response. (Inset) Averaged linear and supralinear responses. (E) The number of supralinear events evoked during the 60 pairings expressed in percent correlates with the magnitude of LTP, implicating the supralinear event as a causative factor. (F) EPSC rise time also correlates with the mean amplitude of the supralinear response.

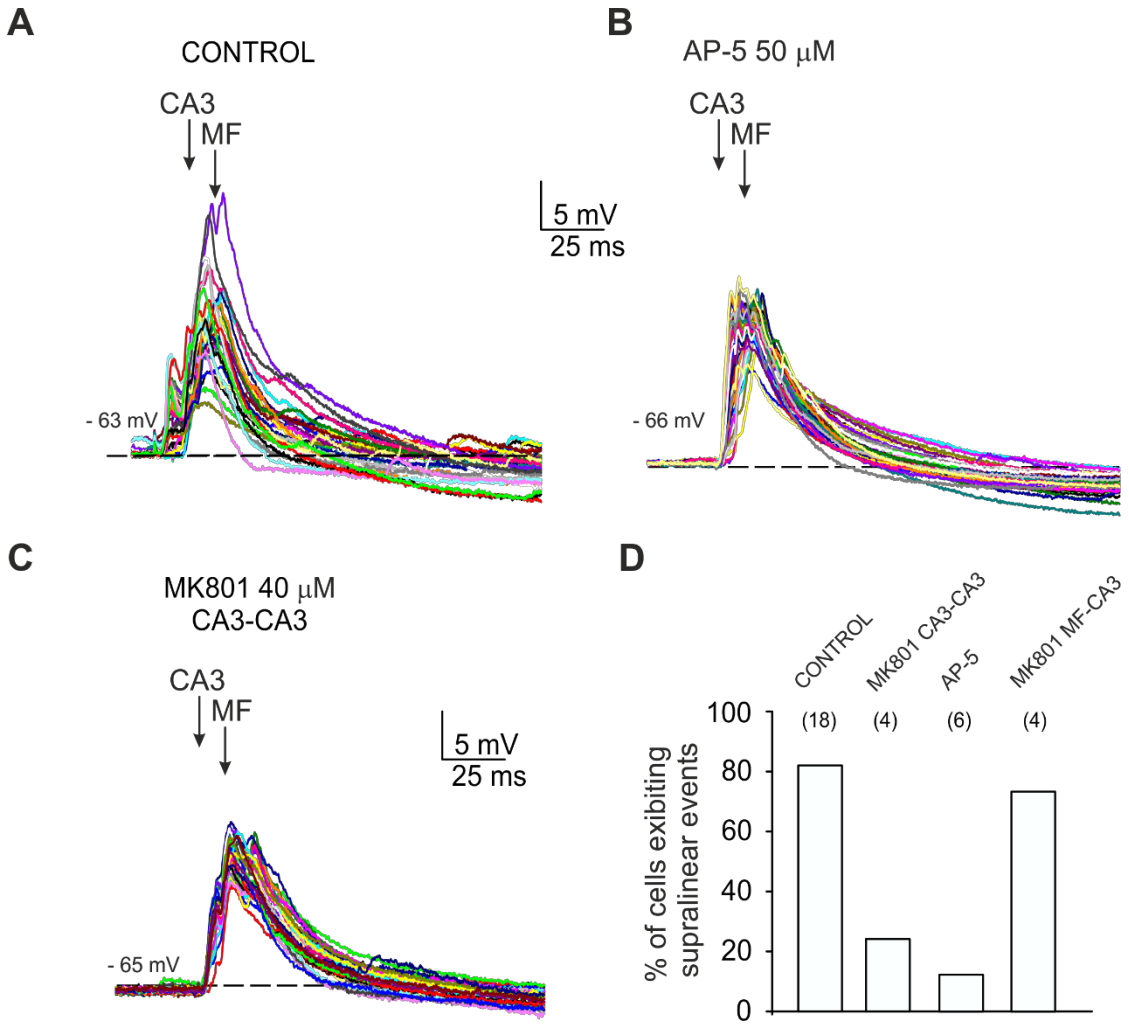

Fig. S5. Induction of a supralinear response depends on the activation of NMDA receptors. (A) Raw data recorded from a CA3 pyramidal cell showing supralinear responses in several trials. (B and C) Supralinear responses are suppressed when NMDA receptors are blocked with AP-5 (B) or MK-801 (C). (D) Pooled data for experiments with NMDA receptor antagonists.

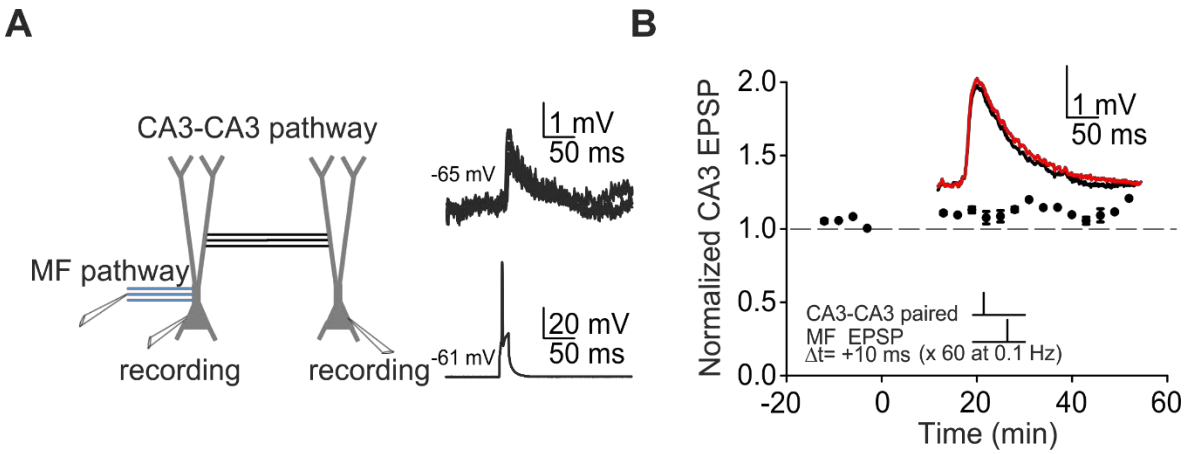

Fig. S6. (A) Activation of a single CA3 recurrent axon by recording from two synaptically connected CA3 pyramidal cells. (B) Repetitive pairing (60 times at 0.1 Hz) of the CA3 recurrent response evoked by stimulating a single axon, followed after 10 ms by a mossy fiber-evoked subthreshold response, did not result in synaptic potentiation (n = 4).

We further characterized the role of the supralinear response in inducing plasticity by recording from the trunk of the apical dendrite (Fig. 4A). After confirming that the response was dependent on NMDA receptor activation, we examined its timing properties (Fig. 4B and Fig. S7C). When the mossy fiber EPSP followed the CA3 recurrent EPSP by 10 ms, the amplitude of the supralinear responses recorded in the dendrite exceeded the amplitude of the mean linear responses by 115.8 ± 11.1% ($n = 9$; $P < 0.001$). A supralinear response was not observed when the timing of the inputs was set such that the mossy fiber EPSP preceded the CA3 recurrent EPSP by 35 ms, the timing used for LTD (16.8 ± 3.1%; $n = 5$; $P = 0.09$), or when the two inputs were activated synchronously (−14.2 ± 1.2%; $n = 4$; $P = 0.13$), conditions that did not induce potentiation.

If the hypothesis that EPSP-dependent LTP depends on an interaction occurring in the apical dendrite is correct, then the supralinear response would be expected to be more apparent in recordings from dendrites receiving clustered synaptic input compared with somatic recordings. Thus, we obtained simultaneous recordings from a first-order apical dendritic branch and from the soma (Fig. S8). In these experiments, it was possible to select a locus of stimulation that evoked a CA3 recurrent EPSP of greater amplitude in the dendritic recording than in the somatic recording (Fig. 4D and Fig. S8C). When we then paired the response with a mossy fiber-evoked EPSPs that followed at 10 ms, the percentage increase of the supralinear responses was always greater in the dendrite than in the soma (by 52 ± 9.7%; $n = 6$; $P < 0.001$). In contrast, when a stimulation site was chosen that evoked a smaller EPSP in the recorded dendrite than in the soma, the magnitude of the supralinear responses was smaller in the dendritic recording compared with the somatic recording (by 42 ± 9.7%, $n = 3$; $P < 0.005$; Fig. 4E).

The ratio in amplitude of the dendritic versus the somatic CA3 recurrent EPSP reflects the proximity of the dendritic recording electrode to the source of the supralinear response. Accordingly, we observed a correlation between dendritic/somatic CA3 recurrent EPSP amplitude and the magnitude of the dendritic supralinear response ($r = 0.81$; $P < 0.001$), compatible with findings identifying circumscribed dendritic segments as the functional units for clustered synaptic plasticity (30, 31).

We conclude that an NMDA receptor-mediated supralinear response, corresponding to a dendritic NMDA spike (23–27), is sufficient to induce LTP between CA3

pyramidal cells. In neocortical pyramidal cells, activation of multiple synapses (from 9 to 43) is necessary to evoke an NMDA spike (32–34). A similar mechanism is involved in the generation of the supralinear response in CA3 pyramidal cells. When a paired recording approach was used to excite a single CA3 recurrent axon, which activates fewer than 10 synapses per targeted pyramidal cell (35), repetitive pairing of the unitary CA3 recurrent EPSP with an evoked mossy fiber EPSP failed to induce LTP (n = 4) (Fig. S6).

Another characteristic of NMDA spikes is that they do not require activation of sodium or calcium channels (23–25). Similarly, we found that a supralinear NMDA receptor-mediated response was reliably induced in the absence of a calcium plateau, but we could evoke a calcium spike through a 20–30% increase in the stimulation intensity applied to the CA3 recurrent input and mossy fiber input to depolarize the CA3 neuron beyond −30 mV (n = 4) (Fig. S7 A and B). However, LTP was still induced in the presence of nifedipine (5 μM) to block high-threshold calcium channels (54.7 ± 17.6%; n = 4; $P < 0.001$) and nickel (50 μM) to block low-threshold calcium channels (52.4 ± 9.8%; n = 4; $P < 0.001$). Blocking sodium channels with QX-314 also did not prevent the supralinear NMDA receptor-mediated response, but did abolish the sodium spikelet and calcium plateau, even when stimulation strength was increased (Fig. S7 B and C).

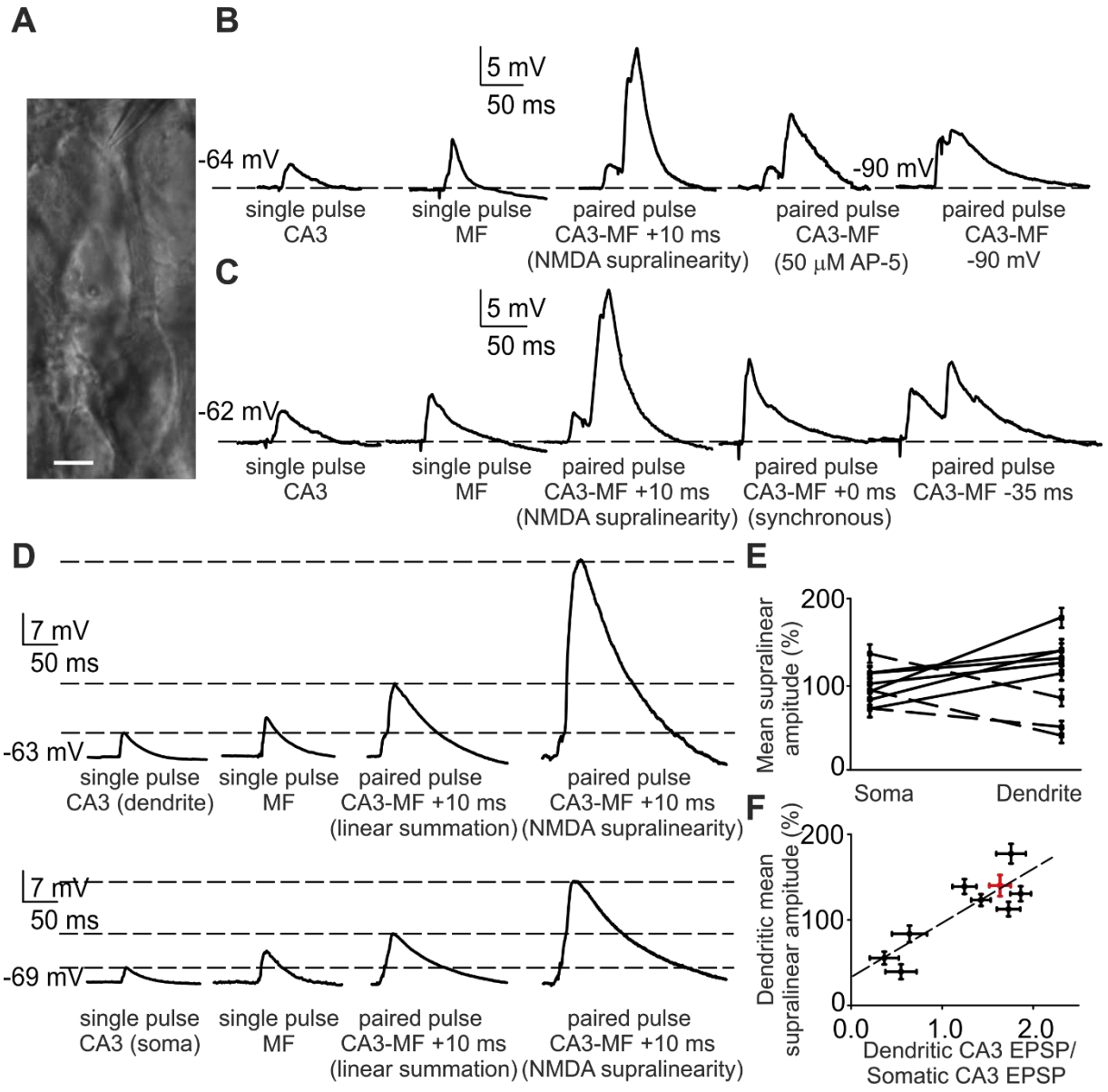

Fig. 4. The supralinear response evoked at CA3 recurrent synapses is mediated by an NMDA spike. (A) Image of a CA3 pyramidal cell during recording from the proximal apical dendrite. (Scale bar: 15 μm.) (B) A current-clamp recording from the apical dendrite (158 μm from the soma) in control conditions (before repetitive pairing) showing a supralinear summation of CA3 and mossy fiber-evoked responses. Traces are averages of 10 sweeps. The first two traces show averaged EPSPs evoked by a CA3 input and by a mossy fiber input alone. When mossy fiber stimulation follows CA3 stimulation with a delay of 10 ms, a supralinear response can be evoked. All traces with +10 ms pairings are scaled to the mean single-pulse CA3 EPSP. Supralinear summation is prevented by an NMDA receptor antagonist or by clamping the cell at −90 mV. (C) The timing of inputs is critical for induction of supralinear responses. A supralinear response is generated when a CA3 recurrent response is followed after 10 ms by a mossy fiber response, as in our LTP protocol (dendritic recording: 172 μm from the soma). Synchronous stimulation or a mossy fiber response preceding a CA3 recurrent response by 35 ms (as in the LTD protocol) does not produce a supralinear response. (D) Simultaneous recording from a first-order apical dendritic branch (upper traces) and from the soma

(lower traces) showing averaged traces of a CA3 recurrent EPSP, a mossy fiber EPSP, a paired linear response, and a paired supralinear response. The greater amplitude of the signals in the dendritic recording indicates that for this cell, the synapses stimulated by the CA3 recurrent input are close to the recorded dendritic branch but far from the soma. In these cases, the supralinear response is greater (less attenuated) in the dendritic recording compared with the somatic recording. (E) In contrast, in cases where the stimulated CA3 recurrent input induces a smaller EPSP in the recorded dendrite than in the soma (dashed lines), the measured supralinearity is smaller in the dendritic recording than in the somatic recording. (F) Consequently, the magnitude of the supralinear responses recorded in the dendrite increases as a function of the ratio of the amplitude of the dendritic/somatic CA3 recurrent EPSP.

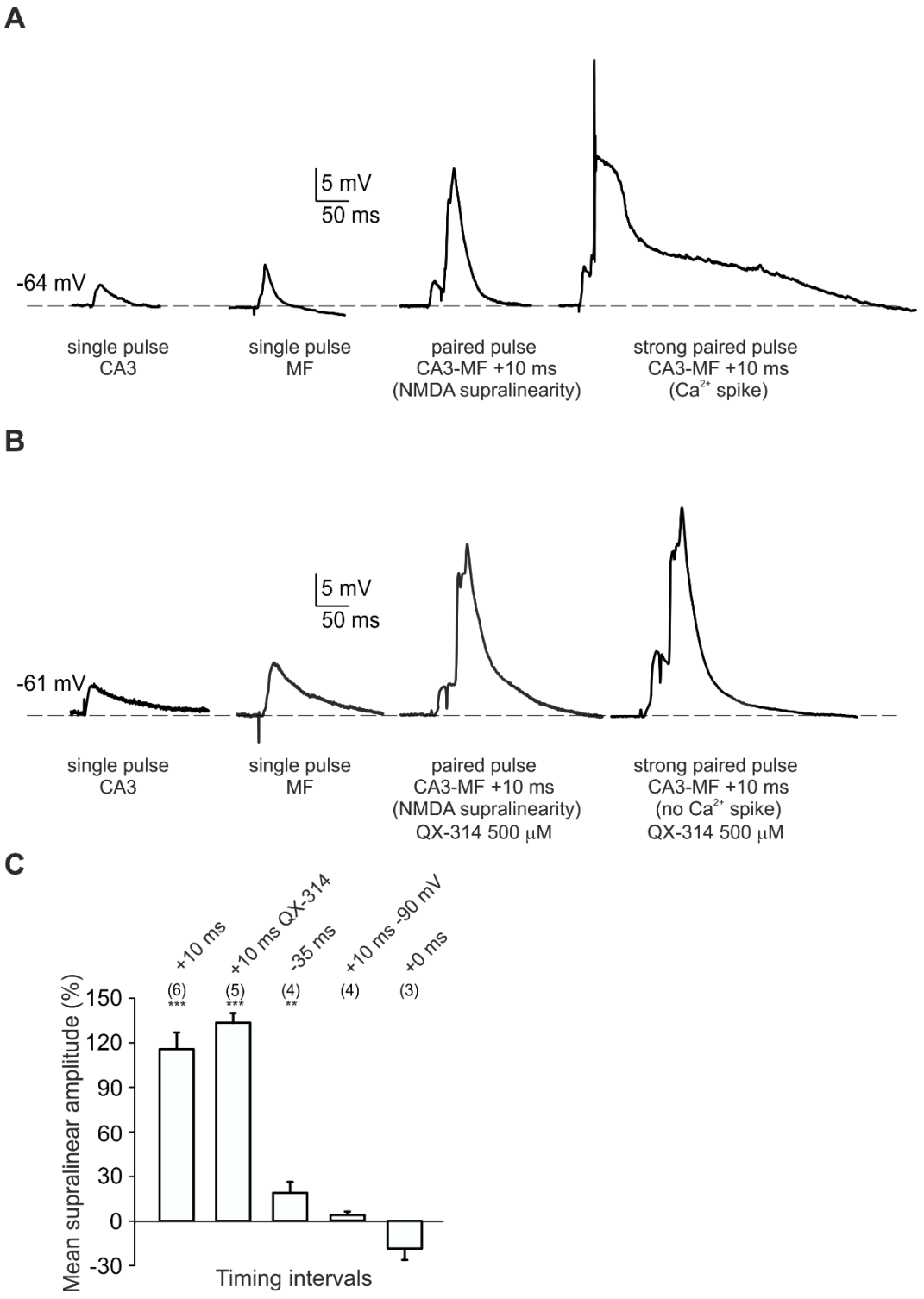

Fig. S7. Characterization of supralinear responses. (A) The supralinear summation of synaptic responses does not require calcium spikes. A dendritic recording from the cell shown in Fig. 3B reveals that a much stronger stimulation than that needed to induce an NMDA spike is required to evoke a calcium plateau response. (B) In the presence of intracellular QX-314 (500 μM), which blocks sodium channels (69) and reduces calcium currents (70), a calcium plateau no longer can be evoked, but the supralinear NMDA response is maintained. (C) Summary data illustrating the mean amplitude of supralinear events recorded in the apical dendrite under various timing and pharmacologic conditions.

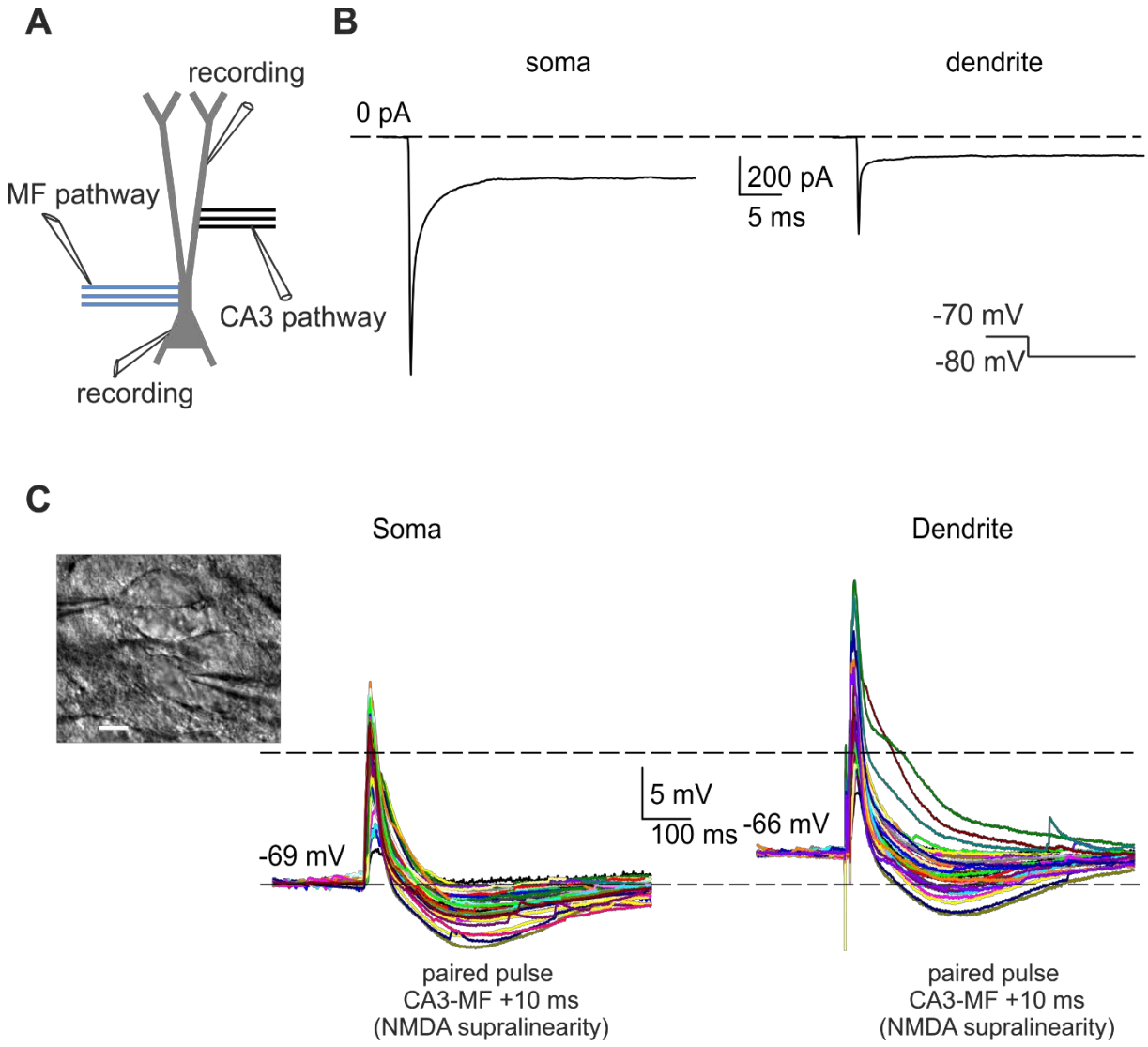

Fig. S8. Comparison of evoked responses recorded in the soma and a first-order apical dendritic branch. (A) Configuration of recording and stimulating electrodes. (B) Passive membrane properties of the somatic and dendritic compartments. (C) Individual traces recorded in the soma and dendrite of the cell from Fig. 3D showing distant-dependent attenuation of supralinear responses in the soma. (Inset) image of a CA3 pyramidal cell during simultaneous recording from the first-order apical dendritic branch (right electrode) and soma (left electrode). (Scale bar: 20 μm).

DISCUSSION

The molecular processes underlying LTP/LTD expression induced by various established experimental protocols are well understood; however, the physiological conditions under which synaptic plasticity occurs remain unclear. Several previous studies have addressed this issue using STDP protocols, which correspond more closely to in vivo patterns of activity and follow timing dependent contingencies of presynaptic and postsynaptic spikes as predicted by Hebb's rule for neural learning. Central to STDP is the back-propagating action potential initiated in the postsynaptic cell that depolarizes the dendrites, thereby fulfilling a critical requirement for the activation of NMDA receptors; however, accumulating evidence suggests that for most forms of Hebbian plasticity, back-propagating action potentials are not essential and are in fact less effective than active dendritic responses in triggering synaptic plasticity (36). Furthermore, the STDP requirement for repetitive pairing of EPSPs and action potentials is problematic for plasticity involving mossy fiber synaptic input, because dentate granule cells in vivo exhibit very low levels of activity (6, 37, 38) and function as conditional detonators, evoking action potentials in a targeted CA3 pyramidal cell only infrequently (10). Here we propose that a subthreshold mechanism depending on mossy fiber-evoked EPSPs may compensate for the extreme sparseness of electrical activity in the granule cell population in vivo (6, 37–40).

Pairing of subthreshold synaptic responses has been shown to induce plasticity in a variety of neuronal circuits (13), a phenomenon variously referred to as EPSC-dependent LTP (LTPEPSC) (41), subthreshold postsynaptic depolarization LTD (dLTD) (42), input-timing-dependent-plasticity (ITDP) (43), or subthreshold-depolarization dependent plasticity (SDDP) (44). The mossy fiber-dependent associative plasticity characterized in the present study represents an especially powerful form of subthreshold signal-induced plasticity. The exceptional effectiveness of the mossy input reflects on one hand its strategic localization at the base of the apical dendrite, where signals will passively propagate to depolarize more distal spines receiving CA3 recurrent input (12), and on the other hand the simultaneous release of large numbers of vesicles from a single terminal, essentially achieving cooperativity from a unitary fiber (8, 11). This production of a large AMPA receptor-mediated signal thus obviates the high-frequency temporal summation required to

induce plasticity in most other circuits (45, 46). Furthermore, a large long-duration EPSP may be more efficient than a brief back-propagating action potential at counteracting the slow kinetics of magnesium unblock from NMDA channels (36, 47).

Our experiments show that the main determinant of heterosynaptic LTP induced by pairing evoked subthreshold potentials is a supralinear dendritic response. Candidate mechanisms for active dendritic responses are sodium spikes, calcium spikes, and NMDA spikes (48). Experiments with pharmacological blockers allow us to rule out sodium spikes and calcium spikes. Even though a calcium plateau could be evoked with stronger synaptic stimulation, such plateau potentials were never observed during our LTP protocol. In addition, dendritic calcium waves would not be triggered at the low frequency of mossy fiber stimulation that we used (49). Thus, by exclusion, the remaining candidate for the generation of a dendritic supralinear response is the NMDA spike.

Additional evidence for NMDA spikes is their sensitivity to specific antagonists and to hyperpolarization-induced block via magnesium, as well as the fact that they were evoked only when a critical number of NMDA receptor-containing synapses was activated within a given dendritic branch. Accordingly, NMDA spikes were observed with bulk stimulation, but not when a unitary input to a CA3 pyramidal cell was activated. Also facilitating the generation of NMDA spikes is the finding that NMDA receptors at CA3–CA3 synapses (50), as at CA1–CA3 synapses (51), conduct significant current at membrane potentials near resting potential.

Of note, numerous studies have shown that the induction of LTP by STDP depends ultimately on the generation of a supralinear dendritic response, rather than on the back-propagating spike per se (36). Thus, the dendritic mechanism for EPSP dependent LTP and for STDP shares a common final step. Back propagating spikes, as well as dendritic sodium and calcium spikes, are propagating signals, however, whereas NMDA spikes are restricted in their spatial extent by the requirement of glutamate binding to NMDA receptors. Thus, STDP may exert a more global effect within the dendritic tree than NMDA spike dependent LTP.

The input timing requirements that allow subthreshold responses to induce synaptic plasticity may arise under a variety of physiological conditions. The CA3 pyramidal cell network exhibits peaks of activity phase locked to theta oscillations (52); thus, when a given CA3 pyramidal cell receives theta-timed input from neighbouring CA3 cells, appropriately timed subthreshold mossy fiber input would induce LTP. LTD

would result if subthreshold mossy fiber input arrives before CA3 input, or asynchronously (53). Thus, the giant mossy fiber signal may operate as a gate directing CA3 recurrent synapses toward LTP or LTD, depending on the timing relationship of the inputs.

In conclusion, we have characterized a dendritic interaction that contributes to the induction of plasticity at CA3 recurrent synapses by generating NMDA spikes. The finding that EPSPs evoked by mossy fibers are sufficient to induce persistent changes in synaptic function provides further evidence of the importance of analog signaling in the nervous system, not only for the regulation of neurotransmitter release (54–56), but also for dendritic information processing and synaptic plasticity (43, 56–61).

MATERIALS AND METHODS

All experiments were performed in slice cultures prepared according to the Gähwiler method (62). Although there are slight modifications in the circuitry of slice cultures, these changes are apparent primarily in the CA1 area, whereas the connectivity of granule cells and the number of mossy fiber contacts in the CA3 area closely match the morphological characteristics observed in vivo (63). Slice cultures were prepared from 6-d-old Wistar rat pups killed by decapitation following a protocol approved by the Veterinary Department of the Canton of Zurich (approval ID 41/2011). In brief, 400-μm-thick hippocampal slices were fixed to glass coverslips using clotted chicken plasma, placed in sealed test tubes with serum-containing medium, and kept in a moving incubator at 36 °C for 21–28 d. Experiments were performed at 34 °C using the standard patch-clamp recording technique. All data are expressed as mean ± SEM.

Electrophysiological Recordings. Slice cultures were placed in a recording chamber mounted on an upright microscope (Zeiss Axioskop FS1) and superfused with an external solution (pH 7.4) containing 148.8 mM Na^+, 2.7mM K^+, 149.2 mM Cl^-, 2.8 mM Ca^{2+}, 2.0 mM Mg^{2+}, 11.6 mM HCO_3^-, 0.4 mM $H_2PO_4^-$, 5.6 mM D-glucose, and 10mg/L phenol red. All experiments were performed at 34 °C. Whole-cell recordings of CA3 pyramidal cells and dentate granule cells were obtained with patch pipettes (4–6 MΩ) filled with 135 mM K-gluconate, 5 mM KCl, 10 mM Hepes, 1

mM EGTA, 5 mM phosphocreatine, 2 mM MgATP, 0.4 mM NaGTP, and 0.07 mM $CaCl_2$ (pH 7.2). For the determination of current/voltage relationships, command potentials had a duration of 1 s to ensure steady-state responses. Data were recorded with an Axopatch 200B amplifier (Molecular Devices), digitized at 4 kHz for current-clamp and 5 kHz for voltage-clamp, and analyzed off-line with pCLAMP 10 (Molecular Devices) and Origin (Microcal Software). In some experiments, inhibitory postsynaptic potentials were reduced in the recorded CA3 pyramidal cells by adding picrotoxin (1 mM) to the patch solution. Series resistance (typically 5–15 MΩ) was monitored regularly, and cells were excluded if a change of >20% occurred during the recording.

Drugs and Chemicals. AP-5, MK801, NBQX, nifedipine, picrotoxin, QX-314, and S-MCPG were purchased from Abcam. ATP, phosphocreatine, EGTA, GTP, and nickel were purchased from Sigma/Fluka, and DCG-IV was purchased from Tocris Cookson.

Data Analysis. Data points for synaptic plasticity experiments are values averaged over 3 min. Thus, the first point plotted after the 10-min pairing protocol (60 times at 0.1 Hz) is at 13 min. Numerical data in the text are expressed as mean ± SEM. Statistical comparisons were performed using the Student t test. Differences were considered significant at $P < 0.05$.

BIBLIOGRAPHY

1. McNaughton B, Morris RGM (1987) Hippocampal synaptic enhancement and information storage within a distributed memory system. Trends Neurosci 10(10): 408–415.

2. Rolls ET, Treves A (1990) The relative advantages of sparse versus distributed encoding for associative neuronal networks in the brain. Network 1:407–421.

3. Nakazawa K, et al. (2002) Requirement for hippocampal CA3 NMDA receptors in associative memory recall. Science 297(5579):211–218.

4. Nakashiba T, Young JZ, McHugh TJ, Buhl DL, Tonegawa S (2008) Transgenic inhibition of synaptic transmission reveals role of CA3 output in hippocampal learning. Science 319(5867):1260–1264.

5. Nakashiba T, Buhl DL, McHugh TJ, Tonegawa S (2009) Hippocampal CA3 output is crucial for ripple-associated reactivation and consolidation of memory. Neuron 62(6): 781–787.

6. Leutgeb JK, Leutgeb S, Moser MB, Moser EI (2007) Pattern separation in the dentate gyrus and CA3 of the hippocampus. Science 315(5814): 961–966.

7. Nakashiba T, et al. (2012) Young dentate granule cells mediate pattern separation, whereas old granule cells facilitate pattern completion. Cell 149(1):188–201.

8. Rollenhagen A, et al. (2007) Structural determinants of transmission at large hippocampal mossy fiber synapses. J Neurosci 27(39):10434–10444.

9. Henze DA, Urban NN, Barrionuevo G (2000) The multifarious hippocampal mossy fiber pathway: A review. Neuroscience 98(3):407–427.

10. Henze DA, Wittner L, Buzsáki G (2002) Single granule cells reliably discharge targets in the hippocampal CA3 network in vivo. Nat Neurosci 5(8):790–795.

11. Bischofberger J, Engel D, Frotscher M, Jonas P (2006) Timing and efficacy of transmitter release at mossy fiber synapses in the hippocampal network. Pflugers Arch 453(3):361–372.

12. Amaral DG, Witter MP (1989) The three-dimensional organization of the hippocampal formation: A review of anatomical data. Neuroscience 31(3):571–591.

13. Feldman DE (2012) The spike-timing dependence of plasticity. Neuron 75(4):556–571.

14. Salin PA, Scanziani M, Malenka RC, Nicoll RA (1996) Distinct short-term plasticity at two excitatory synapses in the hippocampus. Proc Natl Acad Sci USA 93(23): 13304–13309.

15. Vogt K, Mellor J, Tong G, Nicoll R (2000) The actions of synaptically released zinc at hippocampal mossy fiber synapses. Neuron 26(1): 187–196.

16. Ueno S, et al. (2002) Mossy fiber Zn2+ spillover modulates heterosynaptic N-methyl-Daspartate receptor activity in hippocampal CA3 circuits. J Cell Biol 158(2):215–220.

17. Connors BW, Prince DA (1982) Effects of local anesthetic QX-314 on the membrane properties of hippocampal pyramidal neurons. J Pharmacol Exp Ther 220(3):476–481.

18. Harris EW, Cotman CW (1986) Long-term potentiation of guinea pig mossy fiber responses is not blocked by N-methyl-D-aspartate antagonists. Neurosci Lett 70(1): 132–137.

19. Zalutsky RA, Nicoll RA (1990) Comparison of two forms of long-term potentiation in single hippocampal neurons. Science 248(4963):1619–1624.

20. Debanne D, Gähwiler BH, Thompson SM (1998) Long-term synaptic plasticity between pairs of individual CA3 pyramidal cells in rat hippocampal slice cultures. J Physiol 507(Pt 1):237–247.

21. Kobayashi K, Poo MM (2004) Spike train timing-dependent associative modification of hippocampal CA3 recurrent synapses by mossy fibers. Neuron 41(3):445–454.

22. Hunt DL, Puente N, Grandes P, Castillo PE (2013) Bidirectional NMDA receptor plasticity controls CA3 output and heterosynaptic metaplasticity. Nat Neurosci 16(8): 1049–1059.

23. Schiller J, Major G, Koester HJ, Schiller Y (2000) NMDA spikes in basal dendrites of cortical pyramidal neurons. Nature 404(6775):285–289.

24. Antic SD, Zhou WL, Moore AR, Short SM, Ikonomu KD (2010) The decade of the dendritic NMDA spike. J Neurosci Res 88(14):2991–3001.

25. Major G, Larkum ME, Schiller J (2013) Active properties of neocortical pyramidal neuron dendrites. Annu Rev Neurosci 36:1–24.

26. Wei DS, et al. (2001) Compartmentalized and binary behavior of terminal dendrites in hippocampal pyramidal neurons. Science 293(5538):2272–2275.

27. Makara JK, Magee JC (2013) Variable dendritic integration in hippocampal CA3 pyramidal neurons. Neuron 80(6):1438–1450.

28. Sayer RJ, Friedlander MJ, Redman SJ (1990) The time course and amplitude of EPSPs evoked at synapses between pairs of CA3/CA1 neurons in the hippocampal slice. J Neurosci 10(3):826–836.

29. Henze DA, Cameron WE, Barrionuevo G (1996) Dendritic morphology and its effects on the amplitude and rise-time of synaptic signals in hippocampal CA3 pyramidal cells. J Comp Neurol 369(3):331–344.

30. Govindarajan A, Israely I, Huang SY, Tonegawa S (2011) The dendritic branch is the preferred integrative unit for protein synthesis-dependent LTP. Neuron 69(1): 132–146.

31. Takahashi N, et al. (2012) Locally synchronized synaptic inputs. Science 335(6066): 353–356.

32. Larkum ME, Nevian T, Sandler M, Polsky A, Schiller J (2009) Synaptic integration in tuft dendrites of layer 5 pyramidal neurons: A new unifying principle. Science 325(5941):756–760.

33. Chalifoux JR, Carter AG (2011) Glutamate spillover promotes the generation of NMDA spikes. J Neurosci 31(45):16435–16446.

34. Oikonomou KD, Short SM, Rich MT, Antic SD (2012) Extrasynaptic glutamate receptor activation as cellular bases for dynamic range compression in pyramidal neurons. Front Physiol 3:334.

35. Mitra A, Mitra SS, Tsien RW (2012) Heterogeneous reallocation of presynaptic efficacy in recurrent excitatory circuits adapting to inactivity. Nat Neurosci 15(2):250–257.

36. Lisman J, Spruston N (2005) Postsynaptic depolarization requirements for LTP and LTD: A critique of spike timing-dependent plasticity. Nat Neurosci 8(7):839–841.

37. Jung MW, McNaughton BL (1993) Spatial selectivity of unit activity in the hippocampal granular layer. Hippocampus 3(2):165–182.

38. Wiebe SP, Stäubli UV (1999) Dynamic filtering of recognition memory codes in the hippocampus. J Neurosci 19(23):10562–10574.

39. Chawla MK, et al. (2005) Sparse, environmentally selective expression of Arc RNA in the upper blade of the rodent fascia dentata by brief spatial experience. Hippocampus 15(5):579–586.

40. Alme CB, et al. (2010) Hippocampal granule cells opt for early retirement. Hippocampus 20(10):1109–1123.

41. Krasteniakov NV, Martina M, Bergeron R (2004) Subthreshold contribution of Nmethyl-D-aspartate receptors to long-term potentiation induced by low-frequency pairing in rat hippocampal CA1 pyramidal cells. Neuroscience 126(1):83–94.

42. Sjöström PJ, Turrigiano GG, Nelson SB (2004) Endocannabinoid-dependent neocortical layer-5 LTD in the absence of postsynaptic spiking. J Neurophysiol 92(6):

3338–3343.

43. Dudman JT, Tsay D, Siegelbaum SA (2007) A role for synaptic inputs at distal dendrites: Instructive signals for hippocampal long-term plasticity. Neuron 56(5):866–879.

44. Fino E, Deniau JM, Venance L (2009) Brief subthreshold events can act as Hebbian signals for long-term plasticity. PLoS ONE 4(8): e6557.

45. Buchanan KA, Mellor JR (2007) The development of synaptic plasticity induction rules and the requirement for postsynaptic spikes in rat hippocampal CA1 pyramidal neurones. J Physiol 585(Pt 2):429–445.

46. Sjöström PJ, Turrigiano GG, Nelson SB (2007) Multiple forms of long-term plasticity at unitary neocortical layer 5 synapses. Neuropharmacology 52(1):176–184.

47. Kampa BM, Clements J, Jonas P, Stuart GJ (2004) Kinetics of Mg2+ unblock of NMDA receptors: Implications for spike-timing dependent synaptic plasticity. J Physiol 556(Pt 2):337–345.

48. Sjöström PJ, Rancz EA, Roth A, Häusser M (2008) Dendritic excitability and synaptic plasticity. Physiol Rev 88(2):769–840.

49. Kapur A, Yeckel M, Johnston D (2001) Hippocampal mossy fiber activity evokes Ca2+ release in CA3 pyramidal neurons via a metabotropic glutamate receptor pathway. Neuroscience 107(1):59–69.

50. Debanne D, Guérineau NC, Gähwiler BH, Thompson SM (1995) Physiology and pharmacology of unitary synaptic connections between pairs of cells in areas CA3 and CA1 of rat hippocampal slice cultures. J Neurophysiol 73(3):1282–1294.

51. Kovalchuk Y, Eilers J, Lisman J, Konnerth A (2000) NMDA receptor-mediated subthreshold Ca(2+) signals in spines of hippocampal neurons. J Neurosci 20(5):1791–1799.

52. Mizuseki K, Royer S, Diba K, Buzsáki G (2012) Activity dynamics and behavioral correlates of CA3 and CA1 hippocampal pyramidal neurons. Hippocampus 22(8):1659–1680.

53. Debanne D, Gähwiler BH, Thompson SM (1994) Asynchronous pre- and postsynaptic activity induces associative long-term depression in area CA1 of the rat hippocampus in vitro. Proc Natl Acad Sci USA 91(3):1148–1152.

54. Alle H, Geiger JR (2008) Analog signalling in mammalian cortical axons. Curr Opin Neurobiol 18(3):314–320.

55. Christie JM, Chiu DN, Jahr CE (2011) Ca(2+)-dependent enhancement of release by subthreshold somatic depolarization. Nat Neurosci 14(1):62–68.

56. Debanne D, Bialowas A, Rama S (2013) What are the mechanisms for analogue and digital signalling in the brain? Nat Rev Neurosci 14(1):63–69.

57. McNaughton BL, Douglas RM, Goddard GV (1978) Synaptic enhancement in fascia dentata: Cooperativity among coactive afferents. Brain Res 157(2):277–293.

58. Gustafsson B, Wigström H, Abraham WC, Huang YY (1987) Long-term potentiation in the hippocampus using depolarizing current pulses as the conditioning stimulus to single volley synaptic potentials. J Neurosci 7(3):774–780.

59. Artola A, Bröcher S, Singer W (1990) Different voltage-dependent thresholds for inducing long-term depression and long-term potentiation in slices of rat visual cortex. Nature 347(6288):69–72.

60. Golding NL, Staff NP, Spruston N (2002) Dendritic spikes as a mechanism for cooperative long-term potentiation. Nature 418(6895):326–331.

61. Hardie J, Spruston N (2009) Synaptic depolarization is more effective than back propagating action potentials during induction of associative long-term potentiation in hippocampal pyramidal neurons. J Neurosci 29(10):3233–3241.

62. Gähwiler BH (1981) Organotypic monolayer cultures of nervous tissue. J Neurosci Methods 4(4):329–342.

63. Mori M, Abegg MH, Gähwiler BH, Gerber U (2004) A frequency-dependent switch from inhibition to excitation in a hippocampal unitary circuit. Nature 431(7007):453–456.

64. Salin PA, Scanziani M, Malenka RC, Nicoll RA (1996) Distinct short-term plasticity at two excitatory synapses in the hippocampus. Proc Natl Acad Sci USA 93(23):13304–13309.

65. Mori M, Abegg MH, Gähwiler BH, Gerber U (2004) A frequency-dependent switch from inhibition to excitation in a hippocampal unitary circuit. Nature 431(7007):453–456.

66. Debanne D, Guérineau NC, Gähwiler BH, Thompson SM (1995) Physiology and pharmacology of unitary synaptic connections between pairs of cells in areas CA3 and CA1 of rat hippocampal slice cultures. J Neurophysiol 73(3): 1282–1294.

67. Kamiya H, Shinozaki H, Yamamoto C (1996) Activation of metabotropic glutamate receptor type 2/3 suppresses transmission at rat hippocampal mossy fibre synapses. J Physiol 493(Pt 2): 447–455.

68. Mori M, Abegg MH, Gähwiler BH, Gerber U (2004) A frequency-dependent switch from inhibition to excitation in a hippocampal unitary circuit. Nature 431(7007):453–456.

69. Connors BW, Prince DA (1982) Effects of local anesthetic QX-314 on the membrane properties of hippocampal pyramidal neurons. J Pharmacol Exp Ther 220(3):476–481.

70. Talbot MJ, Sayer RJ (1996) Intracellular QX-314 inhibits calcium currents in hippocampal CA1 pyramidal neurons. J Neurophysiol 76(3):2120–2124.

DENDRITIC NMDA SPIKES ARE NECESSARY FOR TIMING-DEPENDENT ASSOCIATIVE PLASTICITY IN THE HIPPOCAMPUS

Federico Brandalise, Stefano Carta, Fritjof Helmchen,
John Lisman, Urs Gerber

Nature Communications, 2016
Under Revision

Contribution to this study: F. Brandalise designed the study together with U.G. and J.L., and performed the majority of the experiments.

SUMMARY

The computational repertoire of neurons is enhanced by regenerative electrical signals initiated in dendrites acting as cell-intrinsic amplifiers of synaptic depolarization. Among these signals, dendritic NMDA spikes are of interest in light of their correlation with LTP induction. Because it is not possible to block NMDA spikes pharmacologically while maintaining NMDA receptors available to initiate synaptic plasticity, it remains unclear whether NMDA spikes alone can trigger LTP. We used dendritic recordings and calcium imaging to analyze the role of NMDA spikes in associative LTP in CA3 pyramidal cells. We show that NMDA spikes produce regenerative branch-specific calcium transients. Decreasing the probability of NMDA spikes reduces LTP whereas increasing their probability enhances LTP. NMDA spikes and LTP occur without back-propagating action potentials. However, action potentials can facilitate LTP induction by promoting NMDA spikes. Thus, NMDA spikes are necessary and sufficient to produce the critical postsynaptic depolarization required for associative LTP in CA3 pyramidal cells.

INTRODUCTION

The Hebbian postulate, whereby a synapse is strengthened when presynaptic input is successful in evoking postsynaptic activity, is accepted as the basis for many forms of learning. This process is initiated by strong depolarization of the postsynaptic neuron, which activates NMDA receptors and results in the calcium elevation that triggers the biochemical processes leading to LTP. The depolarization produced by a single synaptic input is insufficient to induce LTP; rather, LTP is associative in nature, requiring the summated input from many excitatory synapses. A key aspect of Hebbian plasticity is the requirement of a feed-back signal that informs the synapse whether the integrated postsynaptic activity was sufficient to induce an action potential. An attractive candidate for this feedback event is the back-propagating action potential (bAP)[1,2]. However, a number of observations have called into question the relevance of the bAP for LTP[3,4]. Importantly, LTP can be induced at various synapses in the absence of bAPs[5-13]. In these studies, regenerative dendritic events referred to as dendritic spikes (dSpikes) may produce the depolarization needed to trigger LTP. These can be local events, often confined to a single dendritic

branch[14]. Theory suggests that such spatially restricted depolarization may have the advantage of allowing memory storage at a much finer scale than the widespread dendritic regions affected by bAPs[15]. At present, however, the evidence that dSpikes provide the critical depolarization necessary for LTP remains correlative.

Dendritic spiking mechanisms are complex, involving both bAPs as well as dSpikes (dendritic sodium spikes, dendritic calcium spikes, and dendritic NMDA spikes[14]). Although all these events may influence dendritic depolarization, determining which factor is essential for LTP is complicated. We have investigated LTP at recurrent collateral synapses in the CA3 hippocampal region and characterized the underlying roles of bAPs and dSpikes. Using a combination of electrophysiological and two-photon Ca^{2+} imaging techniques, we identify dendritic NMDA spikes as the causal signal that initiates LTP at synapses between hippocampal CA3 pyramidal cells.

RESULTS

NMDA spikes induce branch-restricted Ca^{2+} transients and LTP

We evoked NMDA spikes, which are a class of dSpike dependent on NMDA receptor activation[16,17], using a subthreshold input timing-dependent plasticity (ITDP) protocol. CA3 recurrent (rCA3) axons were stimulated followed 10 ms later by mossy fiber (MF) stimulation (Fig. 1a). In these experiments action potentials were prevented by intracellular application of QX-314 (500 µM)[18]. 60 pairings at 0.1 Hz, produced LTP at the stimulated rCA3 synapses (41.9 ± 2.3% after 30 min, n = 13 of 16, $P < 0.001$; Fig. 1a), whereas MF EPSPs remained unaffected (Fig. 1b and [9]). Scaling membrane potential traces to normalize the amplitude of the evoked rCA3 EPSP preceding MF stimulation revealed a bimodal distribution of summated EPSPs corresponding to linear and supralinear responses (Fig. 1c). The supralinear responses exhibited all-or-none properties as a function of stimulation intensity and were blocked by NMDAR antagonists, thus meeting two important criteria for NMDA spikes[19] (Supplementary Fig. 1 and Fig. 1d; see Methods for NMDA spike analysis). To facilitate analysis, all experiments were performed with intracellular picrotoxin (1 mM) to suppress $GABA_A$-mediated inhibition. However, ITDP-triggered LTP can also be induced in the presence of picrotoxin[9].

We next examined a third criterion for NMDA spikes, the localized elevation of calcium. Two-photon Ca^{2+} imaging with Fluo-5F showed that during the pairing protocol Ca^{2+} transients occurred in the region of the dendritic rCA3 synapses close to the stimulation electrode (Fig. 1e and Supplementary Fig. 2d), consistent with the finding that NMDA spikes are triggered by NMDA receptors expressed at rCA3 rather than at MF synapses[9]. Importantly, whenever an evoked dendritic Ca^{2+} transient was detected, a coincident NMDA spike was likely to be present in the electrophysiological recording (in 93.8 ± 3.5% of cases, *n* = 13; Fig. 1f and Supplementary Fig. 2e). In addition, the integral of all Ca^{2+} transients detected within the field of view close to the stimulation electrode correlated with the amplitude of the NMDA spike (Supplementary Fig. 3e-g). Dendritic Ca^{2+} imaging also provided information about the localization and spatial extent of NMDA spikes. Ca^{2+} transients were restricted to individual branches, spreading only for short distances (11.8 ± 1.2 µm, *n* = 13 cells; Fig. 1e, h and Supplementary Fig. 2h-j). Furthermore, within a branch there were local hotspots (~1 µm diameter) that were repeatedly elicited during the pairing protocol, likely reflecting the sites of synaptic input (*n* = 7/7; Fig. 1h, i and Supplementary Fig. 2h-j), as reported previously[10,11,19,20,21]. Branch-specific Ca^{2+} transients could be observed in apical (*n* = 7) or basal dendrites (*n* = 9) depending on the position of the stimulation electrode (see Methods for further description). This pattern reflects the location of rCA3 synapses and the innervation pattern of CA3 pyramidal cells by MFs, whose giant terminals target the most proximal apical and basal region of the dendrites[22], and thus are strategically positioned to provide the associative input to evoke NMDA spikes at the more distally located rCA3 synapses. Dendritic Ca^{2+} transients can arise not only in conjunction with NMDA spikes but also with back-propagating APs, dendritic sodium spikes, and Ca^{2+} spikes. Under our experimental conditions, however, the dendritic Ca^{2+} transients corresponded to NMDA spikes, on the basis of their duration (~50 ms)[23,24], absence of a sodium spikelet[23,24], and restricted spatial propagation[19,24] (Supplementary Fig. 4). Furthermore, dendritic NMDA spikes were evoked with a lower stimulation threshold than Ca^{2+} spikes, and were not prevented by pharmacological blockade of sodium and Ca^{2+} channels[9,25,26]. Both the NMDA spikes and the corresponding dendritic Ca^{2+} transients were greatly decreased in number after NMDAR blockade with the competitive antagonist D-AP5 (50 µM) (NMDA spikes: from 44.2 ± 2.7% in control, *n* = 13, to 4.8 ± 1.7%, *n* = 6, $P < 0.001$; Ca^{2+}

transients: from 41.9 ± 2.3%, n = 13, to 5.1 ± 2.7%, n = 6, P < 0.001; Fig. 1d,g and Supplementary Fig. 2f,g). Taken together, the results demonstrate that these supralinear events are chiefly NMDA spikes localized to individual dendritic branches.

Are the NMDA spikes evoked by the ITDP protocol expressed in only one region of the dendritic tree or can multiple areas be implicated? We addressed this question by examining the EPSP/EPSC rise time as a proxy for the distance of the stimulated rCA3 inputs from the soma (Supplementary Fig. 5). In the majority of cells (10/13), the relatively low-intensity stimulation employed (minimal stimulation (60% failures) + 20% in all experiments) evoked rCA3 EPSPs with unimodal distributions of rise time, which is consistent with the generation of the EPSP at a specific dendritic distance from the soma, even though a CA3 pyramidal cell typically receives multiple synaptic contacts from a given neighboring cell[27]. Moreover, plotting the rise time of the rCA3 EPSP against the mean distance from the soma of the observed Ca^{2+} transients yielded a linear relation (Supplementary Fig. 5e). Nevertheless, in 3/13 experiments the Ca^{2+} transients were detected in two distinct areas of the dendritic tree; consistently in these cases the rise time analysis revealed a bimodal distribution (Supplementary Fig. 6).

A strong indication that NMDA spikes are important for the induction of LTP was obtained by examining the relationship between the probability of evoking dendritic Ca^{2+} transients characteristic of NMDA spikes and the magnitude of LTP. This revealed a high correlation (r = 0.79, n = 16; Fig. 1j). In experiments where paired stimulation evoked Ca^{2+} transients in less than 10% of the 60 trials, rCA3 synapses did not undergo potentiation (1.1 ± 0.1%, n = 3, P = 0.5; Fig. 1j and Supplementary Fig. 7). Thus, the paired stimulation paradigm *per se* does not induce potentiation, but rather a critical number (~10) of NMDA spikes is required. Furthermore, the number of branches exhibiting a dendritic Ca^{2+} transient during a paired stimulation correlates with the amplitude of the NMDA spike (Fig. 1k).

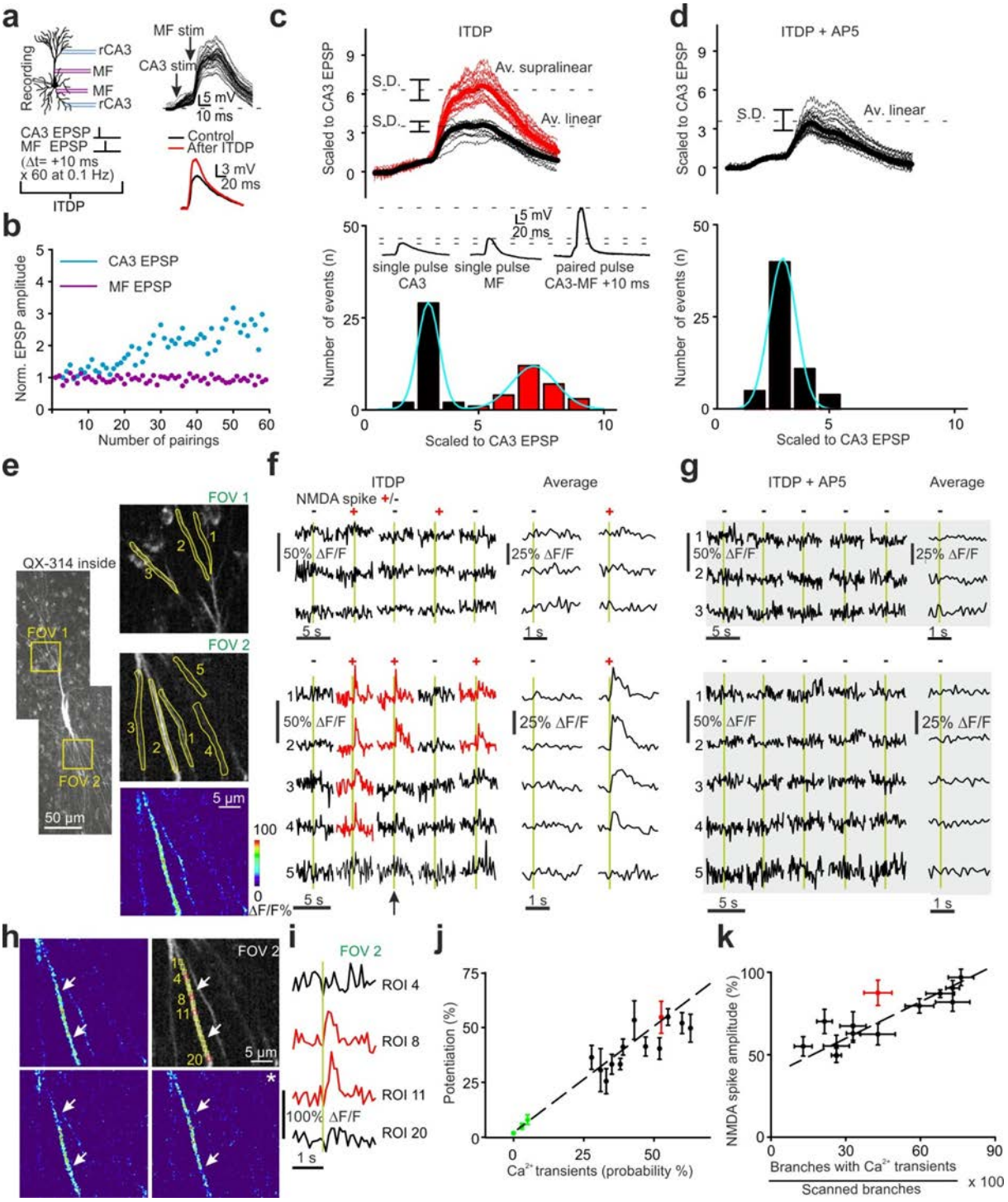

Figure 1. Branch-specific NMDAR-dependent dendritic Ca^{2+} transients evoked by subthreshold synaptic pairing are associated with LTP induction. **(a)** Left: ITDP protocol for pairing rCA3 and MF inputs to a hippocampal CA3 pyramidal cell in slice culture. The recording pipette contained 500 µM QX-314. Right: Examples of pairing-evoked EPSPs and averaged traces of the rCA3 EPSP before and after LTP. **(b)** Time course throughout the pairing protocol of EPSP amplitudes normalized to baseline. rCA3-evoked but not MF-evoked EPSPs are potentiated. **(c)** Scaled voltage traces (normalized to initial rCA3 EPSP amplitude) reveal a bimodal distribution of response amplitude corresponding to linear (black) and supralinear (red) summation. Inset: individual traces for a rCA3 EPSP, a mossy fiber EPSP and a summated supralinear EPSP. **(d)** Supralinear responses are suppressed

by NMDAR blockade (D-AP5) resulting in a unimodal distribution of summated EPSP amplitudes. **(e)** Fluo-5F labeled CA3 pyramidal neuron. Fluorescence measurements to detect pairing-induced Ca^{2+} transients were obtained in 3 ROIs for apical dendritic branches in FOV 1 and 5 ROIs for basal dendritic branches in FOV 2. Lower right image shows localized Fluo-5F $\Delta F/F$ fluorescence change for one pairing trial (arrow in f). **(f)** Example Ca^{2+} transients from ROIs selected in e, recorded during 5 representative consecutive pairings (green bars). Trials with linear ("-") and supralinear ("+") EPSP summation are indicated. Ca^{2+} transients for FOV2 were averaged separately for linear (*n* = 14/30) and supralinear (*n* = 16/30) trials. **(g)** NMDAR blockade abolished dendritic Ca^{2+} transients as shown for the same ROIs as in f. **(h)** A series of uniformly sized ROIs (~1 µm x 1 µm) numbered from 1 – 20 were positioned along a responsive dendritic segment (delineated by arrows) as identified from the heat map in e. Images from three pairing trials in which an NMDA spike was evoked. **(i)** Ca^{2+} transients associated with an NMDA spike for ROI 8 and 11 (red traces) and for ROIs outside the active region (black traces) for the image in i marked with an asterisk. **(j)** The magnitude of LTP of the rCA3 EPSP correlates across cells with the incidence of Ca^{2+} transients during pairing (number of trials with Ca^{2+} transients in at least one ROI divided by the total number of ITDP pairings). In cells where the pairing protocol failed to evoke Ca^{2+} transients (green data points), EPSPs were not potentiated. Red data point corresponds to the example cell shown in d. **(k)** Pooled data showing the increase in NMDA spike amplitude as a function of the prevalence of dendritic Ca^{2+} transients (*r* = 0.73, *n* = 16).

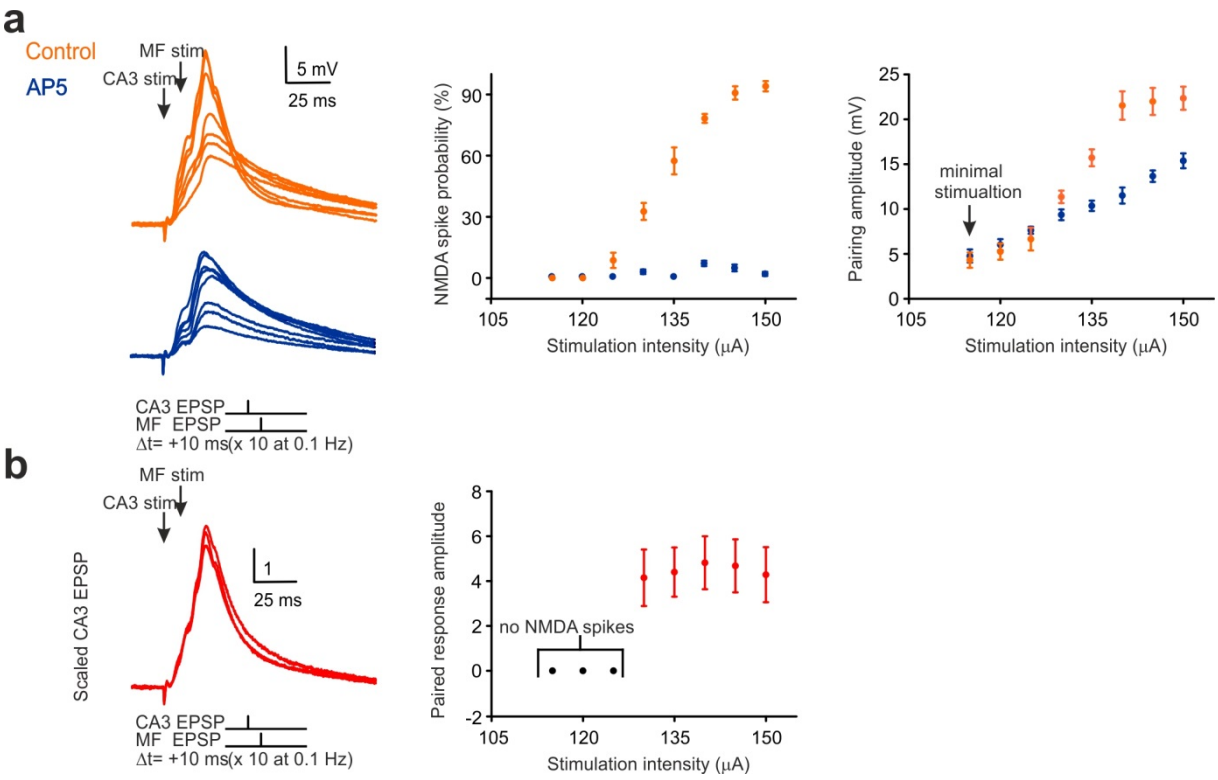

Supplementary Figure 1. The supralinear events evoked in CA3 pyramidal cells fulfill the criteria for NMDA spikes, exhibiting a threshold, sensitivity to NMDAR blockade, and all-or-none expression. (a) Left panel: Experimental design: each trace is an average of 10 sweeps obtained by pairing a rCA3 EPSP followed by a MF EPSP according to the ITDP protocol shown below. Families of traces were generated by progressively increasing the stimulation intensity beyond threshold intensity under control conditions and after NMDAR blockade. Center panel: Pooled data for the probability of triggering a supralinear response as a function of stimulation intensity (n = 5). As NMDA spikes are all-or-none events[17], the response amplitude is expected to increase abruptly once that threshold is exceeded. However, as the data points represent responses averaged over ten trials that include both failures and successes, the amplitude increases incrementally reflecting the change in probability of surpassing threshold with stronger stimulation. Right panel: averaged responses showing the change in amplitude of the paired EPSP with incrementing stimulation intensity. In the presence of D-AP5 supralinear events are prevented and the amplitude of the averaged responses with increasing stimulation intensity follows a linear function mediated by AMPA receptors. **(b)** The all-or-none nature of the NMDA spike is revealed when failures are excluded and the amplitude of only supralinear events is plotted, which is consistent with the bimodal distribution of rCA3/MF summated responses (**Fig. 1c**; Brandalise and Gerber, 2014). It should be noted that although NMDA spikes are all-or-none events, their amplitude is determined by the number of synapses activated and can therefore vary from trial to trial if the number of stimulated inputs changes. However, when data from several cells are averaged, this variability is no longer apparent.

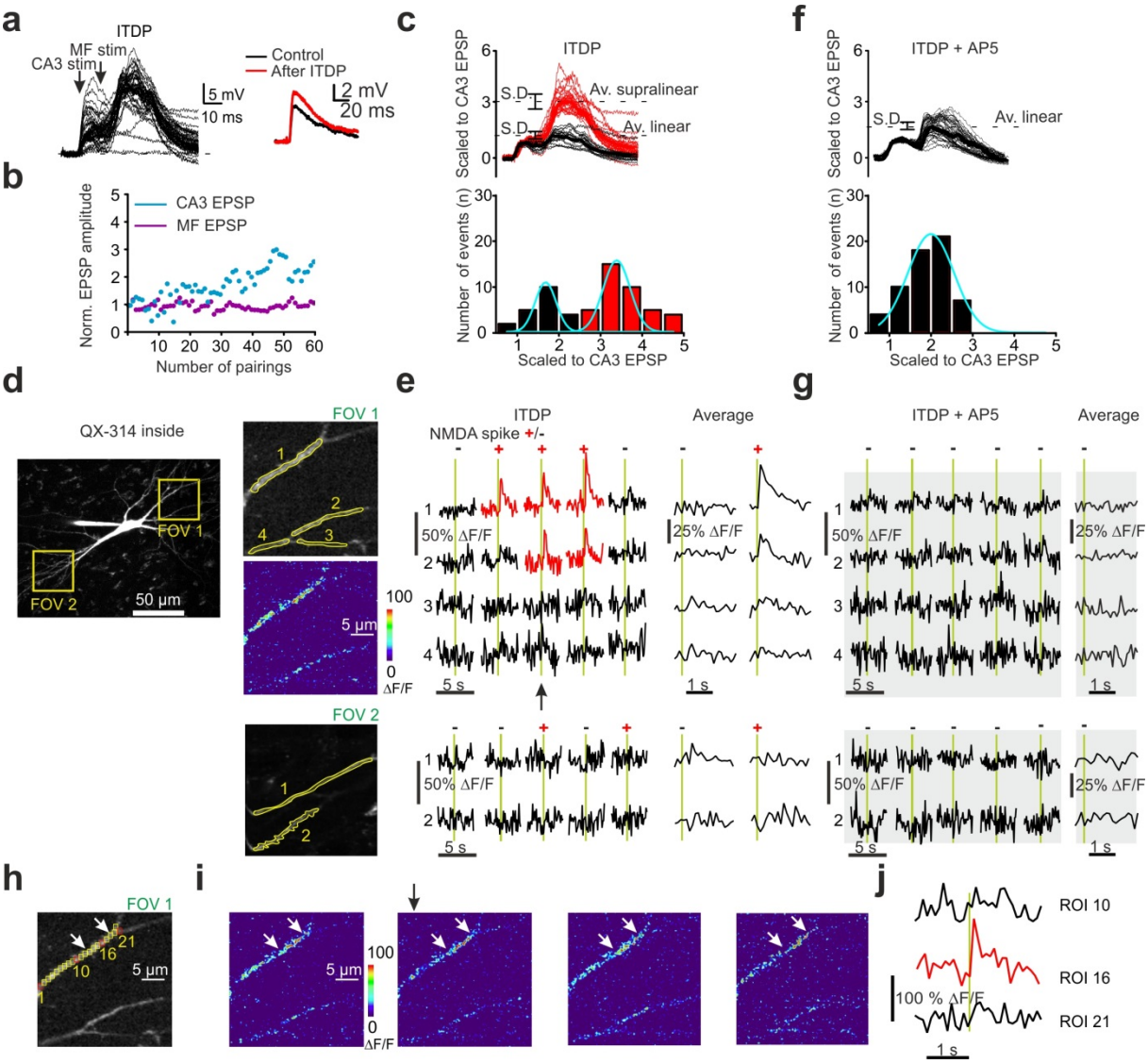

Supplementary Figure 2. Peak dendritic Ca^{2+} transients associated with NMDA spikes exhibit highly consistent inter-trial localization. (a) Raw data recorded during the ITDP protocol from a representative CA3 pyramidal cell in which sodium currents were blocked with intracellular QX-314 (500 µM) to prevent back-propagating APs and dendritic sodium spikes. After 60 pairings, the rCA3 EPSP undergoes LTP. **(b)** Time course of the experiment showing that rCA3-evoked EPSPs were potentiated whereas MF-evoked EPSPs were not at the ITDP stimulation frequency of 0.1 Hz. **(c)** The same 60 traces were scaled to normalize the amplitude of the evoked rCA3 EPSP that precedes the MF EPSP. This procedure reveals the presence of linear (black) as well as supralinear events (red), which are bimodally distributed. Note that at the end of the 60 pairings the rCA3 EPSP is potentiated by 84.9 ± 10.6% as a consequence of short-term facilitation. **(d)** Responses were analyzed in the basal (FOV 1) and apical dendrites (FOV 2). In FOV 1, two of four dendritic segments exhibit Ca^{2+} transients during NMDA spikes. The same stimulation failed to evoke Ca^{2+} transients in the dendrites imaged in FOV 2. **(e)** Dendritic Ca^{2+} transients evoked during 5 consecutive pairings (green bars) of rCA3 and MF EPSPs in which "+" and "-" mark the trials associated with supralinear and linear EPSPs, respectively. Averaged Ca^{2+} transients are from 30 consecutive pairings. The arrow indicates the trial corresponding to the image showing the change in Fluo-5F fluorescence in d. Averaged responses are shown on the right. **(f)** NMDA spikes are no longer observed after blocking NMDARs (D-AP5) and, consequently, the

amplitudes of the events exhibit a unimodal distribution. **(g)** When NMDA spikes are prevented, dendritic Ca^{2+} transients are not observed. **(h)** A series of uniformly sized ROIs (~1 µm x 1 µm) numbered from 1 – 21 were positioned along a responsive dendritic segment as identified by the heat map in d. **(i)** Images from four consecutive pairing trials in which an NMDA spike was evoked. The Ca^{2+} hotspot lies at the center of the dendritic section demarcated by the white arrows (ROI 16). The black arrow indicates the trial corresponding to the traces in j. **(j)** Time-course of the calcium response associated with an NMDA spike for ROI 16 (red trace) and for ROIs outside the white arrows (black traces). For pooled data of NMDA spike magnitude see Supplementary Fig. 4b.

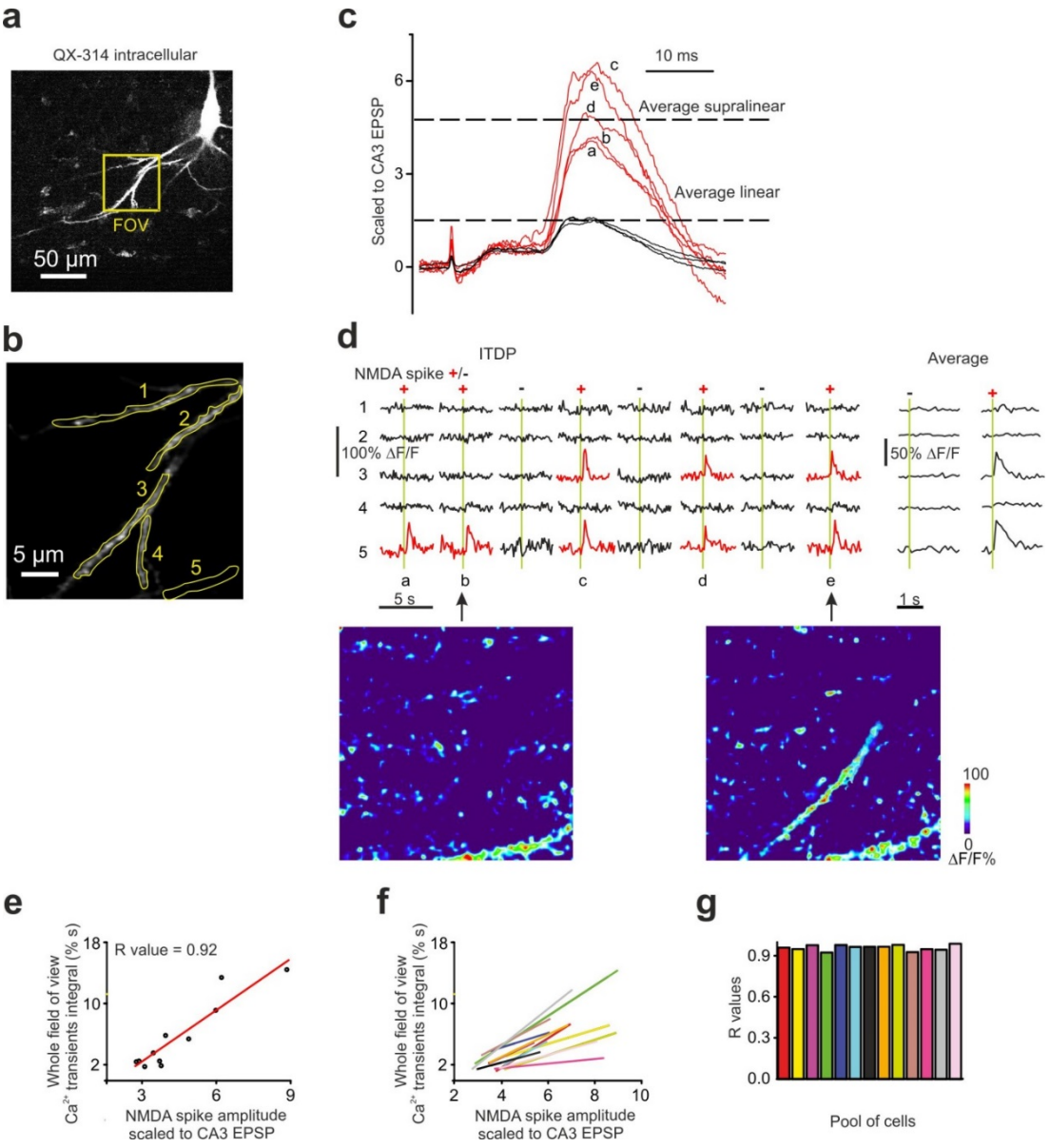

Supplementary Figure 3. Event analysis showing a correlation between the number of branches exhibiting dendritic Ca^{2+} transients and the amplitude of electrophysiologically recorded NMDA spikes. (a) FOV in the basal dendrites. **(b)** Dendritic Ca^{2+} transients were analyzed in five ROIs. **(c)** Eight consecutive superimposed events evoked by pairing a rCA3 EPSP with a subsequent MF EPSP (normalized to the amplitude of the rCA3 EPSP) which generated three linear responses and five supralinear

responses generated by NMDA spikes. **(d)** Fluo-5F fluorescence imaging shows that in most cases the dendritic Ca^{2+} transients in these ROIs are associated with NMDA spikes (+) and are restricted to specific branch segments (for this cell: ROIs 1,3,5,6). The arrow indicates the trial for the image showing the change in Fluo-5F fluorescence in B. **(e)** Correlation between the spatially and temporally integrated Ca^{2+} transient magnitude (integrated over the whole FOV shown in b; 2-s post-stimulation integration time window; in units of "%s") and the NMDA spike amplitude, normalized to the amplitude of the evoked rCA3 EPSP preceding MF stimulation, for the example cell shown in a-d. Only supralinear events were analyzed. **(f)** Same as in e, plotting linear regression lines for all recorded cells shown in Figure 1i. **(g)** Comparison of correlation coefficients for all regression lines shown in f. Mean correlation coefficient $r = 0.96 \pm 0.01$, $n = 13$.

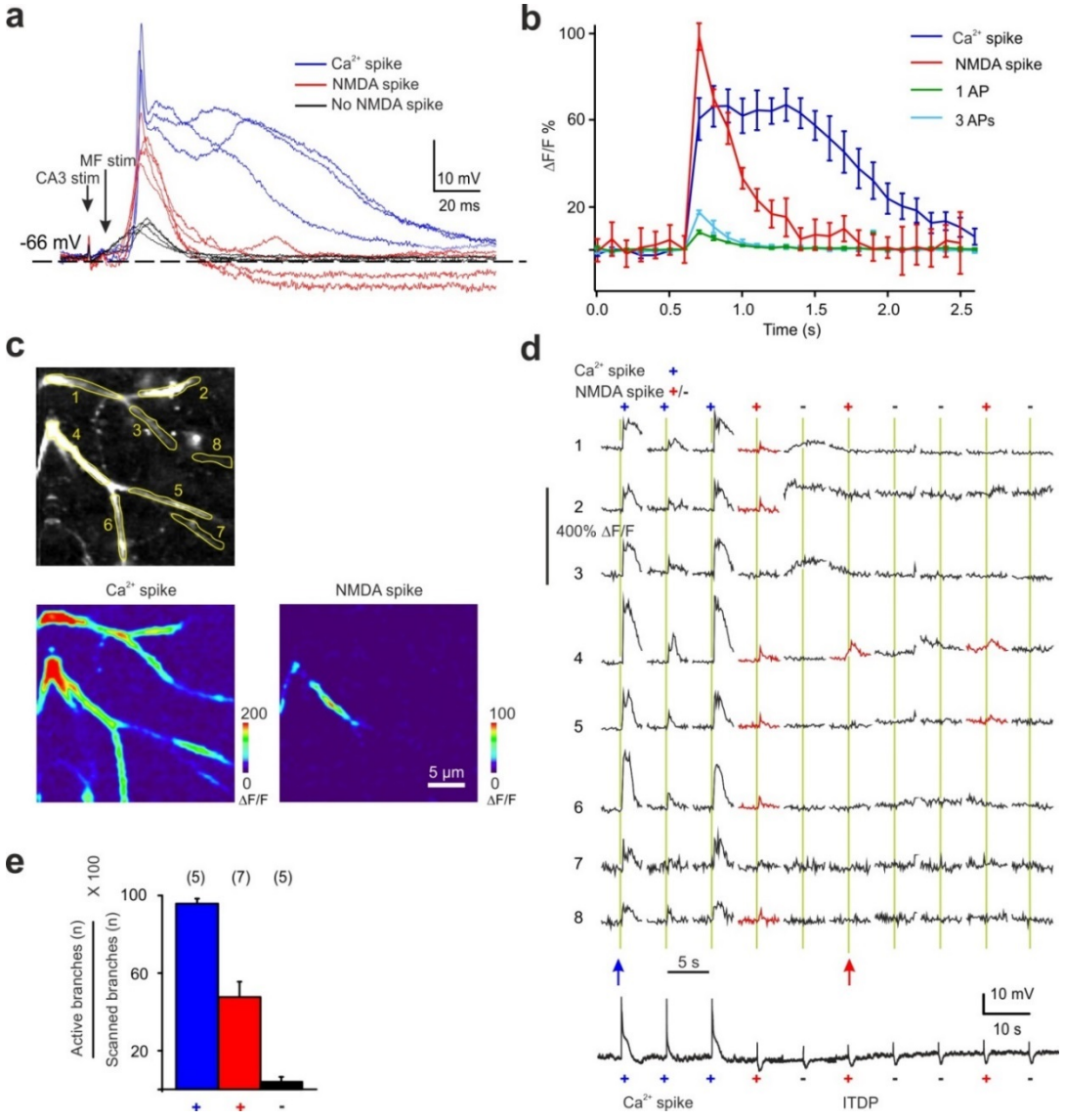

Supplementary Figure 4. Comparison of dendritic Ca^{2+} transients evoked either by NMDA spikes, by voltage-gated Ca^{2+} channels, or by back-propagating APs. (a) Responses in current clamp mode obtained by sequential pairing of a rCA3 EPSP and a MF EPSP with a delay of 10 ms. Incrementing stimulation intensities evoke first a linear response, then a supralinear NMDA spike, and finally a supralinear Ca^{2+} spike. **(b)** Distinct

dendritic Ca^{2+} transients associated with various dendritic electrical responses (*n* = 5). To allow comparison of response magnitudes, the same spatially restricted ROI (1 µm x 1 µm) was focused on the hotspot generated by the dendritic NMDA spike in the heat map to plot the averaged Ca^{2+} transients corresponding to the different responses (see Fig.1h,1; Supplementary Fig. 2h–j). Ca^{2+} transient integrals over a 2 s window were 121.1 ± 19.9%s (Ca^{2+} spike), 30.4 ± 4.5%s (NMDA spike), 2.0 ± 0.3%s (1AP), and 3.1 ± 1.2%s (3 APs). **(c)** Dendritic ROIs selected for the analysis of Ca^{2+} transients associated with an NMDA spike as compared with a Ca^{2+} spike. Ca^{2+} spikes are associated with a generalized dendritic Ca^{2+} signal, whereas the Ca^{2+} transients seen with NMDA spikes are spatially restricted. **(d)** Responses to 10 consecutive paired stimuli imaged in 8 ROIs. A blue "+" indicates Ca^{2+} spikes, which were evoked by suprathreshold stimuli, that is, sufficient to evoke APs; a red "+" indicates NMDA spikes, which were generated by subthreshold stimuli; a black "-" indicates trials in which the same intensity subthreshold stimuli elicited linear responses. Note that whereas NMDA spikes trigger Ca^{2+} transients that are restricted to a small subset of dendritic segments, Ca^{2+} spikes lead to a generalized response that is detected in all imaged dendritic branches. The blue arrow indicates traces corresponding to the image labeled Ca^{2+} spike in a. The red arrow indicates traces corresponding to the image labeled NMDA spike in A. Lowermost trace shows the current clamp recording during this imaging experiment. **(e)** Pooled data showing the proportion of imaged dendritic branches within a responsive FOV that exhibited a Ca^{2+} transient during a Ca^{2+} spike (blue) (95.5 ± 2.2%; *n* = 5) an NMDA spike (red) (52.6 ± 5.6%, *n* = 5), or no dendritic spike (black) (4.0 ± 2.2%, *n* = 5).

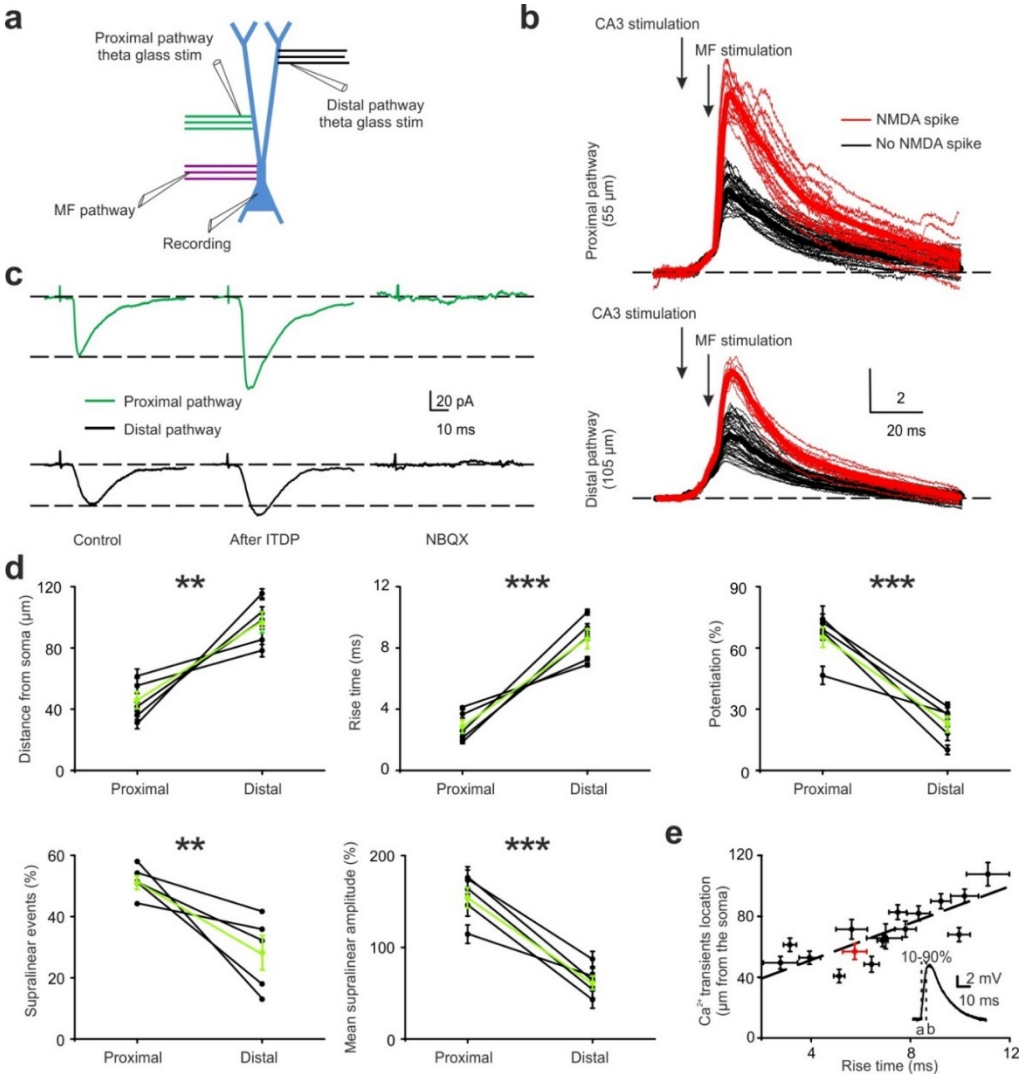

Supplementary Figure 5. Focal dendritic stimulation with theta glass electrodes confirms that the potentiation of rCA3 synapses with the ITDP protocol decreases as a function of their distance from the soma. (a) Experimental configuration with two theta glass stimulating electrodes positioned close to the dendrites at two different distances from the MF input, which is always close to the soma. **(b)** Responses to 60 repetitive pairings of a rCA3 EPSP followed by a MF EPSP to induce ITDP, normalized to the amplitude of the rCA3 EPSP. Both the amplitude and the probability for generating an NMDA spike are greater at proximal synapses versus distal synapses. **(c)** Averaged traces for rCA3 EPSCs showing a faster rise time and greater LTP at proximal versus distal synapses. **(d)** Pooled data comparing the rise time (proximal: 2.9 ± 0.4 ms, n = 5; distal: 8.6 ± 0.6 ms, n = 5, P = 0.006), the distance from soma of the stimulation electrode (proximal: 45.6 ± 5.6 µm, n = 5; distal: 23.0 ± 3.9 µm, n = 5, P < 0.001), the amount of potentiation (proximal: 65.6 ± 4.9%, n = 5; distal: 96.4 ± 6.8%, n = 5, P < 0.001), the number of NMDA spikes occurring during the 60 pairings (proximal: 51.7 ± 2.3%, n = 5; distal: 28.9 ± 5.6%, n = 5, P < 0.005), and the mean amplitude of the evoked NMDA spikes (proximal: 156.3 ± 11.1%, n = 5; distal: 63.8 ± 7.4%, n = 5, P < 0.001). **(e)** Pooled data for cells plotted in Fig. 1h demonstrating the positional correspondence of evoked EPSPs and imaged Ca^{2+} transients. rCA3 EPSP rise time (as a proxy for distance of the evoked EPSP from the recording electrode) was plotted against distance from the soma where Ca^{2+} transients were detected (r = 0.79 ± 0.01, n = 13). The red data point corresponds to the cell shown in Fig. 1.

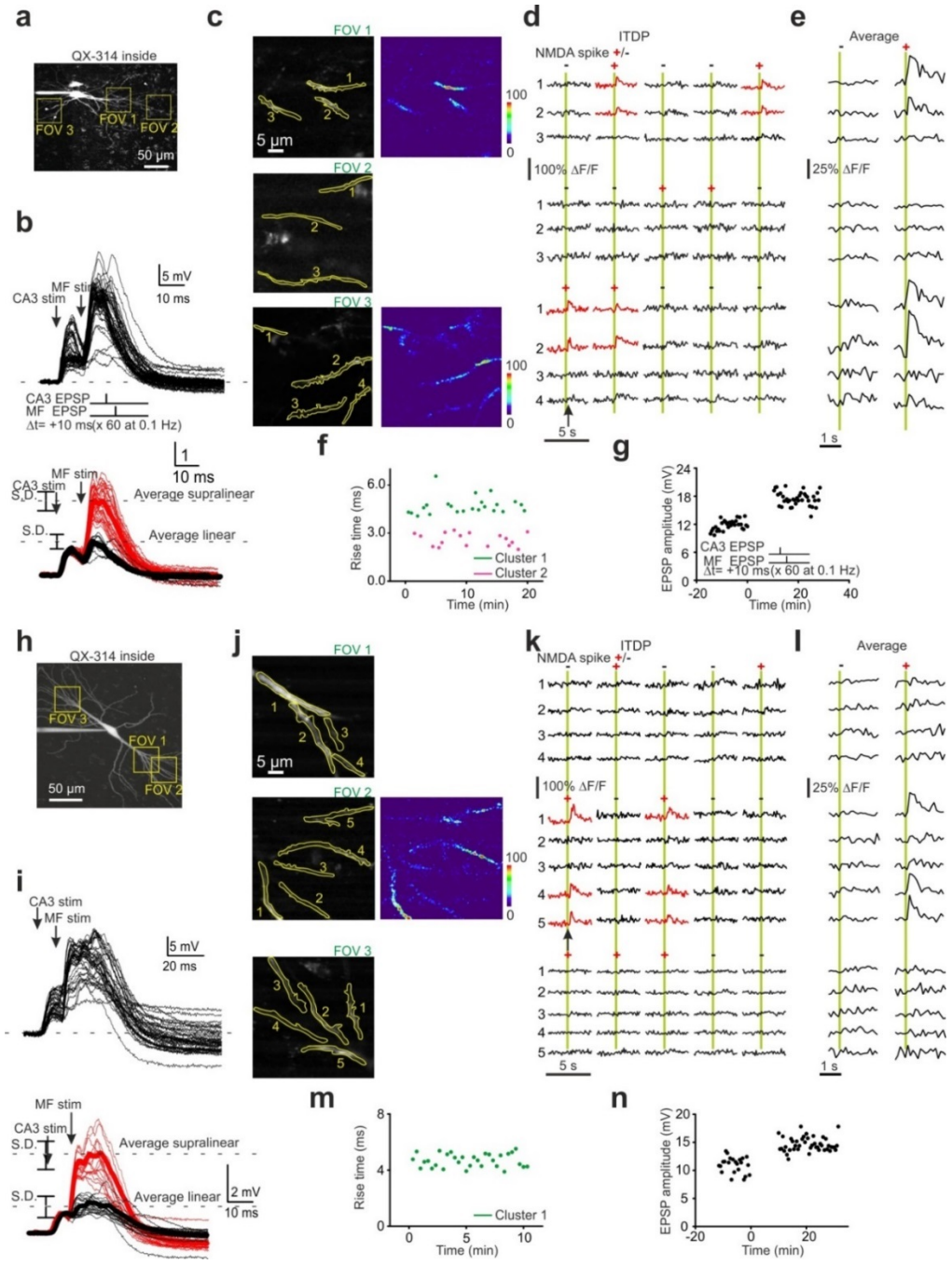

Supplementary Figure 6. In some experiments, stimulation led to activation of two spatially distinct groups of rCA3 inputs to a CA3 pyramidal cell evoking differentially localized dendritic Ca^{2+} transients. (a) A CA3 pyramidal cell labeled with Fluo-5F (100 µM) and Alexa 495 (10 µM) in which three fields of view were selected for analysis. **(b)** Above are raw data and below are traces normalized to the amplitude of the evoked rCA3 EPSP preceding the MF stimulus during 60 repetitive pairings (bottom). **(c)** ROIs in which dendritic Ca^{2+} transients were analyzed showing that Ca^{2+} transients were evoked in FOV 1 and FOV 2. **(d)** Responses to 5 representative consecutive pairings (green bars) imaged in the 3 fields of view during the ITDP protocol. **(e)** Averaged traces reveal that dendritic Ca^{2+} transients were associated with NMDA spikes (+) and were generated in two distinct circumscribed areas of the dendritic tree (FOV 1 in the apical part of the dendritic tree and FOV 3 in the basal tree). **(f)** Plotting the rCA3 EPSP rise time during the control period preceding the ITDP protocol revealed a bimodal distribution (cluster 1 and cluster 2), consistent with the

stimulation of two distinct groups of synapses localized in different parts of the dendritic tree. This phenomenon, in which two separate areas of the dendritic tree were activated with one extracellular stimulation electrode, was observed in 3 out of 13 cells. **(g)** Time course for LTP induction at the rCA3 input in response to the ITDP protocol. **(h-n)** Data from a similar experiment recorded from a different CA3 pyramidal cell. In this case, however, plotting the rCA3 EPSP rise time during the control period preceding the ITDP protocol revealed a homogeneous distribution indicating that the stimulated input activates a single clustered group of synapses. This pattern of dendritic activation fits with the imaging data in which Ca^{2+} transients were observed in only one FOV.

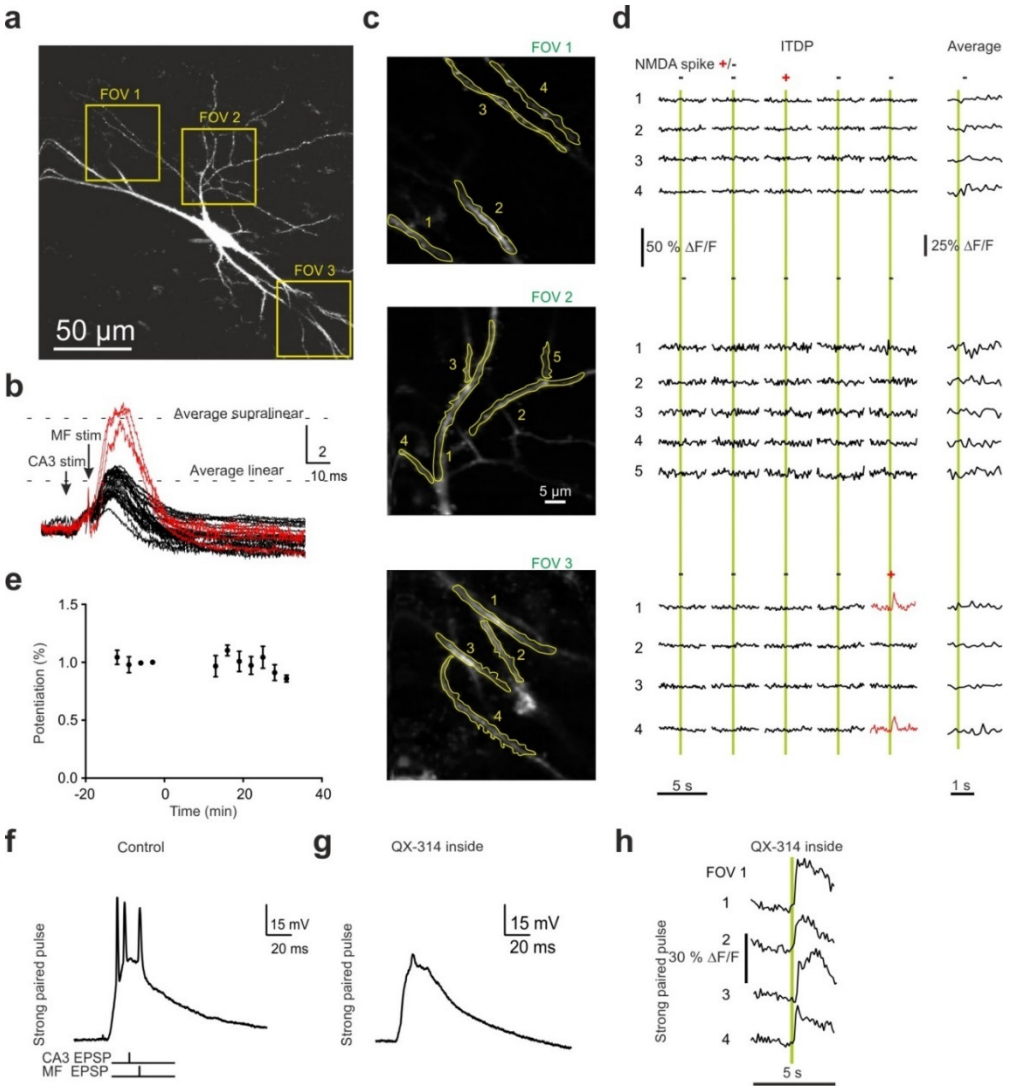

Supplementary Figure 7. When ITDP fails to trigger NMDA spikes, dendritic Ca^{2+} transients are not detected and LTP is not induced. (a) One of the group of three CA3 pyramidal cells represented as green data points in Figure 1h. **(b)** In these cells an NMDA spike was generated in less than 15% of the 60 pairings during the ITDP protocol. Responses are shown normalized to the amplitude of the rCA3 EPSP. **(c)** Images from three FOVs in regions of the dendritic tree indicated in a. **(d)** Recordings in the three FOVs during 5 consecutive pairings (green bars) of the ITDP protocol. Note that for this cell dendritic Ca^{2+} transients were almost never detected in any of the three FOVs. **(e)** Time course of the mean amplitude of the rCA3 EPSP before and after the ITDP protocol for the three cells represented as green data points in Figure 1h in which NMDA spikes were triggered rarely

and LTP was not induced. **(f)** A positive control showing that the absence of NMDA-spike-mediated Ca^{2+} transients is not due to a failure of Fluo-5F dialysis. At the beginning of the recording, prior to intracellular dialysis with QX-314, a high intensity paired pulse stimulus induces a complex Ca^{2+} spike. **(g)** After QX-314 dialysis the same intensity of stimulation evokes a complex Ca^{2+} spike without spikelets (as described previously[31]). **(h)** Ca^{2+} transients were detected in all ROIs during the occurrence of a complex Ca^{2+} spike.

NMDA spikes provide the postsynaptic depolarization for ITDP

We next sought to address the causal role of NMDA spikes in LTP induction by bidirectionally manipulating the probability of evoking NMDA spikes. In a first set of experiments, we examined whether LTP induction would be facilitated by enhancing the activation of extrasynaptic NMDA receptors, as these play a key role in the generation of NMDA spikes[24,25]. Using the above-described ITDP pairing protocol with sodium channels blocked by intracellular QX-314, we reduced the stimulation intensity below the threshold to evoke NMDA spikes reliably (in only 5.4 ± 2.0% of pairings, n = 8). Repetitive pairing for 60 times with this weak ITDP protocol failed to induce LTP (0.9 ± 0.5%, n = 8, P = 0.6; Fig. 2a, b). However, after inhibiting glutamate transporters with TBOA, a procedure that promotes glutamate spillover and activation of extrasynaptic NMDARs[28], stimulation with the same intensity significantly increased the probability of evoking NMDA spikes (in 46.4 ± 2.6% of pairings, n = 8, P < 0.001) and their normalized amplitude (from 95.3 ± 13% to 132.9 ±10.4%, n = 8, P < 0.01; Fig. 2b, c). Moreover, LTP was now observed at the rCA3 synapses (65.1 ± 4.3%, n = 8, P < 0.001, Fig. 2a, b).

In the next experiments, we reduced the probability of evoking NMDA spikes by hyperpolarizing the membrane potential and looked at the resulting change in the ability to induce LTP. At ~-60 mV (-60.5 ± 3.4 mV, n = 7), the pairing of rCA3 and MF inputs consistently resulted in NMDA spikes (45.6 ± 2.9% of pairings, n = 7, P < 0.001) whereas at more hyperpolarized membrane potentials (-74.2 ± 2.3 mV, n = 7), NMDA spikes were rarely evoked (in 6.1 ± 1.5% of pairings, n = 7; Fig. 2d-h). LTP could not be induced in the experiments with hyperpolarized membrane potential in which NMDA spikes were infrequent (rCA3 EPSP amplitude change: -1.2 ± 0.5%, n = 7, P = 0.7), while in the same cells at -60 mV LTP was observed in 7/7 experiments (58.1 ± 2.9%, n = 7, P < 0.001; Fig. 2g).

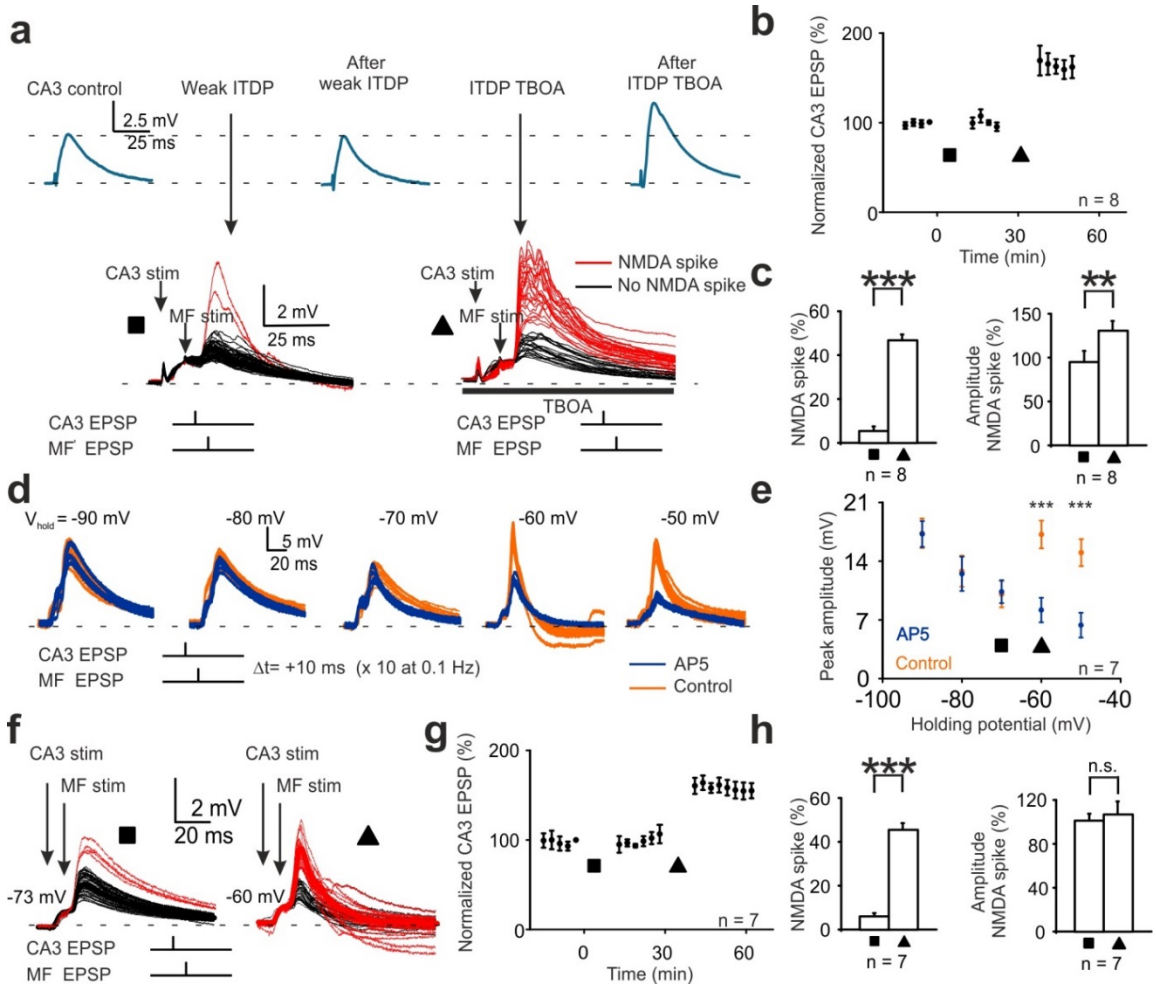

Figure 2. LTP induction can be manipulated bidirectionally by altering the probability of NMDA spikes. **(a)** Example voltage recording during a weak ITDP protocol, which was below threshold for consistently evoking NMDA spikes and did not potentiate the rCA3 EPSP (top, blue traces). Increasing glutamate spillover with 10 µM TBOA during a second pairing protocol in the same cell enhanced the probability of NMDA spikes (red traces) and induced LTP (square: ITDP; triangle: ITDP + TBOA). **(b)** Pooled data for rCA3 EPSP amplitude after the weak ITDP protocol was applied in the absence and presence of TBOA (rCA3 EPSP amplitude was measured after TBOA washout). **(c)** Pooled data for the probability of evoking an NMDA spike and for the NMDA spike amplitude in the two conditions. **(d)** Decreasing NMDA spike probability by hyperpolarizing the membrane potential. An evoked rCA3 EPSP was paired with a subsequent MF EPSP at decrementing holding potentials with and without NMDAR blockade (D-AP5). For each condition, pairing was repeated only 10 times to avoid inducing LTP. **(e)** Pooled data show a linear decrease in summated EPSP amplitude during NMDAR blockade when the holding potential becomes more depolarized (blue traces). Repeating the experiment without NMDAR blockade reveals a non-linear enhancement in EPSP amplitude at membrane potentials less negative than -70 mV (orange traces). **(f)** When the ITDP protocol was delivered at a hyperpolarized holding potential (more negative than -70 mV, square), where NMDARs do not contribute significantly to synaptic responses, NMDA spikes were rarely evoked. When the same protocol was repeated at -60 mV (triangle), NMDA spikes were evoked with high probability. **(g)** Time course of rCA3 EPSP amplitude showing that the ITDP protocol has no effect at -73 mV (square) but induces LTP at -60 mV (triangle). **(h)** Pooled data for NMDA spike incidence and amplitude for the two conditions.

NMDA spikes provide the postsynaptic depolarization for STDP

A dendritic event implicated in synaptic plasticity is the bAP[1,2]. However, it is possible that a bAP by itself has little direct effect on LTP induction and only becomes important if it triggers other dendritic events[3]. Because all of the above experiments were performed under conditions where action potentials were prevented, it was of interest to examine whether bAPs play a role in triggering NMDA spikes and if so, whether this process is reliable. We therefore paired the rCA3 EPSP with a back-propagating AP instead of a MF EPSP, which corresponds to a classical spike-timing dependent plasticity (STDP) protocol. Simultaneous recordings were obtained from a second-order apical dendrite and the soma (Supplementary Fig. 8). The stimulating electrode was positioned so as to activate rCA3 fibers that targeted mainly the dendrite recorded from, as indicated by the faster rise time and the greater amplitude of the rCA3 EPSP recorded in the dendrite versus the soma (dendrite: 6.1 ± 0.5 ms, soma: 9.2 ± 0.8 ms, P = 0.008; dendrite: 8.2 ± 1.9 mV, soma: 4.9 ± 0.7 mV, n = 5, P = 0.007; Fig. 3c). When this EPSP was followed after 10 ms by a single AP triggered with somatic current injection, an NMDA spike was never observed (n = 5; Fig. 3a, d). The contribution of NMDARs to the responses generated by this single AP STDP protocol as compared to the ITDP protocol was small but not negligible (13 ± 1.6% versus 102.1 ± 7.9%, n = 5, P = 0.0001; Fig. 3d). Weak activation of NMDARs as occurs in response to such a single bAP might therefore not be sufficient to produce LTP, as reported in other cell types[29-32]. To test this possibility directly we paired the bAP with synaptic input over 50 trials at 0.3 Hz. As show in Fig. 3a, e, this protocol did not induce LTP (2.2 ± 2.4%, n = 5, P = 0.7). Thus, simply activating NMDARs may be insufficient for LTP induction if the generated response is below threshold to evoke an NMDA spike. Previous studies in other cell types have shown that whereas STDP is difficult to evoke using a single bAP, brief bursts of bAPs can be effective[2,31,32]. When the rCA3 EPSP was paired after a 10 ms delay with three APs at 200 Hz, an NMDA spike of dendritic origin was evoked with high probability (61.2 ± 9.3%, n = 5; Fig. 3a, d). Repetitive pairing with this STDP protocol induced strong LTP (44.9 ± 9.9%, n = 5, P = 0.0033; Fig. 3a, e). Thus, AP firing has to attain a critical frequency to evoke NMDA spikes and to induce LTP (Supplementary Fig. 9).

To further clarify the role of bAPs in modulating the probability of evoking an NMDA spike, we tested a STDP protocol in which a hyperpolarizing pulse was applied

through the dendritic recording electrode during the triggering of the three APs, which prevented NMDA spikes (Fig. 3f, h). Importantly, the injected current did not hyperpolarize the membrane below the threshold for AP generation (Fig. 3f) and did not markedly reduce the “non-regenerative” NMDA component of the response (11.7 ± 2.6%; n = 5, P = 0.002; Fig. 3h). Again, rCA3 fibers were stimulated that targeted mainly the dendrite recorded from, as indicated by the faster rise time and the greater amplitude of the rCA3 EPSP recorded in the dendrite versus the soma (dendrite: 5.6 ± 0.6 ms, soma: (8.7 ± 0.7 ms recording, n = 5, P = 0.0008). With this protocol LTP was not induced (3.76 ± 3.84%, n = 5, P = 0.3; Fig. 3f, i), showing that the occurrence of bAPs *per se* is not sufficient to initiate synaptic plasticity. In the same cell the omission of the hyperpolarizing pulse recovered NMDA spikes (59.5 ± 7.2%, n = 5, Fig. 3h) and repetitive pairing now induced LTP (43.9 ± 2.9%, n = 5, P < 0.0001; Fig. 3f, i). Taken together these data show that NMDA spikes are the critical event in both subthreshold and suprathreshold forms of LTP at rCA3 synapses.

The bAPs associated with STDP protocols also activate voltage-gated Ca^{2+} channels that may trigger dendritic Ca^{2+} spikes[2,33,34]. After pharmacological block of Ca^{2+} currents, however, the supralinear response persisted (Supplementary Fig. 9f, g).

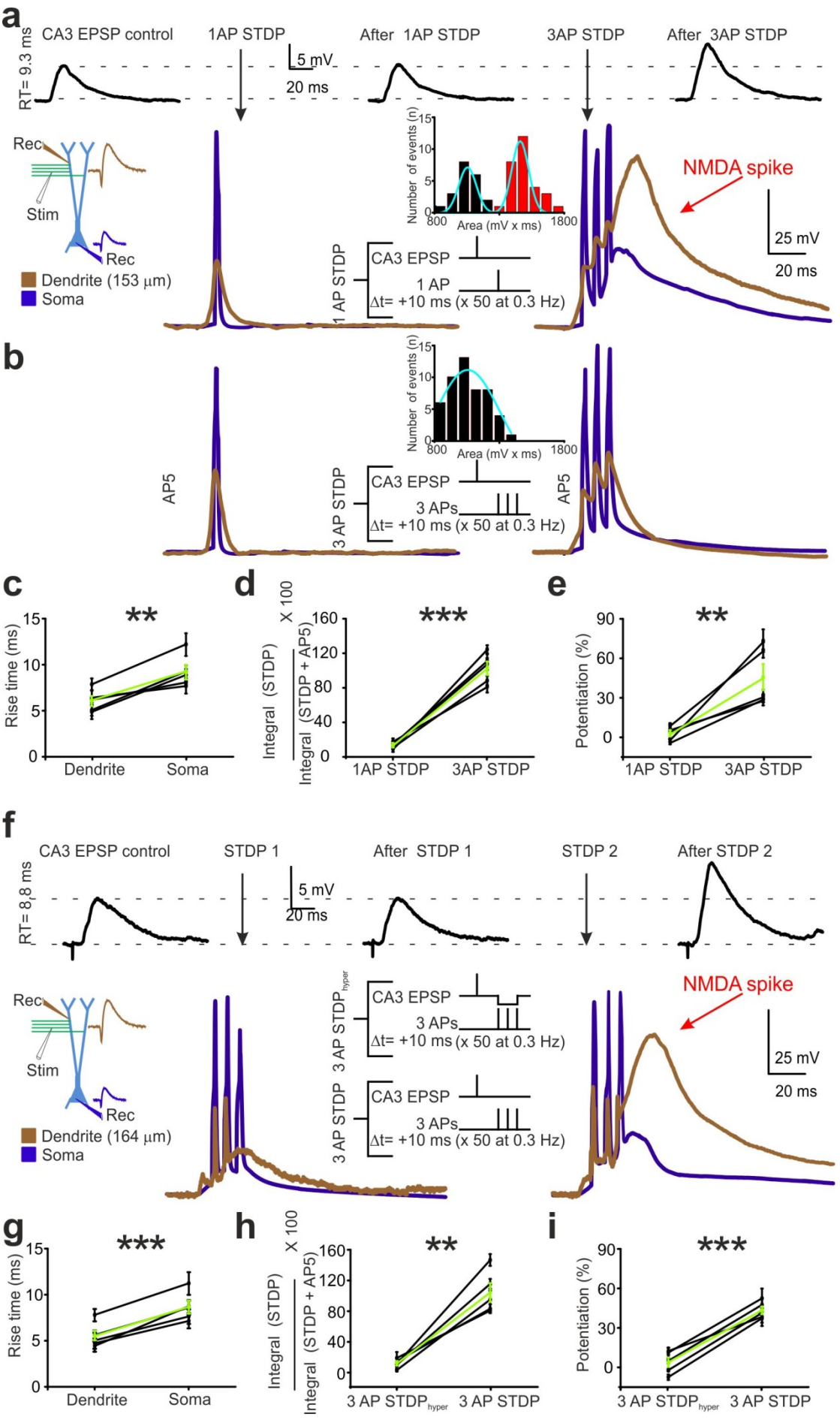
a
CA3 EPSP control
1AP STDP
After 1AP STDP
3AP STDP
After 3AP STDP
RT= 9.3 ms
5 mV
20 ms
Rec
Stim
Rec
Dendrite (153 µm)
Soma
Number of events (n)
Area (mV x ms)
800
1800
CA3 EPSP
1 AP
Δt= +10 ms (x 50 at 0.3 Hz)
1 AP STDP
NMDA spike
25 mV
20 ms
b
AP5
3 AP STDP
CA3 EPSP
3 APs
Δt= +10 ms (x 50 at 0.3 Hz)
c
Rise time (ms)
Dendrite
Soma
d
Integral (STDP) / Integral (STDP + AP5) X 100
1AP STDP
3AP STDP
e
Potentiation (%)
f
CA3 EPSP control
STDP 1
After STDP 1
STDP 2
After STDP 2
RT= 8,8 ms
Dendrite (164 µm)
3 AP STDP hyper
g
h
i
3 AP STDP hyper

Figure 3. STDP protocols induce LTP only if NMDA spikes are generated. **(a)** Representative voltage traces recorded simultaneously at the soma and a second-order dendrite (see schematic), first during an STDP protocol pairing rCA3 EPSPs with a single AP evoked by brief somatic current injection (2 ms; 4 nA; left), followed by pairing with three evoked APs delivered at a frequency of 200 Hz (right). A 1 AP STDP protocol failed to potentiate EPSPs whereas 3 AP STDP resulted in LTP (top traces). Note that the 1 AP STDP protocol was generally insufficient to generate a supralinear dendritic response, whereas the 3 AP STDP protocol caused dendritic spikes visible in the dendritic recording and to a lesser extent, because of cable filtering, in the somatic recording. Inset: Area under the evoked responses was plotted to distinguish between linear and supralinear events. **(b)** Supralinear responses with the 3 AP STDP protocol were prevented following NMDAR blockade (D-AP5, 1.4 ± 3.2%, $n = 5$, $P < 0.0001$). Inset: Supralinear responses are prevented when NMDARs are blocked. **(c)** Faster EPSP rise times in dendrite versus soma indicates that for these experiments a majority of the synapses activated by stimulation of rCA3 collaterals were located at or near the dendritic branch recorded from. The green line denotes the pooled average of all cells. **(d)** The NMDAR contribution generated by the different STDP protocols was estimated by calculating the ratio between the areas under the voltage traces in the absence and presence of D-AP5. **(e)** When the STDP protocol did not adequately activate NMDARs to generate a supralinear response, LTP was not induced. **(f)** A hyperpolarizing pulse applied during the 3 AP STDP protocol decreased the probability of evoking an NMDA spike and prevented LTP induction. As a result, a supralinear response was not generated, either in the soma (blue trace) or the dendrite (brown trace). Furthermore, the rCA3 EPSP was not potentiated (black traces: rCA3 EPSP recorded in the soma). When the same protocol was repeated, but without the hyperpolarizing pulse, supralinear responses were generated and LTP was induced. **(g)** Pooled data showing faster rise times for the rCA3 EPSP in the dendritic as compared to the somatic recording indicating that primarily dendritic inputs were stimulated. **(h)** Quantification of the contribution mediated by NMDARs to the recorded responses shows that the STDP protocol that included a hyperpolarizing pulse (3AP STDPhyper) inhibited the generation of a supralinear signal versus without the hyperpolarization (3AP STDP). **(i)** In addition, the STDP protocol that included a hyperpolarizing pulse greatly reduced the magnitude of LTP at the rCA3 synapse.

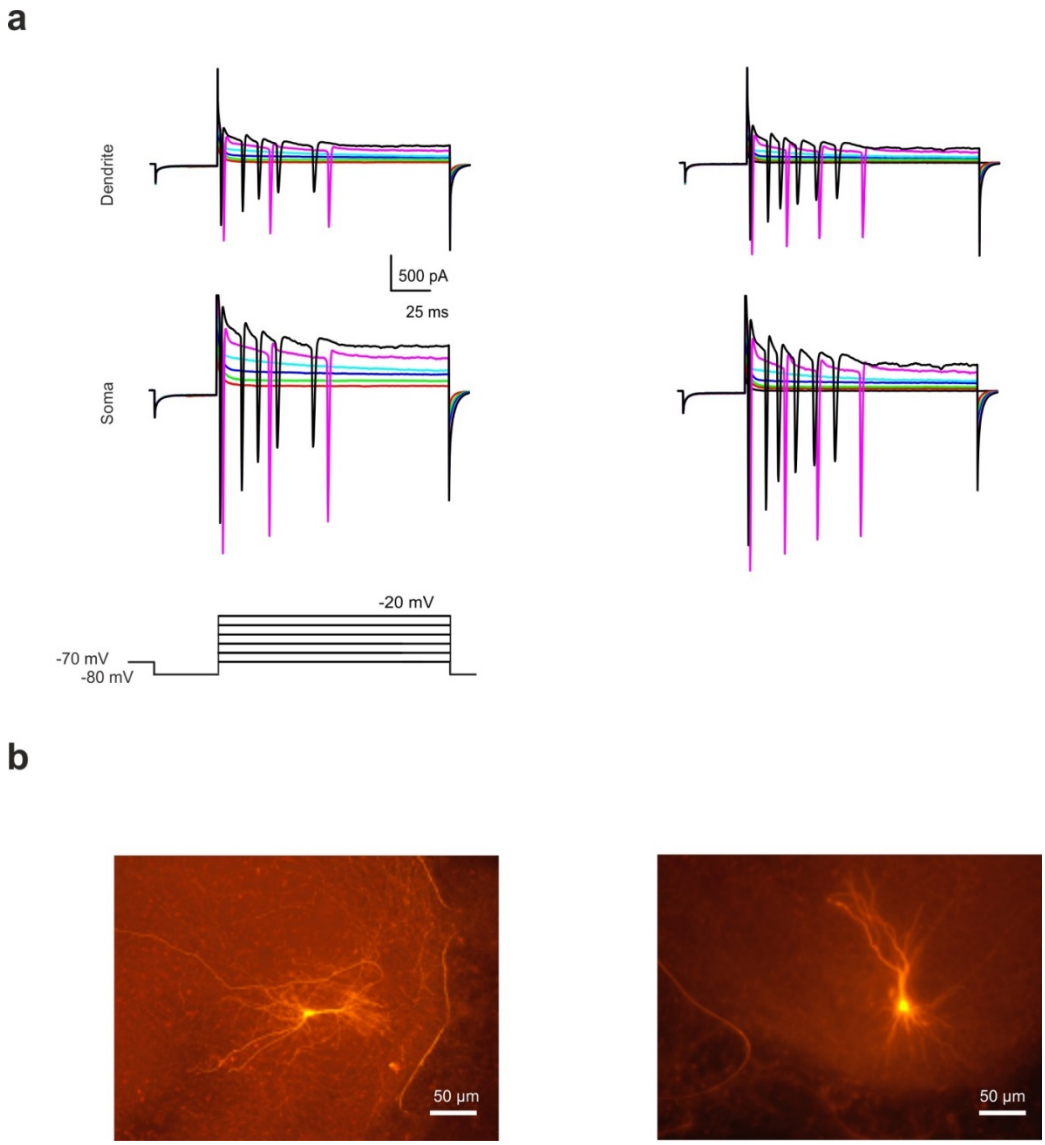

Supplementary Figure 8. Criteria to confirm that the electrodes are targeting the same neuron in dual patch recordings from the soma and a dendrite. (a) At the beginning of experiments with dual patch recordings from the same cell, voltage steps (inset) were applied to the voltage-clamped CA3 pyramidal cell through the somatic electrode. The synchronicity of the evoked suprathreshold responses (action currents) indicates that both electrodes were contacting the same cell, thereby ruling out synaptic responses between the two cells. **(b)** Biocytin was included in both recording pipettes and slices were fixed in PFA after experiments. Immunostaining revealed only one labeled neuron per slice confirming that both patch pipettes were in the same neuron.

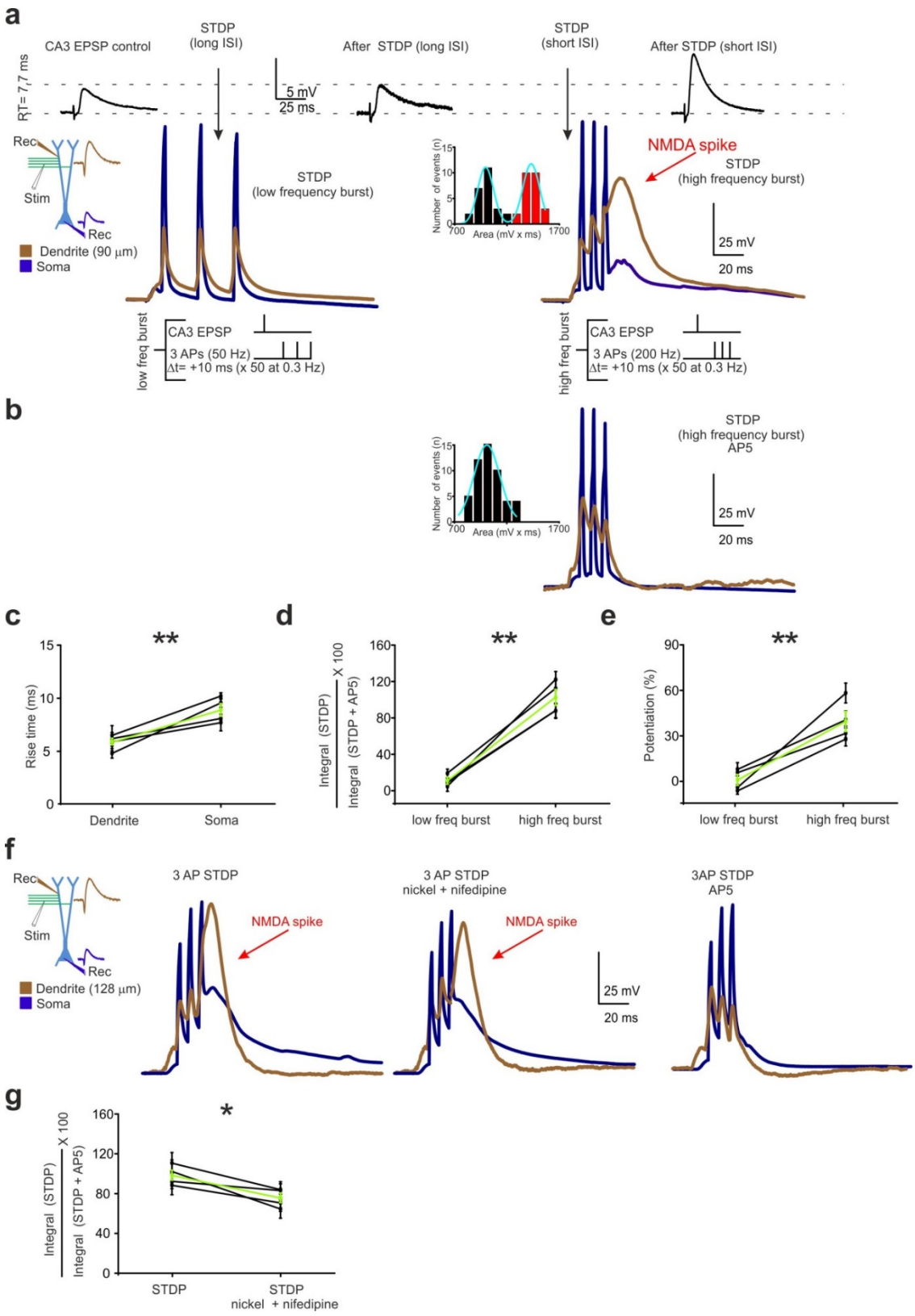

Supplementary Figure 9. A critical frequency of AP firing must be exceeded during STDP in order to evoke an NMDA spike and to induce LTP. (a) Representative traces from experiments in which simultaneous recordings from the soma and from a second order dendrite are compared during a standard STDP protocol consisting of a rCA3 EPSP followed by three APs at low (50 Hz) or high frequency (200 Hz) evoked by a three pulse current injection (2 ms; 4 nA for each AP). rCA3 EPSPs do not potentiate with the low frequency

protocol but undergo LTP with the high frequency STDP protocol (black traces: rCA3 EPSPs recorded in the dendrite). Below: Only the high frequency STDP protocol reliably generates a supralinear response (62.8 ± 8.8%, n = 5, P < 0.001). EPSP–AP pairing with a low-frequency (50 Hz) burst of APs failed to trigger NMDA spikes and to induce LTP. Inset: Area under the evoked responses was plotted to distinguish between linear and supralinear events. **(b)** The supralinear response is abolished following NMDAR blockade (D-AP5). Inset: Supralinear responses are prevented when NMDARs are blocked. **(c)** Faster EPSP rise times in dendrite versus soma indicates that for these experiments a majority of the synapses activated by stimulation of rCA3 collaterals were located at or near the dendritic branch recorded from. The green line denotes the pooled average of all cells. **(d)** The contribution mediated by NMDARs to responses generated by the low and high frequency STDP protocols was quantified by calculating the ratio between the areas under the traces in the absence and the presence of D-AP5 (low frequency burst: 10.6 ± 3.0%, high frequency burst: 102.5 ± 8.7%, n = 5, P < 0.001). **(e)** Pooled data showing that potentiation at the rCA3 synapse is only induced in response to the high frequency STDP protocol (low frequency: 2.1.5 ± 5.5%, high frequency: 59.4 ± 7.4%, n = 5, P < 0.001). **(f)** Evidence that an NMDA spike rather than a Ca^{2+} spike underlies the supralinearity observed with the high frequency STDP protocol. The supralinearity in response to the STDP protocol is maintained in the presence of voltage-gated Ca^{2+} channel antagonists (nifedipine 5 μM, nickel 50 μM), albeit with reduced magnitude (area under the trace: from 98.6 ± 5.0% in control conditions to 75.8 ± 4.8% in presence of Ca^{2+} channel blockers, n = 4, P < 0.05, paired t test). Blocking NMDARs abolishes the supralinear response. **(g)** The magnitude of the supralinearity was estimated by calculating the ratio between the areas under the traces in the absence and the presence of D-AP5. This analysis reveals that antagonists of voltage-dependent calcium channels lead to a reduction in the responses. Thus, the back propagating APs induced by somatic spiking during the high frequency STDP protocol also activate Ca^{2+} channels, as reported previously[6].

DISCUSSION

We have presented several lines of evidence for a direct causal role of dendritic NMDA spikes in the induction of LTP at excitatory recurrent synapses onto CA3 pyramidal cells. We were able to evoke dendritic electrical signals definitively identified as NMDA spikes and to show that manipulations that increased the probability of NMDA spikes increased LTP whereas manipulations that decreased their probability reduced LTP. NMDA spikes were the critical trigger both when LTP was induced with subthreshold events using an ITDP protocol as well as with bAPs using a classical STDP paradigm. Thus, our results also provide new insights into the function of bAPs. According to the text-book description of STDP, such spikes, when timed after the onset of EPSPs, provide the crucial depolarization to initiate LTP. However, for CA3 pyramidal cells this timing rule is not absolute, depending on the age of the animal[35,36]. As shown here and previously[9], at synapses between CA3 pyramidal cells LTP can be induced in the absence of bAPs. Nevertheless, bAPs, which can be boosted during concurrent synaptic input[37], may have an indirect role in inducing synaptic plasticity. In our study, brief bursts of bAPs evoked NMDA spikes, which in turn induced LTP. Thus, the NMDA spike rather than the bAP is the final effector of LTP at the CA3 synapses we have studied. Determining the postsynaptic depolarization necessary for LTP in CA3 recurrent synapses is of particular significance because both theoretical and experimental work point to the critical role of this brain region in autoassociative memory[38-40].

Our findings raise the question whether NMDA spike-mediated subthreshold LTP induction represents a special property of recurrent synapses in the CA3 area or whether NMDA spikes may also be involved at other synapses. Previous work in diverse brain areas has shown that dendritic spikes generate the supralinear signal triggering plasticity at synapses where LTP can occur independently of bAPs[5,6,11,12,13]. Specifically for NMDA receptor-dependent dendritic spikes, *in vivo* investigations have provided correlative evidence for their role in synaptic plasticity in CA1 pyramidal cells[41], in motor cortex[10], and in barrel cortex[11]. Although these studies did not rigorously establish the unique role of NMDA spikes as in our experiments, they are consistent with our conclusion that dSpikes rather than bAPs provide the critical depolarization for LTP. Thus, NMDA spikes appear to be

important for LTP at synapses in diverse brain regions, but other synapses have been shown depend on other types of supralinear signaling[8,12,13,14]. It should be noted that under *in vivo* conditions, the impact of NMDA spikes on the induction of plasticity may be less pronounced than in our strictly controlled *in vitro* experiments. Similarly, although STDP protocols have been shown to alter neuronal properties at the single neuron level *in vivo*[42], STDP effects reported from *in vitro* experiments tend to be stronger and more robust, presumably because of the absence of modulatory variables relating to behavioral state, background neuronal activity, and physiological brain rhythmicity, which are difficult to control for during *in vivo* experiments[43].

Our data indicate that on the order of 10 NMDA spikes (~20% of the responses during the 60 trial protocol lasting 6 minutes) are sufficient to induce LTP, which is in the same range as the number of bursts that a hippocampal pyramidal cell fires as an animal traverses the cell's place field[44]. Significant LTP may thus be induced by a single experience. In this respect it is of interest that the long-term representation of space by CA1 hippocampal place cells in navigating mice depends directly on the prevalence of dendritic branch spikes[41,45]. Our data provide further support for the concept of the dendritic branch rather than the dendritic spine as the functional unit for LTP induction[46-48]. NMDA spikes in CA3 pyramidal cells are generated when approximately 15 synapses are activated synchronously on a dendritic segment[20,49], which is a relatively small number considering that 15 synapses represent < 5% of the synapses present in a dendritic segment[20]. This observation is consistent with the compartmentalization of correlated inputs onto single dendritic segments during hippocampal development[50-52]. Such clustered input provides the structural basis for the generation of spatially-restricted NMDA spikes and their critical role in LTP induction.

MATERIALS AND METHODS

Preparation of acute hippocampal slices

Acute slices were prepared from 3-week-old Wistar rats following a protocol approved by the Veterinary Department of the Canton of Zurich. (approval ID 81-2014). Rats were decapitated and brains quickly removed in an ice-cold artificial cerebrospinal fluid (ACSF) solution containing the following (in mM): 125 NaCl, 2.5

KCl, 1.25 NaH_2PO_4, 25 $NaCHCO_3$, 1 $MgCl_2$, 2 $CaCl_2$, 10 glucose (pH 7.4) and equilibrated with 95% O_2 and 5% CO_2. 300 µm thick transverse acute slices were prepared with a vibratome (HM 650V, Microm International) in ice-cold ACSF. Sections were incubated in ASCF for 20 min at 34 °C and then kept at room temperature for at least 1 hour before recording. Experiments with acute slices are depicted in Supplementary Figure 10.

Preparation of hippocampal slice cultures

All other experiments were performed in slice cultures, which form a quasi-monolayer that facilitates dendritic imaging. Slice cultures were prepared from 6-d-old Wistar rats according to the Gähwiler method[53]. Transverse slices were prepared (400 µm) and fixed to coverslips with clotted chicken plasma. These were placed in sealed test tubes with serum-containing medium and maintained in a moving incubator at 36 °C for 21 – 28 days.

Patch-clamp recording

Hippocampal slice cultures or acute slices were mounted in a recording chamber positioned on an upright microscope (Zeiss Axioskop FS1) or for combined imaging, a Scientifica microscope. Slices or slice cultures were superfused with an external solution (pH 7.4) containing (in mM): 137 NaCl, 2.7 KCl, 11.6 $NaHCO_3$, 0.4 NaH_2PO_4, 2 $CaCl_2$, 2 $MgCl_2$, 5.6 D-glucose, and 0.001% phenol red to monitor pH for slice cultures and 125 NaCl, 2.5 KCl, 1.25 NaH_2PO_4, 25 $NaCHCO_3$, 2 $CaCl_2$, 2 $MgCl_2$, 10 glucose (pH 7.4) and equilibrated with 95% O_2 and 5% CO_2 for acute slices. All experiments were performed at 34 °C. Patch pipettes had a resistance between 5 - 7 MΩ for somatic whole-cell recordings of CA3 pyramidal cells and between 9 - 11 MΩ for recordings from second order dendrites. Both somatic and dendritic patch pipettes were filled with (in mM): 135 K-gluconate, 5 KCl, 10 Hepes, 1 m EGTA, 5 phosphocreatine, 2 MgATP, 0.4 NaGTP, and 0.07 $CaCl_2$ (pH 7.2). In experiments in which imaging was performed, Fluo-5F (100 µM) and Alexa 495 (10 µM) were added to the solution. Resting membrane potential of the hippocampal CA3 pyramidal cells was −64.1 ± 2.9 mV, n = 53). Voltage commands were corrected for the liquid junction potential (8.3 mV). No differences were apparent in the properties of NMDA spikes recorded in slice cultures and in acute slices (Supplementary Fig. 10).

For the determination of current-voltage relationships, command potentials had a duration of 1 s to ensure steady-state responses. Data were recorded with Axopatch 200B amplifiers (Molecular Devices), digitized at 4 kHz for current-clamp and 5 kHz for voltage-clamp, and analyzed off-line with pCLAMP 10 (MolecularDevices) and Origin (OriginLab). In all experiments, inhibitory postsynaptic potentials were reduced in the recorded CA3 pyramidal cells by adding picrotoxin (1 mM) to the patch solution. Series resistance (typically 8.5 – 14.5 MΩ for somatic recordings and 15 – 35 MΩ for dendritic recordings) was monitored regularly, and cells were excluded if a change of >20% occurred during the recording. For experiments involving extracellular stimulation, the electrode placement, the paired pulse ratio, the response latency, and the sensitivity of transmission to DCG-IV were assessed to differentiate between responses mediated by MFs versus rCA3 fibers (Supplementary Fig. 11).

Stimulation paradigm

CA3 pyramidal cells receive excitatory input in a spatially segregated manner:

1) Mossy fibers (MFs), the axons of the dentate granule cells, contact the emerging trunk of the apical and basal dendritic tree[22].

2) Recurrent collaterals (rCA3s), the axons of neighboring CA3 pyramidal cells, target the intermediate region of the apical and basal dendritic tree[54].

3) Perforant path axons, originating in the entorhinal cortex, contact the distal portion of the apical dendritic tree[54].

Consistent with this innervation pattern, our experiments show that Ca^{2+} transients associated with NMDA spikes occur both in the apical and basal dendritic tree. Dendritic Ca^{2+} transients were evoked mainly in the apical dendritic tree when the rCA3 stimulating electrode was placed in the stratum radiatum of CA3 and the MF electrode in the dentate gyrus. Dendritic Ca^{2+} transients were evoked mainly in the basal dendritic tree when the rCA3 stimulating electrode was placed in the stratum oriens of CA3 and the MF electrode in the dentate gyrus. The identity of the stimulated fiber tracts was ascertained using standard criteria (Supplementary Fig. 11).

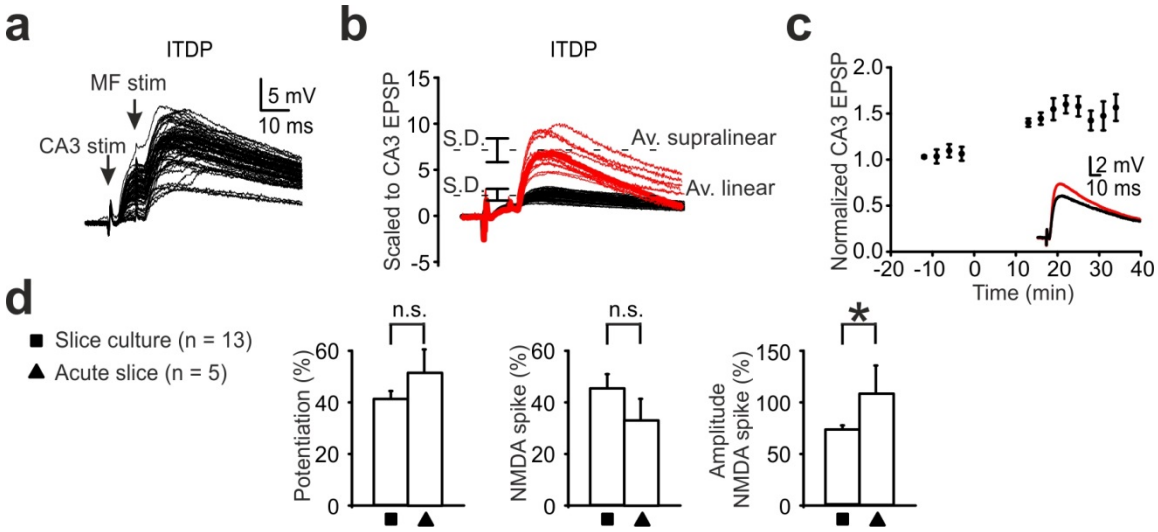

Supplementary Figure 10. NMDA spikes in hippocampal CA3 pyramidal cells exhibit similar properties in acute slices and in organotypic slice cultures. (a) Responses induced by pairing of a rCA3 EPSP followed by a MF EPSP. **(b)** Scaling to normalize the traces to the amplitude of the rCA3 EPSP reveals linear responses (black) and supralinear responses (red) corresponding to NMDA spikes. **(c)** The presence of NMDA spikes is associated with the induction of LTP Inset: rCA3 EPSPs before (black) and after (red) the ITDP pairing protocol. **(d)** Differences in NMDA spike properties recorded in acute slices (no Fluo-5F) versus cultured slices (Fluo-5F) are not significant except for a slight difference in amplitude. Potentiation: acute slice: 51.8 ± 10.5% after 30 min, *n* = 5/7, slice culture: 41.9 ± 2.3% *n* = 13/16, *P* = 0.08. Percent of supralinear events during 60 rCA3/MF pairings: acute slice: 32.5 ± 8.5%, *n* = 5, slice culture: 45.3 ± 3.2%, *n* = 13, *P* = 0.07. Amplitude of supralinear events normalized to rCA3 EPSP amplitude: acute slice: 105.8 ± 27.3%, *n* = 5, slice culture: 71.5 ± 2.7%, *P* = 0.02.

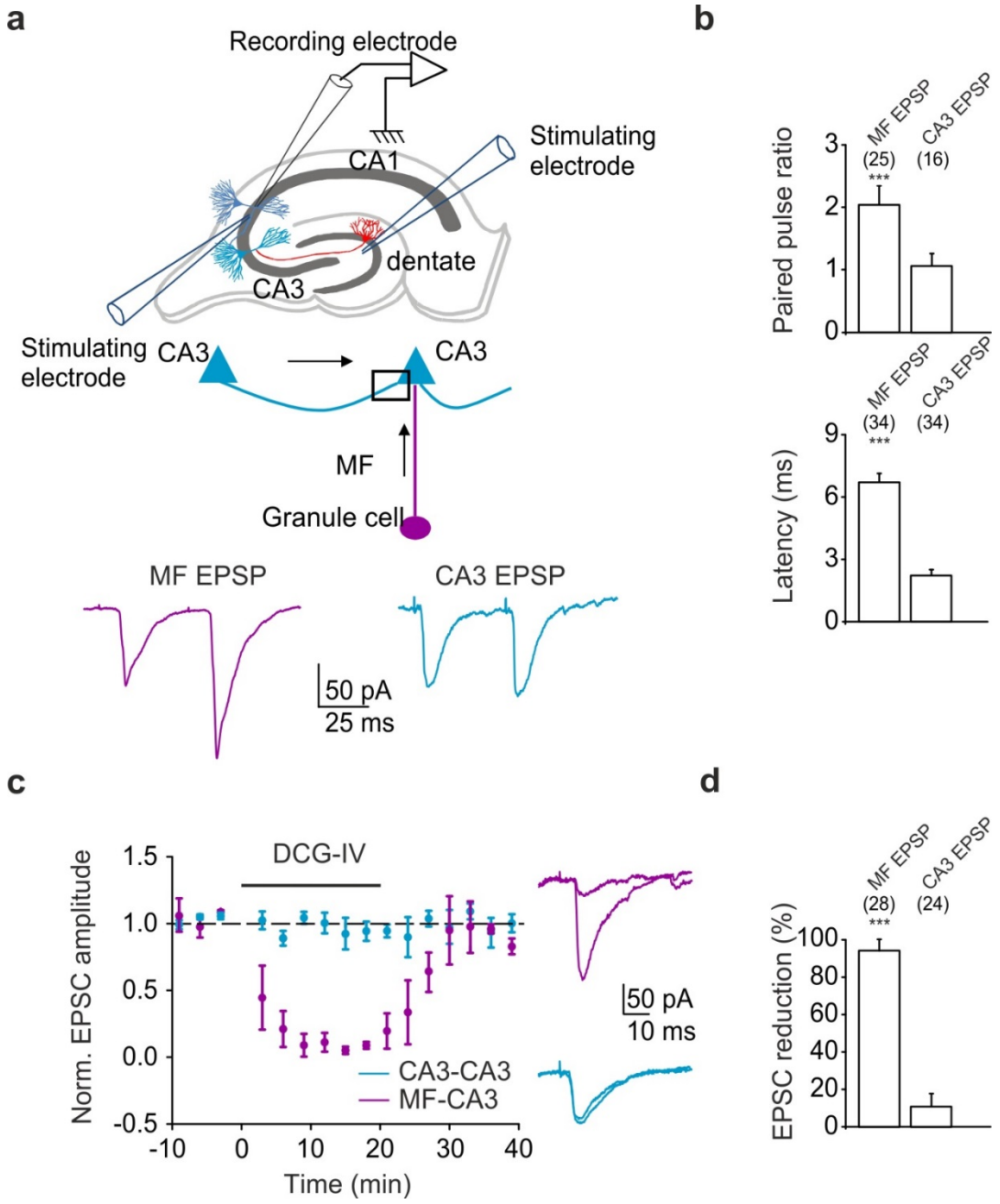

Supplementary Figure 11. Criteria for differentiating between responses evoked by stimulating mossy fibers versus rCA3 fibers. (a) Experimental recording configuration. Insets show representative EPSCs recorded in a CA3 pyramidal cell that were evoked by paired-pulse stimulation with a 50 ms interval either of mossy fiber or of rCA3 fibers. **(b)** Pooled data. Mossy fiber stimulation results in paired-pulse facilitation (ratio: 2.1 ± 0.8, *n* = 25), whereas rCA3 fiber stimulation induces either paired-pulse facilitation or depression (ratio: 1.2 ± 0.6, *n* = 25, *P* < 0.001, paired t-test). Moreover, the latency of evoked EPSCs is greater after stimulating mossy fibers as compared to rCA3 fibers (6.7 ± 0.3 ms, versus 2.4 ± 0.1 ms, *n* = 34, *P* < 0.001 paired t-test). **(c)** Bath-application of DCG-IV (2 µM), a Group II metabotropic glutamate receptor agonist that blocks glutamate release from mossy fibers but not from CA3 pyramidal cell terminals, selectively diminishes mossy fiber but not rCA3 responses (MF: 91.3 ± 5.1%, *n* = 28, *P* < 0.00.1; rCA3: 11.9 ± 6.4%, *n* = 24, *P* = 0.2, paired t-test). **(d)** Pooled data for DCG-IV experiments.

NMDA spike analysis

Supralinear responses, which correspond to NMDA spikes, were revealed by normalizing the amplitude of the evoked rCA3 EPSP preceding MF stimulation (e.g. Fig. 1c). All 60 paired responses were scaled to the amplitude of the rCA3 EPSP revealing a bimodal distribution.

The probability of evoking an NMDA spike, p_{NMDAsp}, was calculated as follows:

$$p_{NMDAsp} = \frac{n_{supra}}{60} \text{ x } 100\%$$

The amplitude of an NMDA spike, A_{NMDAsp}, was expressed as the percentage increase compared to the amplitude of the mean linear response, $\bar{A}_{linear}$ (peak of the first Gaussian, e.g. Fig. 1c):

$$A_{NMDAsp} = \left(\frac{A_{NDMAsp}}{\bar{A}_{linear}} \text{-1}\right) \text{x } 100\%$$

Two-photon Ca^{2+} imaging

CA3 pyramidal neurons were loaded with Fluo-5F (100 µM) and Alexa Fluor 495 (10 µM; Molecular Probes) through the recording pipette for at least 20 min prior to two-photon imaging. Neurons were imaged using a two-photon microscope (Scientifica) equipped with a Ti:sapphire laser (Tsunami, Spectra Physics) tuned to 840 nm and a 40x water-immersion objective lens (0.8 NA, Olympus). Laser power under the objective was typically between 10 - 15 mW. Fluorescence was detected using two photomultiplier tubes using 525/50 nm (green channel) and 620/60 nm (red channel) emission filters. Scanning and image acquisition were controlled by HelioScan software[55] Time series of Fluo-5F fluorescence images were acquired at 10 Hz with 100 x 100 pixel resolution across imaging fields encompassing neuronal dendrites. The dimensions of a field of view (FOV) were 30 µm x 30 µm.

For the imaging experiments the ITDP protocol consisted of 60 pairings. As it was of interest to compare responses between different FOVs, images were obtained sequentially from each FOV resulting in data sets consisting of 30 responses when 2 FOVs were selected or 20 responses when 3 FOVs were selected. Simultaneous data acquisition from more than one FOV would have resulted in images with insufficient resolution for detailed analysis. In this respect it should be noted that we

previously found no change in the probability of evoking an NMDA spike over the time course of the 60 pairings (Supplementary Fig. 4 in Brandalise and Gerber, 2014).

At the end of each experiment, a z-stack of the fluorescently labeled CA3 pyramidal cell was acquired. Dye which inadvertently leaked from the recording pipette was sometimes taken up surrounding by glia cells. Data were analyzed with NIH ImageJ and Igor Pro (WaveMetrics) software. In ImageJ, dendrites segments were manually selected as regions of interest (ROIs). Ca^{2+} signals were expressed as $\Delta F/F = (F-F_0)/F_0$ where F and baseline F_0 represent mean fluorescence values in an ROI. A Ca^{2+} transient was accepted as a signal when its amplitude was greater than 2 times the standard deviation of the noise. The onset of the evoked Ca^{2+} transients was defined by the timing of the electrical stimulation (0.1 Hz). Ca^{2+} transient integrals for ROIs were calculated in MATLAB as temporal integrals over a 2-s post-stimulus time window (units of "%s"; after subtraction of the mean ΔF/F in a 1-s pre-stimulus baseline window). Collapsed z-stack overview images were used to measure the distance from dendritic branches to the recording electrode in the soma. For the analysis of the frequency of Ca^{2+} transients associated with NMDA spikes, as well as their amplitudes and integrals, ROIs were selected such that they enclosed an entire dendritic segment, hence the area covered by ROIs was variable (Fig. 1 and Supplementary Figs. 2,3,4,5,7). For detailed analysis of the spatial extent of the Ca^{2+} transients, a series of uniformly sized ROIs (~1 µm x 1 µm) were positioned along dendrites exhibiting responses as identified by heat maps (Fig. 1h-i and Supplementary Fig. 2h-j).

Statistical analysis

All data are expressed as the mean ± SEM. No data sets were excluded from analysis. Statistical analyses were performed using Origin 2016 (OriginLab) applying Student's paired or unpaired t-test. Before applying the Student t-test, a QQ plot was generated and the Shapiro-Wilk test was performed for each pool of data to confirm a normal distribution. Linear correlations were evaluated with the Pearson coefficient. The size of the data sets was determined based on past experience with experiments involving *in vitro* recordings in brain slices. For the main experiments n = 7 – 15, and for control experiments n = 5 – 10.

BIBLIOGRAPHY

1. Stuart, G. J. & Sakmann, B. Active propagation of somatic action potentials into neocortical pyramidal cell dendrites. *Nature* **367,** 69-72 (1994).

2. Magee, J. C. & Johnston, D. A synaptically controlled, associative signal for Hebbian plasticity in hippocampal neurons. *Science* **275,** 209-213 (1997).

3. Lisman, J. & Spruston, N. Postsynaptic depolarization requirements for LTP and LTD: a critique of spike timing-dependent plasticity. *Nat. Neurosci.* **8,** 839-841 (2005).

4. Lisman, J. & Spruston, N. Questions about STDP as a general model of synaptic plasticity. *Front. Synaptic Neurosci*. **2,** (2010).

5. Golding, N. L. & Spruston, N. Dendritic sodium spikes are variable triggers of axonal action potentials in hippocampal CA1 pyramidal neurons. *Neuron* **21,** 1189-1200 (1998).

6. Golding, N. L., Staff, N. P. & Spruston, N. Dendritic spikes as a mechanism for cooperative long-term potentiation. *Nature* **418,** 326-331 (2002).

7. Sjöström, P. J., Turrigiano, G. G., & Nelson, S. B. Multiple forms of long-term plasticity at unitary neocortical layer 5 synapses. *J. Neurophysiol.* **52,** 176-184. (2007).

8. Dudman, J. T., Tsay, D. & Siegelbaum, S. A. A role for synaptic inputs at distal dendrites: instructive signals for hippocampal long-term plasticity. *Neuron* **56,** 866-879 (2007).

9. Brandalise, F. & Gerber, U. Mossy fiber-evoked subthreshold responses induce timing-dependent plasticity at hippocampal CA3 recurrent synapses*. Proc. Natl. Acad. Sci. USA* **111,** 4303-4308 (2014).

10. Cichon, J. & Gan, W. B. Branch-specific dendritic Ca2+ spikes cause persistent synaptic plasticity. *Nature* **520,** 180-185 (2015).

11. Gambino, F., Pagès, S., Kehayas, V., Baptista, D., Tatti, R., Carleton, A. & Holtmaat, A. Sensory-evoked LTP driven by dendritic plateau potentials *in vivo*. *Nature* **515,** 116-119 (2014).

12. Kim, Y., Hsu, C. L., Cembrowski, M. S., Mensh, B. D. & Spruston, N. Dendritic sodium spikes are required for long-term potentiation at distal synapses on hippocampal pyramidal neurons. *eLife* **4,** e06414 (2015).

13. Basu, J., Zaremba, J. D., Cheung, S. K., Hitti, F. L., Zemelman, B. V., Losonczy, A. & Siegelbaum, S. A. Gating of hippocampal activity, plasticity, and memory by entorhinal cortex long-range inhibition. *Science* **351,** aaa5694 (2016).

14. Stuart, G. J. & Spruston, N. Dendritic integration: 60 years of progress. *Nat. Neurosci.* **18,** 1713-1721 (2015).

15. Poirazi, P., Brannon, T. & Mel, B. W. Pyramidal neuron as two-layer neural network. *Neuron* **37,** 989-999 (2003).

16. Schiller, J., Schiller, Y., Stuart, G. & Sakmann, B. Calcium action potentials restricted to distal apical dendrites of rat neocortical pyramidal neurons. *J. Physiol.* **505,** 605-616 (1997).

17. Schiller, J., Major, G., Koester, H. J. & Schiller, Y. NMDA spikes in basal dendrites of cortical pyramidal neurons. *Nature* **404,** 285-289 (2000).

18. Connors, B. W. & Prince, D. A. Effects of local anesthetic QX-314 on the membrane properties of hippocampal pyramidal neurons. *J. Pharmacol. Exp. Ther.* **220,** 476-481(1982).

19. Major, G., Larkum, M. E. & Schiller, J. Active properties of neocortical pyramidal neuron dendrites. *Annu. Rev. Neurosci.* **36,** 1-24 (2013).

20. Magee, J. C., Christofi, G. E., Miyakawa, H. I., Christie, B. R., Lasser-Ross, N. E. & Johnston, D. Subthreshold synaptic activation of voltage-gated Ca^{2+} channels mediates a localized Ca^{2+} influx into the dendrites of hippocampal pyramidal neurons. *J. Neurophysiol.* **74,** 1335-1342 (1995).

21. Wilson, D. E., Whitney, D. E., Scholl, B., & Fitzpatrick, D. Orientation selectivity and the functional clustering of synaptic inputs in primary visual cortex. *Nat. Neurosci.* **19,** 1003-1009, (2016).

22. Schwegler, H., Lipp, H. P., Van der Loos, H. & Buselmaier, W. Individual hippocampal mossy fiber distribution in mice correlates with two-way avoidance performance. *Science* **214,** 817-819 (1981).

23. Antic, S. D., Zhou, W. L., Moore, A. R., Short, S. M. &, Ikonomu, K. D. The decade of the dendritic NMDA spike. J. Neurosci. Res. **88**, 2991-3001 (2010).

24. Oikonomou, K. D., Short, S. M., Rich, M. T. & Antic, S. D. Extrasynaptic glutamate receptor activation as cellular bases for dynamic range compression in pyramidal neurons. *Front. Physiol.* **3,** 334 (2012).

25. Chalifoux, J. R. & Carter, A. G. Glutamate spillover promotes the generation of NMDA spikes. *J. Neurosci*. **31,** 16435-16446 (2011).

26. Palmer, L. M., Shai, A. S., Reeve, J. E., Anderson, H. L., Paulsen, O. & Larkum, M. E. NMDA spikes enhance action potential generation during sensory input. *Nat. Neurosci.* **17,** 383-390 (2014).

27. Mitra, A., Mitra, S. S. & Tsien, R. W. Heterogeneous reallocation of presynaptic efficacy in recurrent excitatory circuits adapting to inactivity *Nat. Neurosci.* **15,** 250-257 (2011).

28. Arnth-Jensen, N., Jabaudon, D. & Scanziani, M. Cooperation between independent hippocampal synapses is controlled by glutamate uptake. *Nat. Neurosci.* **5,** 325-331 (2002).

29. Markram, H., Lübke, J., Frotscher, M. & Sakmann, B. Regulation of synaptic efficacy by coincidence of postsynaptic APs and EPSPs. *Science* **275,** 213-215 (1997).

30. Pike, F. G., Meredith, R. M., Olding, A. W. & Paulsen, O. Postsynaptic bursting is essential for 'Hebbian'induction of associative long-term potentiation at excitatory synapses in rat hippocampus. *J. Physiol.* **518,** 571-576 (1999).

31. Sjöström, P. J., Turrigiano, G. G. & Nelson, S. B. Rate, timing, and cooperativity jointly determine cortical synaptic plasticity. *Neuron* **32,** 1149-1164 (2001).

32. Kampa, B. M., Letzkus, J. J. & Stuart, G. J. Requirement of dendritic calcium spikes for induction of spike-timing-dependent synaptic plasticity. *J. Physiol*. **574,** 283-290 (2006).

33. Yasuda, R., Sabatini, B. L. & Svoboda, K. Plasticity of calcium channels in dendritic spines. *Nat. Neurosci.* **6,** 948-955 (2003).

34. Grienberger, C., Chen, X. & Konnerth, A. NMDA receptor-dependent multidendrite Ca^{2+} spikes required for hippocampal burst firing *in vivo*. *Neuron* **81,** 1274-1281 (2014).

35. Debanne, D., Gähwiler, B. H. & Thompson, S. M. Long-term synaptic plasticity between pairs of individual CA3 pyramidal cells in rat hippocampal slice cultures. *J. Physiol.* **507,** 237-247 (1998).

36. Mishra, R. K., Kim, S., Guzman, S. J. & Jonas, P. Symmetric spike timing-dependent plasticity at CA3-CA3 synapses optimizes storage and recall in autoassociative networks. *Nat. Commun.* **7,** 11552 (2016).

37. Waters, J. & Helmchen, F. Boosting of action potential backpropagation by neocortical network activity *in vivo*. *J. Neurosci.* **24,** 11127-11136 (2004).

38. McNaughton, B. L. & Morris, R. G. Hippocampal synaptic enhancement and information storage within a distributed memory system. *Trends Neurosci.* **10,** 408-415 (1987).

39. Lisman, J. E. Relating hippocampal circuitry to function: recall of memory sequences by reciprocal dentate–CA3 interactions. *Neuron* **22,** 233-242 (1999).

40. Kesner, R. P. Behavioral functions of the CA3 subregion of the hippocampus. *Learn. Mem.* **14,** 771-781. (2007).

41. Sheffield, M. E. & Dombeck, D. A. Calcium transient prevalence across the dendritic arbour predicts place field properties. *Nature* **517,** 200-204 (2015).

42. Pawlak, V., Greenberg, D. S., Sprekeler, H., Gerstner, W. & Kerr, J. N. Changing the responses of cortical neurons from sub-to suprathreshold using single spikes in vivo. *Elife* **2,** e00012 (2013).

43. Shulz, D. E. & Jacob, V. Spike-timing-dependent plasticity in the intact brain: counteracting spurious spike coincidences. *Front. Synaptic Neurosci.* **2,** 137 (2010).

44. McNaughton, B. L., Barnes, C. A. & O'Keefe, J. The contributions of position, direction, and velocity to single unit activity in the hippocampus of freely-moving rats. *Exp. Brain Res.* **52,** 41-49 (1983).

45. Bittner, K. C., Grienberger, C., Vaidya, S. P., Milstein, A. D., Macklin, J. J., Suh, J., Tonegawa, S. & Magee, J. C. Conjunctive input processing drives feature selectivity in hippocampal CA1 neurons. *Nat. Neurosci.* **18,** 1133-1142 (2015).

46. Polsky, A., Mel, B. W. & Schiller, J. Computational subunits in thin dendrites of pyramidal cells. *Nat. Neurosci.* **7,** 621-627 (2004).

47. Losonczy, A., Makara, J. K. & Magee, J. C. Compartmentalized dendritic plasticity and input feature storage in neurons. *Nature* **452,** 436-441 (2008).

48. Govindarajan, A., Israely, I., Huang, S. Y. & Tonegawa, S. The dendritic branch is the preferred integrative unit for protein synthesis-dependent LTP. *Neuron* **69,** 132-146 (2011).

49. Makara, J. K. & Magee, J. C. Variable dendritic integration in hippocampal CA3 pyramidal neurons. *Neuron* **80,** 1438-1450 (2013).

50. Kleindienst, T., Winnubst, J., Roth-Alpermann, C., Bonhoeffer, T. & Lohmann, C. Activity-dependent clustering of functional synaptic inputs on developing hippocampal dendrites. *Neuron* **72,** 1012-1024 (2011).

51. Takahashi, N., Kitamura, K., Matsuo, N., Mayford, M., Kano, M., Matsuki, N. & Ikegaya, Y. Locally synchronized synaptic inputs. *Science* **335,** 353-356 (2012).

52. Lee, K. F., Soares, C., Thivierge, J. P. & Béïque, J. C. Correlated synaptic inputs drive dendritic calcium amplification and cooperative plasticity during clustered synapse development. *Neuron* **89,** 784-799 (2016).
53. Gähwiler, B. H. Organotypic monolayer cultures of nervous tissue. *J. Neurosci. Meth.* **4**, 329-342 (1981).

54. Amaral, D. G. & Witter, M. P. The three-dimensional organization of the hippocampal formation: a review of anatomical data. *Neuroscience* **31**, 571-591 (1989).

55. Langer, D., van't Hoff, M., Keller, A.J., Nagaraja, C., Pfäffli, O.A., Göldi, M., Kasper H. & Helmchen, F. HelioScan: A software framework for controlling in vivo microscopy setups with high hardware flexibility, functional diversity and extendibility. *J. Neurosci. Meth.* **215,** 38-52 (2013).

ACKNOWLEDGEMENTS

We appreciate the technical assistance of D. Göckeritz-Dujmovic, S. Giger, H. Kasper, F. David, and P. Morciano. We thank B. Gähwiler, M. Santello, and F. Loup for valuable discussions and comments on the manuscript and S. Soldado Magraner for writing MATLAB routines. This work was supported by the Swiss National Science Foundation (grant: 31003A_162558) to UG and the NIH (grant: U01NS0905583) to JL.

AUTHOR CONTRIBUTIONS

F.B. performed electrophysiological and calcium imaging experiments and designed experiments. S.C. performed calcium imaging experiments. F.H. analyzed data and wrote the paper. J.L. designed experiments and wrote the paper. U.G. analyzed data, designed experiments and wrote the paper.

CONDITIONING BY SUBTHRESHOLD SYNAPTIC INPUT CHANGES THE CHARACTERISTIC FIRING PATTERN OF CA3 HIPPOCAMPAL NEURONS

Saray Soldado Magraner*, Federico Brandalise*, Suraj Honnuraiah, Michael Pfeiffer, Urs Gerber & Rodney Douglas

In preparation

*The authors contributed equally to the work

Contribution to this study: F. Brandalise designed the study together with S.S.M. and R.D., and performed the experiments with S.S.M.

SUMMARY

The intrinsic firing patterns of neurons recorded in vitro are commonly used as means of classifying neuronal types and correlating them with morphological types. Here we investigated the stability of the intrinsic firing patterns in the CA3 field of the rat hippocampus. We found that neurons change their responses very significantly following only a short period of low frequency subthreshold stimulation of their afferents. Cluster analysis of the discharge patterns before and after conditioning by afferent stimulation revealed systematic transitions between discharge types. These transitions were generally towards adapting and intrinsic burst behaviours, irrespective of the initial pattern exhibited by the cell. These results could be reproduced by a conductance based electrophysiological model, in which conditioning by stimulation results in an increase of calcium and M-type potassium conductances. We conclude that CA3 neurons adapt their conductance profile to the statistics of ongoing activity in their embedding circuits and consequently, that their response to step currents should not be used as a basis for neuronal classification.

INTRODUCTION

It is widely accepted that the diversity of morphological, molecular, and electrophysiological properties exhibited by neurons of the neocortex and hippocampus reflects functionally distinct classes of cells (Ramon y Cajal 1893; McCormick et al. 1985; Ren et al. 1992; DeFelipe 1993; Kawaguchi and Kubota, 1997; Markram et al. 2004; Somogyi and Klausberger 2005). In particular, neurons have been described electrophysiologically according to the pattern of their action potential discharge in response to applied intra-somatic step currents. Many studies have reported that excitatory and different types of inhibitory neurons, identified by morphology and molecular markers, exhibit distinct firing patterns (Connors and Gutnick 1990; Cauli et al. 2000; Markram et al. 2004; Butt et al. 2005; Dumitriu et al. 2007). These responses may be for example: adapting, accelerating, bursting, or fast spiking. With rare exceptions (Steriade 2004), the patterns are assumed to be a sufficiently stable property of a neuron that they can be used as a basis for phenotypic classification (for example: Markram et al. 2004; Ascoli et al. 2008).

A prominent view is that genetic factors determine both the morphology and the

distinct firing patterns of individual neurons. This assumption is followed by the Petilla convention, which proposes a nomenclature for firing patterns of GABAergic cortical interneurons as part of standardized classification criteria (Ascoli et al. 2008). However, there are substantial reasons to doubt that discharge patterns are static properties of neurons. The discharge response of a neuron depends on the distribution and activations of the membrane conductances that it expresses (Hille 2001; Markram et al. 2004). This distribution is subject to homeostatic control including up- or down-regulation of conductances in response to the neuron's own activity (Turrigiano et al. 1995; Turrigiano and Nelson 2004; Marder and Goaillard 2006). For example, STG neurons of the lobster change their firing patterns in response to network isolation by changing the balance between inward and outward currents (Turrigiano et al. 1995). Furthermore, neurons have conserved molecular pathways that link network activity to the recruitment of genes and signaling factors implicated in neural excitability (Flavell and Greenberg 2008; Cohen and Greenberg 2008), and activity-dependent maturation is indeed necessary for the emergence of the whole spectrum of electrical types (García et al. 2011). In final agreement with this hypothesis, a very recent study shows for the first time that the electrical properties of different types of basket cells can be interchanged in response to neural activity (Dehorter et al. 2015).

These lines of evidence suggest that the firing patterns of cortical neurons are not a static characteristic of the cell, but rather the consequence of adaptive mechanisms that adjust the behavior of the neuron in response to the patterns of activity in its embedding network. We have explored this hypothesis using whole-cell recordings from neurons in the CA3 region of rat hippocampus in organotypic cultures. The discharge patterns of neurons in response to constant current injection were characterized before and after a conditioning phase of periodic subthreshold synaptic stimulation. It was found that pre-conditioned cells could indeed be classified according to the type of their discharge pattern. However, conditioning by subthreshold synaptic input elicited significant changes in the behavior of nearly all neurons examined, requiring substantial re-classification of their type. We used a conductance-based single-compartment neuron model to explore what changes in the neuronal conductance profile could explain the observed changes in discharge pattern. We found that the results can be explained by input-dependent recruitment of voltage dependent calcium and M-type potassium ion channels. We conclude that

CA3 neurons can indeed adapt their output patterns in response to circuit activity by specific tuning of key conductances.

MATERIALS AND METHODS

All experiments were conducted in accordance with guidelines and regulations of the cantonal veterinary office of Zurich; Licence Nr 81-2014.

Electrophysiological Recordings

Rat hippocampal organotypic cultures (Gähwiler 1981) of average postnatal age 21 days were transferred to a recording chamber and mounted on an upright microscope (Axioskop FS1; Zeiss). The cultures were superfused with an external solution (pH 7.4) containing (in mM) 148.8 Na^+, 2.7 K^+, 149.2 Cl^-, 2.8 Ca^{2+}, 2.0 Mg^{2+}, 11.6 HCO_3^-, 0.4 $H_2PO_4^-$, 5.6 D-glucose, and 10 mg/l Phenol Red. All experiments were performed at 34^{O}C. Whole-cell recordings of CA3 neurons were obtained with patch pipettes (4-7 MΩ). Pipettes were filled (in mM) with potassium 126 gluconate, 4 NaCl, 1 $MgSO_4$, 0.1 BAPTA-free, 0.05 BAPTA-Ca^{2+}, 15 glucose, 3 ATP, 5 HEPES (pH was adjusted to 7.2 with KOH) 0.1 GTP, and 10.4 byocitin. IPSPs in the recorded cells were reduced by adding picrotoxin (1 mM) to the intracellular patch solution.

The recording pipettes were manually positioned under microscope control. Recorded neurons were located mostly in the pyramidal cell layer. Electrophysiology and subsequent histology suggest that the neurons described below include both pyramidal cells and smooth cells.

Current-voltage relationships were determined by step command potentials and had duration of 1 s to ensure steady-state responses. Data were recorded using an Axopatch 200B amplifier (Molecular Devices). Series resistance was monitored regularly, and was typically between 5 and 15 MΩ. Cells were excluded from further analysis if this value changed by more than 20% during the recording. Junction potential was not corrected.

Mossy fibers were stimulated with a bipolar tungsten electrode. The intensity of the stimulus was adjusted to evoke subthreshold post-synaptic potential responses of 15 mV on average in the recorded neuron (minimal stimulation + 20% stimulation intensity).

Action potential discharges were evoked by injected current steps (-0.08 up to 1.8

nA; step increment 0.05 - 0.15 nA, depending on the input resistance of the recorded cell) each lasting 5 seconds. After this control, the neurons were conditioned by mossy fibers activation, consisting of a double pulse (0.1 ms duration pulses, interval 10 - 20 ms) at a frequency of 1 Hz, repeated 500 times. Thus, the conditioning period was approximately 8 minutes. Immediately after this conditioning, the firing pattern of the neuron was assessed again using the same step protocol. The step protocols were repeated 3 times with 5 min intervals to assess stability.

Histology

Hippocampal slice cultures were prepared for morphological assessment by fixing in freshly prepared 4% paraformaldehyde in 0.1 M phosphate buffer (PB) at pH 7.4 overnight at 4^0C; washing three times in phosphate-buffered saline (PBS, 1.5 mM KH_2PO_4, 8.5 mM Na_2 HPO_4, 137 mM NaCl, and 3 mM KCl, pH 7.4); and permeabilizing at room temperature in PBS that contained 10% heat-inactivated donkey serum, and 1% Triton X-100. Then they were incubated overnight at 4^0C with streptavidin conjugated with Alexa (546 λm). The cultures were washed again three times in PBS, and then mounted in Fluorostab (Bio-Science Products AG, Emmenbrucke, Switzerland) and coverslipped. High-resolution images were obtained using laser scanning confocal microscopy (Leica TCS SP2, Leica Microsystems, Heidelberg, Germany). We distinguished between pyramidal and smooth cells based on the size and shape of the somatic compartment and dendritic arbor and the presence or absence of dendritic spines.

Data analysis

Signals were digitized at 4 kHz for current clamp and 5 kHz for voltage clamp. These data were analyzed off-line using pCLAMP 10 (Molecular Devices) and MatlabR2011b (MathWorks).

Analysis of the voltage traces was performed similar to Chen et al. 2015. The average resting membrane potential of each neuron was estimated as the mean membrane potential during the first 100 ms of current-injection protocol (before injection of the step-current pulses). Input resistance was obtained by measuring the voltage drop across the hyperpolarizing trace of the step-current pulses. APs were located using median filtering, and the threshold was inferred as the point at which the derivative of the voltage trace exceeded 5 mV/ms. AP amplitude was measured

from threshold-to-peak and AP afterhyperpolarization (AHP) from the threshold-to through. Half-width was estimated as the full width at half-maximal amplitude.
Statistical comparisons between conditions were performed as paired t tests.

Cluster analysis of discharge traces

The firing patterns of the neurons were categorized by hierarchical clustering of their discharge patterns. The dataset consisted of all voltage traces recorded from neurons in response to step-wise current injections with different amplitudes, including recordings before and after conditioning. For any one neuron, the collection of responses to different current injections represents the signature of the electrical type. However, for inherent verification of our cluster procedure, we chose to treat each response independently. In this way successful clustering could be confirmed by its ability to assign responses from the same neuron into the same category.
The clustering measured similarity of a feature vector derived from the voltage traces. First the recorded voltage traces were converted into a time series of the instantaneous firing rates. The instantaneous firing rate at each spike was taken as 1/Inter-spike-Interval (ISI). Then the instantaneous rates where linearly interpolated across the spike times at 1 ms time intervals over 6 seconds (5 second current injection step, plus 1 second on and offset), and normalized by the maximum firing rate. Finally, a characteristic feature vector of a common length of 600 elements was obtained by down-sampling the interpolated rate traces by a factor of 10, in order to make them computationally tractable to the similarity measurement.
Similarity distances between pairs of traces were calculated using the Dynamic Time Warping (DTW) metric (Berndt and Clifford 1994). DTW takes into account that two similar signals can be out of phase temporarily, and aligns them in a non-linear manner through dynamic programming (Keogh and Ratanamahatana 2005). The algorithm takes two time series Q = $\langle q_1, q_2, \ldots, q_n \rangle$ and C = $\langle c_1, c_2, \ldots, c_m \rangle$ and computes the best match between the sequences by finding the path of indices that minimizes the total cumulative distance

$$DTW(Q, C) = min \sum_{k=1}^{K} w_k \quad (1)$$

where w_k is the cost of alignment associated with the k^{th} element of a warping path

W. A warping path starts at q_1 and c_1 respectively, and finds a monotonically increasing sequence of indices i^k and j^k, such that all elements q_j in *Q* and c_j in *C* are visited at least once, and for the final step of the path i^{end} = n and j^{end} = m holds. The optimal DTW distance is the cumulative distances y (i, j), corresponding to the costs of the optimal warping path ⟨q_1,...,q_i⟩ and ⟨c_1, ... , c_j⟩. This distance can be computed iteratively by dynamic programming:

$$y(i,j) = d(q_j, c_j) + min\{y(i-1, j-1), y(i-1, j), y(i, j-1)\} \qquad (2)$$

where d (q_i, c_j) is the absolute difference between the elements of the sequence. The optimal warping path is obtained by backtracking from the final element y (n, m), and finding which of the three options (increasing i only, increasing j only, or increasing i and j simultaneously) led to the optimal warping distance, until i = 1, j = 1 is reached. A warping window constraint of 10% of the vector size was chosen (Keogh and Ratanamahatana 2005).

The pairwise DTW distances were used to perform hierarchical clustering by Ward's algorithm (Ward Jr 1963). The number of classes increases with the level of the hierarchy. We choose to cut the tree at a level that provided sufficient structure to interpret the hierarchy in terms of recognized response types (for example, Ascoli et al. (2008)).

Every recording for a given cell was treated as an independent observation, and could in principle be assigned to any cluster. If the electrophysiological state of the cell is expressed in all of its responses, then we expect that all the independent observations derived from that cell should be assigned to the same cluster. However, traces derived from current injections to the same cell in different conditions (pre- or post-stimulation) are expected to be assigned to different clusters if there is significant change in the underlying electrophysiological state.

In fact, the independent traces did not cluster perfectly. Instead, the majority of independent observations derived from a given state clustered together and there were a few that fell into other clusters. Therefore, we chose to label the electrical type of each cell according to the cluster that contained the mode of the traces for one set of current injections. Cells for which no clear dominant cluster could be identified, e.g. because half of the traces fell into one cluster, and half of them into another, were labeled as unclassified. A cluster transition was recognized whenever the cell was

assigned to different clusters before and after the stimulation protocol.

The analysis was performed using custom-written software in MatlabR2011b. The implementation of the DTW algorithm was obtained from Matlab Central (http://www.mathworks.com/matlabcentral/fileexchange/43156-dynamic-time-warping–dtw).

Neuron simulation model

A single cylindrical compartment, conductance-based neuronal model was used for all simulations. The length and diameter of the cylinder are set at equal dimensions to avoid spatial discretization problems in a single compartment (Cooley and Dodge Jr 1966; De Schutter and Bower 1994). The geometrical dimensions and passive properties associated with the model were obtained from Hemond et al. (2008). We have set the length and diameter of our compartment to 50 μm to obtain the input resistance of 150 MΩ in our model cell that approximates the mean input resistance of our experimental cells (144.8 MΩ). The active properties were modeled by including appropriate voltage and calcium gated ion channels whose density and kinetics were obtained from experimental recordings performed in CA3 neurons (Hemond et al. 2008).

The simulations were performed using NEURON (Hines and Carnevale 1997). We choose an integration step of 25 μs, which was approximately 1% of the shortest time constant in the model. The voltage- and time-dependent currents followed the Hodgkin and Huxley formalism (1952):

$$C\,\frac{dV}{dt} = -(I_{Na} + I_{Kdr} + I_{Kd} + I_{KA} + I_{Km} + I_{CaK} + I_{CaL} + I_{CaN} + I_{CaT} + I_{Leak}) \quad (3)$$

Each current I_x is described by the equation

$$I_{(v,t)} = \bar{g} \cdot m \cdot h \cdot \left(V_{(t)} - E\right) \quad (4)$$

where $\bar{g}$ is the maximal conductance, m and h are activation and inactivation terms, V is the membrane potential, and E the reversal potential of the channel. The reversal potentials for Na^+ and K^+ were E_{Na} = 50 mV and E_K = 85 mV, respectively. The equations describing the different channel kinetics (m, h) for every current were obtained from Hemond et al. (2008). Following this reference, the three calcium

conductances (T, M and L) were incorporated into a single parameter g_{Ca}.

The set of maximal conductance values that are consistent with all our experimentally observed firing patterns are shown in the supplementary Figure S1 and S2.

The intracellular calcium dynamics were modeled (Hemond et al. 2008), as follows:

$$\frac{d[Ca^{2+}]}{dt} = \frac{I_{Ca}}{2Fv} - \frac{[Ca^{2+}]_i - 0.0001}{\tau_{Ca}} \qquad (5)$$

The first term of the above equation describes the change caused by Ca^{2+} influx into a compartment with volume v. F is the Faraday constant, I_{Ca} is the calcium current and τ_{Ca} is the time constant of Ca^{2+} diffusion.

	Intrinsic Burst		Adapting		Accelerating		Non-Adapting		Delayed	
Maximal Conductances	Cylinder	Realistic CA3	Cylinder	Realistic CA3	Cylinder	Realistic CA3	Cylinder	Realistic CA3	Cylinder	Realistic CA3
g_{Na}	0.04	0.022	0.04	0.022	0.04	0.022	0.04	0.022	0.04	0.022
g_{Kdr}	0.01	0.01	0.01	0.01	0.01	0.02	0.01	0.01	0.02	0.01
g_{Ka}	0.07	0.02	0.04	0.02	0.04	0.02	0.12	0.02	0.08	0.02
g_{CaT}	0.001	0.00002	0.00	0.00001	0.0003	0.00001	0.00	0.00	0.0001	0.00
g_{CaN}	0.001	0.00002	0.00	0.00001	0.0003	0.00001	0.00	0.00	0.0001	0.00
g_{CaL}	0.001	0.00002	0.00	0.00001	0.0003	0.00001	0.00	0.00	0.0001	0.00
g_{CaK}	0.0001	0.00002	0.00	0.00	0.0005	0.00001	0.00	0.00	0.0006	0.00
g_{Km}	0.0006	0.021	0.00052	0.017	0.00	0.00	0.000003	0.00	0.000003	0.00
g_{Kd}	0.00045	0.002	0.00025	0.00	0.0008	0.005	0.00	0.00	0.00035	0.002
I	1	1.83	0.62	1.37	1.95	1.1	0.53	0.58	0.55	0.583

Figure S1: Model maximal conductance values for the experimental fits. List of the absolute conductance values used to reproduce the traces of main Figure 4 in the single compartment NEURON model. The conductances were tuned manually in order to fit qualitatively the overall dynamics of the voltage experimental traces. The bottom row lists the value of the current (in nA) used to reproduce every voltage trace. For more detailed description of the model see Methods.

Conductances Ranges	1	2	3
g_{Kdr}	0.015 : 0.05 : 0.04		
g_{Ka}	0.01 : 0.01 : 0.09		
g_{Ca}	0	0.2 : 0.1 : 0.6	0.8 : 0.1 : 1
g_{CaK}	0 : 0.1 : 0.9		
g_{Km}	0	0.4 : 0.1 : 1	
g_{Kd}	0 : 0.1 : 0.3	0.4 : 0.05 : 0.8	0.9 : 0.1 : 1
I	0.45 : 0.05 : 0.65	0.75 : 0.05 : 1	1.75 : 0.05 : 1.95
Total conductance vectors	861		
Total traces	5166		

Figure S2: Range of maximal conductance values used to generate the model database of voltage traces. A model database of voltage traces, which includes all the observed experimental firing patterns, was generated by varying 6 maximal conductances (g_{Kdr}, g_{Ka}, g_{Ca}, g_{CaK}, g_{Km} and g_{Kd}) over a given range. Each row in the table lists the ranges of conductance values employed in every channel. The different ranges of conductances (columns) were produced in order to account for the different firing patterns reproduced in the model. Different ranges of current I were also needed to reveal the different firing types. A total of 861 conductance vectors were generated by combining the different conductances. The firing pattern of every conductance vector was produced at several levels of step-current injection, obtaining a total of 5166 voltage traces. Note that g_{CaT}, g_{CaN} and g_{CaL} are englobed under the single parameter g_{Ca}.

RESULTS

Firing patterns of CA3 neurons change after subthreshold stimulation

Whole-cell patch clamp recordings of CA3 neurons were performed in hippocampal organotypic cultures. The intrinsic firing patterns of the neurons were recorded before and after conditioning by extracellular stimulation of the mossy fibers, originating in the dentate gyrus (Figure 1A). The conditioning stimuli consisted of paired pulses (0.1 ms duration pulses, interval 10 – 20 ms) applied at 1 Hz, and repeated 500 times for a total period of approximately 8 minutes. The amplitude of the pulses was adjusted for each recorded cell to elicit only subthreshold excitatory post-synaptic potentials (EPSPs) (Figure 1B). The mossy fiber protocol is a modification of that described by Brandalise and Gerber (2014), which has been previously shown to elicit heterosynaptic plasticity in CA3 pyramidal-pyramidal synapses. To confirm that the EPSP elicited was mossy fiber-mediated, we perfused the Group II metabotropic glutamate receptor agonist DCG-IV (2 mM) (see supplementary Figure S6A) which abolished the synaptic response.

The firing patterns of neurons were assessed with a sequence of constant current injections. For convenience we used the terminology of the Petilla classification (Ascoli et al. 2008) to label these patterns. Interestingly, we observed that in nearly seventy percent of cases (68% of n = 50) the characteristic pattern obtained during the pre-conditioning trials was changed in the post-conditioning trials that followed mossy fiber stimulation. For example, the cell shown in Figure 1C had a non-adapting pattern before stimulation. After conditioning, this response changed to intrinsic burst. These changes in firing pattern were present immediately after the stimulation protocol, and were stable at least 15 minutes after the stimulation.

In preliminary experiments we observed that the likelihood of inducing a change in discharge pattern depended on the amplitude of the subthreshold EPSP evoked by mossy fiber stimulation. Cells with EPSP amplitudes below 10 mV had a lower probability of transition (below 50%) (see supplementary Figure S3). Higher amplitudes in contrast, evoked changes in firing in over 70% of the cases while remaining safely subthreshold (relative to a threshold of about 33 mV, with a current rheobase of 0.23 nA). Intracellular dialysis could be excluded as the cause of the pattern transitions, because these effects were also observed under conditions where dialysis was minimized (n = 10) (see supplementary Figure S7).

We attempted to resolve if synaptic input was necessary to elicit the changes, or they could be induced directly at the soma. To this end, we used intra-somatic injection of paired current pulses whose parameters were chosen to elicit approximately a similar somatic voltage response to that generated by the mossy fiber stimulation (see supplementary Figure S4). These direct somatic stimuli evoked changes in discharge that were similar to those elicited by the indirect mossy stimulation in over 60% of the cells (n = 13). This result suggests that the mechanism inducing the change is depolarizing mediated and acts at the single cell level.

The mossy fiber conditioning was followed by a significant 36 MΩ (25%) decrease in input resistance (R_{in}), from (144.8 ± 73.0) to (108.4 ± 65.3) (see supplementary Figure S5). There was also a significant 5 mV (7 %) depolarization of the resting membrane potential (V_m) (-65.3 ± 5.0) with respect to resting level (-70.4 ± 5.7) (n = 50). However, the changes could not be induced by simply holding the resting membrane potential at different values, nor was the change induced by the step-currents used to measure the discharge patterns (see supplementary Figure S6). No significant changes in V_m and R_{in} in cells were found in unconditioned cells (n = 10). Another factor to note is the total amount of current injected during the protocol. The duration of the stimulation adds to 1 second, when the mossy fiber current pulses are concatenated over 500 times. The step pulse currents used to reveal the discharge properties of the cell last 5 seconds in total, and were not sufficient to elicit changes (see supplementary Figure S6B). The transient dynamic quality of the stimulus (in this case a paired pulse) is thus crucial in eliciting the changes observed.

Cluster analysis of experimental traces: quantification of identity changes in neurons

It is generally assumed that individual neurons have a characteristic electrophysiological state based on the distributions of various membrane conductances. This state will express a discharge pattern that is a signature of its electrical type (e-type). That is, cells of the similar morphological type are expected to be in similar electrophysiological states, and so exhibit similar discharge patterns. In this view, response type is a property of morphological type. However, our observations suggest that the electrophysiological state is not stable. Instead, the state may be changed by input stimuli.

On inspection the changes in response induced by conditioning appeared to be from more regular patterns before condition towards early bursting patterns afterward. We sought to quantify these changes using hierarchical clustering methods (Druckmann

et al. 2013; Tricoire et al. 2011; Hosp et al. 2014) to establish more objectively which states are associated with which response patterns, and to quantify the frequencies of transitions between them.

Previous studies have used clustering methods to quantify the similarity between vectors of features extracted from the voltage traces, such as action potential (AP) amplitude, firing rate, or accommodation index (Druckmann et al. 2013; Tricoire et al. 2011; Hosp et al. 2014). However, in our dataset several commonly used features including characteristics of the action potential such as AP width, amplitude and afterhyperpolarization (AHP) showed no difference before and after the stimulation (see supplementary Figure S8). Consequently, we chose to use instead Dynamic Time Warping (DTW) as a comparison metric, because it operates directly on the action potential sequence rather than relying on a pre-defined set of features.

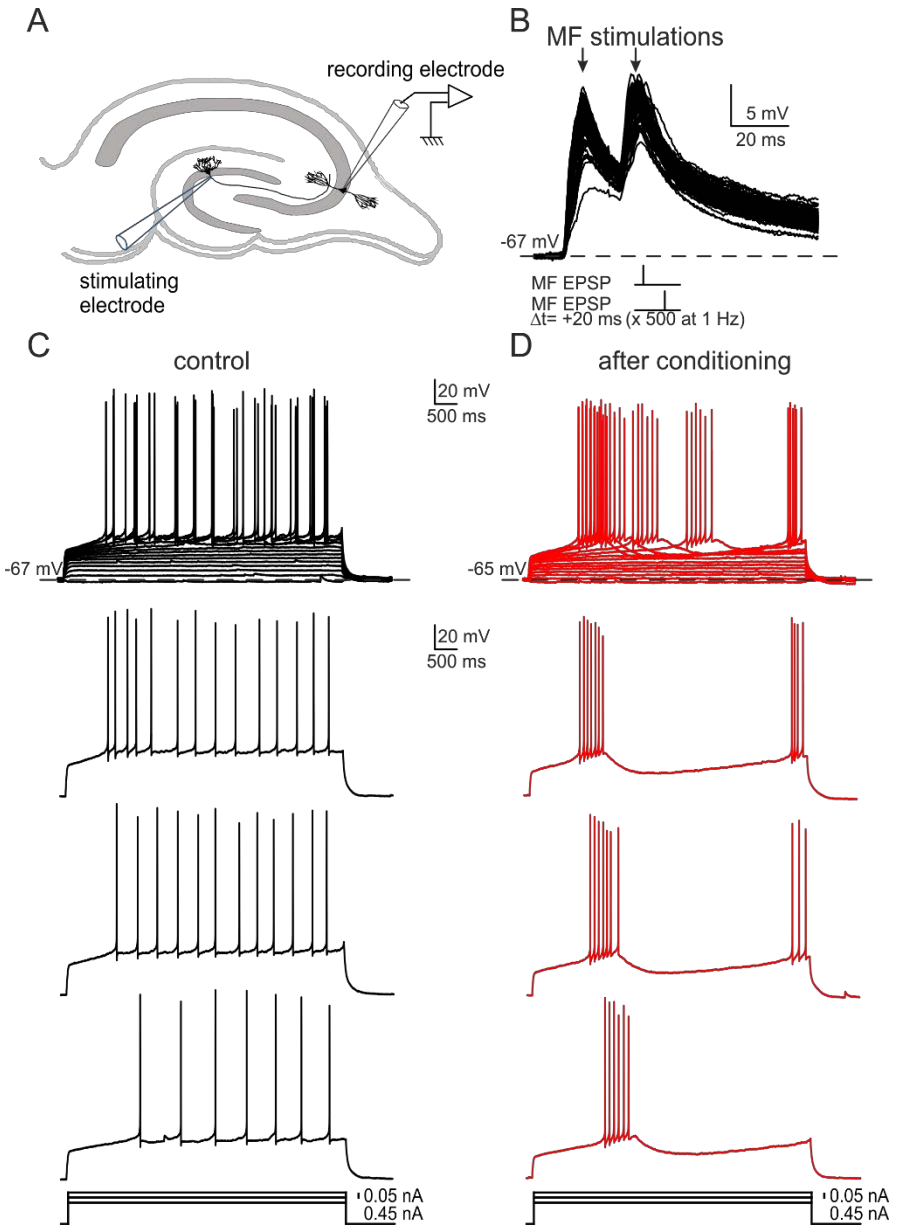

Figure 1: Transition of firing patterns of a CA3 cell after subthreshold paired-pulse stimulation of afferents. A) Configuration of recording and stimulating electrodes (on the CA3 region of the hippocampus and on the Dentate Gyrus, respectively). B) Typical conditioning protocol on a CA3 cell. EPSPs were evoked in response to stimulation of the mossy fibers with double current pulses, separated by 20 ms and repeated 500 times at 1 Hz. The series of repeated pulses are shown superimposed. C) Discharge pattern of the cell under control conditions. Spike response was measured through a series of constant step current injections of 0.05 nA of increasing amplitude. The upper panel shows the superimposed stack of voltage traces elicited in the cell. Below, three upper traces are separated for clarity. Under control conditions this neuron exhibited a non-adapting discharge pattern according to the Petilla classification. D) After conditioning by afferent stimulation, as shown in B, the discharge switched to an intrinsic burst pattern. The injected current protocol is represented beneath each set of voltage traces.

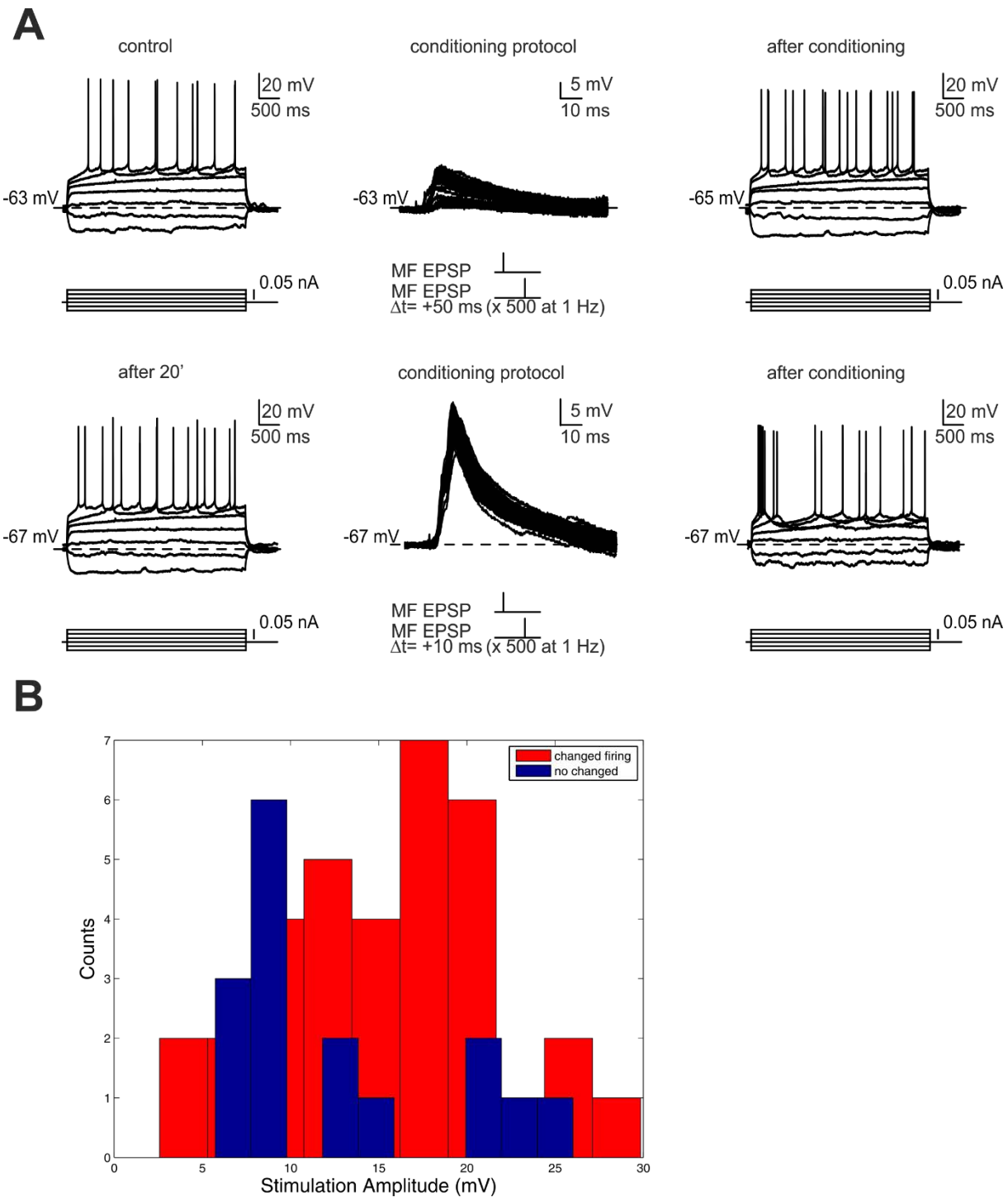

Figure S3: EPSPs of 5mV in average fail to induce transitions. A) On the upper panel a cell shows a non-adapting pattern in control conditions. After conditioning with mossy fiber stimulation with EPSPs of an average amplitude of 5mV, the firing pattern remains non-adapting. On the lower panel, the same cell is stimulated thereafter with EPSPs with an amplitude greater than 15 mV, and the firing of the cell changes to intrinsic burst. B) Histogram showing the distribution of EPSP amplitudes on the conditioned cells of our dataset. As it can be noted, cells in which the EPSP falls below 10 mV have a lower probability of transition (below 50%) in comparison to the ones above (over 70%).

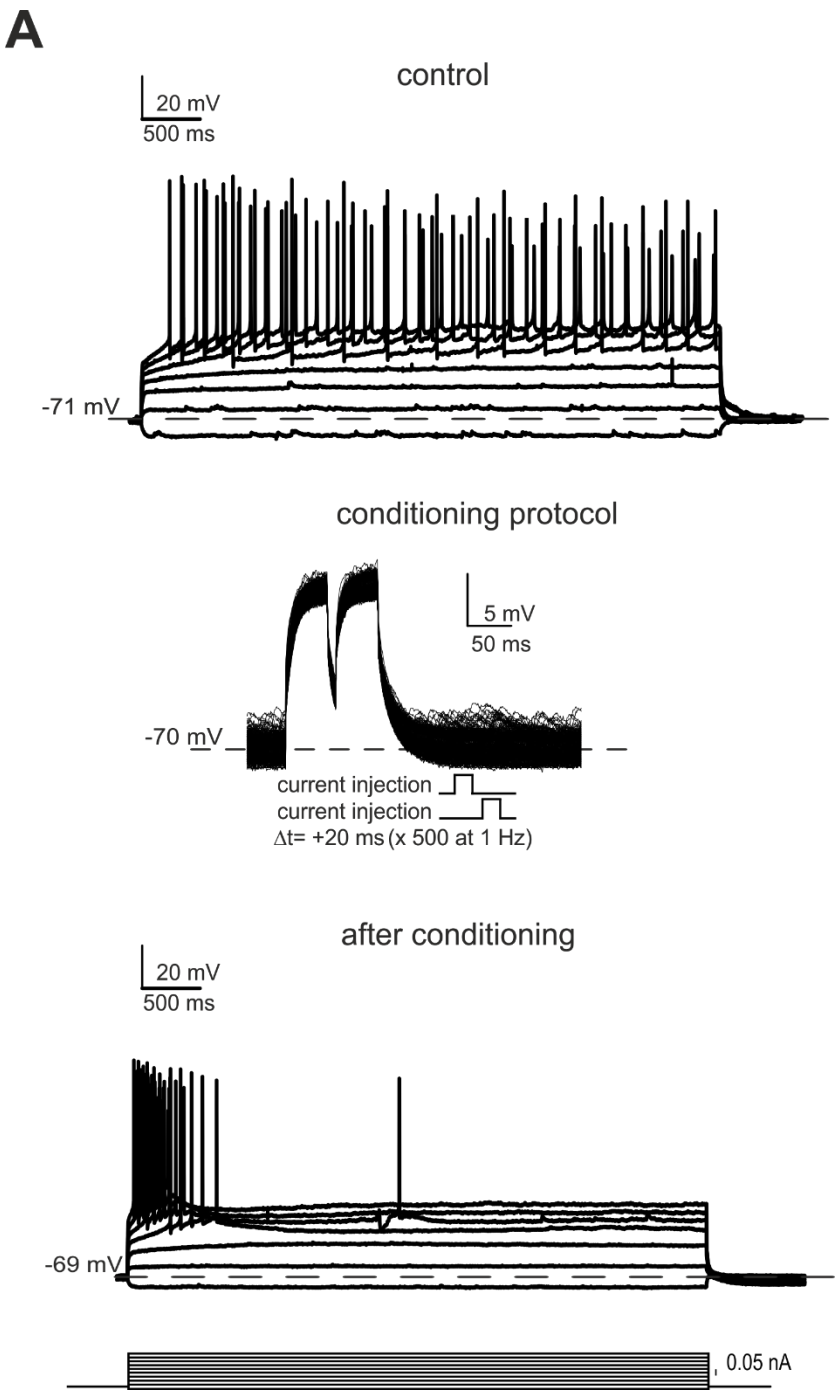

Figure S4: Firing pattern transitions elicited by structured somatic current injection. A) CA3 cells were stimulated by direct somatic current injection. EPSPs of average 15 mV were elicited with double current pulses, separated by 20 ms and repeated 500 times at 1 Hz, similar in form to that generated by mossy fiber stimulation. This example cell exhibits a transition from non-adapting to intrinsic burst firing. Spike response was measured through a series of constant step current injections of increasing amplitude. The injected current protocol is represented at the bottom of the figure. The center panel shows the voltage response elicited in the cell when the stimulation protocol was applied. The series of 500 repeated pulses are shown superimposed. 60% of the cells changed their firing after the conditioning protocol (n = 13).

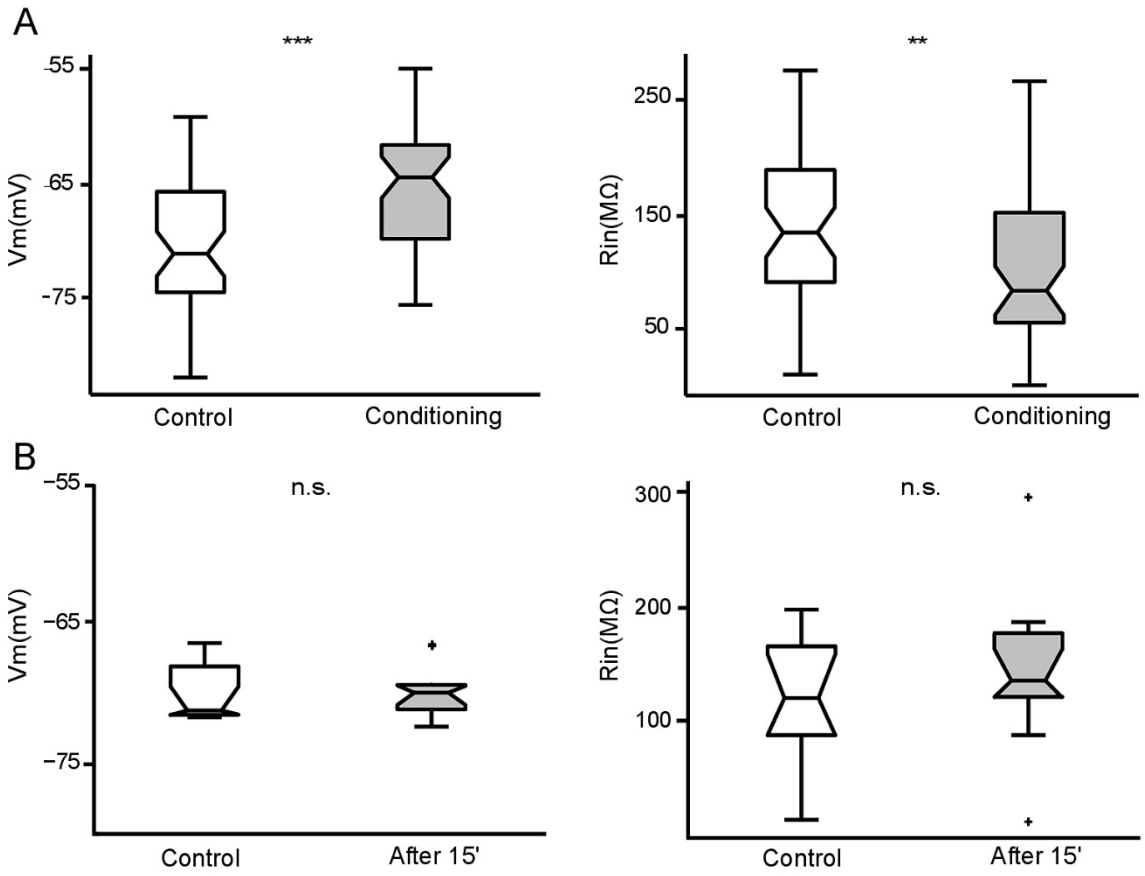

Figure S5: Resting membrane potential and input resistance of conditioned and non-conditioned cells. A) Conditioned cells. The cells show an increase in Vm and a decrease on Rin after the mossy fiber stimulation protocol. Mean values: Vm control = -70.4 ± 5.7, Vm conditioning = -65.3 ± 5.0. Rin control = 144.8 ± 73.0, Rin conditioning = 108.4 ± 65.3. Asterisks indicate significance for a paired t-test (***, $p<0.001$), (**, $p<0.01$) (n=50). B) Tiring firing pattern of unconditioned cells was measured by step-wise current injection, and checked again after 15 minutes. The Vm and Rin of these cells did not change significantly. Mean values: Vm control = -69.3 ± 2.0, Vm after 15' = -69.1±1.9. Rin control = 148.8 ± 56.1, Rin after 15' = 158.9 ± 55.6 (n=10). On each box, the central mark is the median, the edges of the box are the 25th and 75th percentiles, the whiskers extend to the most extreme data points not considered outliers, and outliers are plotted individually.

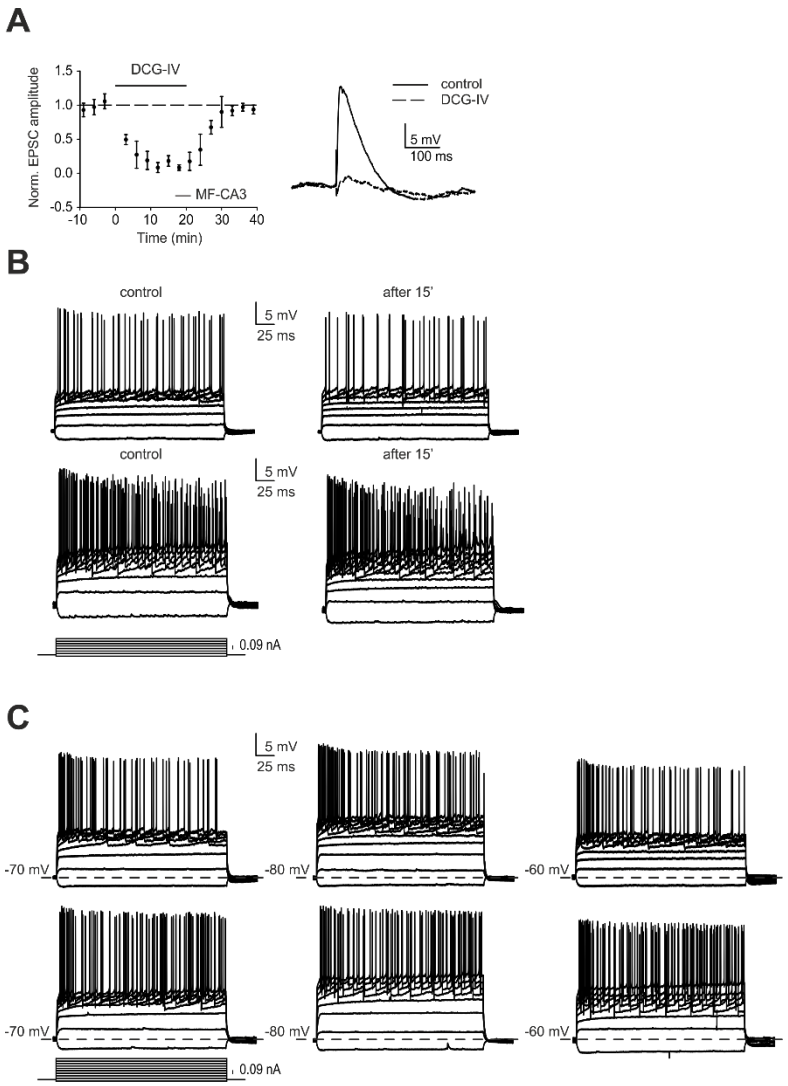

Figure S6: Mossy Fiber stimulation and stability controls. A) To proof that the stimulated input is purely mossy fiber-mediated EPSP avoiding a possible contamination by CA3-CA3 recurrent synapses, we perfused DCG-IV (2 mM), a mGlu2 agonist that blocks glutamate release from mossy fiber but not CA3 pyramidal cell terminals (Cosgrove et al. 2010), in 18 of our conditioned cells at the end of the experiment. (Left) During DGC-IV perfusion stimulated EPSPs amplitude significantly decreased by 88.2 ± 2.1 % ($P < 0.001$ on a t-test; $n = 18$) confirming that we selectively stimulated MF inputs. (Right) Average of 10 stimulated EPSPs before and after DGC-IV perfusion. B) Firing pattern transitions are not elicited by step current injection alone. Examples of two cells whose firing pattern have been measured by step-wise current injection (protocol showed in the inset). The cells do not show changes in firing pattern up to 15 min later (n=10). C) Firing pattern transitions are not elicited sustained shifts in membrane potential. Examples of two cells that have been hold at different membrane potentials through steady current injection (-70, -80 and -60 approximately). After changing the holding potential of the recorded neuron the firing patter was measured by step-wise current injection (protocol showed inthe inset). No transitions of firing pattern were observed at any of the different holding potentials (n=8).

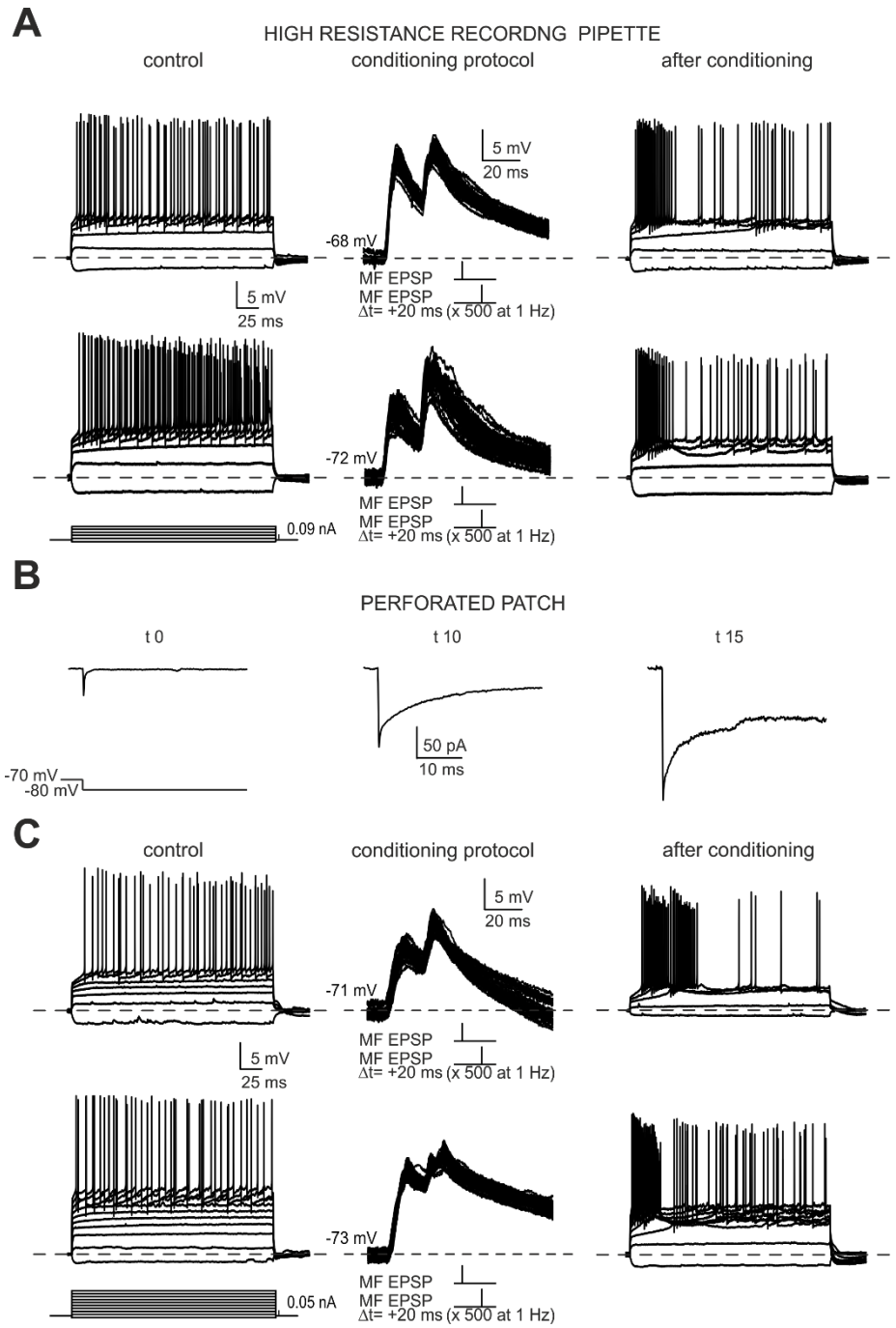

Figure S7: Firing pattern transitions on CA3 neurons are not induced by intracellular dialysis. A) Patch with high resistance pipette (10M). Control cells exhibit non-adapting (upper panel) and accelerating (lower panel) firing pattern. After conditioning, both change to intrinsic burst firing pattern. Mossy fiber stimulation protocol shown in middle panel. B) Example of hippocampal CA3 cell recorded with perforated patch. After 15 min, the antibiotic amphothericin-B (0.24 mg/ml) creates holes in membrane that provide direct access to cell. Current responses to hyperpolarizing voltage step (from -70 to -80 mV) at t=0, t=10 and t=15 min. C) Two examples of firing pattern transitions of conditioned cells recorded with perforated patch. Control cells exhibit accelerating (upper panel) and non-adapting (lower panel) patterns. After conditioning, they switch towards intrinsic burst firing.

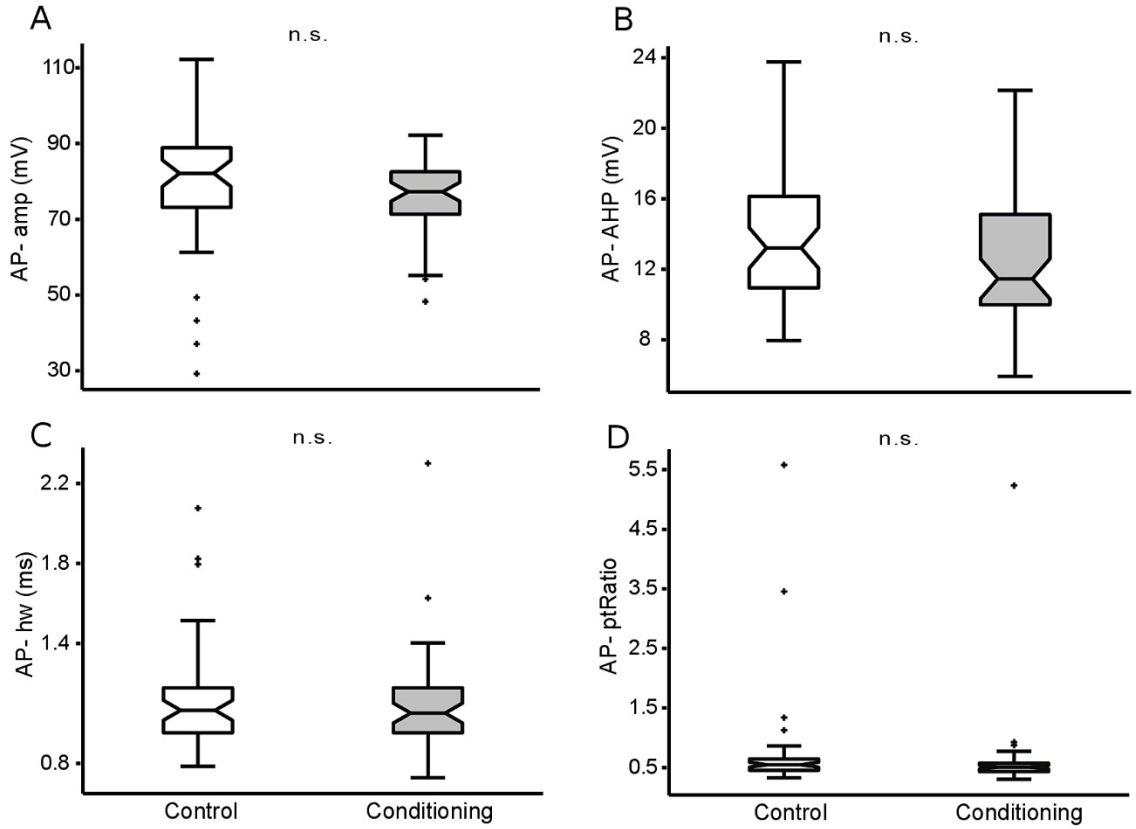

Figure S8: Action Potential parameters do not change after conditioning. A) Amplitude of the action potential. Mean values: APamp control = 78.63 ± 14.95, APamp conditioning = 75.60 ± 9.77 B) Afterhyperpolarization. Mean values: AP-AHP control =13.62 ± 3.76, AP-AHP conditioning = 12.66 ± 4.15 C) Half with. Mean values: APhw control = 1.11 ± 0.26, APhw conditioning = 1.1 ± 0.24 D) Peak to though ratio. Mean values: APptRatio control = 0.73±0.83, APptRatio conditioning = 0.61 ± 0.68. Differences are assessed by a paired t-test. (ns= non significant, $p > 0.05$) (n = 50). On each box, the central mark is the median, the edges of the box are the 25th and 75th percentiles, the whiskers extend to the most extreme data points not considered outliers, and outliers are plotted individually. The parameters for each cell were measured from the first action potential elicited at the middle trace of step current injection.

The results of the cluster analysis of discharge patterns are shown in Figure 2. We cut the clustering tree at a level that separates the traces into 5 distinct families. Traces that are representative of each family are shown in Figure 2B. Beneath each representative trace the average of the firing rate vectors for that cluster are depicted. The clustering algorithm captures well the typical time courses of the firing patterns. One main branch of the cluster tree contains accelerating and non-adapting firing patterns, while the other contains adapting and intrinsic bursting patterns together with a smaller group of traces that have delayed spiking profiles.

The consistency of the algorithm is confirmed by its successful clustering of independent feature vectors derived from the same set of current injections (same cell under the same conditions) into a single cluster. Indeed, in 86% of cases (43 of the 50 cells) the algorithm successfully allocated the majority of vectors from the same set of current injections into single clusters. Vectors from the 7 remaining cells were not consistently classified. For 50% of the cells all of their voltage traces fell into the same cluster, and for 90% of the cells at least 50% did (see supplementary Figure S9). The allocation of some responses from the same cell into more than a single cluster does however follow a biological logic. For example, for cells classified as accelerating, some of their voltage traces could reasonably fall into the non-adapting cluster because acceleration may vanish at high current injections. A similar reasonable misclassification is possible for adapting traces. In this case low current injections may be classified as non-adapting because the currents are not high enough to elicit adaptation (see supplementary Figure S10). In particular, many of the traces belonging to the delayed spiking cluster come from cells whose traces at low current injections were assigned to the accelerating cluster, or belonged to non-adapting cells with spiking delay.

The transitions between cluster types induced by the stimulation protocol are shown in Figure 2C. This figure considers only those cells in which responses both before and after conditioning could be clearly assigned to the same or different clusters. In total, 68% of the cells (n=50) changed their original cluster as a result of subthreshold conditioning.

This quantitative result supports the qualitative observation that cells tend to transition towards more adapting and intrinsic burst profiles. Among the 20 cells initially falling into the non-adapting cluster, 70% exhibited such changes in response, with 35% moving into the intrinsic bursting category, and 35% exhibiting

adapting spike patterns. Of six cells that began in the adapting cluster, 5 cells (83%) switched to the intrinsic bursting type.

Most of the cells for which the firing pattern did not change were already in the most common target states of transitions. For example, 89% of the intrinsic bursting cells did not change cluster. This provides further evidence for a predominantly unidirectional change of firing patterns in response to conditioning. The 7 cells that could not be consistently classified under control conditions, were all correctly classified after the stimulation. They showed the same transition tendencies: 5 of the 7 cells (71.4%) moved into the intrinsic bursting cluster, and 2 cells (28.6 %) became adapting.

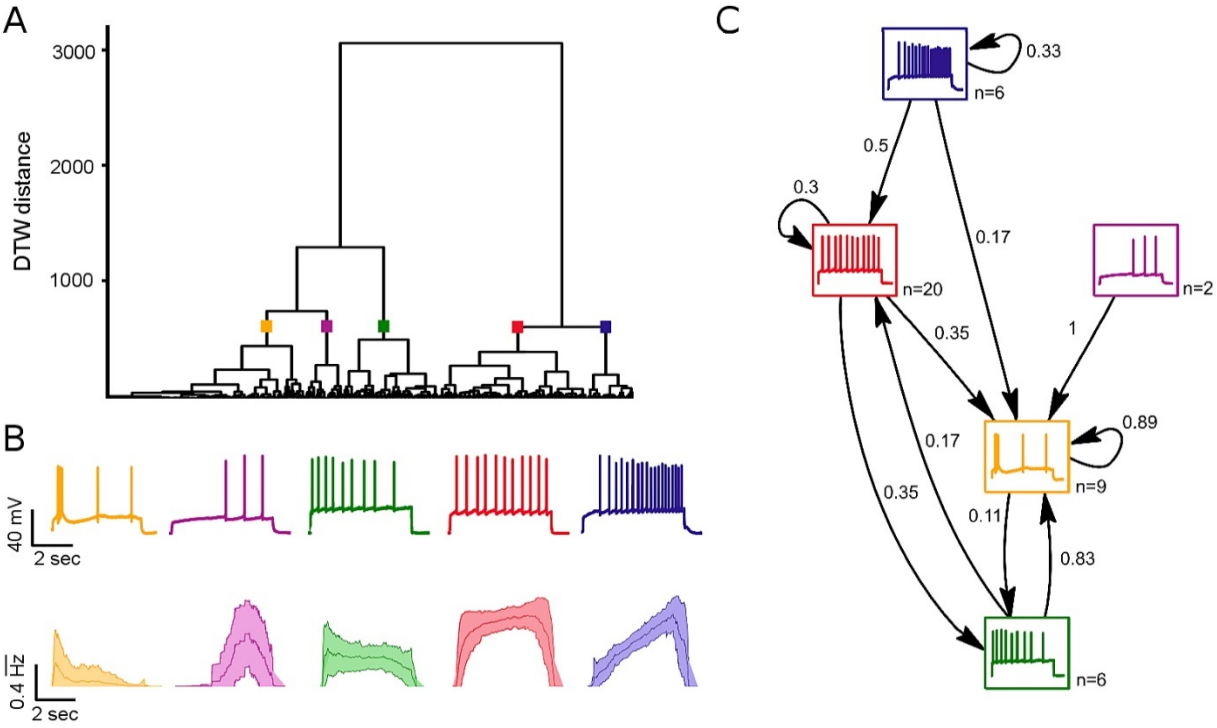

Figure 2: Hierarchical clustering of experimental discharge traces. A) Dendrogram of clustered traces. Two main families can be identified: one containing adapting and bursting traces, together with delayed spiking patterns; and another branch containing regular and accelerating traces (n = 50). B) Representative traces from each cluster, together with its pattern name according to the Petilla classification. Below, average instantaneous firing rate over all traces belonging to the same cluster. Dashed lines indicate standard deviations. The instantaneous firing rate (in Hz) is normalized to 1. C) Transitions observed between firing patterns before and after conditioning. Each cell is assigned to a single cluster for both the control and conditioned cases. Arrows indicate transitions between types whenever a cell changed cluster. Self-loops indicate that the firing pattern was retained after conditioning. Numbers indicate percentages of observed transitions, and the number of cells in each category under control conditions is displayed next to each pattern type. Cells tend to transition towards adapting and bursting patterns following conditioning (n = 43). Seven cells were assigned as unclassified.

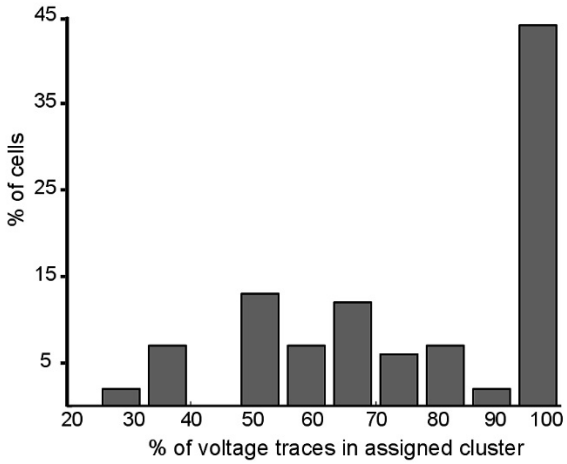

Figure S9: Clustering performance on the step wise voltage traces. The capacity of the clustering algorithm to group together independent voltage traces derived from the same set of current injections was evaluated. Histogram x-axis accounts for the percentage of voltage traces from the same set that are assigned to a unique cluster. Y-axis, shows the percentage of cells that fulfil the x condition. Ideal performance of the algorithm would allocate 100% of voltage traces coming from same set of current injections to the same cluster. For most of the cells, at least half of the voltage traces fall into one cluster, and almost 45% of the cells have all traces (100%) assigned to same cluster (n = 50).

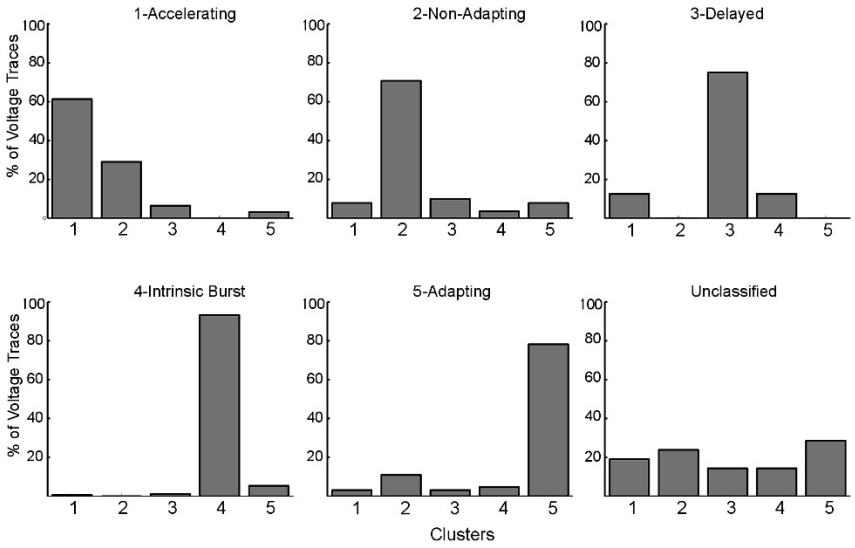

Figure S10: Misclassified voltage traces from an assigned cell. Each panel shows the percentage of voltage traces of the cells assigned to a given cluster, which have been assigned by the algorithm to the other clusters. For example, first panel shows that 30% of voltage traces of cells classified as Accelerating fall into the Non-Adapting cluster. At higher current injection the accelerating pattern is lost. Because of high firing rate the algorithm now classifies the traces as non-adapting. Numbers on the x axis correspond to the different cluster classes. 1-Accelerating, 2-Non-Adapting, 3-Delayed, 4-Intrinsic Burst, 5-Adapting. Last panel shows the distribution of voltage traces of unclassified cells (n = 50).

Changes of firing patterns occur in different morphological types of CA3 neurons

We explored whether the transitions of response were characteristic of distinct morphological types of cells. During experiments the neurons were selected for recording without being able to visualize their morphological type. Recorded cells were filled with biocytin, and so their basic morphology could be established post hoc using conjugated biotin fluorofor that enhances visualization of labeled cells. We filled 30 of the 50 cells reported here. Figure 3 shows representative examples of the somatic and dendritic morphology of these neurons. Because of the somatic and dendritic shape, and the presence or absence of dendritic spines we segregated the cells between pyramidal and smooth.

It was found that response to conditioning was not determined by morphological type. For example, Figure 3A shows a pyramidal cell that underwent a transition from a non-adapting burst to intrinsic burst profile. Another pyramidal cell in Figure 3B had a delayed accelerating profile before, and intrinsic burst behavior afterward. A smooth cell (i.e. rounded somata and bipolar shape) in Figure 3C moved from a non-adapting continuous to an adapting continuous profile. The subjective observation was further confirmed by analyzing the cluster transitions of both pyramidal and smooth cells. The pattern of transitions was found to be identical for the two populations (see supplementary Figure S11).

We noticed however, that 4 of the cells in the non-adapting cluster had high firing rates under control conditions (see supplementary Figure S12). Two of them had smooth cell morphologies, which could potentially be Fast Spiking interneurons. The other two cells corresponded to very densely spiny cells, with stellate morphologies. Interestingly, although transitions towards bursting or classic adapting behaviors were not observed on these cells, there was a visible modulation on the delay of the first spike in both cell types suggesting that the stimulation protocol had a differential effect on this particular neural population.

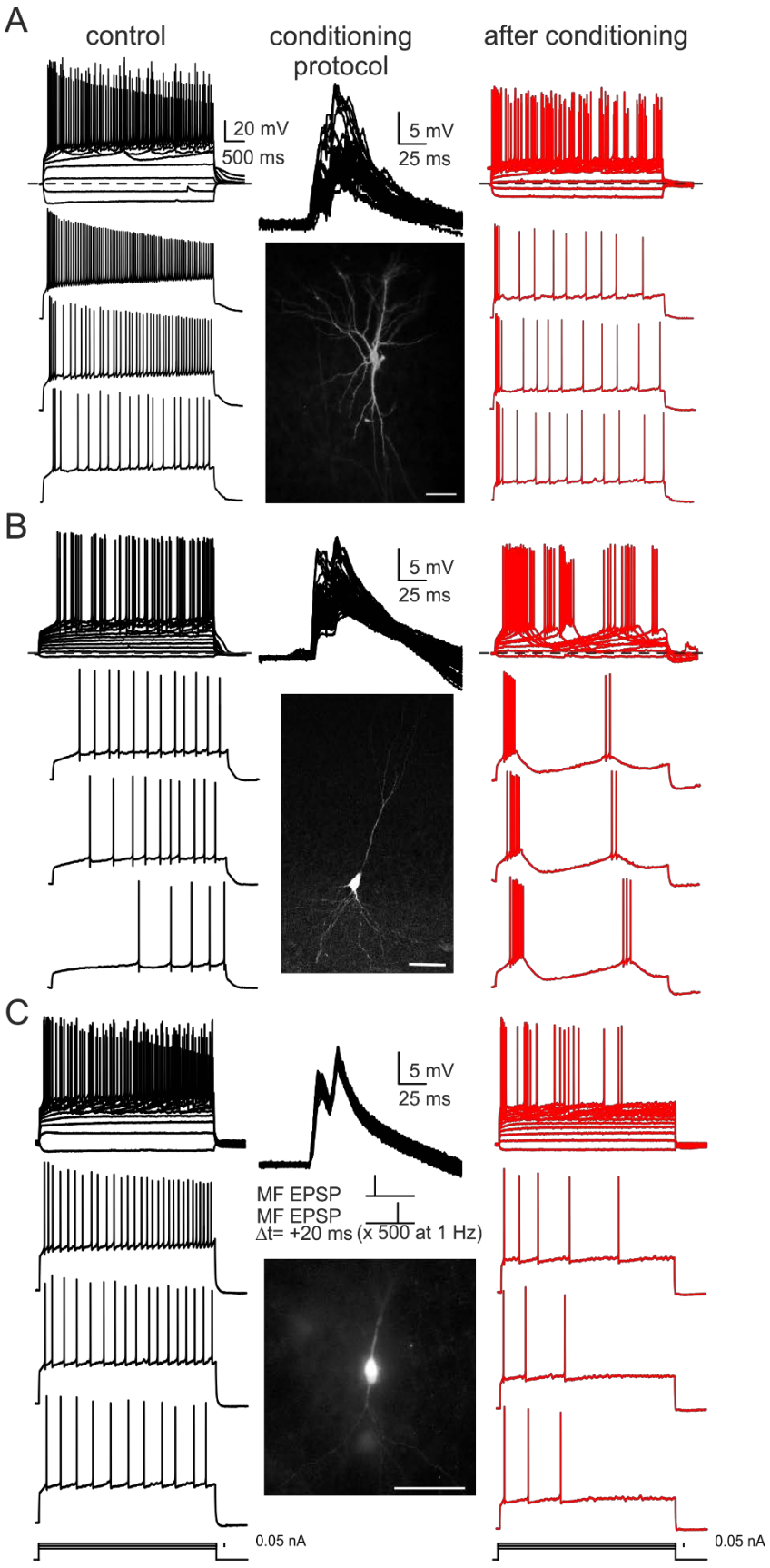

Figure 3: Firing pattern transitions occur in neurons with diverse morphologies and initial conditions. Three examples of neurons in the CA3 area that present different morphologies and different firing patterns in control conditions are shown.

The discharge patterns were measured by injection of step currents of increasing amplitude. Control measurements (black traces, left) were followed by stimulation of the mossy fibers (as described in Figure 1A). Thereafter patterns were measured again (red traces, right). Middle panels show EPSP shapes elicited by the conditioning; and below the cell morphology obtained by labeling the cells with biocytin. A) Pyramidal cell switches from non-adapting burst to intrinsic burst firing. B) Pyramidal cell switches from delay accelerating to intrinsic burst pattern. C) Smooth cell switches from non-adapting continuous to adapting continuous firing. (Scale bars = 50 µm). As shown in Figure 2, transitions of pattern towards adapting or initial burst profiles occur most frequently, and these transitions are independent of the morphological type of the cell and its initial firing pattern (see supplementary Figure S11).

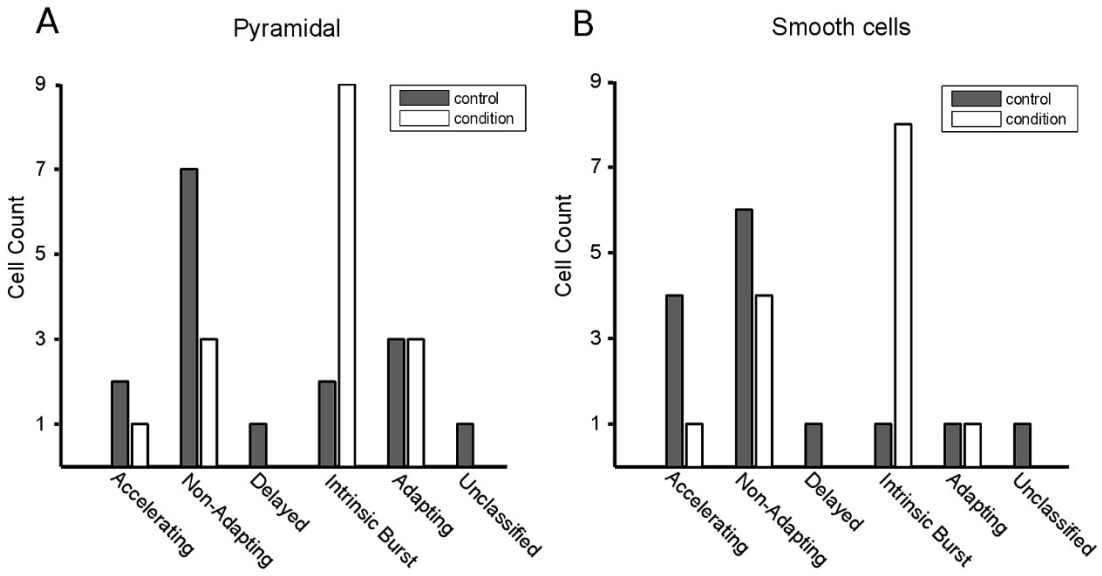

Figure S11: Pyramidal and smooth cells cluster counts before and after stimulation. A) Pyramidal neurons in each cluster before and after stimulation. Histogram shows number of pyramidal cells falling into the 5 different clusters, before and after conditioning. There is an increase of cells in the intrinsic burst cluster after conditioning, and no decrease on the adapting one; whereas the other clusters show a decrease of cells after stimulation (n = 16). B) The similar changes are found for the smooth cells (n = 14). Neurons morphologies were subjectively classified on basis of somatic shape and size, dendritic structure and the presence or absence of dendritic spines.

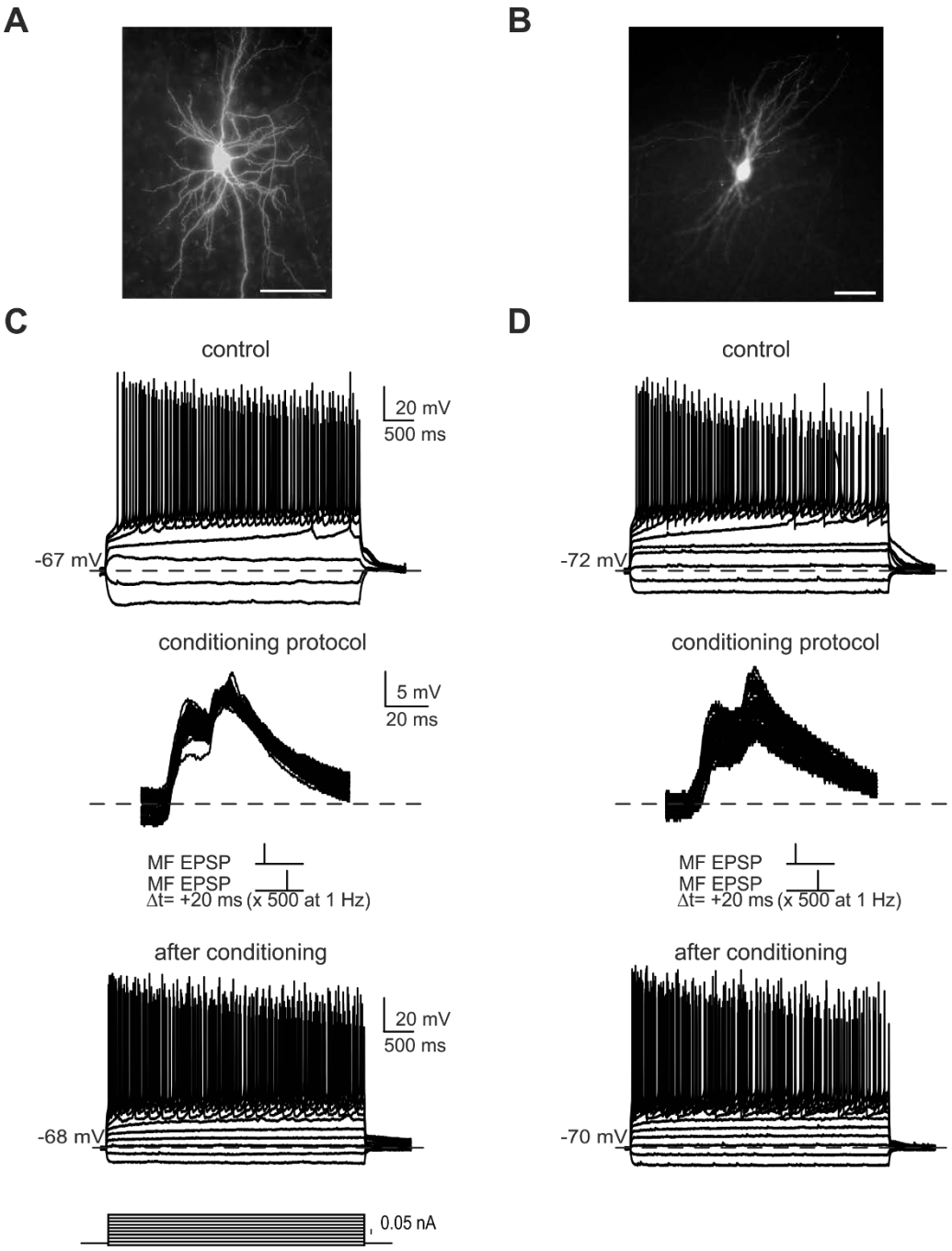

Figure S12: Selected cells with high frequency firing do not switch to intrinsic burst firings. A) Biocytin filled spiny cell with stellate morphology. B) Smooth cell with rounded somata and short dense dendritic arbor. Firing patterns in control (upper) and after stimulation (bottom) are shown beneath each cell for both the stellate (C) and the smooth cell (D). The neurons present a non-adapting pattern both, before and after conditioning. Middle panel shows EPSPs elicited in the cell via mossy fiber stimulation. Note that after conditioning, cells do not change the Petilla firing pattern mode, although there is a visible modulation on the delay to first spike (’ramping response’). There is also a visible decrease in the input resistance of both cells. Scale bar = 50 µm.

A conductance based model explains the transitions between firing patterns

The consistent transition towards adapting and intrinsic bursting behaviors suggests a common underlying mechanism for most cell types. A prime candidate for this mechanism is a change in the profile of active conductances contributing to action potential discharge dynamics.

We explored this possibility using simulations of action potential discharge in a conductance-based single compartment neuron model containing 9 voltage and calcium gated ion channels (see Methods). The densities and kinetics of these channels were derived from experimental measurements of CA3 pyramidal neurons (Hemond et al. 2008). We tuned only their maximum conductances to reproduce the discharge patterns observed in our experiments. The allowable ranges of the maximum conductances were restricted to those reported in the literature (Hemond et al. 2008).

The model reproduces the main features of discharge classes obtained by clustering of the experimental data (Figure 4). The occasional decrease in spike amplitude seen in some of the experimental traces is probably due to sodium inactivation. We choose not to include this feature in the model, because it does not affect the overall dynamics of the spike discharge. The absolute values for the conductances required to reproduce all traces are shown in supplementary Table S1. The conductances whose values were changed to model transitions between different firing patterns were the following. Four types of potassium channel (g_{Km}, g_{Kd}, g_{CaK} and g_{KA}), and the three calcium conductances (g_{CaT}, g_{CaN} and g_{CaL}). Following (Hemond et al. 2008) these last conductances were changed proportionally, and so they are represented by a single parameter, g_{Ca}. The action potential conductances (g_{Kdr} and g_{Na}) were held fixed, except for the case of the regular pattern shown in Figure 4A, where a slight increase of the g_{Kdr} conductance was necessary to match the rate of the experimental trace. Figure 4 shows that the model requires quite different ion channel configurations to reproduce different discharge patterns. The presence of key modulatory conductances is crucial for the reproduction of the different timing properties of the cell's spike discharge. In this manner, for delayed discharge pattern (Figure 4B), the presence of g_{Kd} is required for a delayed onset of the spiking, and the slow inactivation of g_{Kd} is important for generating the accelerating discharge pattern (Figure 4C). We found that a shift of +10mV in the inactivation of g_{Kd} significantly improved the accelerating index and reduced the tuning cost for

obtaining accelerating discharge pattern (Miller et al. 2008). In the case of the adapting and intrinsic burst pattern (4D and E), the inclusion of g_{Km} and g_{Ca} (given there are basal levels of g_{CaK}) is necessary for the slowing down of the action potentials after the initial discharge. The rest of the conductances were varied in order to match the characteristics of the experimental trace shown, however, we find that g_{Ca}, g_{CaK}, g_{Km} and g_{Kd} are essential to match the overall dynamics of discharge responses observed experimentally.

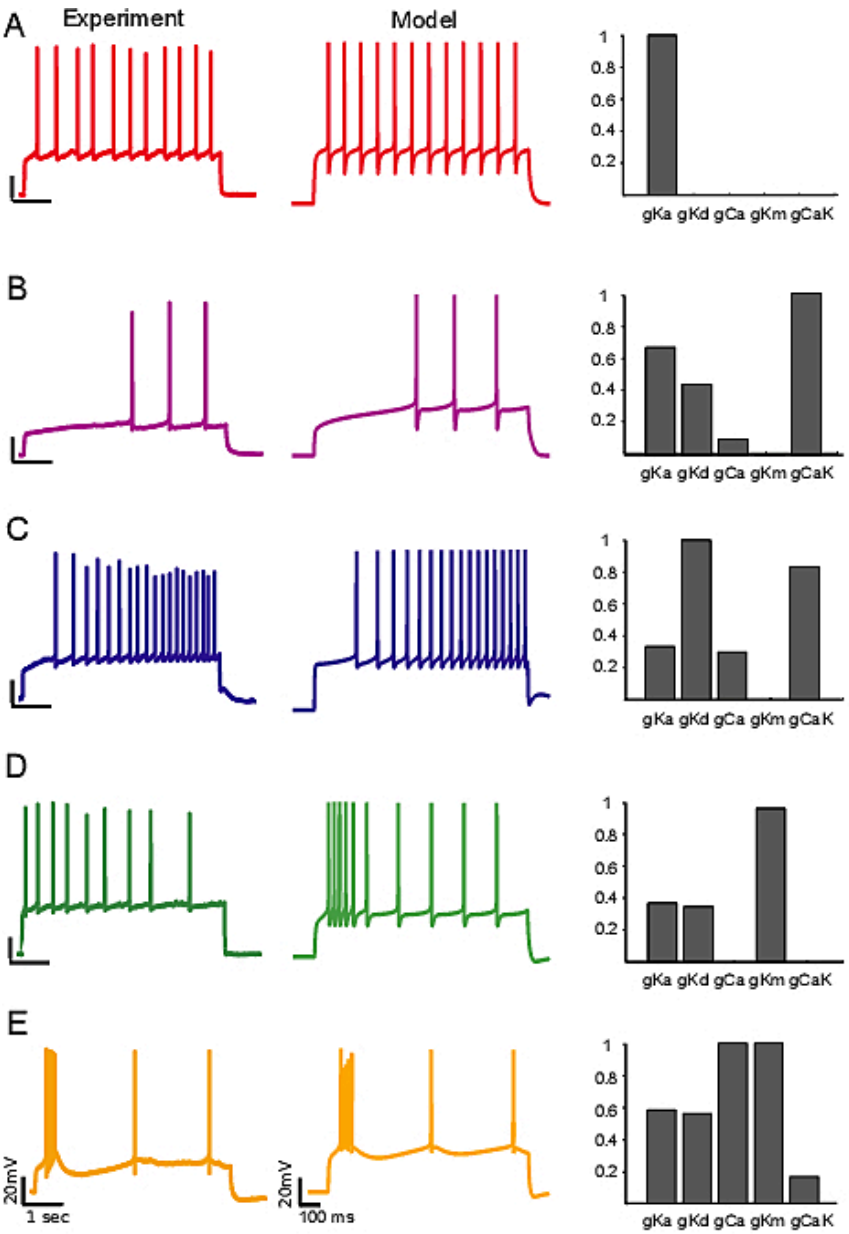

Figure 4: Conductance-based model with 9 different ion channels reproduces the diversity of experimental traces. For each of the clusters in Figure 2, a representative experimental pattern (left) could be reproduced by the single compartment model (center). Example patterns: A) Non-Adapting; B) Delayed; C) Accelerating; D) Adapting; E) Intrinsic Burst. Right column shows profiles of the 5 conductances used to generate each of the different model patterns. Conductance values are normalized to 1. Only the 5 conductances that needed to be changed between patterns are displayed (g_{KA}, g_{Kd}, g_{Ca}, g_{Km}, g_{CaK}). For each firing pattern a different profile of conductances was necessary to achieve a good fit. The different model patterns could not be generated by varying the amplitude of injected current alone. The exact conductance values used to produce every model pattern and the amount of current injection are shown in the supplementary Table S1.

Clustering of model traces

We compared the performance of the clustering procedure on the model and the experimental data. In a first step we tuned the maximal conductance densities of the model to match the various experimentally observed firing patterns. This tuning was performed manually, and the match to the traces was qualitative. Our intention in this step was simply to obtain a database of representative ranges of conductances that could plausibly explain the discharge patterns observed experimentally. To do this, the maximal conductances of the different channels were swept through ranges that would likely encompass the experimentally observed patterns (see supplementary Figure S2). In this way a total of 861 conductance profiles were generated. We obtained the discharge response of each profile to different levels of current injection, giving a total of 5166 voltage traces with their associated conductance profiles.

The dynamic time-warping algorithm was used to match optimally every single experimental trace against the collection of traces in this model database, and so obtain an estimate of the conductance profile likely to be present in the experimental neuron. These estimates also define the subset of model traces that best represent their experimental counterparts. This subset was then fed to hierarchical clustering procedure, as performed previously for the experimental data (Figure 2).

The result of hierarchical clustering of the model traces is shown in Figure 5A. There are four main families, corresponding to adapting, intrinsic bursting, accelerating and non-accommodating behavior. The classification of the model traces is very similar to the experimental one, except for the absence of the small class of delayed-spiking patterns (second cluster of Figure 2), which in the case of the model were allocated mostly to the accelerating cluster. Figure 5B characterizes the crucial conductances determining the transitions of discharge patterns. These are g_{Km}, g_{CaK}, and g_{Ca}. g_{Kd} plays a role in generating acceleration, but does not contribute to the transitions. In panel C each point indicates the location of an experimental discharge response in this conductance space. The color of a point shows its cluster assignment. There is a systematic segregation of the data, indicating how the discharge classes of Figure 5A conform to localized regions of conductance space. This correspondence of firing patterns and biophysical parameters offers an interpretation of the causes of transitions between firing behaviors induced by mossy fiber stimulation (Figure 2C). The shift towards adapting and intrinsic bursting behavior corresponds to an increase in calcium related, and g_{Km} conductances (Figure 5D, E).

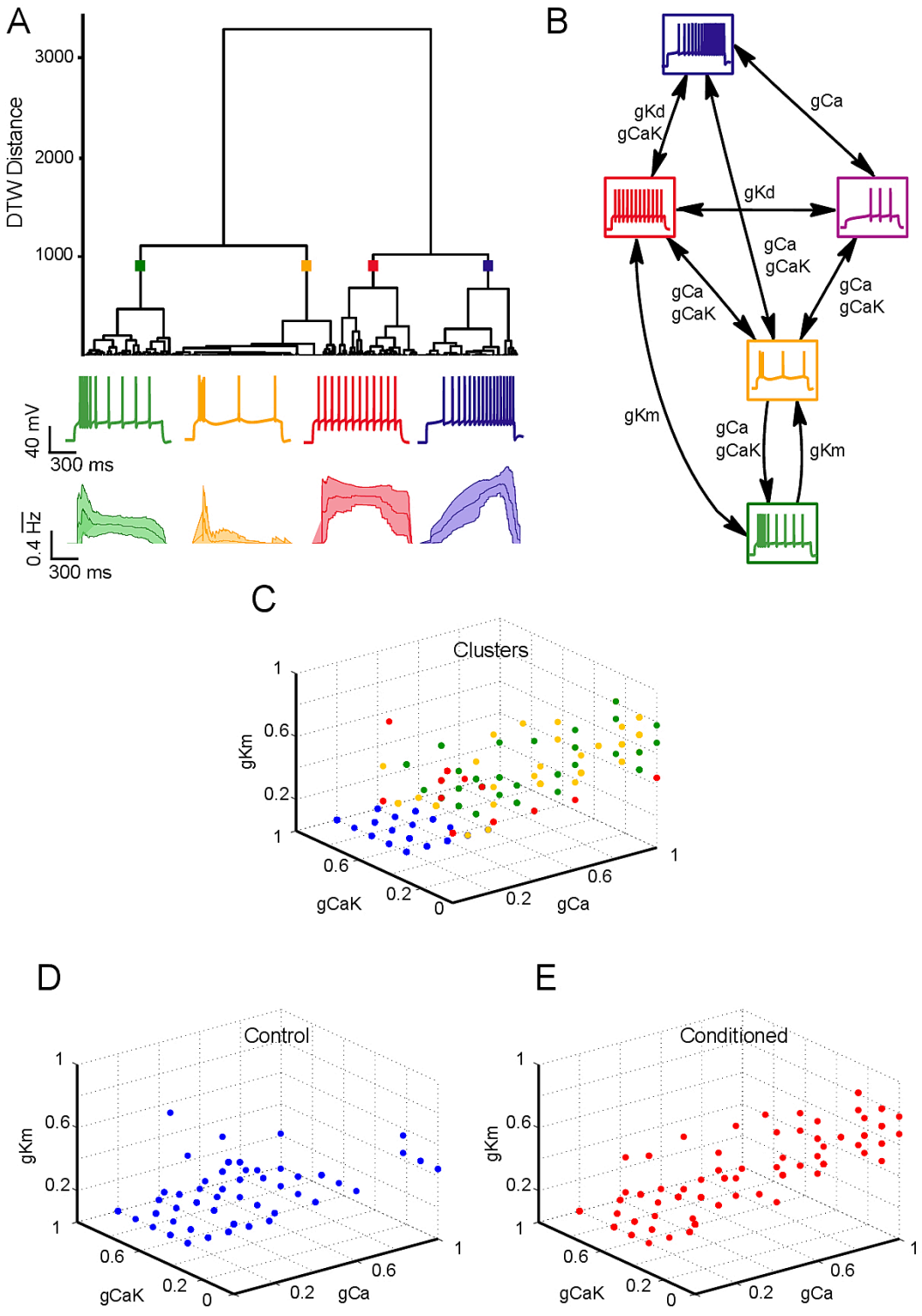

Figure 5: Hierarchical clustering of the model-generated discharge traces mapped to the experimental traces. Every experimental trace was matched to a model trace using the DTW algorithm as a search tool on a model database of traces. Hierarchical clustering was then applied to the model traces. A) The clustering algorithm distinguishes four main families, which correspond to adapting, intrinsic burst, non-adapting and accelerating patterns. Below the dendrogram, a

representative model trace of every cluster is depicted. Underneath, average instantaneous firing rate within each cluster with its standard deviation. (n=50) B) Conductance road map showing the key conductances responsible for a transition in firing pattern on the model generated traces. The main channels implicated are g_{Ca}, g_{CaK}, g_{Kd} and g_{Km}. C) Distribution of the conductance vectors of the model traces clustered in (A) in 3D space. Axes correspond to: calcium conductance variable (g_{Ca}); calcium-dependent potassium channel (g_{CaK}); and potassium channel (g_{Km}). The dots are color coded according to their cluster assignment. D) Distribution of the conductance vectors in 3D space of the model traces matched to cells in control conditions E) Distribution of the conductance vectors of traces matched to cells after conditioning. Conditioned cells present a higher content of g_{Ca} and g_{Km}.

DISCUSSION

We have shown that the characteristic firing patterns of neurons in the CA3 region of the hippocampus can be modified by subthreshold paired pulse stimulation of the soma. The pulses can be elicited either indirectly by stimulation of the mossy fibers; or directly by somatic current injection (see supplementary Figure S4). These results indicate that suprathreshold behavior of neurons on the time scale of hundreds of milliseconds can be modified by the statistics of ongoing subthreshold activity.

Hierarchical cluster analysis of action potential discharge traces in these cells confirmed the major classes of response pattern previously observed in hippocampal neurons: regular, accelerating, adapting, and intrinsic bursting. However, conditioning by pulse stimuli resulted in transitions from one response class to another. Typically, these transitions were towards more adapting and intrinsic burst responses. The changes were present immediately after the 8-minute conditioning protocol, suggesting that the mechanism underlying the transition operates on a timescale of at most, some 100s of seconds.

The changes in pattern could be reproduced in simulations of a conductance- based model of neuron electrophysiology. We were able to reproduce all of the experimental responses with this model, and so obtained estimates of the conductance profiles underlying the behavior of each experimental cell before and after conditioning. We found that the shift in responses towards adapting and intrinsic bursting can be explained by recruitment of calcium and M-type potassium

conductances. The collection of calcium conductances (T, N and L) were treated as a single $g_{Ca,}$ with changes in g_{Ca} being applied as proportional changes to each of its components. The conditioning protocol consisted of a train of paired pulses applied either by stimulation of the mossy fibers, or by intrasomatic current injection. We found that the somatic voltage responses of 15 mV amplitude in average are more likely to have an effect. For our typical input resistance of 144MΩ, this means that 0.1 nA current pulse amplitudes are adequate to evoke a transition in discharge pattern. This current is only a half of the median rheobase current (0.23nA) in our cells, indicating that the mechanism that modulates the discharge conductances operates in a current range well below the necessary for generating the discharge itself. We used only paired pulses in these experiments. Future work must explore in more detail the range of stimuli required to elicit the transition, and so establish to what aspects of the input current statistics the postsynaptic neuron is sensitive.

Developmental timing of firing pattern formation

This study was performed on organotypic cultures, derived from brain slices of newborn rats that are incubated for three weeks using the roller-tube technique (Gähwiler 1981). Organotypic cultures have been used extensively to characterize electrophysiological properties of hippocampal neurons and it is known that the tissue preserves the anatomical organization of the adult hippocampus, as well as its connectivity and characteristic spontaneous activity (Gähwiler 1988; Okamoto et al. 2014). Furthermore, it has been validated as a reliable in vitro model for studying CNS injuries, and for pharmacological screenings (Finley et al. 2004; Sundstrom et al. 2005).

Our hippocampal slices are derived from immature brains, and this raises questions of whether the observed transitions of firing patterns are likely to happen in vivo or whether they reflect activity-dependent acquisition of firing properties of neurons in the developing brain. Electrical maturation of neurons is a long lasting process that extends until late postnatal days (Yuste 2005), and which has been shown to require cortical activity (García et al. 2011). For example, at the time of our recordings (around P20) some channels such as K_{V3} are not yet fully expressed (Okaty et al. 2009). Thus, the conditioning protocol could influence the activity-dependent maturation of the electrical properties of the neurons recorded, biasing them towards one particular electrical type. Such sensitivity to network activity statistics implies that

the intrinsic firing characteristics of neurons are determined by their embedding network during development rather than being explicitly encoded in their genotype. Unraveling the rules by which these cells acquire their characteristic firing properties will provide valuable information on how neurons are dynamically integrated into circuits by adapting their discharge behavior according to their synaptically received network spiking statistics. Additionally, further studies on brain slices and in vivo are needed to understand if this functional plasticity is present also in the adult brain, and whether it holds also for other brain regions such as the cerebral cortex.

Relationship between electrical properties and neuron type

We identified both pyramidal and smooth cells amongst those recorded (see Figure 3), indicating that diverse types of CA3 neurons may change their discharge type. Although we observe most of the firing patterns described by the Petilla convention (Ascoli et al. 2008), that schema describes a greater diversity of morphological and molecular types of interneurons (Markram et al. 2004; Somogyi and Klausberger 2005) than we were able to recognize. Thus, a significantly larger database, together with full morphological and molecular characterization of different interneurons will be required in order to extend our observations of dynamic discharge types to the full Petilla set.

For example, four cells of our dataset showed under control conditions a high frequency non-adapting discharge, two of them with interneuron-like morphologies, potential Fast Spiking interneurons. The other two cells corresponded to very densely spiny cells, with stellate morphologies. Interestingly, transitions towards bursting or classically adapting behaviors were not observed on these cells, although there was a visible modulation on the delay of the first spike in both cell types (see supplementary Figure S12). This may indicate that these cells may respond under a different set of rules to the stimulation protocol provided. The modulation on the delay of the first spike also agrees with a recent study by Dehorter et al. 2015, in which basket cells are shown to tune this same feature in response to the excitability of the surrounding network.

In a previous study, Druckmann et al. (2013) used automated statistical analysis to construct an extensive database of firing patterns. They too found a hierarchical organization of the traces, in which base class of patterns were first categorized into adapting and fast spiking profiles. One of the distinction between these two patterns

is the presence or absence of calcium channels. A genetic predisposition for certain firing patterns and different likelihoods of transitions in response to changes of network activity could thus be explained by the different initial densities of conductances in different cell types.

Using biophysical models to understand changes in firing patterns

In order to understand the biophysical origins of different firing patterns, and to gain insights into the internal mechanisms that may cause the transitions observed, we used a conductance-based single compartment model with 9 different ion channels based on Hemond et al. (2008). They could reproduce several experimental firing patterns observed in CA3 neurons, as we could with minimum tuning of their conductance parameters.

Here we have shown that the pattern transitions among all the known firing patterns can be easily achieved through modifying only the specific maximal conductances of a few key ion channels (see Figure 5B). We propose that the main candidates for eliciting any type of transitions are g_{Kd}, g_{Km} and g_{Ca} coupled with g_{CaK}. We are aware that these are only potential candidates, and the same effect on firing pattern transition could be elicited considering other ion channels, or combinations of them. The key principle here is the effect on the dynamics of spike discharge that the increase on a certain conductance elicits. In this manner, the effect on the spike delay mediated by a slow inactivating hyperpolarizing current, such as g_{Kd} can also be elicited by a slow non-inactivating depolarizing current such as g_{Nap}. It could thus be possible that different cells recruit different set of conductances depending on their initial conductance profile.

Our single compartment electrophysiological model should not be seen as representing only a somatic compartment. Instead it is a single compartment model that approximates the entire neuron. The model focuses on how distinct firing patterns can emerge through different configurations of a given set of conductances, rather than the influences of detailed cellular morphology. We found, as did Hemond et al. (2008) that this single compartment model was well able to reproduce the experimentally observed traces. A more detailed model consumes much greater resources, and would increase the computational cost for generating the database of variable conductance vectors used in Figure 5. The diversity of cell morphologies and the paucity of information concerning the distributions of ion channels across a model

with detailed morphology would have made fitting intractable, without providing further insights into the central question of this paper. Nevertheless, we confirmed that the results for the single compartment model shown in Figure 4 could be reproduced in the morphologically realistic model described by (Hemond et al. 2008) (see supplementary Figure S13). Although the maximal conductance values had to be reestablished, we observe that the principal key channels responsible for the firing pattern transitions are conserved in both the single compartment and in the realistic CA3 model.

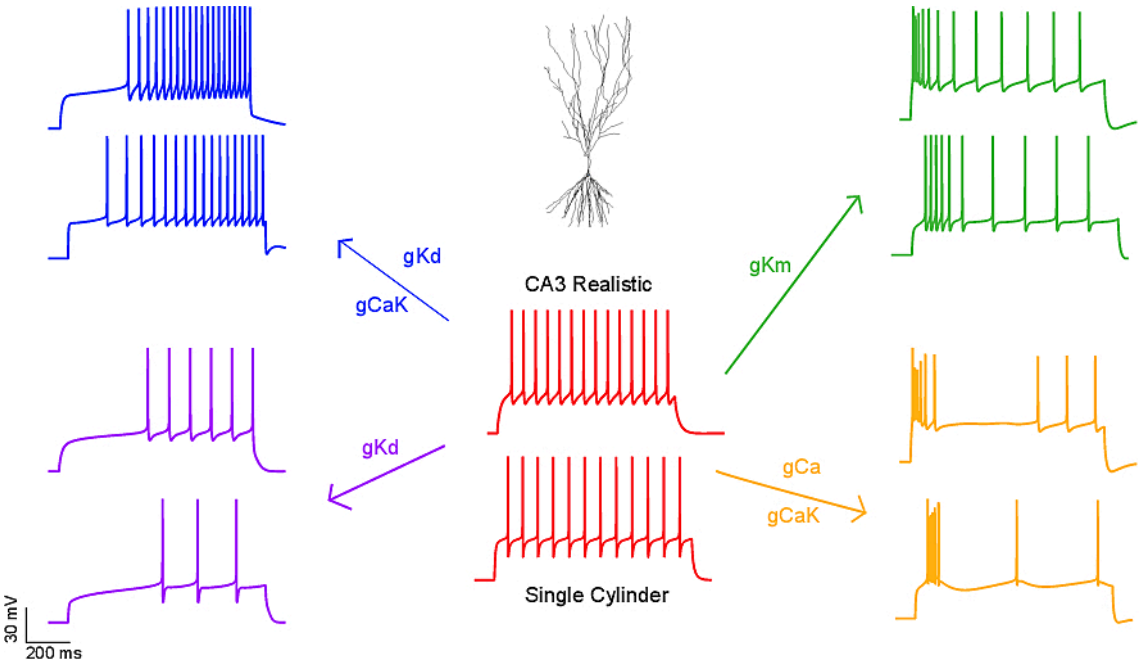

Figure S13: Firing pattern transitions can be reproduced in both, a single compartment model and a realistic CA3 pyramidal model. We find that the key ion channels responsible of the firing pattern transitions are kept in both the single compartment model and the realistic one. The upper trace represents the model traces reproduced on the CA3 realistic pyramidal cell, and below the same firing pattern on the single cylinder is shown. The maximal conductance values used to reproduce every pattern are shown in the Supplementary Table 2.

Candidate mechanisms for firing pattern transitions

One possible explanation for the transitions is that continuous stimulation of the neuron may alter the ion concentrations in the cellular environment; for example, by altering potassium and calcium concentrations (Jensen et al. 1994; Su et al. 2001). However, our simulations show that the time constant of decay of the intracellular calcium is too short to allow significant accumulation (see supplementary Figure S15). Even if it were greatly increased, the accumulation of calcium in the cell would be insufficient to elicit a radical change in firing pattern (see supplementary Figure S15).

The more likely explanation proposed here is that the conditioning stimulation causes recruitment of g_{Ca}, and g_{Km} conductances (given basal levels of g_{CaK}). Activity dependent changes of conductance have been extensively studied, and shown to be triggered even by learning paradigms (Zhang and Linden 2003; McKay et al. 2013). The work of Turrigiano et al. (1994) suggested that a calcium dependent mechanism could modulate the neural conductances in STG lobster neurons, and that this would translate into changes in the cells' firing patterns. Later work showed that depolarizing pulses at 1Hz could alter the density of the calcium-dependent outward current I_{CaK} and the transient outward current I_A in the STG (Golowasch et al. 1999). These studies led to theories of homeostatic plasticity (Turrigiano and Nelson 2004; Abbott and Nelson 2000), which propose that cells maintain both the turnover of ion channels, and a stable level of activity, to compensate for changes in synaptic strength. However, the time scale of such mechanisms typically extends over hours, and presumably involves processes of gene transcription (Lee et al. 2005), whereas in our experiments the changes were observed immediately after conditioning. Aizenman and Linden (2000) observed rapid changes of excitability of cerebellar cells after synaptic stimulation, and proposed a calcium-dependent modification though phosphorylation of g_{CaT} and g_{CaK} to account for the observed changes. Interestingly, these are the same candidate channels that we have identified as underlying the discharge pattern changes in this study.

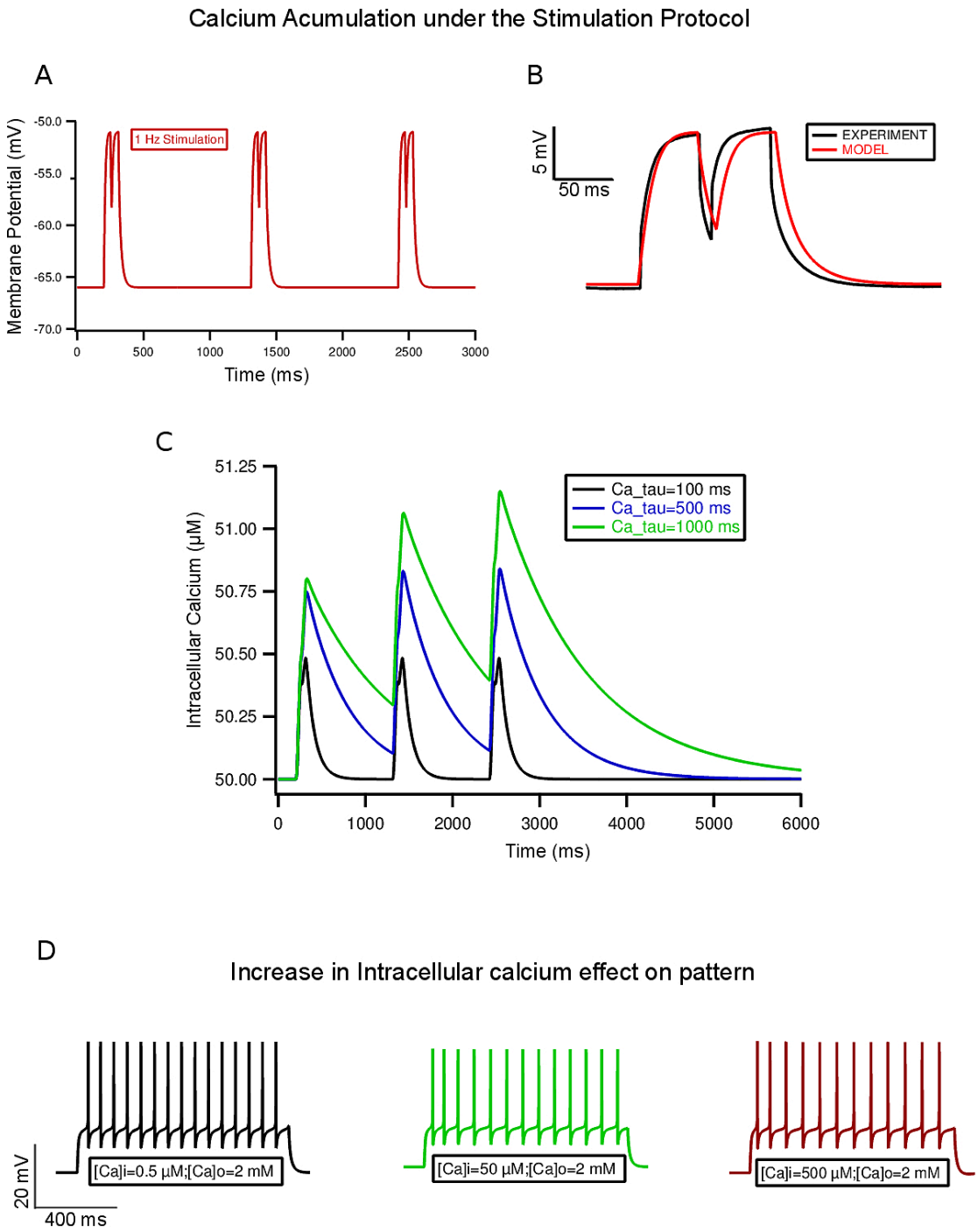

Figure S15: Firing pattern transitions in model are not due to calcium accumulation. A) Protocol applied to the model cell: 1Hz current stimulation by double current pulses that elicited a depolarization of 10mV, repeated 500 times. B) Comparison of model pulses with those elicited in the somata of experimental cells. C) Due to kinetics of calcium decay, the ion does not accumulate over period of stimulation (black trace). Decay must be much longer for calcium to accumulate significantly (green trace). D) Hypothetical increase in intracellular increase has little effect on pattern of discharge, even when increased 1000 fold (from left to right).

Activity dependent recruitment of conductances

How can the simple subthreshold stimulation protocol rapidly and selectively recruit the candidate conductances? Previous studies had proposed a combination of biophysical and biochemical mechanisms that translate into such rapid specific recruitment (Shin et al. 1999). Rapid up- or down-regulation of ion channels via phosphorylation or vesicle modulation due to calcium signaling has been demonstrated (Flavell and Greenberg 2008; Davis et al. 2001; Zhang and Linden 2003).

We speculate that the conductances could be recruited through a resonance mechanism. It has been known for decades that neural conductances can act as inductors that make the neuron respond preferentially at certain frequency bands (Hutcheon and Yarom 2000). These resonant properties of cells may underlie important functional implications in response to neural activity and different brain rhythms (Llinas 1988; Buzáski and Draguhn 2004). The characteristic resonance frequency band of every channel would be defined by their particular time constant, and it is their interaction and distinct levels of expression, which confers to the cell its particular resonance properties. An input current signal expressing a certain frequency band could recruit conductances with matching properties within the cell and so trigger a fast biochemical positive or negative feedback process that would up- or down-regulate the maximal conductance of that particular channel (or also other channels). In support of this argument, it has been shown that ion channels possess a complex of scaffold proteins containing certain protein kinases that could selectively regulate channel conductance through phosphorylation (Davis et al. 2001).

Future work must consider the spectral properties of the paired pulse signal, and explore the possibility of frequency based conductance recruitment by direct intrasomatic injection of spectrally shaped noise. Following this line of thought, we predict that stimulations at other frequency bands not covered by our stimulation protocol would result in a different conductance regulation and so different discharge transitions than the ones observed in this study.

Functional implications of spike pattern changes

The fact that neurons possess the internal machinery to mediate the transitions observed raises questions about the computational consequences of such behavior.

As proposed by (Shin et al. 1999), a neuron that can dynamically adapt its output firing in response to the input statistics that it receives would have important evolutionary advantages. If such neuron could adjust its threshold and dynamic range upon activity, it could respond to a set of stimuli over a broad range of amplitudes and frequencies without compromising the sensitivity of the cell. Interestingly, in most cells the slope of their average firing rate vs. input current (FI) curve decreased after stimulation (see supplementary Figure S14). This shift is caused by the transition of firing patterns towards adapting and intrinsic bursting profiles.

Spike frequency accommodation has been shown to possess characteristics of a high-pass filter (Benda and Herz 2003). Since stimulations occurred at characteristic frequencies, the cells may have recruited a specific set of conductances that shift their integration properties such as to gain sensitivity in the new spectrum range. Differences in filtering properties of brain stem neurons have also been shown to facilitate the extraction of spatial information from natural sounds (Remme et al. 2014).

Besides maximization of sensitivity, it has also been shown in modeling studies that a neuron that can adapt to its own input statistics maximizes the mutual information between the input received and the output firing rate (Stemmler and Koch 1999). This type of effect can emerge following firing rate homeostasis rules and promote metaplasticity (Honnuraiah and Narayanan 2013), or on the other hand it can be their cause (Joshi and Triesch 2009). It is thus possible that due to all these functional implications, the firing patterns that have been observed are the consequences of a natural selection process that confers evolutionary advantages already acting at the single cell level. Further studies will be needed in order to unravel the role that such firing pattern transitions may have for computations in neural circuits. A first step towards this goal must be to explore more generally how the form and frequency spectrum of somatic input signals on the long time scale affect the distinct firing patterns that neurons exhibit on the short scale.

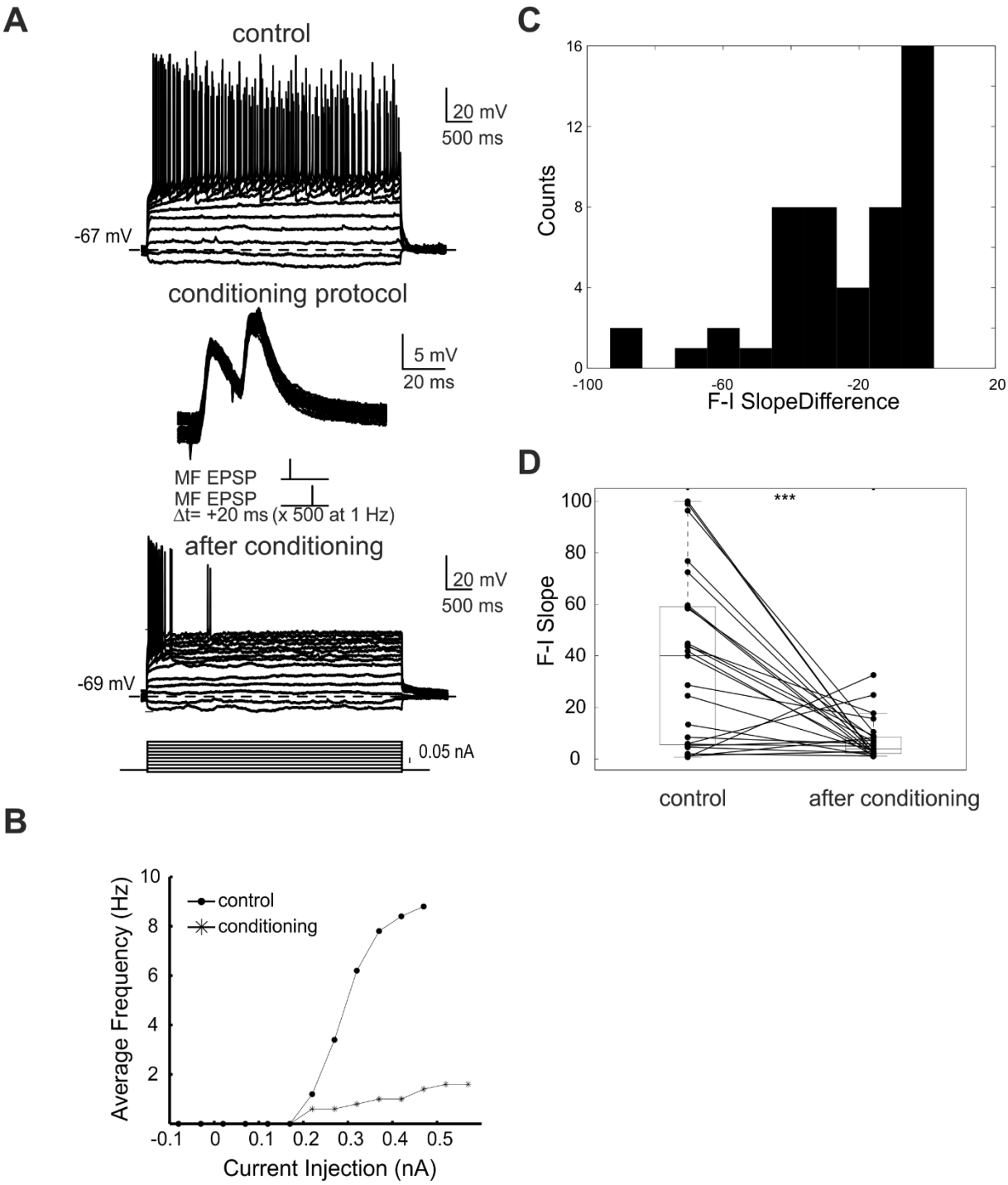

Figure S14: Slope reduction of the average frequency-current curve. A) Characteristic example of the change in firing pattern of a cell upon mossy fiber stimulation. B) Average frequency discharge elicited by the step current injections shown in A, before and after stimulation. C) Histogram which shows the distribution of the F-I slope difference (Slope of conditioned cells minus slope of control cells) across the population. D) Whisker plot showing the F-I slope in both control and after conditioned stimulus. Asterisks indicate significance for a paired t-test (***, $p<0.001$). Lines represent single cells (n=50).

CONCLUSION

We have shown that hippocampal neurons in organotypic cultures can rapidly adapt their supratheshold action potential discharge patterns in response to subthreshold paired pulse conditioning stimuli delivered to their somata either by activation of their synapses, or directly by intrasomatic current injection. We propose that these changes are mediated by recruitment of calcium and M-type potassium conductances, conditional on the statistics of their somatic input currents. Such a mechanism would allow the neuron to adapt its output behavior to the requirements of the network in which it is embedded. Our results also imply that the discharge characteristics of neurons in this hippocampal region are not constant, and so should not be used as a basis for phenotypic classification of a neural type.

ACKNOWLEDGMENTS

We thank Kevan Martin for critical comments on the manuscript, Beat Gähwiler for useful discussions, and Gabriela Michel for proofreading the manuscript. This work was supported by EU SECO Grant EU216593 and ETH Grant 2-73246-8 to K.A.C.M and Swiss National Science Foundation grant 31003A-143373 / 1 to U.G.

BIBLIOGRAPHY

Abbott LF and Nelson SB. 2000. Synaptic plasticity: taming the beast. Nature neuroscience. 3:1178–1183.

Aizenman CD and Linden DJ. 2000. Rapid, synaptically driven increases in the intrinsic excitability of cerebellar deep nuclear neurons. Nature neuroscience. 3(2):109–111.

Ascoli GA, Alonso-Nanclares L, Anderson SA, Barrionuevo G, Benavides-Piccione R, Burkhalter A, Buzsáki G, Cauli B, DeFelipe J, Fairen A, et al. 2008. Petilla terminology: nomenclature of features of gabaergic interneurons of the cerebral cortex. Nature Reviews Neuroscience. 9(7):557–568.

Benda J and Herz AV. 2003. A universal model for spike-frequency adaptation. Neural computation. 15(11):2523–2564.

Berndt DJ and Clifford J. 1994. Using dynamic time warping to find patterns in time series. In KDD workshop, volume 10, pages 359–370. Seattle, WA.

Brandalise F and Gerber U. 2014. Mossy fiber-evoked subthreshold responses induce timing-dependent plasticity at hippocampal ca3 recurrent synapses. Proceedings of the National Academy of Sciences. 111(11):4303–4308.

Butt SJ, Fuccillo M, Nery S, Noctor S, Kriegstein A, Corbin JG, and Fishell G. 2005. The temporal and spatial origins of cortical interneurons predict their physiological subtype. Neuron. 48(4):591–604.

Buzsáki G and Draguhn A. 2004. Neuronal oscillations in cortical networks. Science. 304(5679):1926–1929.

Cauli B, Porter JT, Tsuzuki K, Lambolez B, Rossier J, Quenet B, and Audinat E. 2000. Classification of fusiform neocortical interneurons based on unsupervised clustering. Proceedings of the National Academy of Sciences. 97(11):6144–6149.

Chen I, Helmchen F, Lütcke H. 2015. Specific early and late oddball-evoked responses in excitatory and inhibitory neurons of mouse auditory cortex. Journal of Neuroscience**.** 35(36):12560-12573.

Cohen S and Greenberg ME. 2008. Communication between the synapse and the nucleus in neuronal development, plasticity, and disease. Annual review of cell and developmental biology. 24:183.

Connors BW and Gutnick MJ. 1990. Intrinsic firing patterns of diverse neocortical neurons. Trends in neurosciences. 13(3):99–104.

Cooley J and Dodge Jr F. 1966. Digital computer solutions for excitation and propagation of the nerve impulse. Biophysical journal. 6(5):583.

Cosgrove KE, Galvan EJ, Meriney SD, and Barrionuevo G. 2010. Area ca3 interneurons receive two spatially segregated mossy fiber inputs. Hippocampus. 20(9):1003–1009.

Davis MJ, Wu X, Nurkiewicz TR, Kawasaki J, Gui P, Hill MA, and Wilson E. 2001. Regulation of ion channels by protein tyrosine phosphorylation. American Journal of Physiology-Heart and Circulatory Physiology. 281(5):H1835–H1862.

Dehorter N, Ciceri G, Bartolini G, Lim L, del Pino I, and Marín O. 2015. Tuning of fast-spiking interneuron properties by an activity-dependent transcriptional switch. Science. 349(6253): 1216-1220.

De Schutter E and Bower JM. 1994. An active membrane model of the cerebellar purkinje cell. I. simulation of current clamps in slice. Journal of neurophysiology. 71(1):375–400.

DeFelipe J. 1993. Neocortical neuronal diversity: chemical heterogeneity revealed by colocalization studies of classic neurotransmitters, neuropeptides, calcium-binding proteins, and cell surface molecules. Cerebral Cortex. 3(4):273–289.

Druckmann S, Hill S, Schurmann F, Markram H, and Segev I. 2013. A hierarchical structure of cortical interneuron electrical diversity revealed by automated statistical analysis. Cerebral Cortex. 23(12):2994–3006.

Dumitriu D, Cossart R, Huang J, and Yuste R. 2007. Correlation between axonal morphologies and synaptic input kinetics of interneurons from mouse visual cortex. Cerebral cortex. 17(1):81–91.

Finley M, Fairman D, Liu D, Li P, Wood A, and Cho S. 2004. Functional validation of adult hippocampal organotypic cultures as an in vitro model of brain injury. Brain research. 1001(1):125–132.

Flavell SW and Greenberg ME. 2008. Signaling mechanisms linking neuronal activity to gene expression and plasticity of the nervous system. Annual review of neuroscience. 31:563.

Gähwiler B. 1981. Organotypic monolayer cultures of nervous tissue. Journal of neuroscience methods. 4(4):329–342.

Gähwiler B. 1988. Organotypic cultures of neural tissue. Trends in neurosciences. 11(11):484–489.

García NVDM, Karayannis T, and Fishell G. 2011. Neuronal activity is required for the development of specific cortical interneuron subtypes. Nature. 472(7343):351–355.

Golowasch J, Abbott L, and Marder E. 1999. Activity-dependent regulation of potassium currents in an identified neuron of the stomatogastric ganglion of the crab cancer borealis. Journal of Neuroscience. 19:RC33–1.

Hemond P, Epstein D, Boley A, Migliore M, Ascoli GA, and Jaffe DB. 2008. Distinct classes of pyramidal cells exhibit mutually exclusive firing patterns in hippocampal area ca3b. Hippocampus. 18(4):411–424.

Hille B. 2001. Ion channels of excitable membranes, volume 507. Sinauer Sunderland, MA.

Hines ML and Carnevale NT. 1997. The neuron simulation environment. Neural computation. 9(6):1179–1209.

Honnuraiah S and Narayanan R. 2013. A calcium-dependent plasticity rule for hcn channels maintains activity homeostasis and stable synaptic learning. PloS one. 8(2):e55590.

Hosp JA, Struber M, Yanagawa Y, Obata K, Vida I, Jonas P, and Bartos M. 2014. Morpho-physiological criteria divide dentate gyrus interneurons into classes. Hippocampus. 24(2):189–203.

Hutcheon B and Yarom Y. 2000. Resonance, oscillation and the intrinsic frequency preferences of neurons. Trends in neurosciences. 23(5):216–222.

Jensen MS, Azouz R, and Yaari Y. 1994. Variant firing patterns in rat hippocampal pyramidal cells modulated by extracellular potassium. Journal of Neurophysiology. 71(3):831–839.

Joshi P and Triesch J. 2009. Rules for information maximization in spiking neurons using intrinsic plasticity. In International Joint Conference on Neural Networks (IJCNN) 2009: pages 1456–1461. IEEE.

Kawaguchi Y and Kubota Y. 1997. Gabaergic cell subtypes and their synaptic connections in rat frontal cortex. Cerebral Cortex. 7(6):476–486.

Keogh E and Ratanamahatana CA. 2005. Exact indexing of dynamic time warping. Knowledge and information systems. 7(3):358–386.

Lee PR, Cohen JE, Becker KG, and Fields RD. 2005. Gene expression in the conversion of early-phase to late-phase long-term potentiation. Annals of the New York Academy of Sciences. 1048(1):259–271.

Llinas RR. 1988. The intrinsic electrophysiological properties of mammalian neurons: insights into central nervous system function. Science. 242(4886):1654–1664.

Marder E and Goaillard JM. 2006. Variability, compensation and homeostasis in neuron and network function. Nature Reviews Neuroscience. 7(7):563–574

Markram H, Toledo-Rodriguez M, Wang Y, Gupta A, Silberberg G, and Wu C. 2004. Interneurons of the neocortical inhibitory system. Nature Reviews Neuroscience. 5(10):793–807.

McCormick DA, Connors BW, Lighthall JW, and Prince DA. 1985. Comparative electrophysiology of pyramidal and sparsely spiny stellate neurons of the neocortex. Journal of neurophysiology. 54(4):782–806.

McKay BM, Oh MM, and Disterhoft JF. 2013. Learning increases intrinsic excitability of hippocampal interneurons. The Journal of Neuroscience. 33(13):5499–5506.

Miller MN, Okaty BW, and Nelson SB. 2008. Region-specific spike- frequency

acceleration in layer 5 pyramidal neurons mediated by kv1 subunits. The Journal of Neuroscience. 28(51):13716–13726.

Okamoto K, Ishikawa T, Abe R, Ishikawa D, Kobayashi C, Mizunuma M, Norimoto H, Matsuki N, and Ikegaya Y. 2014. Ex vivo cultured neuronal networks emit in vivo-like spontaneous activity. The Journal of Physiological Sciences. 64(6):421–431.

Okaty BW, Miller MN, Sugino K, Hempel CM, and Nelson SB. 2009. Transcriptional and electrophysiological maturation of neocortical fast-spiking gabaergic interneurons. The Journal of Neuroscience. 29(21):7040–7052.

Ramon y Cajal S. 1893. Nuevo concepto de la histologia de los centros nerviosos.

Remme MW, Donato R, Mikiel-Hunter J, Ballestero JA, Foster S, Rinzel J, and McAlpine D. 2014. Subthreshold resonance properties contribute to the efficient coding of auditory spatial cues. Proceedings of the National Academy of Sciences. 111(22):E2339–E2348.

Ren J, Aika Y, Heizmann C, and Kosaka T. 1992. Quantitative analysis of neurons and glial cells in the rat somatosensory cortex, with special reference to gabaergic neurons and parvalbumin-containing neurons. Experimental brainresearch, 92(1):1–14.

Shin J, Koch C, and Douglas R. 1999. Adaptive neural coding dependent on the time-varying statistics of the somatic input current. Neural computation. 11(8):1893–1913.

Somogyi P and Klausberger T. 2005. Defined types of cortical interneurone structure space and spike timing in the hippocampus. The Journal of physiology. 562(1):9–26.

Stemmler M and Koch C. 1999. How voltage-dependent conductances can adapt to maximize the information encoded by neuronal firing rate. Nature neuroscience. 2(6):521–527.

Steriade M. 2004. Neocortical cell classes are flexible entities. Nature reviews neuroscience. 5(2):121–134.

Su H, Alroy G, Kirson ED, and Yaari Y. 2001. Extracellular calcium modulates persistent sodium current-dependent burst firing in hippocampal pyramidal neurons.

The Journal of Neuroscience. 21(12):4173–4182.

Sundstrom L, Pringle A, Morrison B, and Bradley M. 2005. Organotypic cultures as tools for functional screening in the cns. Drug discovery today. 10(14):993–1000.

Tricoire L, Pelkey KA, Erkkila BE, Jeffries BW, Yuan X, and McBain CJ. 2011. A blueprint for the spatiotemporal origins of mouse hippocampal interneuron diversity. The Journal of Neuroscience. 31(30):10948–10970.

Turrigiano G, Abbott L, and Marder E. 1994. Activity-dependent changes in the intrinsic properties of cultured neurons. Science. 264(5161):974–976.

Turrigiano G, LeMasson G, and Marder E. 1995. Selective regulation of cur- rent densities underlies spontaneous changes in the activity of cultured neurons. The Journal of neuroscience. 15(5):3640–3652.

Turrigiano GG and Nelson SB. 2004. Homeostatic plasticity in the developing nervous system. Nature Reviews Neuroscience. 5(2):97–107.

Ward Jr JH. 1963. Hierarchical grouping to optimize an objective function. Journal of the American statistical association. 58(301):236–244.

Yuste R. 2005. Origin and classification of neocortical interneurons. Neuron. 48(4):524–527.

Zhang W and Linden DJ. 2003. The other side of the engram: experience- driven changes in neuronal intrinsic excitability. Nature Reviews Neuroscience. 4(11):885–900.

GENERAL DISCUSSION

NMDA SPIKE-MEDIATED PLASTICITY

Synaptic plasticity is arguably the most ubiquitous and powerful process underlying brain computation. Accumulating evidence from both *in vitro* (Brandalise et al. 2014; Kim et al. 2015) and *in vivo* experiments (Gambino et al. 2014; Chicon & Gan, 2015) indicate that a supralinear dendritic signal is necessary to provide the strong depolarization required for initiating NMDA receptor-dependent plasticity.

In the first part of my PhD project I was able to demonstrate that intrinsic regenerative signals in dendrites can be triggered through heterosynaptic stimulation of recurrent CA3 pyramidal cells fibers followed by mossy fibers, and that the resulting summation of the evoked EPSPs can generate dendritic events identified as NMDA spikes (Brandalise et al. 2014). In subsequent experiments, I obtained several lines of evidence for a direct causal role of dendritic NMDA spikes in the induction of LTP at excitatory recurrent synapses of CA3 pyramidal cells (Brandalise et al. 2016 *under revision*). Recent *in vivo* investigations have provided data suggesting that NMDA receptor-dependent dendritic spikes may contribute to synaptic plasticity (Gambino et al. 2014;Sheffield & Dombeck 2015; Chicon & Gan 2015), but because of technical limitations it was not possible to establish a causal relationship between the occurrence of these supralinear dendritic events and the induction of LTP. However, in the *in vitro* experiments I performed, it is clear that dendritic NMDA spikes are a crucial source of supralinear depolarization, and that these are necessary and sufficient for the induction of LTP.

Hebbian plasticity, which leads to increased strength in the functional connectivity between two neurons when repeated activation of the presynaptic neuron induces firing in the postsynaptic neuron (Hebb 1949), is considered to underlie the formation of episodic memory and spatial navigation maps in the hippocampus (O'Keefe, 1999; Bittner et al 2015; Shieffield & Dombeck 2015). Current textbooks state that back-propagating action potentials are the basis for triggering LTP, which drives Hebbian remodeling of brain circuits (Markram et al. 2012; Feldman 2012). However, the mechanisms initiating the induction of synaptic potentiation remain under debate. This issue is of importance for several reasons. First, delineating the precise conditions required to trigger plasticity will provide insights into the induction threshold, which determines the reliability of information storage by synapses. Second, if the generally accepted spike timing-dependent

plasticity (STDP) paradigm in which an EPSP paired with a single AP is sufficient to remodel synapses were correct, the resulting functional networks would be unstable. In other words, the threshold to maintain stable plasticity would be to too low if a single action potential were capable of altering synaptic weights, which would lead to corruption of the content encoded in the network. This issue has been raised previously. An early STDP model depending on pairs of spikes (pre-post and post-pre) focused mainly on the timing of the input occurrence to predict the synaptic change and only worked for a restricted number of protocols (Pfister & Gerstner 2006). Other models such as the BMC rule, postulated the existence of a sliding modification threshold of synaptic weight that leads to LTP when it is exceeded or LTD when it is below. A modification of the STDP protocol, called “Triplet STDP” (Gjorgjieva et al. 2011), was therefore proposed that takes into account the synaptic weight as well as input timing, and that is consistent with a much broader class of experimental data.

It might, however, be argued that dendritic spikes (dSpikes) also exhibit a threshold that is too low to ensure reliable storage of information. For example, dSpikes can be induced by pairing subthreshold inputs when they occur with the appropriate timing (also called input timing dependent plasticity, ITDP), and thus allow relatively weak inputs to initiate LTP. As the generation of an NMDA spike requires a clustered pattern of ten to fifteen simultaneous inputs (Major et al., 2013), rather than a single back-propagating AP, the threshold for this form of LTP is in fact very high, thereby conferring stability on synaptic memory storage (see Fig. 1). Thus, not only do the triggering inputs have to be activated in a narrow time window (temporal constraint), but they must also converge on the same dendritic branch (spatial constraint).

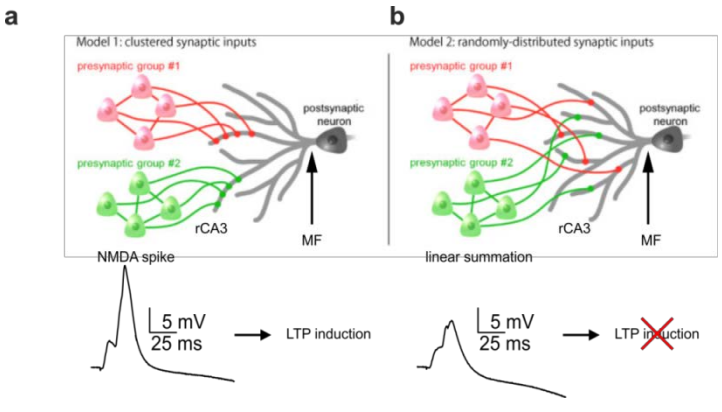

Fig 1. Requirements for NMDA spike induction: (a) Clustered activation of synapses by recurrent inputs onto the same branch occurring in combination with a source of depolarization (such as the MF EPSP); (b) If recurrent inputs are randomly distributed, the induction of NMDA spikes as well as synaptic potentiation is prevented. (modified from Takahashi et al. 2012).

The identification of NMDA spikes as fundamental to synaptic plasticity is also important in that it extends the repertoire of dendritic signaling beyond the digital domain of the back-propagating action potential to a more versatile analog dimension, thus enlarging the range of graded computations. NMDA spikes, like action potentials, have a fixed threshold but their amplitude is variable depending on the extent of clustered input, the density of postsynaptic NMDA receptors, the efficiency of glutamate transporters (an increase in “ambient glutamate” promotes the activation of extrasynaptic NMDA receptors that in turn facilitates NMDA spike induction; Chalifoux and Carter 2011), as well as the driving force set by the local membrane potential (Major et al. 2013). These mechanisms may also compensate for the different properties of proximal versus distal dendrites, which leads to preferential generation of dSpikes in higher resistance distal dendritic compartments (Weber et al. 2016). Furthermore, the modulation of active dendritic signals can affect both their amplitude as well as the probability that they will be evoked. In our experiments we used an intensity for paired stimulation (minimal stimulation plus 20%) that triggered NMDA spikes with a probability of about 40%. In addition, we showed that the minimal number of NMDA spikes necessary to induce LTP during our pairing protocol is approximately 10 events and that the number of evoked NMDA spikes correlates with the amount of potentiation.

The intensity of neuronal input represents another gate for the NMDA spike induction probability. We have recently observed a mechanism that can enhance input intensity in which prolonged paired stimulation of mossy fiber input at relatively low frequency (1 Hz) induced a shift from an accommodating to a bursting firing pattern of CA3 pyramidal cells (Magraner et al. 2016 in preparation). Burst firing will exert a more powerful recurrent activation of neighboring CA3 pyramidal cells. In addition, the temporal summation associated with bursting input will induce stronger depolarization of an activated dendritic branch facilitating the generation of an NMDA spike. Interestingly, theoretical considerations led to the prediction that burst patterns rather than single spikes would favor LTP induction (Lisman 1997).

NMDA spikes are also subject to local modulation as a result of the calcium influx occurring during a dSpike. In a preliminary set of experiments in which two consecutive ITDP protocols were applied, the activated synapses did not exhibit a potentiation of EPSPs and, surprisingly, the amplitude of dSpikes was significantly reduced compared to experiments in which only one ITDP protocol was applied (Fig

2b). Calcium imaging of the stimulated branches revealed a more restricted propagation of the calcium transients associated with the NMDA spike with the double ITDP protocol compared to single protocol (Fig 2c-d).

We hypothesize that this is due to calcium-mediated upregulation of potassium channels in the activated branch. This homeostatic regulation may be a local mechanism to prevent excessive potentiation caused by repetitive input, which may favor competition between the stimulated synapses where the dSpike is triggered and surrounding unstimulated synapses (Poo et al. 2016).

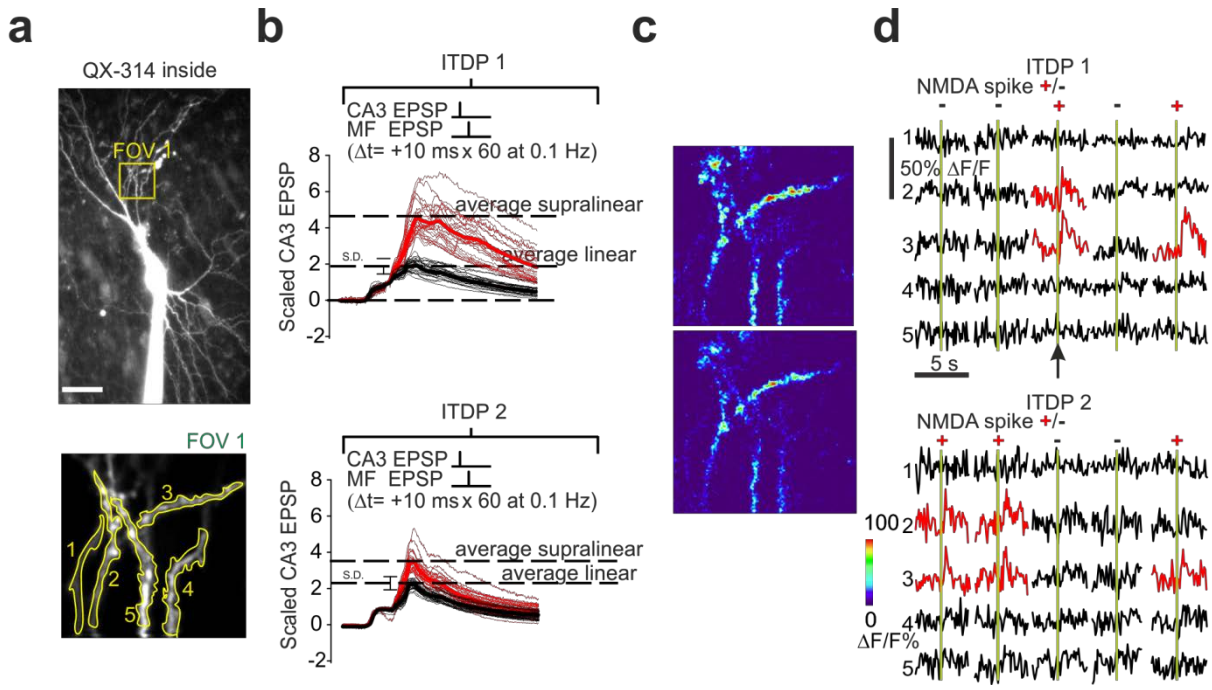

Fig. 2. Local regulation of NMDA spike amplitude. (a) A labeled CA3 pyramidal neuron (scale bar: 30 μm). (b) First (ITDP1) and second (ITDP2) ITDP protocol (responses scaled to CA3 EPSP). Note the significant reduction in the amplitude of the supralinear response when two consecutive ITDP protocols were applied. (c) Heat map of the Ca^{2+} transients detected during NMDA spike occurrence. Both amplitude and spatial propagation are reduced with the double ITDP protocol. (d) Example Ca^{2+} transients from ROIs selected in a, recorded during 5 representative consecutive pairings (green bars) for both ITDP1 and ITDP2. Trials withlinear ("-") and supralinear ("+") EPSP summation are indicated.

Thus, the computational and modulatory power of each synaptic input to the postsynaptic neuron will depend on the amplitude and the induction probability of NMDA spikes.

What are the consequences of this variability? Here I suggest that dSpike-mediated plasticity exploits the sparsity of hippocampal mossy fiber input to CA3

pyramidal cells to allow pattern completion of stored memory in an input-dependent manner on different branches of a given postsynaptic neuron.

A large number of theoretical models (Treves & Rolls 2001; Rolls & Webb 2012) have suggested that the CA3 matrix operates as a single network favoring arbitrary associations between connections arriving from different cortical areas (visual cortex, auditory cortex etc). These inputs converge in the hippocampus via the perforant path and discarge both the recurrent network and the granule cells of the dentate gyrus. In turn, as previously reported (Yeckel & Berger 1990), these inputs reach the CA3 pyramidal cells in a precise temporal sequence in which the recurrent input precedes the mossy fiber EPSP with timing similar to our ITDP protocol. Thus, these synapses will undergo LTP if associated with mossy fiber activation. The potentiated recurrent synapses that belong to a separate branch, once reactivated by the corresponding cue that was present during the original storage of the episodic event would provide enough depolarization to make the postsynaptic neuron fire, and consequently implementing recall also under conditions where only one cue is activated by way of hippocampo-neocortical backprojections (Rolls 1995; Rolls 2008).

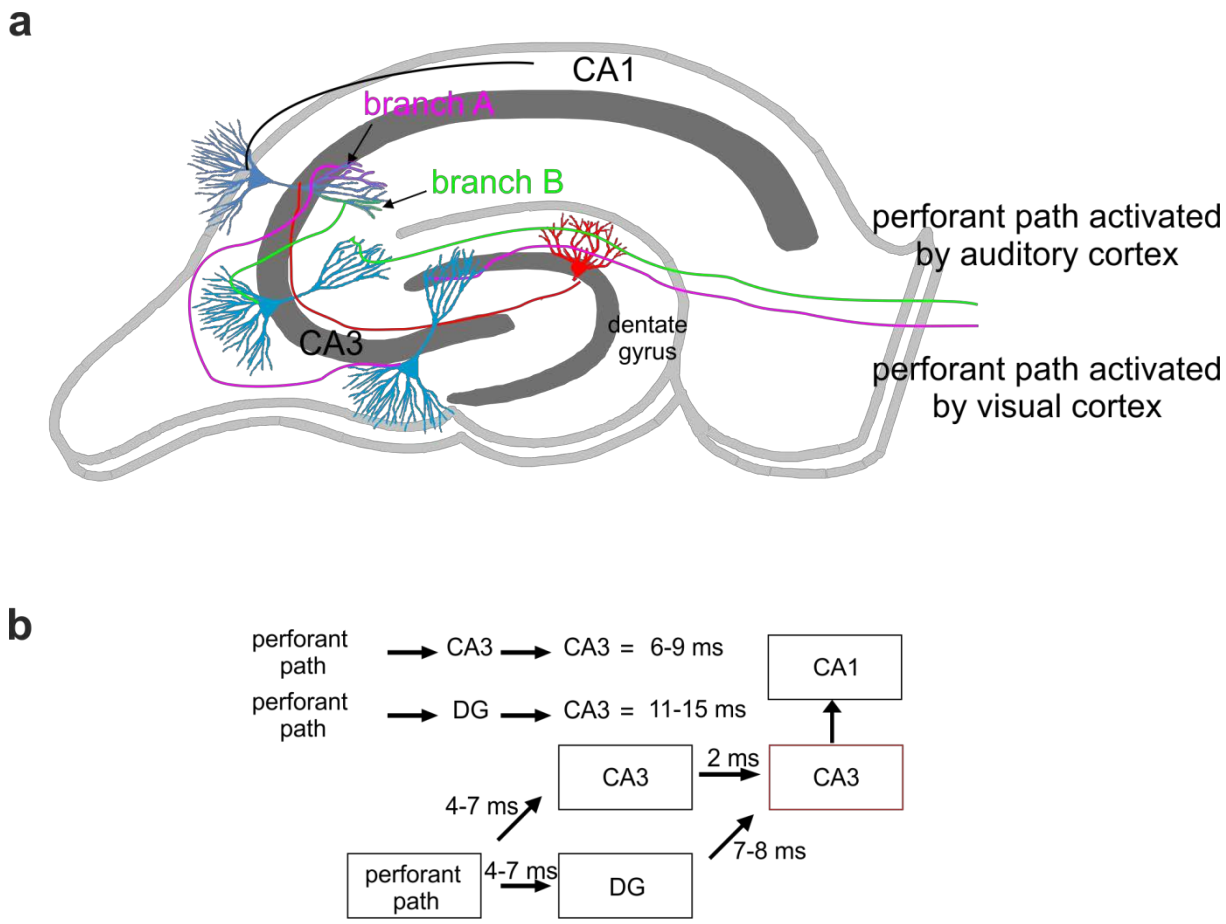

Fig.3. a) The hippocampal network: The hippocampus forms principally a uni-directional network, with input from the entorhinal cortex (EC) that makes connections with the dentate gyrus (DG) and CA3 pyramidal neurons (CA3) via the perforant path. The entorhinal cells giving rise to the perforant path can be activated by different cortical areas as in this example the auditory cortex (green) and visual cortex (pink). These neurons converge their axons on branches of common post-synaptic CA3 pyramidal cells. b) Scheme of the different hippocampal connections. Note that the two pathways have a different total input latency so that the recurrent input is preceding the mossy fiber EPSP.

Approximately fifty mossy fiber inputs contact a CA3 pyramidal neuron where they target the principal trunk in a region between 50 to 80 µm from the soma (Urban et al. 2001). The resulting evoked EPSPs will therefore exhibit a progressive decrement in amplitude because of cable filtering at increasingly distant sites within the dendritic tree (Williams & Mitchell 2008). Due to the extremely sparse activity levels of granule cells, each MF is independent of the others converging on the same neuron. This functionality is consistent with the finding that for each pyramidal cell

only a single MF is active for a given place field (McNaughton 1989; Buckmaster 1994; Lisman 1999).

In the pool of all the MFs targeting a CA3 pyramidal cell we detected “strong” and “weak” inputs as assessed by the amount of depolarization they evoke in the postsynaptic neuron (this distinction is dynamic since presynaptic LTP or LTD can modulate the strength of each MF synapse). Strong MF synapses elicit subthreshold signals that spread further into the dendritic tree thereby relieving Mg^{2+} also at relatively distal recurrent synapses where they can allow the generation of NMDA spikes. Thus, MF inputs exert a graded effect on the dendritic tree with strong MF inputs influencing a larger proportion of the CA3 pyramidal cell dendritic arbor than weak MF inputs. In contrast, a bAP spreads through the dendritic tree in an all-or-none fashion, although branch point failures or high impedence in distal thin branches can block the signal (see INDUCTION OF SYNAPTIC PLASTICITY). The proposal that dSpikes rather than bAPs are the final effectors that initiate plasticity contradicts currently accepted dogma and has therefore come under criticism. Below I have summarized the main issues that have been raised.

1) *The induction of NMDA spikes is facilitated by subthreshold stimulation but this effect is limited by cable filtering only to relatively proximal synapses. If NMDA spikes are the causal events triggering LTP how can very distal synapses be potentiated?*

   Rebuttal: As shown by our group and others (Brandalise et al. 2014; Makara & Magee, 2013), the NMDA spike is indeed preferentially generated in proximal dendrites of the CA3 pyramidal cell because of the proximity to the mossy fiber input. In the distal dendrites, where excitatory input arrives via the perforant path, a different form of dendritic spike can be evoked: the dendritic Na^+ spike (Kim et al. 2012; Kim et al. 2015). Thus, as NMDA spikes do not occur distally, dendritic Na^+ spikes can trigger LTP induction at these synapses suggesting that the repertoire of distinct dendritic spikes may have compartmental specificity depending on both passive (input resistance, branch diameter etc.) as well as active dendritic properties (channel density, excitation/inhibition ratio, input segregation).
2) *NMDA spikes can manifest as long duration events that include a plateau phase and therefore cannot mediate high frequency coding typical for action potentials.*

Rebuttal: Assessment of NMDA spike-associated plateaus suggests that these events are likely to represent an artefact resulting from the glutamate-uncaging technique employed in many studies in which NMDA receptors on multiple neighboring synapses as well as in extrasynaptic regions are activated, a situation which does not correspond to the sparse receptor activation expected under physiological conditions (Oikonomou et al. 2014). Furthermore, the decay time of NMDA spikes is modulated by calcium and voltage-gated potassium channels, by I_h channels, and by $GABA_B$ receptor activation, all of which serve to curtail the duration of NMDA spikes (see Table 2).

Table 2

Channels expressed in CA3 pyramidal neurons	**Role of these channels in dSpike modulation**	**References**
Kv4.2 (not calcium-dependent)	Interaction between active dendritic integration compartments Modulate threshold for dSpike	Yang et al., 2015 Losonczy et al., 2008
HCN1	Interaction between active dendritic integration compartments Modulate threshold for dSpike	Harnett et al., 2015 Harnett et al., 2013
$GABA_B$ receptor	Modulate threshold and duration of dSpike	Lovett-Barron et al., 2012
BK	Modulate threshold and duration of dSpike	Golding et al., 1999 Zhang et al., 2014

3) *As bAPs are sufficient to induce LTP, dSpikes are not necessarily required for synaptic plasticity.*

Rebuttal: When an action potential is generated at the axon hillock it exerts a double action: it provides a source of depolarization that can trigger plasticity at dendritic synapses and it produces the output that evokes an EPSP in postsynaptic neurons. During the last decade, however, modeling studies have indicated that a neuron can integrate signals as a two layer processor (Poirazi and Mel, 2003), meaning that under certain conditions dendrites can actively integrate inputs independently of somatic activity. A bAP would not be

compatible for such compartmentalized computation. In contrast, NMDA spikes, which are restricted to the dendritic branch from where they originate, can mediate signals that support independent local processing and storage of information.

4) *Conversely, if dSpikes are sufficient for LTP, are bAPs that spread through the dendritic tree simply an epiphenomenon?*

   Rebuttal: Absolutely not. We have shown that a burst of three action potentials, but not one action potential, can reliably induce LTP when paired with a recurrent EPSP by providing the depolarization necessary to trigger an NMDA spike. However, under conditions where a burst of bAPs fails to elicit an NMDA spike, LTP is not induced.

In addition to underscoring the importance of dSpikes, my findings provide further support for the concept that the dendritic branch rather than the dendritic spine is the functional unit for LTP induction (Branco et al. 2010; Govindarajan et al. 2011). Repetitive synaptic stimulation induces calcium transients in a specific locus within the dendritic branch with high fidelity in consecutive trials. In hippocampal pyramidal cells, NMDA spikes are generated when approximately 15 synapses are activated synchronously within a dendritic segment (Makara & Magee, 2013), which is a relatively low number considering that 15 synapses represent less than 5% of the total present on a dendritic segment (Major et al., 2013). Furthermore, developmental processes favor the compartmentalization of correlated inputs onto single dendritic segments thereby providing a structural basis for the generation of spatially-restricted dendritic spikes (Kleindienst et al. 2011; Winnubst & Lohmann 2015). This requirement of functionally clustered input to generate NMDA spikes thus represents a critical threshold to curtail non-discriminant LTP.

In conclusion, my experimental data show that dendritic NMDA spikes are critical for the induction of associative LTP in the hippocampus. This finding adds a new facet to our understanding of the mechanisms that underlie synaptic plasticity and should aid in the development of more physiologically relevant computational models of memory encoding.

The fact that activation of the mossy fiber synapse, which establishes a specialized type of neuronal connection in the brain, was necessary to evoke NMDA spike-mediated LTP in my experiments might suggest that this form of LTP is unique

to CA3 pyramidal cells. However, other groups have observed an association between NMDA spikes and synaptic plasticity in layer 2/3 pyramidal cells in mouse somatosensory cortex during rhythmic sensory whisker stimulation (Gambino et al. 2014), in layer V pyramidal neurons in the mouse motor cortex (Chicon & Gan 2015), and in CA1 pyramidal cells during new environment exploration (Scheffield & Dombek 2015).

We thus believe that this newly characterized form of LTP induction is widespread in the brain and may represent a key mechanism underlying action potential-independent plasticity.

FUTURE RESEARCH DIRECTIONS

Ever since dSpikes were first described (Schiller et al. 1997; Schiller et al. 2000), their physiological significance has been called into question as they had only been observed *in vitro* (Antic et al. 2010). Because of technical challenges, it took over a decade until Larkum and colleagues (Palmer et al. 2014) were able to demonstrate the presence of NMDA spikes *in vivo*. These experiments in layer 2/3 pyramidal neurons from rat somatosensory cortex showed that NMDA spikes enhance action potential generation during sensory processing. Subsequent *in vivo* investigations have found that supralinear dendritic responses occur in diverse brain areas where they contribute to LTP induction in barrel cortex (Gambino et al., 2014) and motor cortex (Chicon & Gan, 2015) and initiate spatial representation in CA1 pyramidal cells (Scheffield & Dombeck, 2015).

Even though the experiments for my PhD project were performed with organotypic or acute hippocampal slices from rat brain, the findings are consistent with responses observed in the behaving animal under conditions such as spatial navigation. Our data show that on the order of 10 NMDA spikes evoked during the 60 trial protocol that lasted ten minutes was sufficient to induce LTP, which is in the same range as the number of bursts that a hippocampal place cell fires as the animal traverses its place field (McNaughton et al. 1983). In this respect, it is noteworthy that the long-term representation of space by hippocampal place cells in navigating mice depends directly on the generation of dendritic branch spikes (Sheffield and Dombeck, 2015). In their study dendritic spikes exhibited kinetic and spatial

properties consistent with NMDA spikes, but could not be definitively categorized for technical reasons.

My future aim is to obtain further evidence *in vivo* for the hypothesis that NMDA spikes are critical for the induction of LTP. Specifically, we intend to test whether NMDA spikes recorded from CA3 pyramidal cells in actively navigating mice correlate with the formation of place fields and with pattern completion functions. To address this question, we have designed *in vivo* experiments in collaboration with the group of Prof. Fritjof Helmchen to image dendritic spikes in CA3 pyramidal cells in awake behaving mice. For these experiments we have obtained the transgenic mouse line, C57BL/6-Tg(Grik4-cre) G32-4Stl/J (Jackson Laboratory) (Madisen et al. 2010), with robust Cre expression in the hippocampal CA3 pyramidal cell layer (Nakazawa et al., 2002). We have now crossed this line with a GCaMP6 separate line (Allen Institute for Brain Science) to generate mice with transgenic expression of a fast and sensitive calcium indicator in CA3 pyramidal cells.

We are currently recording dendritic signals of CA3 pyramidal cells in anesthetized mice as a first *in vivo* approach. Even though these are preliminary data (only two animals have been imaged so far) it is encouraging to see that it was possible to distinguish between events that invade all of the imaged dendritic arbor (most likely induced by bursting activity) and other events that were much more localized and restricted to a single portion of a dendrite in a similar fashion as in our *in vitro* experiments (see Fig. 4).

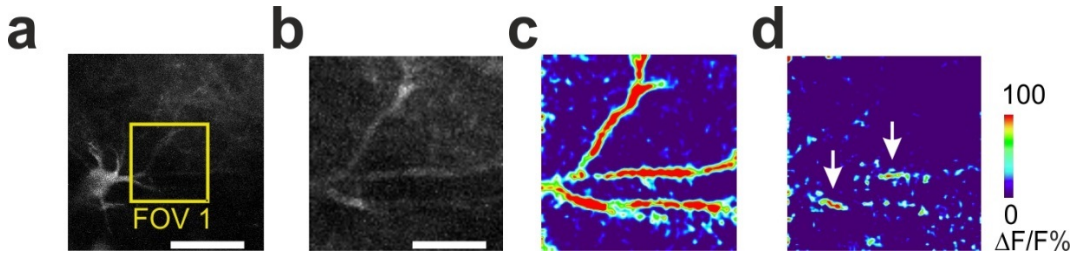

Fig. 4. Global versus local calcium transients detected in CA3 pyramidal cell in anesthetized mice. (a) Labeled CA3 pyramidal neuron (scale bar: 50 μm). (b) Enlarged image of the field of view where calcium transients were recorded. (scale bar: 15 μm) (c) Heat map of the calcium transients detected during a global event that invades the entire imaged dendritic arbor. (d) Heat map of calcium transients restricted to a single portion of two out of three dendrites. Note that the portion closer to the soma does not exhibit any calcium transients supporting the exclusive dendritic initiation and propagation of the event.

In the second phase of the *in vivo* approach, dendritic signals will be imaged from place cells, which will be identified by the presence of calcium signals occurring with greater probability when mice traverse specific locations on the track (place fields).

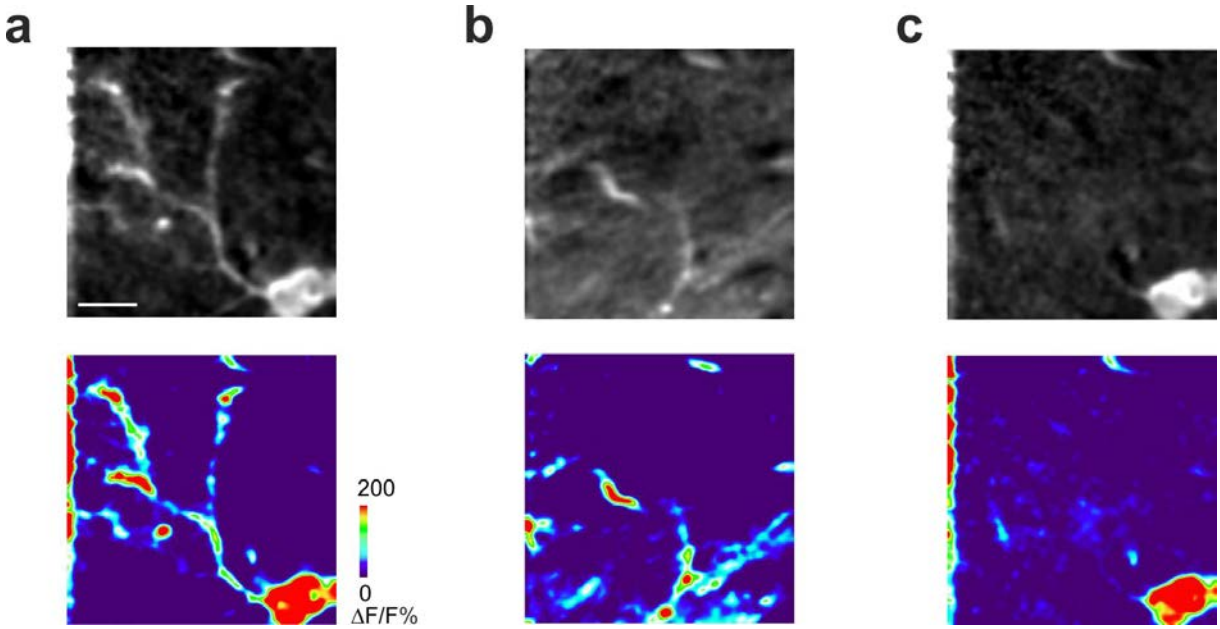

Fig. 5. Variability of calcium transients detected in CA3 pyramidal cell in awake mice. Labeled CA3 pyramidal neuron (scale bar: 30 μm). (a) Coincident somatic firing and a bAP observed in all visible dendritic branches (b) Dendritic branch spiking in the absence of detectable somatic firing was also observed. (c) Example of an event where somatic firing was not propagated to the dendritic arbor.

This experiment will establish whether CA3 pyramidal cells generate dSpikes for the representation of space, as was recently shown for CA1 pyramidal cells (Sheffield & Dombeck, 2015). More in detail, we propose to analyze the different types of calcium transients (see Fig. 5) and to quantify the number of events occurring under different behavioral conditions such as: 1) when exploring a new environment (using a virtual reality screen positioned in front of the treadmill); 2) when the location of the reward in the virtual environment is changed, 3) after re-mapping in response to alterations in the virtual reality map. Furthermore, it will be of interest to test additional behavioral paradigms by training mice on a linear treadmill while different visual orientation cues are presented at different distances along the running path. As CA3 pyramidal cells are instrumental for pattern completion during navigational tasks (Neunuebel & Knierim, 2014), we will test whether dSpikes

contribute to this specific function by comparing responses under full cue and partial cue conditions. Dendritic NMDA spikes will be identified on the basis of their restricted propagation and by pharmacological characterization. Our working hypothesis is that dSpikes are crucial for the storage of associations between inputs originating from very different areas of the cerebral cortex, for example, between information originating in the auditory cortex about the sound produced by an object and information originating in the parietal cortex about its location. NMDA spike-mediated plasticity may potentiate subsets of clustered recurrent synapses activated by different inputs converging onto the same CA3 pyramidal neuron. Subsequent presentation of a partial cue would be then sufficient to induce neuronal spiking allowing the retrieval of the whole representation.

The recognition that pyramidal cell dendrites actively participate in processing incoming signals through the generation of dSpikes is revolutionizing our understanding of the mechanisms that mediate synaptic plasticity. A future challenge will be to characterize the roles of dSpikes in neurological disorders that affect dendritic structure and function such as fragile X syndrome and Rett syndrome for which there are currently no effective treatments. Research in this area will lead to insights aiding in the design of new therapeutic strategies. Progress on this front will depend, however, on a deeper understanding of the functions of dSpikes during normal neuronal function. At present, dSpikes remain incompletely characterized and have only been observed and investigated in relatively few brain areas and cell types. I believe that the results obtained during the course of my PhD project contribute to this rapidly expanding field of research and will provide a new perspective on information processing at the level of the individual neuron.

REFERENCES

Aizenman, E., Lipton, S. A., & Loring, R. H. (1989). Selective modulation of NMDA responses by reduction and oxidation. *Neuron*, 2(3), 1257-1263.

Antic, S. D., Zhou, W. L., Moore, A. R., Short, S. M., & Ikonomu, K. D. (2010). The decade of the dendritic NMDA spike. *Journal of Neuroscience Research*,*88*(14), 2991-3001.

Augustinaite, S., Kuhn, B., Helm, P. J., & Heggelund, P. (2014). NMDA spike/plateau potentials in dendrites of thalamocortical neurons. *The Journal of Neuroscience*, *34*(33), 10892-10905.

Basu, J., Zaremba, J. D., Cheung, S. K., Hitti, F. L., Zemelman, B. V., Losonczy, A., & Siegelbaum, S. A. (2016). Gating of hippocampal activity, plasticity, and memory by entorhinal cortex long-range inhibition. *Science*,*351*(6269), aaa5694.

Bell, C. C., Han, V. Z., Sugawara, Y., & Grant, K. (1997). Synaptic plasticity in a cerebellum-like structure depends on temporal order. *Nature*, 387(6630), 278-281.

Bi, G. Q., & Poo, M. M. (1998). Synaptic modifications in cultured hippocampal neurons: dependence on spike timing, synaptic strength, and postsynaptic cell type. *The Journal of Neuroscience*, *18*(24), 10464-10472.

Bi, G. Q., & Poo, M. M. (2001). Synaptic modification by correlated activity: Hebb's postulate revisited. *Annual Review of Neuroscience*, 24(1), 139-166.

Bienenstock, E. L., Cooper, L. N., & Munro, P. W. (1982). Theory for the development of neuron selectivity: orientation specificity and binocular interaction in visual cortex. *The Journal of Neuroscience*, *2*(1), 32-48.

Bittner, K. C., Grienberger, C., Vaidya, S. P., Milstein, A. D., Macklin, J. J., Suh, J., ... & Magee, J. C. (2015). Conjunctive input processing drives feature selectivity in hippocampal CA1 neurons. *Nature Neuroscience*, 18(8), 1133.

Bliss, T. V., & Lømo, T. (1973). Long-lasting potentiation of synaptic transmission in the dentate area of the anaesthetized rabbit following stimulation of the perforant path. *The Journal of Physiology*, *232*(2), 331-356.

Blitzer, R. D. (2005). Long-term potentiation: mechanisms of induction and maintenance. *Science Signaling*, *2005*(309), tr26-tr26.

Bloodgood, B. L., & Sabatini, B. L. (2007). Nonlinear regulation of unitary synaptic signals by CaV 2.3 voltage-sensitive calcium channels located in dendritic spines. *Neuron*, 53(2), 249-260.

Bollmann, J. H., & Engert, F. (2009). Subcellular topography of visually driven dendritic activity in the vertebrate visual system. *Neuron*, *61*(6), 895-905.

Branco, T., Clark, B. A., & Häusser, M. (2010). Dendritic discrimination of temporal input sequences in cortical neurons. *Science*, *329*(5999), 1671-1675.

Brandalise, F., & Gerber, U. (2014). Mossy fiber-evoked subthreshold responses induce timing-dependent plasticity at hippocampal CA3 recurrent synapses. *Proceedings of the National Academy of Sciences*, *111*(11), 4303-4308.

Brager, D. H., & Johnston, D. (2007). Plasticity of intrinsic excitability during long-term depression is mediated through mGluR-dependent changes in Ih in hippocampal CA1 pyramidal neurons. *The Journal of Neuroscience*, 27(51), 13926-13937.

Buckmaster, P. S., & Schwartzkroin, P. A. (1994). Hippocampal mossy cell function: a speculative view. *Hippocampus*, *4*(4), 393-402.

Burnashev, N., Zhou, Z., Neher, E., & Sakmann, B. (1995). Fractional calcium currents through recombinant GluR channels of the NMDA, AMPA and kainate receptor subtypes. *The Journal of Physiology*, 485(Pt 2), 403.

Burrone, J., O'Byrne, M., & Murthy, V. N. (2002). Multiple forms of synaptic plasticity triggered by selective suppression of activity in individual neurons. *Nature*, 420(6914), 414-418.

Callaway, J. C., & Ross, W. N. (1997). Spatial distribution of synaptically activated sodium concentration changes in cerebellar Purkinje neurons. *Journal of Neurophysiology*, 77(1), 145-152.

Caporale, N., & Dan, Y. (2008). Spike timing-dependent plasticity: a Hebbian learning rule. *Annual Reviews Neuroscience*, *31*, 25-46.

Chalifoux, J. R., & Carter, A. G. (2011). Glutamate spillover promotes the generation of NMDA spikes. *The Journal of Neuroscience*, *31*(45), 16435-16446.

Cichon, J., & Gan, W. B. (2015). Branch-specific dendritic Ca2+ spikes cause persistent synaptic plasticity. *Nature*, *520*(7546), 180-185.

Collingridge, G. L., Kehl, S. J., & McLennan, H. T. (1983). Excitatory amino acids in synaptic transmission in the Schaffer collateral-commissural pathway of the rat hippocampus. *The Journal of Physiology*, *334*(1), 33-46.

Coultrap, S. J., Freund, R. K., O'Leary, H., Sanderson, J. L., Roche, K. W., Dell'Acqua, M. L., & Bayer, K. U. (2014). Autonomous CaMKII mediates both LTP and LTD using a mechanism for differential substrate site selection. *Cell reports*, *6*(3), 431-437.

Desai, N. S., Rutherford, L. C., & Turrigiano, G. G. (1999). BDNF regulates the intrinsic excitability of cortical neurons. *Learning & Memory*, 6(3), 284-291.

de Almeida, L., Idiart, M., & Lisman, J. E. (2009). The input–output transformation of the hippocampal granule cells: from grid cells to place fields.*The Journal of Neuroscience*, *29*(23), 7504-7512.

Debanne, D., Gähwiler, B. H., & Thompson, S. M. (1994). Asynchronous pre-and postsynaptic activity induces associative long-term depression in area CA1 of the rat hippocampus in vitro. *Proceedings of the National Academy of Sciences*, *91*(3), 1148-1152.

Debanne, D., Gähwiler, B. H., & Thompson, S. M. (1998). Long-term synaptic plasticity between pairs of individual CA3 pyramidal cells in rat hippocampal slice cultures. *The Journal of Physiology*, *507*(1), 237-247.

Fan, Y., Fricker, D., Brager, D. H., Chen, X., Lu, H. C., Chitwood, R. A., & Johnston, D. (2005). Activity-dependent decrease of excitability in rat hippocampal neurons through increases in Ih. *Nature Neuroscience*, 8(11), 1542-1551.

Feldman, D. E. (2012). The spike-timing dependence of plasticity. *Neuron*,*75*(4), 556-571.

Franklin, J. L., Fickbohm, D. J., & Willard, A. L. (1992). Long-term regulation of neuronal calcium currents by prolonged changes of membrane potential. *The Journal of Neuroscience*, 12(5), 1726-1735.

Gambino, F., Pagès, S., Kehayas, V., Baptista, D., Tatti, R., Carleton, A., & Holtmaat, A. (2014). Sensory-evoked LTP driven by dendritic plateau potentials in vivo. *Nature*, *515*(7525), 116-119.

Garaschuk, O., Schneggenburger, R., Schirra, C., Tempia, F., & Konnerth, A. (1996). Fractional Ca2+ currents through somatic and dendritic glutamate receptor channels of rat hippocampal CA1 pyramidal neurones. *The Journal of Physiology*, 491(Pt 3), 757.

Garner, A. R., Rowland, D. C., Hwang, S. Y., Baumgaertel, K., Roth, B. L., Kentros, C., & Mayford, M. (2012). Generation of a synthetic memory trace. *Science*, 335(6075), 1513-1516.

Gjorgjieva, J., Clopath, C., Audet, J., & Pfister, J. P. (2011). A triplet spike-timing–dependent plasticity model generalizes the Bienenstock–Cooper–Munro rule to higher-order spatiotemporal correlations. *Proceedings of the National Academy of Sciences*, 108(48), 19383-19388.

Gibb, A. J., & Edwards, F. A. (1994). Patch clamp recording from cells in sliced tissues. In *Microelectrode Techniques: The Plymouth Workshop Handbook. Cambridge, UK: The Company of Biologists* (pp. 225-274).

Golding, N. L., & Spruston, N. (1998). Dendritic sodium spikes are variable triggers of axonal action potentials in hippocampal CA1 pyramidal neurons. *Neuron*, 21(5), 1189-1200.

Golding, N. L., Staff, N. P., & Spruston, N. (2002). Dendritic spikes as a mechanism for cooperative long-term potentiation. *Nature*, *418*(6895), 326-331.

Gordon, U., Polsky, A., & Schiller, J. (2006). Plasticity compartments in basal dendrites of neocortical pyramidal neurons. *The Journal of Neuroscience*, *26*(49), 12717-12726.

Govindarajan, A., Israely, I., Huang, S. Y., & Tonegawa, S. (2011). The dendritic branch is the preferred integrative unit for protein synthesis-dependent LTP. *Neuron*, *69*(1), 132-146.

Grienberger, C., Chen, X., & Konnerth, A. (2014). NMDA receptor-dependent multidendrite Ca 2+ spikes required for hippocampal burst firing in vivo. *Neuron*, *81*(6), 1274-1281.

Grunditz, Å., Holbro, N., Tian, L., Zuo, Y., & Oertner, T. G. (2008). Spine neck plasticity controls postsynaptic calcium signals through electrical compartmentalization. *The Journal of Neuroscience*, *28*(50), 13457-13466.

Gustafsson, B., Wigstrom, H., Abraham, W. C., & Huang, Y. Y. (1987). Long-term potentiation in the hippocampus using depolarizing current pulses as the conditioning stimulus to single volley synaptic potentials. *The Journal of Neuroscience*, *7*(3), 774-780.

Han, V. Z., Grant, K., & Bell, C. C. (2000). Reversible associative depression and nonassociative potentiation at a parallel fiber synapse. *Neuron*, 27(3), 611-622.

Hardie, J., & Spruston, N. (2009). Synaptic depolarization is more effective than back-propagating action potentials during induction of associative long-term potentiation in hippocampal pyramidal neurons. *The Journal of Neuroscience*, *29*(10), 3233-3241.

Harnett, M. T., Makara, J. K., Spruston, N., Kath, W. L., & Magee, J. C. (2012). Synaptic amplification by dendritic spines enhances input cooperativity. *Nature*, *491*(7425), 599-602.

Hebb, D. O. (1949). The first stage of perception: Growth of the assembly. *The Organization of Behavior*, 60-78.

Henze, D. A., Wittner, L., & Buzsáki, G. (2002). Single granule cells reliably discharge targets in the hippocampal CA3 network in vivo. *Nature Neuroscience*, *5*(8), 790-795.

Hoffman, D. A., & Johnston, D. (1999). Neuromodulation of dendritic action potentials. *Journal of Neurophysiology*, 81(1), 408-411.

Huganir, R. L., & Nicoll, R. A. (2013). AMPARs and synaptic plasticity: the last 25 years. *Neuron*, *80*(3), 704-717.

Ishizuka, N., Cowan, W. M., & Amaral, D. G. (1995). A quantitative analysis of the dendritic organization of pyramidal cells in the rat hippocampus. *Journal of Comparative Neurology*, 362(1), 17-45.

Jaffe, D. B., Johnston, D., Lasser-Ross, N., Lisman, J. E., Miyakawa, H., & Ross, W. N. (1992). The spread of Na+ spikes determines the pattern of dendritic Ca2+ entry into hippocampal neurons. *Nature,* 357(6375), 244-246.

Jia, H., Rochefort, N. L., Chen, X., & Konnerth, A. (2010). Dendritic organization of sensory input to cortical neurons in vivo. *Nature*, *464*(7293), 1307-1312.

Kampa, B. M., Clements, J., Jonas, P., & Stuart, G. J. (2004). Kinetics of Mg2+ unblock of NMDA receptors: implications for spike-timing dependent synaptic plasticity. *The Journal of Physiology*, *556*(2), 337-345.

Kampa, B. M., Letzkus, J. J., & Stuart, G. J. (2007). Dendritic mechanisms controlling spike-timing-dependent synaptic plasticity. *Trends in Neurosciences*,*30*(9), 456-463.

Kim, S., Guzman, S. J., Hu, H., & Jonas, P. (2012). Active dendrites support efficient initiation of dendritic spikes in hippocampal CA3 pyramidal neurons. *Nature Neuroscience*, *15*(4), 600-606.

Kim, Y., Hsu, C. L., Cembrowski, M. S., Mensh, B. D., & Spruston, N. (2015). Dendritic sodium spikes are required for long-term potentiation at distal synapses on hippocampal pyramidal neurons. *eLife*, *4*, e06414.

Kleindienst, T., Winnubst, J., Roth-Alpermann, C., Bonhoeffer, T., & Lohmann, C. (2011). Activity-dependent clustering of functional synaptic inputs on developing hippocampal dendrites. *Neuron*, *72*(6), 1012-1024.

Knierim, J. J., Neunuebel, J. P., & Deshmukh, S. S. (2014). Functional correlates of the lateral and medial entorhinal cortex: objects, path integration and local–global reference frames. *Phil. Trans. R. Soc. B*, *369*(1635), 20130369.

Larkum, M. E., Zhu, J. J., & Sakmann, B. (1999). A new cellular mechanism for coupling inputs arriving at different cortical layers. *Nature*, *398*(6725), 338-341.

Lev-Ram, V., Makings, L. R., Keitz, P. F., Kao, J. P., & Tsien, R. Y. (1995). Long-term depression in cerebellar Purkinje neurons results from coincidence of nitric oxide and depolarization-induced Ca 2+ transients. *Neuron*, 15(2), 407-415.

Lisman, J. E. (1997). Bursts as a unit of neural information: making unreliable synapses reliable. *Trends in Neurosciences*, *20*(1), 38-43.

Lisman, J. E. (1999). Relating hippocampal circuitry to function: recall of memory sequences by reciprocal dentate–CA3 interactions. *Neuron*, *22*(2), 233-242.

Lisman, J., Yasuda, R., & Raghavachari, S. (2012). Mechanisms of CaMKII action in long-term potentiation. *Nature Reviews Neuroscience*, *13*(3), 169-182.

Lisman, J., & Spruston, N. (2005). Postsynaptic depolarization requirements for LTP and LTD: a critique of spike timing-dependent plasticity. *Nature Neuroscience*, *8*(7), 839-841.

Lisman, J., & Spruston, N. (2010). Questions about STDP as a general model of synaptic plasticity. *Frontiers in Synaptic Neuroscience*, *26*, 53.

London, M., & Häusser, M. (2005). Dendritic computation. *Annual Reviews. Neuroscience*, *28*, 503-532.

Losonczy, A., & Magee, J. C. (2006). Integrative properties of radial oblique dendrites in hippocampal CA1 pyramidal neurons. *Neuron*, *50*(2), 291-307.

Lovett-Barron, M., Turi, G. F., Kaifosh, P., Lee, P. H., Bolze, F., Sun, X. H., ... & Losonczy, A. (2012). Regulation of neuronal input transformations by tunable dendritic inhibition. *Nature Neuroscience*, *15*(3), 423-430.

Madisen, L., Zwingman, T. A., Sunkin, S. M., Oh, S. W., Zariwala, H. A., Gu, H., ... & Lein, E. S. (2010). A robust and high-throughput Cre reporting and characterization system for the whole mouse brain. *Nature Neuroscience*, 13(1), 133-140

Magee, J. C., & Johnston, D. (1997). A synaptically controlled, associative signal for Hebbian plasticity in hippocampal neurons. *Science*, *275*(5297), 209-213.

Major, G., Larkum, M. E., & Schiller, J. (2013). Active properties of neocortical pyramidal neuron dendrites. *Annual Review of Neuroscience*, *36*, 1-24.

Makara, J. K., & Magee, J. C. (2013). Variable dendritic integration in hippocampal CA3 pyramidal neurons. *Neuron*, *80*(6), 1438-1450.

Makino, H., & Malinow, R. (2011). Compartmentalized versus global synaptic plasticity on dendrites controlled by experience. *Neuron*, *72*(6), 1001-1011.

Markram, H., Lübke, J., Frotscher, M., & Sakmann, B. (1997). Regulation of synaptic efficacy by coincidence of postsynaptic APs and EPSPs. *Science*,*275*(5297), 213-215.

Markram, H., Gerstner, W., & Sjöström, P. J. (2012). Spike-timing-dependent plasticity: a comprehensive overview. *Frontiers in Synaptic Neuroscience*, *4*, 8.

Marr, D., Willshaw, D., & McNaughton, B. (1991). Simple memory: a theory for archicortex. In *From the Retina to the Neocortex* (pp. 59-128). Birkhäuser Boston.

Mayer, M. L., Westbrook, G. L., & Guthrie, P. B. (1984). Voltage-dependent block by Mg2+ of NMDA responses in spinal cord neurones.

McNaughton, B. L., Barnes, C. A., & O'keefe, J. (1983). The contributions of position, direction, and velocity to single unit activity in the hippocampus of freely-moving rats. *Experimental Brain Research*, *52*(1), 41-49.

McNaughton, B. L., & Morris, R. G. (1987). Hippocampal synaptic enhancement and information storage within a distributed memory system. *Trends in Neurosciences*, *10*(10), 408-415.

McNaughton, B. L., Barnes, C. A., Meltzer, J., & Sutherland, R. J. (1989). Hippocampal granule cells are necessary for normal spatial learning but not for spatially-selective pyramidal cell discharge. *Experimental Brain Research*,*76*(3), 485-496.

Min, M. Y., Rusakov, D. A., & Kullmann, D. M. (1998). Activation of AMPA, kainate, and metabotropic receptors at hippocampal mossy fiber synapses: role of glutamate diffusion. *Neuron*, *21*(3), 561-570.

Mori, M., Gähwiler, B. H., & Gerber, U. (2007). Recruitment of an inhibitory hippocampal network after bursting in a single granule cell. *Proceedings of the National Academy of Sciences*, *104*(18), 7640-7645.

Müller, C., Beck, H., Coulter, D., & Remy, S. (2012). Inhibitory control of linear and supralinear dendritic excitation in CA1 pyramidal neurons. *Neuron*, *75*(5), 851-864.

Müller, C., & Remy, S. (2014). Dendritic inhibition mediated by O-LM and bistratified interneurons in the hippocampus. *Frontiers in Synaptic Neuroscience*, *6*, 23.

Murthy, V. N., Schikorski, T., Stevens, C. F., & Zhu, Y. (2001). Inactivity produces increases in neurotransmitter release and synapse size. *Neuron*, 32(4), 673-682.

Nabavi, S., Fox, R., Proulx, C. D., Lin, J. Y., Tsien, R. Y., & Malinow, R. (2014). Engineering a memory with LTD and LTP. *Nature*.

Nakazawa, K., Quirk, M. C., Chitwood, R. A., Watanabe, M., Yeckel, M. F., Sun, L. D., ... & Tonegawa, S. (2002). Requirement for hippocampal CA3 NMDA receptors in associative memory recall. *Science*, *297*(5579), 211-218.

Nowak, L., Bregestovski, P., Ascher, P., Herbet, A., & Prochiantz, A. (1984). Magnesium gates glutamate-activated channels in mouse central neurones. *Nature*

Oikonomou, K. D., Singh, M. B., Sterjanaj, E. V., & Antic, S. D. (2014). Spiny neurons of amygdala, striatum, and cortex use dendritic plateau potentials to detect network UP states. *Frontiers Cellularl Neuroscience*, *8*(292), 10-3389.

O'Keefe, J. (1999). Do hippocampal pyramidal cells signal non-spatial as well as spatial information?. *Hippocampus*, 9(4), 352-364.

Palmer, L. M., Shai, A. S., Reeve, J. E., Anderson, H. L., Paulsen, O., & Larkum, M. E. (2014). NMDA spikes enhance action potential generation during sensory input. *Nature Neuroscience*, *17*(3), 383-390.

Pfister, J. P., & Gerstner, W. (2006). Triplets of spikes in a model of spike timing-dependent plasticity. *The Journal of Neuroscience*, 26(38), 9673-9682.

Poirazi, P., Brannon, T., & Mel, B. W. (2003). Pyramidal neuron as two-layer neural network. *Neuron*, *37*(6), 989-999.

Poo, M. M., Pignatelli, M., Ryan, T. J., Tonegawa, S., Bonhoeffer, T., Martin, K. C., ... & Mullins, C. (2016). What is memory? The present state of the engram. *BMC biology*, 14(1), 1.

Ramirez, S., Liu, X., Lin, P. A., Suh, J., Pignatelli, M., Redondo, R. L., ... & Tonegawa, S. (2013). Creating a false memory in the hippocampus. *Science*,*341*(6144), 387-391.
Remy, S., & Spruston, N. (2007). Dendritic spikes induce single-burst long-term potentiation. *Proceedings of the National Academy of Sciences*, *104*(43), 17192-17197.

Rolls, E. T. (1995). A model of the operation of the hippocampus and entorhinal cortex in memory. *International Journal of Neural Systems*, 6, 51–70.

Rolls, E. T. (2008). Memory, attention, and decision-making. Chapter 2. OUP.

Rolls, E. T., & Webb, T. J. (2012). Cortical attractor network dynamics with diluted connectivity. *Brain Research*, 1434, 212-225.

Rogers, M., & Dani, J. A. (1995). Comparison of quantitative calcium flux through NMDA, ATP, and ACh receptor channels. *Biophysical Journal*, 68(2), 501.

Schneggenburger, R., Zhou, Z., Konnerth, A., & Neher, E. (1993). Fractional contribution of calcium to the cation current through glutamate receptor channels. *Neuron*, 11(1), 133-143.

Sheffield, M. E., & Dombeck, D. A. (2015). Calcium transient prevalence across the dendritic arbour predicts place field properties. *Nature*, *517*(7533), 200-204.

Shatz J. (1992). The developing brain. Sci. Am. 267, 60–6710.1038/scientificamerican0992-60

Sandler, V. M., & Ross, W. N. (1999). Serotonin modulates spike backpropagation and associated [Ca2+] i changes in the apical dendrites of hippocampal CA1 pyramidal neurons. *Journal of Neurophysiology*, 81(1), 216-224.

Sans, N., Petralia, R. S., Wang, Y. X., Blahos, J., Hell, J. W., & Wenthold, R. J. (2000). A developmental change in NMDA receptor-associated proteins at hippocampal synapses. *The Journal of Neuroscience*, 20(3), 1260-1271.

Schiller, J., Schiller, Y., Stuart, G., & Sakmann, B. (1997). Calcium action potentials restricted to distal apical dendrites of rat neocortical pyramidal neurons. *The Journal of Physiology*, *505*(3), 605-616.

Schiller, J., Major, G., Koester, H. J., & Schiller, Y. (2000). NMDA spikes in basal dendrites of cortical pyramidal neurons. *Nature*, *404*(6775), 285-289.

Shi, J., Aamodt, S. M., & Constantine-Paton, M. (1997). Temporal correlations between functional and molecular changes in NMDA receptors and GABA neurotransmission in the superior colliculus. *The Journal of Neuroscience*, 17(16), 6264-6276.

Sjöström, P. J., Turrigiano, G. G., & Nelson, S. B. (2001). Rate, timing, and cooperativity jointly determine cortical synaptic plasticity. *Neuron*, *32*(6), 1149-1164.

Sjöström, P. J., Rancz, E. A., Roth, A., & Häusser, M. (2008). Dendritic excitability and synaptic plasticity. *Physiological Reviews*, *88*(2), 769-840.
Smith, S. L., Smith, I. T., Branco, T., & Häusser, M. (2013). Dendritic spikes enhance stimulus selectivity in cortical neurons in vivo. *Nature*, *503*(7474), 115-120.

Spruston, N., Schiller, Y., Stuart, G., & Sakmann, B. (1995). Activity-dependent action potential invasion and calcium influx into hippocampal CA1 dendrites. *Science*, *268*(5208), 297-300.

Stuart, G., Spruston, N., Sakmann, B., & Häusser, M. (1997). Action potential initiation and backpropagation in neurons of the mammalian CNS. *Trends in Neurosciences*, 20(3), 125-131.

Stuart, G., & Häusser, M. (1994). Initiation and spread of sodium action potentials in cerebellar Purkinje cells. Neuron, 13(3), 703-712.

Stuart, G. J., & Häusser, M. (2001). Dendritic coincidence detection of EPSPs and action potentials. *Nature Neuroscience*, *4*(1), 63-71.

Stuart, G. J., & Sakmann, B. (1994). Active propagation of somatic action potentials into neocortical pyramidal cell dendrites. *Nature*, *367*(6458), 69-72.

Takahashi, N., Kitamura, K., Matsuo, N., Mayford, M., Kano, M., Matsuki, N., & Ikegaya, Y. (2012). Locally synchronized synaptic inputs. *Science*,*335*(6066), 353-356.

Takumi, Y., Ramírez-León, V., Laake, P., Rinvik, E., & Ottersen, O. P. (1999). Different modes of expression of AMPA and NMDA receptors in hippocampal synapses. *Nature Neuroscience*, *2*(7), 618-624.

Thiagarajan, T. C., Lindskog, M., & Tsien, R. W. (2005). Adaptation to synaptic inactivity in hippocampal neurons. *Neuron*, 47(5), 725-737.

Tonegawa, S., Pignatelli, M., Roy, D. S., & Ryan, T. J. (2015). Memory engram storage and retrieval. *Current Opinion in Neurobiology*, *35*, 101-109.

Townsend, M., Yoshii, A., Mishina, M., & Constantine-Paton, M. (2003). Developmental loss of miniature N-methyl-D-aspartate receptor currents in NR2A knockout mice. *Proceedings of the National Academy of Sciences*, 100(3), 1340-1345.

Treves, A., & Rolls, E. T. (1994). Computational analysis of the role of the hippocampus in memory. *Hippocampus*, 4(3), 374-391.

Tsubokawa, H. I. R. O. S. H. I., & Ross, W. N. (1996). IPSPs modulate spike backpropagation and associated [Ca2+] i changes in the dendrites of hippocampal CA1 pyramidal neurons. *Journal of Neurophysiology*, *76*(5), 2896-2906.

Turrigiano, G., Abbott, L. F., & Marder, E. (1994). Activity-dependent changes in the intrinsic properties of cultured neurons. *Science*, 264(5161), 974-976.

Turrigiano, G. G. (1999). Homeostatic plasticity in neuronal networks: the more things change, the more they stay the same. *Trends in Neurosciences*, 22(5), 221-227.

Tzounopoulos, T., Kim, Y., Oertel, D., & Trussell, L. O. (2004). Cell-specific, spike timing–dependent plasticities in the dorsal cochlear nucleus. *Nature Neuroscience*, 7(7), 719-725.

Urban, N. N., Henze, D. A., & Barrionuevo, G. (2001). Revisiting the role of the hippocampal mossy fiber synapse. *Hippocampus*, *11*(4), 408-417.

Wang, Y. T., & Linden, D. J. (2000). Expression of cerebellar long-term depression requires postsynaptic clathrin-mediated endocytosis. *Neuron*, 25(3), 635-647.

Weber, J. P., Andrásfalvy, B. K., Polito, M., Magó, Á., Ujfalussy, B. B., & Makara, J. K. (2016). Location-dependent synaptic plasticity rules by dendritic spine cooperativity. *Nature Communications*, *7*.

Wierenga, C. J., Ibata, K., & Turrigiano, G. G. (2005). Postsynaptic expression of homeostatic plasticity at neocortical synapses. *The Journal of Neuroscience*, 25(11), 2895-2905.

Williams, S. R., & Mitchell, S. J. (2008). Direct measurement of somatic voltage clamp errors in central neurons. *Nature Neuroscience*, *11*(7), 790-798.

Winnubst, J., & Lohmann, C. (2015). Synaptic clustering during development and learning: the why, when, and how. *Frontiers in Molecular Neuroscience*, *5*.

Witt, Andrea, Nancy Macdonald, and Peter Kirkpatrick. "Memantine hydrochloride." *Nature Reviews Drug Discovery* 3.2 (2004): 109-110.)

Witter, M. P., & Moser, E. I. (2006). Spatial representation and the architecture of the entorhinal cortex. *Trends in Neurosciences*, 29(12), 671-678.

Witter, M. P. (2007). The perforant path: projections from the entorhinal cortex to the dentate gyrus. *Progress in Brain Research*, *163*, 43-61.

Yeckel, M. F., & Berger, T. W. (1990). Feedforward excitation of the hippocampus by afferents from the entorhinal cortex: redefinition of the role of the trisynaptic pathway. *Proceedings of the National Academy of Sciences*, 87(15), 5832-5836.

LIST OF PUBLICATIONS

NR2A subunit of the N-methyl D-aspartate receptors are required for potentiation at the mossy fiber to granule cell synapse and vestibulo-cerebellar motor learning. Andreescu CE, Prestori F, **Brandalise F**, D'Errico A, De Jeu MT, Rossi P, Botta L, Kohr G, Perin P, D'Angelo E, De Zeeuw CI. Neuroscience. 2011 Mar 10;176:274-83. I.F. 3.327

Gene Signatures Associated with Mouse Postnatal Hindbrain Neural Stem Cells and Medulloblastoma Cancer Stem Cells Identify Novel Molecular Mediators and Predict Human Medulloblastoma Molecular Classification. Corno D, Pala M, Cominelli M, Cipelletti B, Leto K, Croci L, Barili V, **Brandalise F**, Melzi R, Di Gregorio A, Sergi LS, Politi LS, Piemonti L, Bulfone A, Rossi P, Rossi F, Consalez GG, Poliani PL, Galli R. Cancer Discov. 2012 Jun;2(6):554-68. I.F. 19.453

Golgi cell-mediated activation of postsynaptic $GABA_B$ receptors induces disinhibition of the Golgi cell–granule cell synapse in rat cerebellum. **Brandalise F**, Gerber U and Rossi P. PLoS One. 2012;7(8):e43417. doi: 10.1371/journal.pone.0043417. I.F. 3.23

*****Mossy fiber-evoked subthreshold responses induce timing-dependent plasticity at hippocampal CA3 recurrent synapses. **Brandalise F,** Gerber U**.** Proc Natl Acad Sci U S A. 2014 Mar 18;111(11):4303-8. doi: 10.1073/pnas.1317667111 I.F. 9.67
***** [Recommendation by Prof. Tomoki Fukai in F1000Prime].

Improving Training Condition Assessment in Endurance Cyclists: Effects of Ganoderma lucidum and Ophiocordyceps sinensis Dietary Supplementation. Rossi P, Buonocore D, Altobelli E, **Brandalise F**, Cesaroni V, Iozzi D, Savino E, Marzatico F. Evid Based Complement Alternat Med. 2014;2014:979613. doi: 10.1155/2014/979613.

Distinct molecular components for thalamic-and cortical-dependent plasticity in the lateral amygdala. Osvaldo Mirante, **Federico Brandalise**, Johannes Bohacek, Isabelle M Mansuy. Front Mol Neurosci. 2014 Jul 3;7:62. doi: 10.3389/fnmol.2014.00062. I.F. 5.15

Fear is the mother of invention: anuran embryos exposed to predator cues alter life-history traits, post-hatching behaviour and neuronal activity patterns. Gazzola, Andrea*, **Federico Brandalise***, Diego Rubolini, Paola Rossi, and Paolo Galeotti*. Journal of Experimental Biology 218, no. 24 (2015): 3919-3930. I.F. 2.89
***these authors contributed equally to this work**

Distinct expression patterns of inwardly rectifying potassium currents in developing cerebellar granule cells of the hemispheres and the vermis. **Federico Brandalise**, Rafael Lujan, Roberta Leone, Valentina Cesaroni, Chiara Romano, Urs Gerber, and Paola Rossi. European Journal of Neuroscience, 43(11), 1460-1473 I.F. 3.181

SUBMITTED MANUSCRIPTS

Dendritic NMDA spikes are necessary for timing-dependent associative plasticity at synapses between hippocampal pyramidal cells. **Federico Brandalise,** Stefano Carta, Fritjof Helmchen, John Lisman, Urs Gerber [under revision in Nature Communications].

Structured subthreshold synaptic input changes the characteristic firing pattern of CA3 hippocampal neurons. Saray Soldado Magraner*, **Federico Brandalise***, Suraj Honnuraiah, Urs Gerber, Rodney Douglas. [In preparation for submission].
***these authors contributed equally to this work**

CURRICULUM VITAE

FEDERICO BRANDALISE

Date of birth		April 13, 1986
Place of birth		Tregnago, Verona, Italy
Citizenship		Italian
Languages		Italian, English, German
Education	2005	Scientific High School Diploma– Liceo scientifico Angelo Messedaglia
	2005-2008	Bachelor Degree in Human Biology and Biomedical Science - University of Pavia
		Thesis title: The NR2A subunit of the N-methyl D-aspartate receptor is required for potentiation at the cerebellar mossy fiber to granule cell synapse and vestibulo-cerebellar motor learning.
	2008-2013	Master Degree in Neurobiology - University of Pavia
		Thesis title: Synaptic cross-talk between granule cells and Golgi cells through GABAB mediated modulation of GABAA-dependent neurotransmission in the cerebellum.
	2013-2016	PhD in Neuroscience in the laboratory of Prof. Urs Gerber; Brain research Institute, University of Zurich
Grants		Swiss National Foundation Grant
Affiliations		Swiss Society for Neuroscience American Society for Neuroscience

ACKNOWLEDGMENTS

I would like to use a few lines to thank all the people that have contributed in many ways to the realization of these projects.

The first acknowledgment goes to my PhD committee, for all the feedback and useful suggestions they provided me with during the past three years. A special thanks goes to for Prof. Urs Gerber who, among many other merits, enthusiastically let me take on this investigation, despite the fact that it was a new field for both of us, and who always supported my ideas on how to allow this project to evolve. I am pleased to also mention here Prof. Beat Gähwiler and Prof. Fritjof Helmchem for their constructive mentorship, and for their critical reading of all my manuscripts. During these years, I have learned a great deal from all three of them, especially regarding how to implement a successful scientific approach in designing a neurobiological investigation. I hope that our mutual esteem and friendship will lead to future collaborations.

It is important to mention here also the contribution of Prof. John Lisman, who really inspired several key experiments of the second paper shown in this thesis. I am also delighted to underline here the precious work of Dr. Stefano Carta, who helped me a lot for the initial part of the calcium imaging experiments.

Heartfelt thanks also to Dubravka Göckeritz-Dujmovic for the weekly preparation of the organotypic slice cultures. A significant acknowledgment must be given to all the technical support team of the Brain Research Institute that has made my research possible. It is also my pleasure to remember here the important statistical support of Saray Soldado Magraner and Dr. Ariel Gilad. The third paper of this thesis would not be possible without the modelling expertise of Suraj Honnuraiah and Prof. Rodney Douglas.

Another important acknowledgment goes to the Swiss National Foundation, which granted my PhD Fellowship, making it possible for me to achieve all my goals in these research projects.

I cannot omit thanking my family, who have always supported my decisions and believed in my abilities even over great distances. To conclude, a special thought is dedicated to Roberta, my colleague, my friend and my soon to be wife. You better than anyone understand the effort and the passion that I put into these pages, as you have been with me every evening while I was writing this thesis, helping with suggestions, motivating me to always overcome my limits. A new future is waiting for us, and it looks much brighter with you by my side.